COMPUTATIONAL STUDIES ON METALLOPHOSPHORANES AS INTERMEDIATES IN PALLADIUM-PHOSPHINE CHEMISTRY

Jennifer Goodman

Submitted for the degree of
Doctor of Philosophy

School of Engineering and Physical Sciences
Heriot-Watt University

June 2009

Abstract

The work detailed in this thesis describes density functional (DF) calculations that were performed to investigate the possible role of metallophosphoranes in the reactions of palladium-phosphine complexes.

A study was conducted on X/R exchange in [M(Cl)X(PH_3)(PR_3)] (X = F, OH, NH_2, Me, Ph, Cl; R = H, Me, F; M = Ni, Pd, Pt), to see how metallophosphorane formation, followed by R-transfer, was affected by varying the X ligand, nature of the accepting phosphine (PR_3) or the metal centre. Metallophosphorane formation was easiest with the small, electronegative X ligands such as F and OH and was promoted by electron-withdrawing R substituents on the accepting phosphine. When the metal centre was varied, the trend for the activation barriers was Ni < Pd < Pt. Subsequent R-transfer was always more facile than metallophosphorane formation.

The mechanism of disproportionation of [Pd(Cl)OH(PPh_3)$_2$] was studied using DF calculations on the model system [Pd(Cl)OH(PH_3)$_2$] and hybrid DF:HF methods on the full experimental complex. In the small model a reaction profile was found via a metallophosphorane intermediate formed via a transition state at 28.3 kcal/mol (from the trans reactant) or a transition state at 21.8 kcal/mol (from the cis reactant). A similar mechanism was found with the full experimental complex (highpoint 27.5 kcal/mol) but a more accessible route was located via a zwitterion intermediate, $[PdPPh_3Cl]^-[P(OH)Ph_3]^+$ (highpoint 26.7 kcal/mol).

Possible mechanisms for experimentally-observed Ph/Ph exchange in *trans*-[PdX(Ph)(PPh_3)$_2$] (X = Cl, Br, I) and R/Ph exchange in *trans*-[PdI(R)(PPh_3)$_2$] (R = Me, CH_2CF_3) were studied using DF:HF calculations. For Ph/Ph exchange, the most accessible pathway involved pre-dissociation of a phosphine, followed by intermolecular attack of the palladium-bound phenyl on the remaining phosphorus. The lowest activation barriers were seen when X = I. The equivalent mechanism was also the most accessible for Me/Ph exchange, although the analogous mechanism without pre-dissociation of phosphine was very competitive. R/Ph exchange was computed to be considerably less accessible when R = CH_2CF_3 than when R = Me.

In memory of

Dr. Ernest L. Godfrey

Acknowledgements

I would firstly like to thank my supervisor, Prof. Stuart Macgregor, for his inspiration, guidance and patience. I would also like to thank the previous and current members of CICG for their help, friendship and welcome distractions. I owe special thanks to Stefan for his support, advice, proof-reading and for putting up with me.

My parents and sisters have always been a great source of support and encouragement, which I greatly appreciate. I would also like to thank Sarah for giving me a lovely place to live. I am also grateful for the support I received from Mr. Swan and Dr. Cameron in my earlier education, which helped me to get to where I am today.

ACADEMIC REGISTRY

Research Thesis Submission

Name*:*	Jennifer Goodman		
School/PGI:	Engineering and Physical Sciences		
Version: *(i.e. First, Resubmission, Final)*	Final	Degree Sought (Award **and** Subject area)	PhD in Chemistry

Declaration

In accordance with the appropriate regulations I hereby submit my thesis and I declare that:

1) the thesis embodies the results of my own work and has been composed by myself
2) where appropriate, I have made acknowledgement of the work of others and have made reference to work carried out in collaboration with other persons
3) the thesis is the correct version of the thesis for submission and is the same version as any electronic versions submitted*.
4) my thesis for the award referred to, deposited in the Heriot-Watt University Library, should be made available for loan or photocopying and be available via the Institutional Repository, subject to such conditions as the Librarian may require
5) I understand that as a student of the University I am required to abide by the Regulations of the University and to conform to its discipline.

* *Please note that it is the responsibility of the candidate to ensure that the correct version of the thesis is submitted.*

Signature of Candidate		Date:	

Submission

Submitted By *(name in capitals):*	Jennifer Goodman
Signature of Individual Submitting:	
Date Submitted:	

For Completion in Academic Registry

Received in the Academic Registry by *(name in capitals):*			
Method of Submission *(Handed in to Academic Registry; posted through internal/external mail):*			
*E-thesis Submitted (**mandatory for final theses from January 2009**)*			
Signature:		Date:	

Contents

Chapter 7: Computational background

Chapter 1: Literature Introduction

1.1 Section 1: Introduction to metallophosphoranes

Metallophosphoranes are a class of complexes containing a pentavalent pentacoordinated phosphorus where at least one substituent is a metal fragment. Figure 1.1 shows the general structure of a metallophosphorane, focusing on the key region around the pentacoordinated phosphorus. The geometry around the phosphorus tends to be close to trigonal bipyramidal, with the metal fragment in an equatorial position.

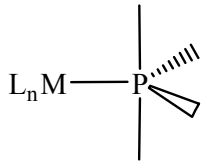

Figure 1.1: General structure of a metallophosphorane.

The discussion of metallophosphoranes will begin by looking at phosphoranes such as PH_5, to understand the bonding around a pentacoordinated phosphorus. Then the molecular orbital diagram for C_{2v} $\{PH_4\}^-$ will be explored, as typically metallophosphoranes are considered to consist of a phosphoranide ligand bound to a metal fragment. The preference of different atoms or groups to lie either equatorial or axial to a pentacoordinated phosphorus will also be discussed.

1.1.1 Bonding around phosphorus in phosphoranes

The bonding character of the phosphorus in a phosphorane is interesting because there are ten electrons in the valence shell, which is a violation of the octet rule and means that the phosphorus is hypervalent. It is useful to model the bonding in the yet unsynthesised molecule PH_5 to gain insight into the bonding around a phosphorane phosphorus. It has been proposed that the 3d orbitals of phosphorus could be utilised, however, the 3s/3p-3d energy gap is large, making their involvement unlikely.[1] Instead, a bonding model was proposed by Rundle[2] where the axial hydrogens and phosphorus in PH_5 are involved in a three-centre-four-electron (3c-4e) bond. This bond consists of the $3p_z$ orbital of phosphorus interacting with the two 1s orbitals from the two axial hydrogens, as shown in Figure 1.2.[3] These combine to form a bonding, a non-bonding (HOMO) and an antibonding molecular orbital (LUMO).

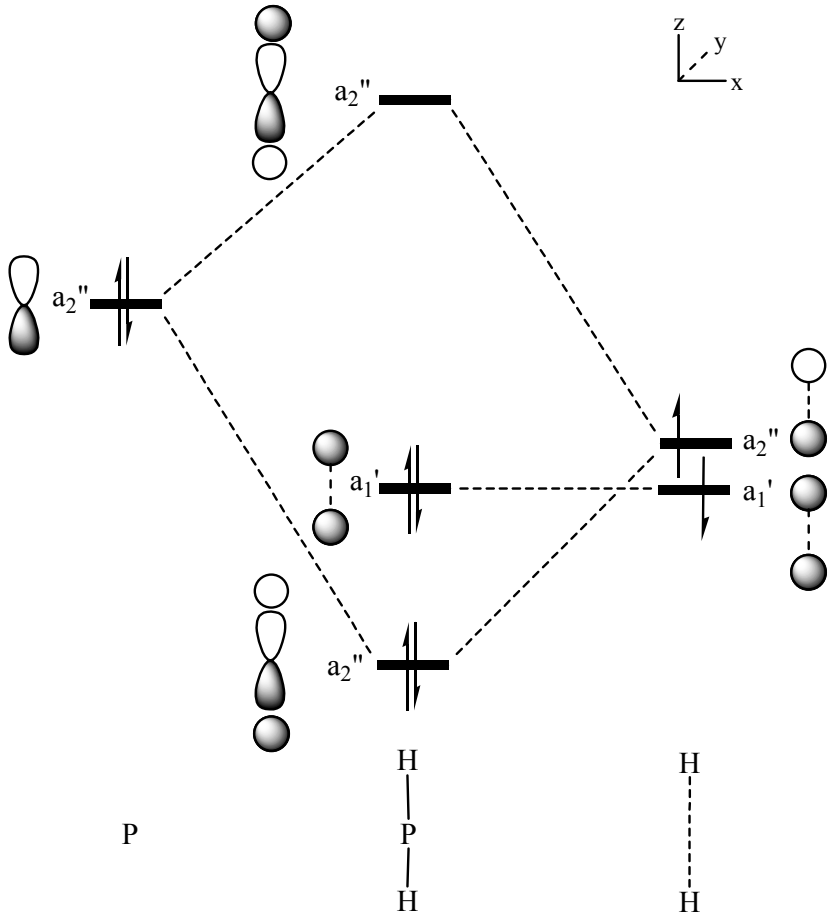

Figure 1.2: The molecular orbitals in the axial 3c-4e bond in PH_5, formed from the linear combination of $3p_z$ from P and two H 1s orbitals. D_{3h} symmetry labels are shown.

The molecular orbitals (MOs) constructed for the axial 3c-4e bond in $\{PH_2\}$ (with p_z orbitals from P) can then be combined with the MOs for a trigonal planar $\{PH_3\}$ fragment (with s, p_x and p_y orbitals from P), as shown in Figure 1.3.[3] The a_1' orbital of the 3c-4e axial bond combines with the a_1' orbital of $\{PH_3\}$, resulting in some of the electron density from the axial bond moving onto the equatorial hydrogens. The other orbitals of a_2'' are unable to mix and remain unchanged.

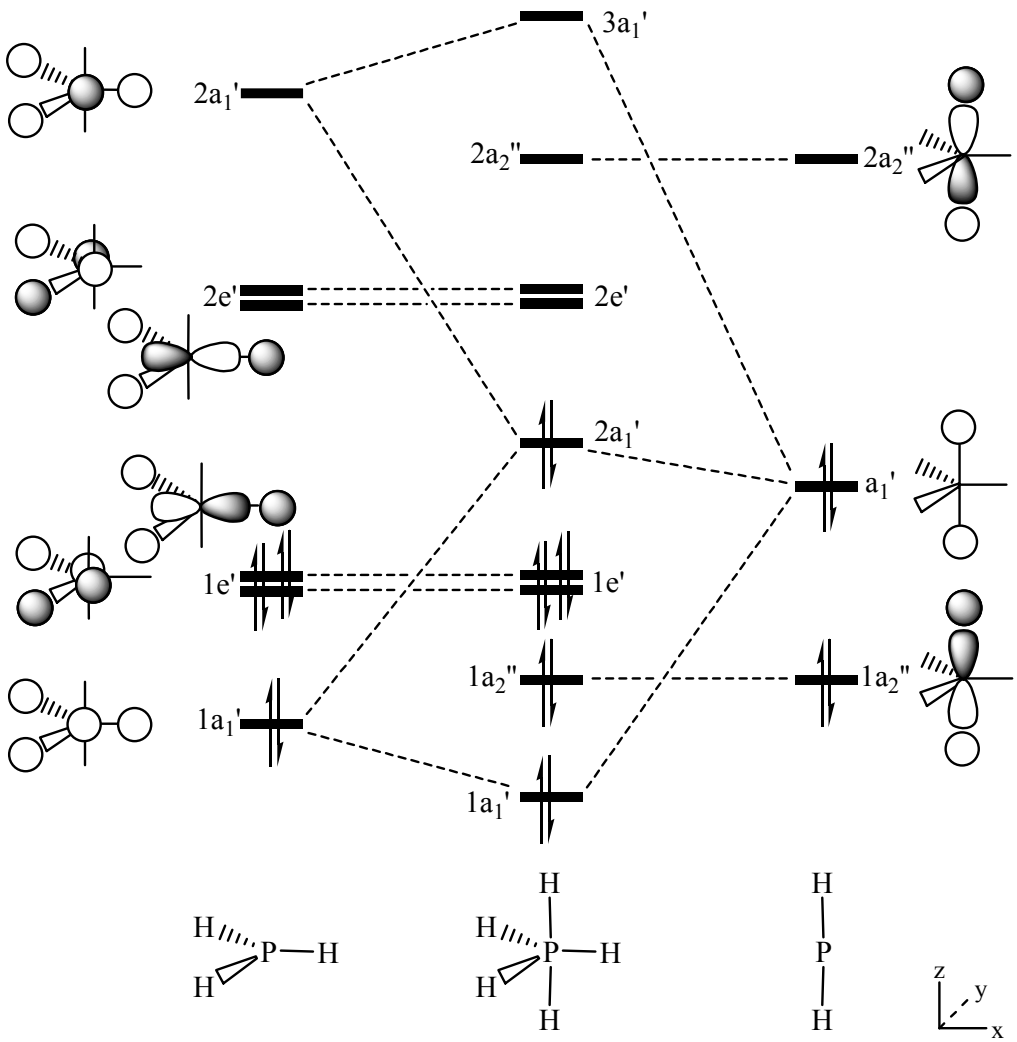

Figure 1.3: The MO diagram for PH_5, constructed from the linear combination of trigonal planar {PH_3} (equatorial H 1s orbitals + P 2s, p_x and p_y orbitals) and linear {PH_2} (axial H 1s orbitals + P p_z).

1.1.2 Bond lengths in phosphoranes

An interesting aspect of trigonal bipyramidal (TBP) phosphoranes is that when a substituent appears in both axial and equatorial sites, such as fluorine in PF_5, the axial bonds are longer than the equatorial P-F bonds.[4] The P-F bond lengths for PF_5[4] and a series of substituted phosphoranes, PR_2F_3, where R = chlorine,[5,6] hydrogen[7] or methyl[8] are shown in Table 1.1.

	PF_5[4]	PCl_2F_3[5]	PH_2F_3[7]	PMe_2F_3[8]
$P\text{-}F_{eq}$	1.532(3)	1.538(7)	1.541(5)	1.533(6)
$P\text{-}F_{ax}$	1.580(2)	1.593(4)	1.619(4)	1.643(3)
Δ ($P\text{-}F_{ax}$ - $P\text{-}F_{eq}$)	0.048(5)	0.055(7)	0.079(6)	0.090(8)
(P-F) mean	1.550(1)	1.575(3)	1.593(2)	1.614(2)

Table 1.1: P-F bond lengths (Å) in phosphorus (V) fluorides, PF_5 and PX_2F_3 where X = F, Cl, H or Me and the X groups are equatorial in the TBP geometries.

The axial P-F bonds are longer than the equatorial in all four compounds. This is likely to be a result of the different types of bonds in a TBP; equatorial bonds are two-centre two-electron bonds whereas axial bonds are three-centre four-electron bonds. Albright *et al.*[9] proposed that there could be mixing between the $1a_1'$ and 1e' orbitals in the equatorial plane of PH_5, which would form sp hybrid orbitals, as shown in Figure 1.4. This would result in there being more s character in the equatorial bonds, making them shorter than the axial bonds.

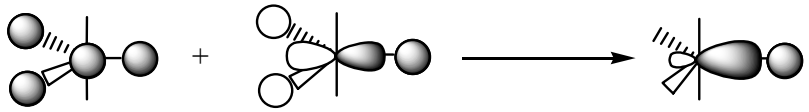

Figure 1.4: sp hybrid orbital produced from mixing equatorial $1a_1'$ and 1e' orbitals.

Table 1.1 also shows that the mean P-F bond lengths and the difference between the axial and equatorial P-F bonds ($\Delta(PF_{ax}\text{-}PF_{eq})$) in a molecule both increase with fluorine substitution. The increase in $\Delta(PF_{ax}\text{-}PF_{eq})$ when changing the substituent (Cl < H < Me) shows that the axial P-F bonds are more sensitive to the nature of the equatorial substituents than the equatorial P-F bonds are. Specifically, the axial P-F bonds are lengthened by increased electron-donating ability of the equatorial substituents.

1.1.3 Ligand site preferences in phosphoranes

There has been a considerable amount of research performed into determining the structure of five-coordinated trigonal bipyramidal (TBP) molecules, focusing especially on site preferences when a mixture of substituents are present. Muetterties *et al.*[10] used ^{19}F NMR to investigate the structures of mono-, di- and trisubstituted phosphorus (V) fluorides in 1963. This work focused on alkyl- and aryl-substituted systems. The following year they published further work where they had extended their study to cover a wider range of substituents.[11] All the results led to the same conclusion: in a

TBP phosphorane, the most electronegative ligands will occupy the axial sites. In RPF_4, R_2PF_3 and R_3PF_2, the aryl or alkyl R groups were always found to occupy equatorial sites. It was suggested that alkyl groups and hydrogen atoms might prefer equatorial sites as there is more s character to the phosphorus bonding orbitals in this plane, as discussed above. Conversely, electronegative ligands prefer the axial sites where they can form more ionic bonds. More recently, in 1989, Christen *et al*.[7] used electron diffraction to determine the gas-phase structures of the hydrogen fluorophosphoranes PHF_4 and PH_2F_3. Their findings support the trend, with all the hydrogens located in equatorial sites. Additionally, an electron diffraction study on PF_4Me and PF_3Me_2[8] revealed that the methyl groups are only observed occupying equatorial sites. The structures of a range of phosphorus (V) chlorofluorides were analysed by Holmes *et al*.[5] using low temperature ^{35}Cl nuclear quadrupole resonance and ^{19}F NMR techniques. This work reinforced the trends seen in the other studies, with the chlorine atoms always occupying equatorial positions in PCl_3F_2 and PCl_2F_3.

Electronegativity is not the only factor that can affect ligand site preference. Emsley and Hall[12] suggested that both electronic and steric factors could influence the preferred position of a ligand. For instance, they propose that if a ligand has lone pairs capable of π-bonding, it will prefer to occupy an equatorial site. This is however dependent on electronegativity. A bulky ligand should also prefer an equatorial site, as there is more space than in an axial site.

1.1.4 Bonding around phosphorus in phosphoranides

When metallophosphoranes are reported in the literature they are commonly considered as a phosphoranide ligand bound to a metal fragment.[13] To gain insight into the bonding picture in a simple phosphoranide such as $\{PH_4^-\}$, a qualitative MO diagram can be produced by removing an equatorial H from the MO diagram for PH_5 shown in Figure 1.5.[9] It can be seen that orbitals $1a_1$, $1a_2$ and $2a_2$ are largely unaffected by the removal of an equatorial H, but the symmetry labels have changed to reflect the change to C_{2v} symmetry. The 1e' and 2e' orbitals from TBP PH_5 have lost their degeneracy and split into pairs of b_1 and b_2 orbitals. There is a degree of sp mixing in the upper a_1 orbitals of $\{PH_4^-\}$. This can be seen in $3a_1$ which is the HOMO and contains the lone pair of electrons on phosphorus.

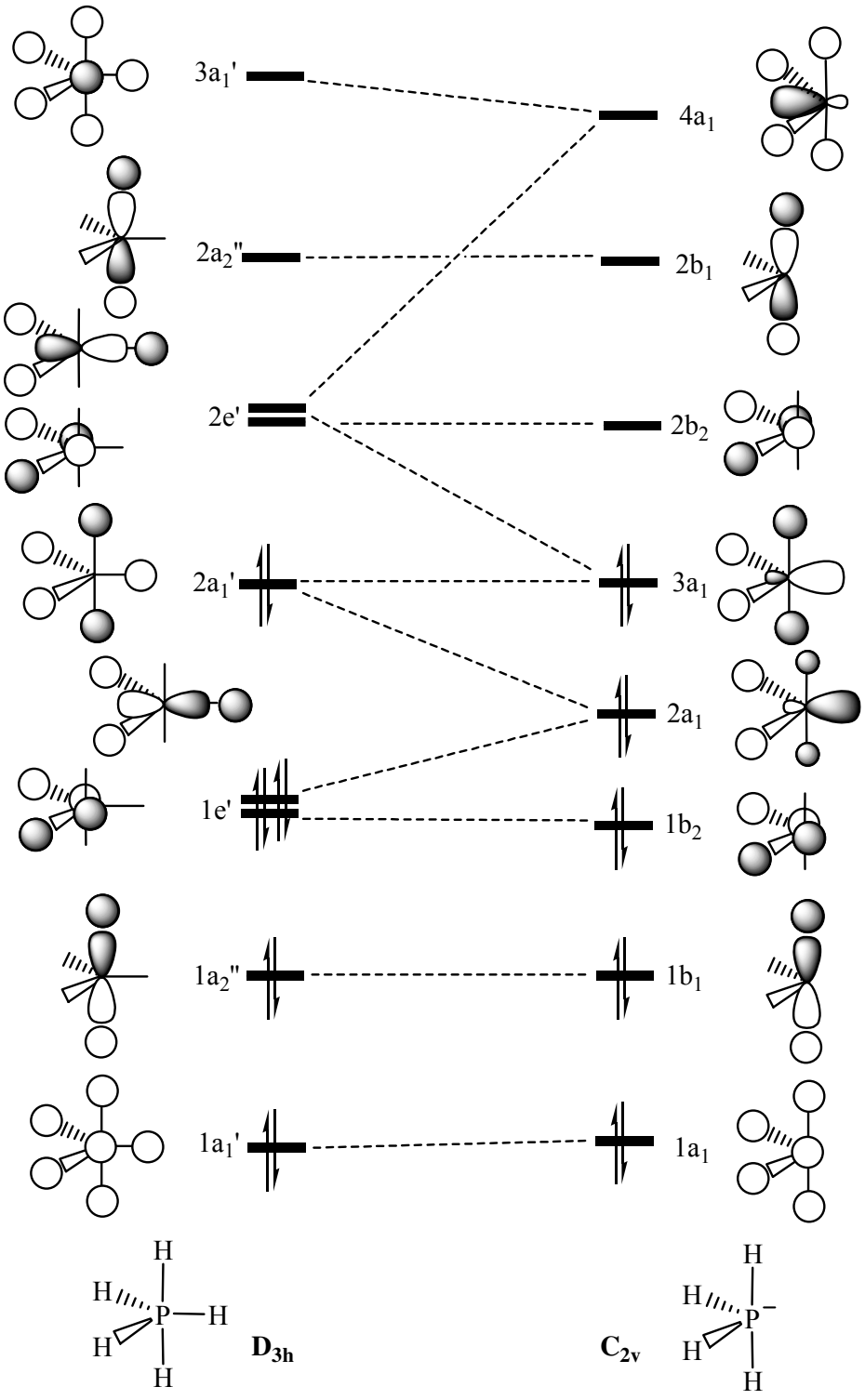

Figure 1.5: The change in the MO diagram from TBP PH_5 when an equatorial H is removed to form $\{PH_4\}^-$.[9]

By identifying the orbitals in $\{PH_4^-\}$ with the correct symmetry to interact with a π-donor or π-acceptor substituent, it is possible to predict which orientation the substituent should prefer. For instance, if a π-acceptor substituent occupies the vacant equatorial site in $\{PH_4^-\}$, there are two possible ways in which it can orient itself to accept electron density from either $1b_1$ or $1b_2$, as shown in Figure 1.6.[3] It can be seen that there is a greater overlap when a π-acceptor substituent interacts with $1b_1$, perpendicular to the

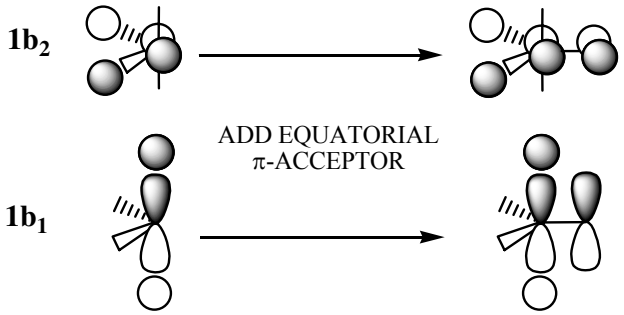

Figure 1.6: The possible orientations for a π-acceptor ligand to interact with a $\{PH_4^-\}$ fragment, where $1b_1$ has the greater overlap.

equatorial plane. Similarly, a π-donor substituent could interact with the unoccupied orbitals $2b_1$ or $2b_2$ in $\{PH_4^-\}$, as shown in Figure 1.7. In this case interaction with the b_2 orbital is favourable, as it avoids an antibonding interaction between the ligand p orbital and the equatorial H s orbitals. This suggests that a π-donor ligand should prefer to interact with $\{PH_4^-\}$ in the equatorial plane.

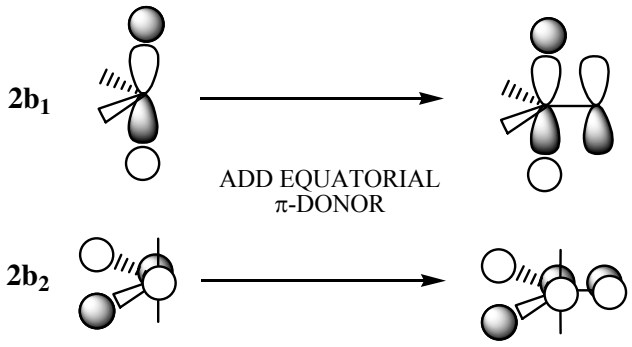

Figure 1.7: The possible orientations for a π-donor ligand to interact with a $\{PH_4^-\}$ fragment, where $2b_2$ has the greater overlap.

This prediction of positional preference has been observed in various substituted fluorophosphoranes. For instance, low temperature NMR studies on PF_4SR (R = Me, Et or Ph), where the lone pair on sulphur acts as a π-donor, showed that the preferred conformation features a sulphur lone pair lying parallel to the equatorial plane, despite

this leading to greater steric crowding.[14] The same orientation was seen using NMR with $PF_3(NH_2)_2$, with both amido lone pairs lying in the equatorial plane.[15]

1.1.5 Metal site preferences in metallophosphoranes

As mentioned before, metallophosphoranes tend to be considered as cationic metal fragments bound to a phosphoranide ligand. Since a late transition metal fragment would normally be bulky and a π-donor, it would be expected to bond to an equatorial site in a phosphoranide. Examination of metallophosphorane structures in the Cambridge Crystallographic Database[16] show that the metal fragment indeed always lies in an equatorial site.

Nakazawa *et al.*[1] were able to gain insight into the nature of the M-P bond in metallophosphoranes by looking at X-ray crystallographic and IR data. They compared the Fe-P bond lengths in $[FeCp\{P(OC_6H_4NMe)_2\}(CO)_2]$, which has two amido and two aryloxy substituents on the phosphorus, to $[FeCp\{P(OC_6H_4NMe)(OC_6H_4O)\}(CO)_2]$, which has one amido and three aryloxy substituents, as shown in Figure 1.8. They argued that if σ donation dominates the Fe-P bond, the complex with the more electron-rich phosphorus would have the shorter Fe-P bond. Conversely, if π-bonding dominates, the complex with the more electron-poor phosphorus would have a shorter Fe-P bond. The X-ray data showed that the Fe-P bond is shorter in the second complex (2.272(1) Å *cf.* 2.291(1) Å),[17] which has a more electron-poor phosphorus, revealing that π-back donation dominates the Fe-P bond. As the number of amido substituents on the phosphorus decreases, the υ_{CO} values in the IR spectra move to a higher energy, indicating greater π-back donation from iron to phosphorus.

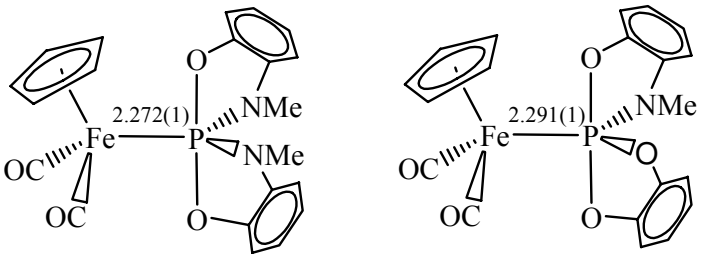

Figure 1.8: The structures of metallophosphoranes $[FeCp\{P(OC_6H_4NMe)_2\}(CO)_2]$ and $[FeCp\{P(OC_6H_4NMe)(OC_6H_4O)\}(CO)_2]$, bond lengths in Å.

A diverse range of metallophosphoranes containing different metals and substituents bound to the pentacoordinated phosphorus will be discussed further in this chapter,

along with the methods of their formation. This will be followed by examples of reactions where metallophosphoranes have been proposed as intermediate species. Finally, there will be a discussion of experimental work that may involve metallophosphoranes as intermediates or transition state structures, the possibility of which will be investigated in this thesis.

1.2 Section 2: General synthetic routes to metallophosphoranes

There are a range of different synthetic routes by which metallophosphoranes can be formed, and most of them can be characterised by one of the general reaction schemes shown in Figure 1.9.

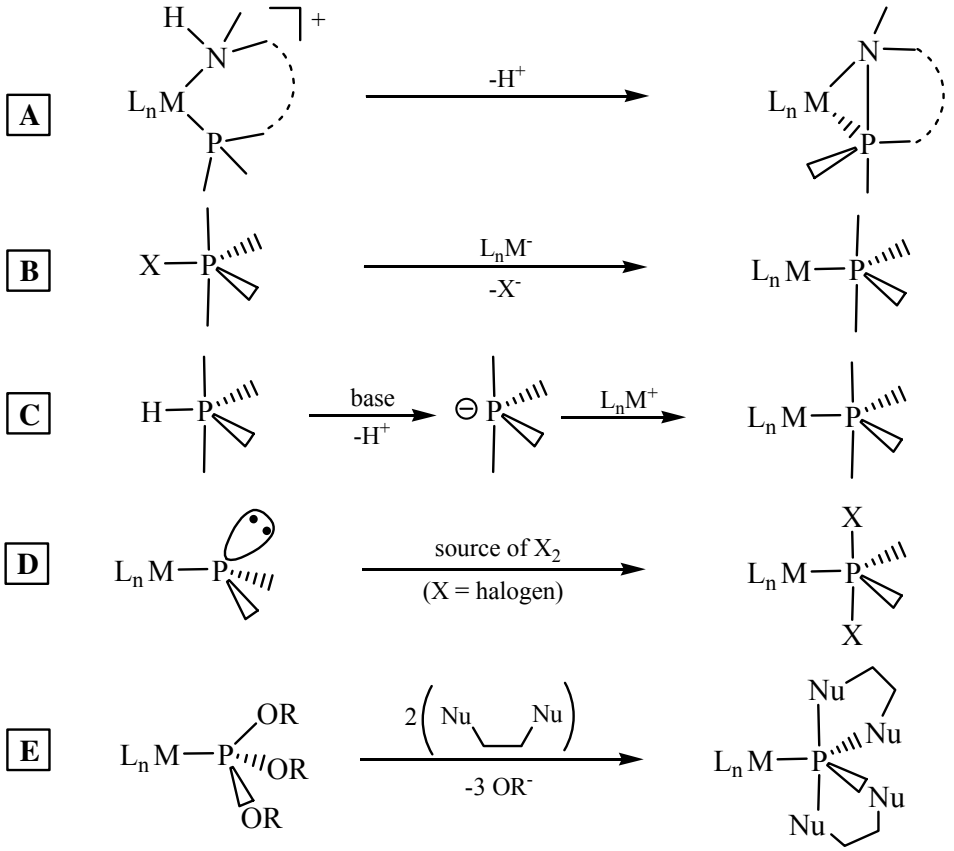

Figure 1.9: General synthetic routes to produce metallophosphoranes.

The first metallophosphoranes to be synthesised were produced using deprotonation, as shown in Route **A**. Generally, LiMe is used to deprotonate a nitrogen in a polycyclic phosphine species, forming a P-N bond and causing the phosphorus to become pentacoordinated. In Route **B**, a TM-anion performs a nucleophilic substitution at a phosphorane phosphorus atom. Metallophosphorane complexes can also be formed via Route **C**, where an electron-poor TM fragment is attacked by a phosphoranide, which has been formed by removal of H^+ from a phosphorane. In Route **D**, metallophosphoranes are synthesised from a halogen, X_2, undergoing oxidative addition to the phosphorus in a TM-phosphide complex. In Route **E**, an organic Lewis base performs a nucleophilic attack on a phosphite phosphorus bound to a TM-centre.

All of the metallophosphorane structures that will be discussed in this chapter have been synthesised using a variation of one of the methods outlined above. The following section will introduce a range of metallophosphorane structures from the literature that illustrate how this field has developed over the last thirty years.

1.2.1 Synthesis and structures of selected metallophosphoranes

The first example of a crystallographically-characterised metallophosphorane structure was published by Riess *et al.*[18] in 1981. They deprotonated a cyclic phosphine ligand on a molybdenum complex, **1**, using LiMe in THF at 60ºC, as shown in Figure 1.10, to produce complex **2**. This is analogous to Synthetic Route **A**, except that the more electronegative oxygen forms a bond to molybdenum.

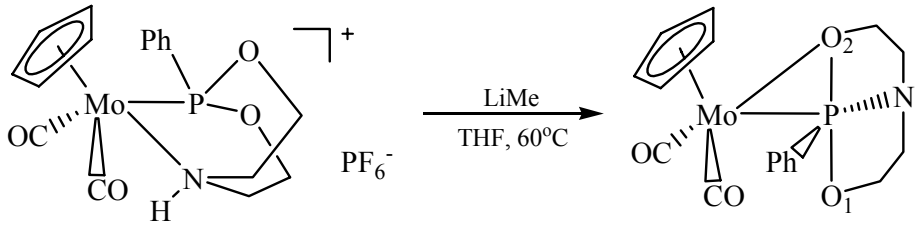

1 **2**

Figure 1.10: Formation of [MoCp{PO_2NPh}$(CO)_2$], **2**, by the deprotonation of **1**.

Complex **2** is the first example of a transition metal complex with a phosphoranide ion as a ligand. It is also the first example of an Mo-P-O three-membered ring. The P-O1 bond is 0.24 Å shorter than the P-O2 bond (1.893(4) Å), and the P-N bond (1.69(5) Å) falls into the expected range for a P-N_{eq} bond[19] in a TBP. The Mo□P distance (2.375(2) Å) is shorter than in [MoCp(NCO)(CO)$(PPh_3)_2$] (2.497(3) Å),[20] a similar molybdenum complex but with a phosphine rather than a phosphoranide ligand. They proposed that the reason for the difference in bond length may lie in the different oxidation states at phosphorus. However, this contradicts the common view of phosphorane ligands being regarded as phosphoranides. The molybdenum, phenyl group and nitrogen occupy equatorial positions in the TBP, while the more electronegative oxygen atoms occupy axial sites. This is consistent with the site preferences discussed earlier in the chapter.

When complex **1** is reacted with LiMe in THF/ether at –20ºC, an alternative metallophosphorane structure, **3**, is formed.[21] Complex **3** appears to be less thermodynamically stable than **2**, as heating **3** for 4 hours in THF at 60ºC produces complex **2**. Tungsten analogues of **2** and **3** were also synthesised using the same

methods as described above, and their structures were characterised using ^{31}P NMR spectroscopy.

The structure of **3** (see Figure 1.11) features a TBP pentacoordinated phosphorus with a Mo-P bond length (2.382(4) Å) similar to in **2**. The nitrogen atom is now in an axial position and coordinated to the metal, and is part of a Mo-P-N three-membered ring. The axial P-N bond is long[19] at 1.908(12) Å, while the P-O bonds are shorter than in **2** now that they occupy equatorial sites (P-O1 = 1.625(10) Å, P-O2 = 1.624(10) Å).

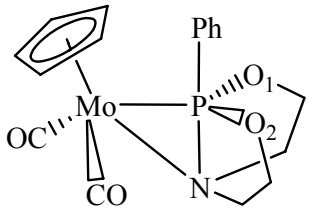

3

Figure 1.11: Alternative isomer of metallophosphorane [MoCp{PO_2NPh}$(CO)_2$], **3**, with the oxygen atoms equatorial in the phosphorane TBP.

Riess *et al.* also used Synthetic Route **A** to form a molybdenum complex containing a cyclamphosphoranide ligand, **5**, where the phosphorus atom is not only pentacoordinated but is also pentacyclic.[22] Complex **5** was formed by treating a molybdenum salt, **4**, with LiMe in THF at room temperature, which resulted in a 91% yield after 1 hour (see Figure 1.12). Despite the polycyclic nature of the phosphoranide, the geometry around phosphorus is very close to a TBP, with a N1-P-N3 angle of 176 ± 0.9º and the three angles in the equatorial plane close to 120º (118.0 ± 0.6º, 116.4 ± 0.6º, 117.6 ± 0.9º). N1 has a typical Mo-N bond length[22] of 2.223(5) Å, but a long P-N bond[22] of 1.854(5) Å, as seen in complex **3**. Unusually for a TBP, the axial P-N3 bond

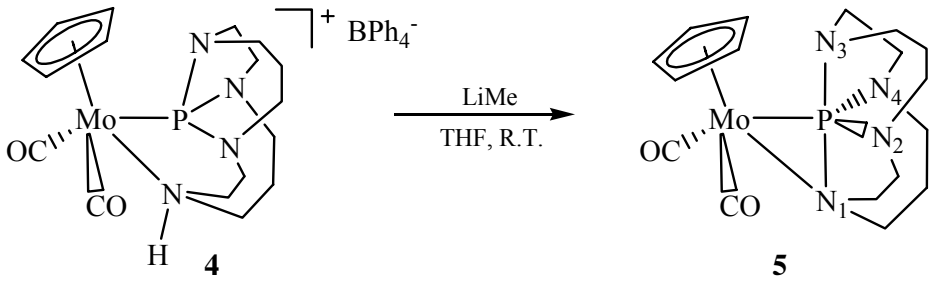

4 **5**

Figure 1.12: Formation of metallophosphorane [MoCp{cyclanP}$(CO)_2$], **5**, by the deprotonation of complex **4**.

is of a similar length to the equatorial P-N bonds, all of which are reasonably short (P-N3 = 1.696(7) Å, P-N2 = 1.697(6) Å, P-N4 = 1.670(7) Å). As discussed earlier in the chapter, normally the axial bonds to substituents in a TBP will be longer than the equatorial bonds. In this case the P-N1 bond is longer due to the coordination of N1 to molybdenum, which in turn shortens the opposite P-N3 bond.

In 1983 Lattman *et al.* published the first example of a metallophosphorane containing a monodentate phosphoranide ligand, **6**.[23] Complex **6** was formed by the nucleophilic attack of a manganese pentacarbonyl anion on the phosphorus in $(C_6H_4O_2)_2PCl$ (Synthetic Route **B**), as shown in Figure 1.13.

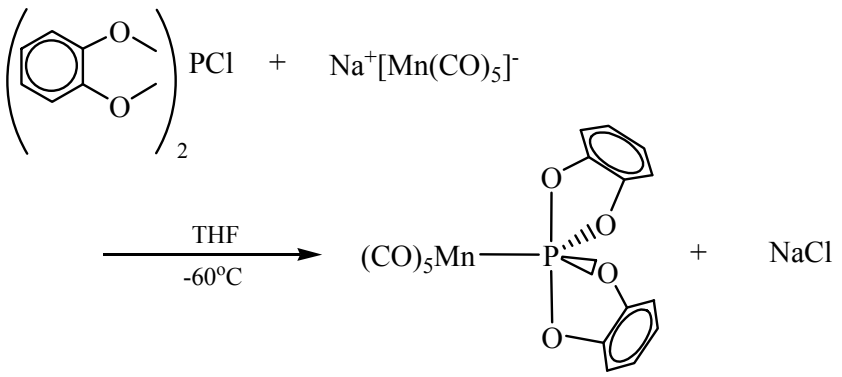

6

Figure 1.13: Formation of metallophosphorane $[Mo\{P(C_6H_4O_2)_2\}(CO)_5]$, **6**.

Two years later, Lattman *et al.* published crystallographic data on a cobalt metallophosphorane, **7**,[24] which contains the same $\{(C_6H_4O_2)_2P\}^-$ phosphoranide ligand as in **6**. Complex **7** was also formed by the nucleophilic attack of a metal ion on $(C_6H_4O_2)_2PCl$, as shown in Figure 1.14. The geometry around pentacoordinated P2 is a distorted TBP, with an O2-P2-O4 angle of 162.1(5)º and the three equatorial angles close to 120º (Co-P2-O1 = 116.4(4)º, Co-P2-O3 = 116.8(4)º, O1-P2-O3 = 126.9(5)º). The Co-P1 bond (2.230(4) Å) is shorter than the Co-P2 bond (2.257(4) Å), which the authors explained by comparing metal-PR_3 bonds with metal-PR_4 bonds in other systems.[25]

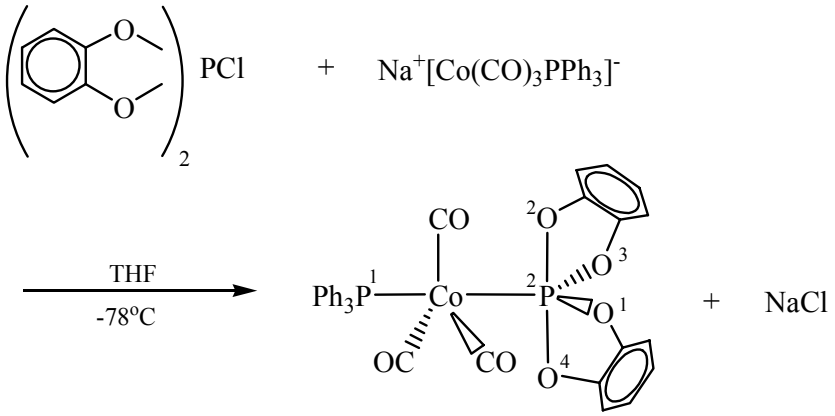

7

Figure 1.14: Metallophosphorane **7** can be formed by attack of an anionic cobalt complex on the phosphorus in $(C_6H_4O_2)_2PCl$.

During the 1980s and early 1990s Lattman and co-workers published the synthesis of a series of metallophosphorane complexes with structures determined by X-ray crystallography. These complexes were produced by deprotonation of a phosphorane followed by coordination to a metal centre, as in Synthetic Route **C**. An example of this is shown in Figure 1.15, where two different complexes are produced, both of which have a pentacoordinated phosphorus ligand.[26,27]

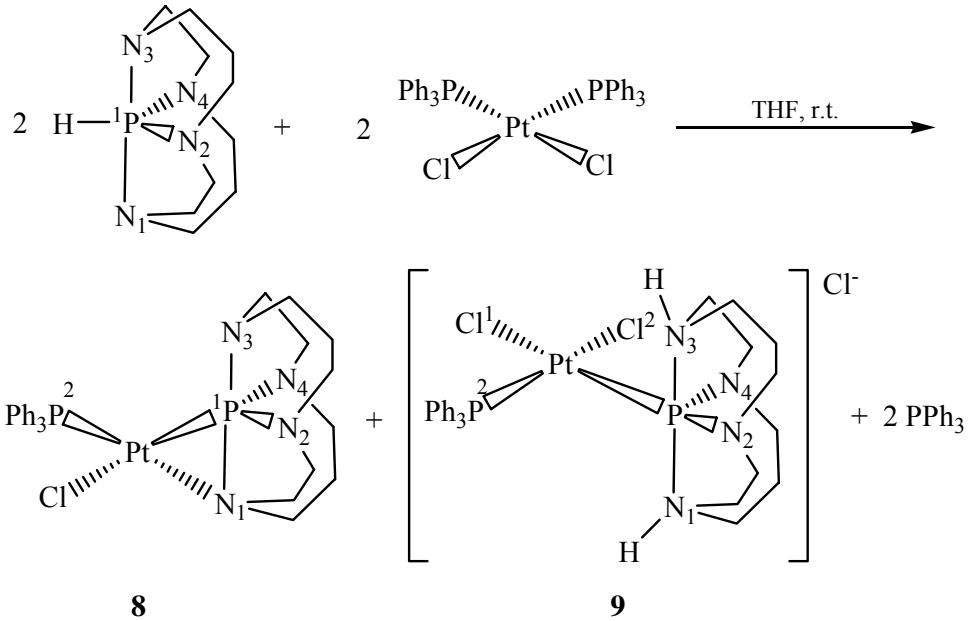

8 **9**

Figure 1.15: Deprotonation of phosphorane {cyclenP}H and coordination to $[PtCl_2(PPh_3)_2]$ forms complexes **8** and **9**.

In metallophosphorane **8**, the {cyclenP}$^-$ ligand is bidentate, bonding to palladium through phosphorus and an axial nitrogen, N1. It is likely that the Pt-P1-N1 three-membered ring is strained, which causes P1-N1 (1.872(11) Å) to be longer than P1-N3 (1.698(11) Å). In contrast to the trends seen in Section 1.3 of this chapter, in **8** the axial P1-N3 bond is of a similar length to the equatorial P1-N2 (1.698(11) Å) and P1-N4 (1.676(11) Å) bonds, as seen in complex **5**. In species **9** the {cyclenP}$^-$ ligand has been protonated twice, and acts as a monodentate ligand. In this case the axial P-N bonds are both relatively long (P1-N1 = 1.936(34) Å, P1-N3 = 1.924(42) Å), though it is typical for the axial P-N bonds in these ligands to be over 1.9 Å when the nitrogens are coordinated or protonated.[26,28] The equatorial P-N bonds (P1-N2 = 1.663(35) Å, P1-N4 = 1.598(37) Å) are shorter than the axial bonds, as expected in a TBP.

Lattman *et al.* have published the crystallographically-determined structures of a wide range of complexes containing a {cyclenP}$^-$ ligand. These complexes feature different transition metals, including cobalt,[29] platinum[30,31] and molybdenum.[32]

The first example of a metallophosphorane containing a monodentate phosphoranide ligand with non-cyclic substituents was published by Ebsworth *et al.*[33] They prepared $[IrCl_2(PCl_4)(CO)(PEt_3)_2]$, **10**, by reacting $[IrCl_2(PCl_2)(CO)(PEt_3)_2]$ with Cl_2 in chloroform, an example of Synthetic Route **D**. This complex is the first example of a phosphoranide with terminal atomic substituents bound to a TM centre. It was not possible to grow single crystals of **10** for X-ray crystallography, so the complex was identified using other analytical techniques and by probing its reactivity. Ebsworth and co-workers also produced a similar iridium complex containing a $\{PF_4\}^-$ group, **11**, as shown in Figure 1.16.[34] Complex **11** was formed in the reaction of $[IrCl_2(PF_2)(CO)(PEt_3)_2]$ with XeF_2 in CH_2Cl_2, and was characterised using X-ray crystallography. $\{PF_4\}^-$ lies trans to Cl, and has a TBP geometry with iridium in an

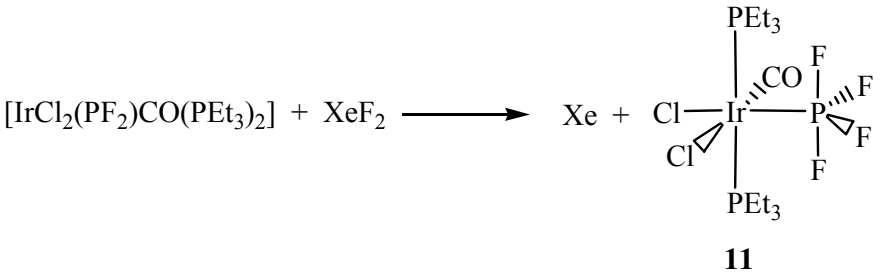

11

Figure 1.16: Synthesis of metallophosphorane $[IrCl_2CO(PEt_3)_2\{PF_4\}]$, **11**.

equatorial position. The axial P-F bonds (1.69(1) Å, 1.64(11) Å) are longer than the equatorial P-F bonds (1.56(2) Å, 1.52(2) Å), as expected in a TBP.

Miyoshi *et al.*[35] later published the synthesis of iron complexes containing $\{PF_4\}^-$, produced by the reaction between a cationic iron complex containing a phosphite ligand and Et_4NF in CH_2Cl_2 at room temperature. As shown in Figure 1.17, two iron metallophosphoranes were produced in the reaction. These products were characterised using ^{31}P and ^{19}F NMR spectroscopy. This reaction is an example of metallophosphoranes formation using a novel method developed by Miyoshi and co-workers, namely a nucleophilic attack on a phosphite phosphorus bound to a transition metal centre,[36] Synthetic Route **E**. They used this method to synthesise a range of iron and ruthenium metallophosphoranes which were characterised using X-ray

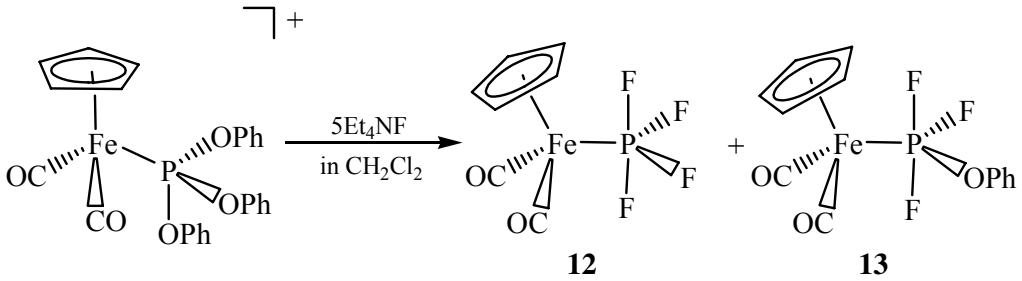

Figure 1.17: Synthesis of two iron metallophosphoranes via a nucleophilic attack on a metal-bound phosphite.

crystallography.[36,37] In these complexes the more electronegative atoms occupy the axial sites around the pentacoordinated phosphorus, as seen previously. For instance, complex **13** has the less electronegative oxygen atom in an equatorial position. In a complex with oxygen and nitrogen substituents, an example of which is shown in Figure 1.18, the nitrogen atoms occupy equatorial sites and the oxygen atoms axial sites.

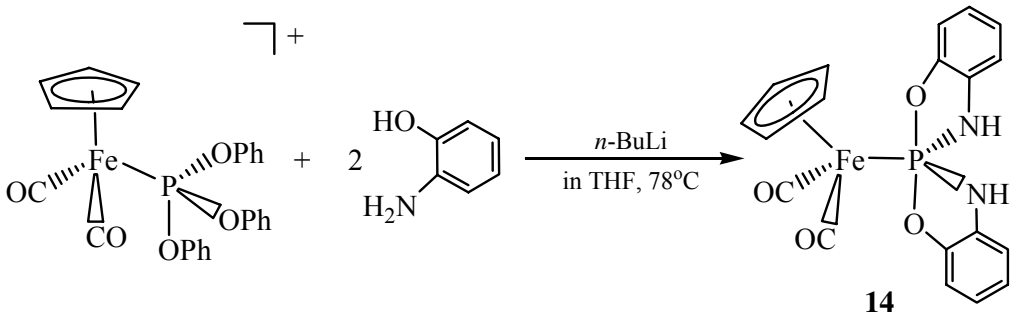

Figure 1.18: Synthesis of an iron metallophosphoranes via the nucleophilic attack of *o*-$HOC_6H_4NH_2$ on a metal-bound phosphite.

More recently, further crystallographically-determined metallophosphorane structures have been published, normally featuring two bidentate ligands on the pentacoordinated phosphorus and mainly palladium,[30,38] rhodium[39,40] or platinum[41] metal centres. The formation and structures of these species build on the earlier chemistry and techniques that have been described.

1.3 Section 3: Reactions with metallophosphoranes as intermediates

There are several reactions where metallophosphoranes have been either proposed or observed as intermediate species. This section will provide an overview of these reactions.

Early work by Riess and Vierling in 1984[42] identified a metallophosphorane complex, **16** (see Figure 1.19), as an intermediate in the migration of a phosphorus-bound allyl onto an iron centre. The σ-allyl ligand isomerises to become a σ-vinyl bound to iron in **17**. Complex **16** was characterised using ^{13}C and ^{1}H NMR spectroscopy and the ν(CO) stretching frequency. Riess *et al.* also observed an analogous metallophosphorane species in a reaction where a phenyl[43] similarly transfers from phosphorus to iron.

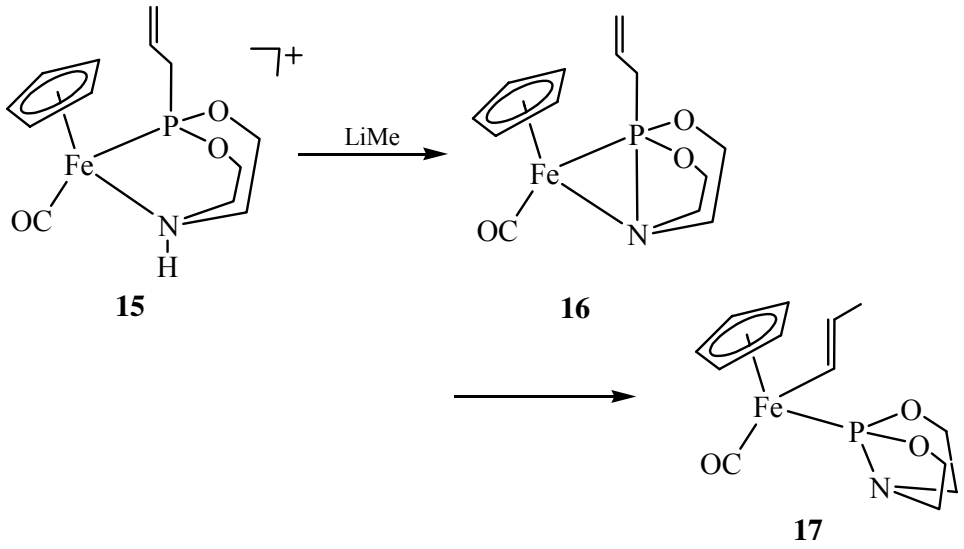

Figure 1.19: Mechanism of allyl-transfer from phosphorus to iron, via a metallophosphorane intermediate (**16**).

In 1992 Miyoshi *et al.*[44] investigated the mechanism by which $[FeCp(CO)_2(PHPh_2)]PF_6$ reacts with $NaBH_4$ to form $[FeCp(H)(CO)_2]$ and $PHPh_2$. They were focusing on the initial part of the reaction, namely phosphine loss, and considered several possible mechanisms. Further tests revealed that the reaction did not proceed via the attack of H^- on either the iron centre or an iron-bound carbonyl group, and did not require dissociation of the phosphine. Therefore, they concluded that the most likely mechanism for the first step in the reaction, forming $[FeCpH(CO)_2]$ and $PHPh_2$, was via a nucleophilic attack by H^- directly on the phosphorus, giving a metallophosphorane intermediate, as shown in Figure 1.20.

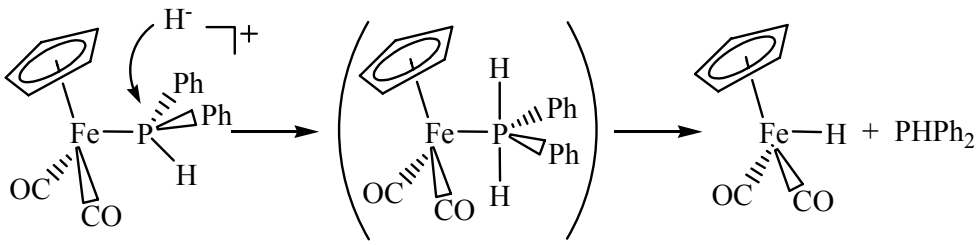

Figure 1.20: Proposed mechanism for reaction of $[FeCp(CO)_2(PHPh_2)]^+$ with $NaBH_4$ via a metallophosphorane intermediate.

The mechanisms proposed by Miyoshi and co-workers were further strengthened by the isolation of an iron metallophosphorane complex similar to those suggested as intermediate structures.[45] The structure of metallophosphorane $[FeCp(CO)_2\{P(o\text{-}OC_6H_4NH)_2\}]$, formed by the reaction of $[FeCp(CO)_2\{P(OMe)_3\}]^+$ with aminophenol, was shown in Figure 1.18. The structure was characterised using IR, ^{31}P NMR and ^1H NMR spectroscopies. It was reported that the metallophosphorane was formed by the attack of the organic Lewis base on the phosphorus.

Further work by Miyoshi and co-workers[46] published in 1994 focused on another range of iron complexes, $[FeCpL_2(P(NC_4H_8)_n(OMe)_{3-n})]^+$ (L = CO, PMe_3; n = 1-3), and their reaction with KOH. The fact that the reaction proceeded with L = CO or PMe_3 shows that it does not require the presence of carbonyl, so it is not directly involved in the reaction mechanism. Although they were unable to detect an intermediate structure, they suggested that a nucleophilic attack of hydroxide on the phosphorus was the most feasible mechanism, as shown in Figure 1.21.

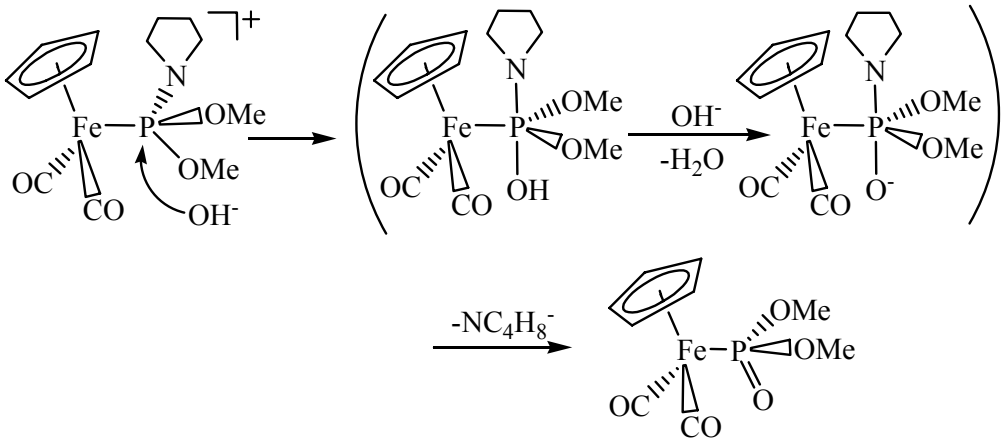

Figure 1.21: Proposed mechanism for reaction of $[FeCp(CO)_2\{P(NC_4H_8)(OMe)_2\}]^+$ with KOH via a metallophosphorane intermediate structure.

A case where a metallophosphorane was observed as a reaction intermediate was published by Miyamoto *et al*. in 2003.[47] They reacted $[IrCl_2Cp^*(PMe_3)]$ with a phosphorane bearing two 8-oxy-1-naphthyl groups in the presence of *t*-BuLi in THF to form Ir(III) metallophosphorane structure **18**, as shown in Figure 1.22. The structure of **18** was characterised using ^{31}P and ^{1}H NMR spectroscopy. This was then converted by heating to Ir(III) complexes **19** and **20** by heating in xylene or ethanol, to remove PMe_3 or Cl^- respectively. This second stage of the reaction involves a 1,2-shift of a carbon on an 8-oxy-1-naphthyl group from phosphorus to iridium.

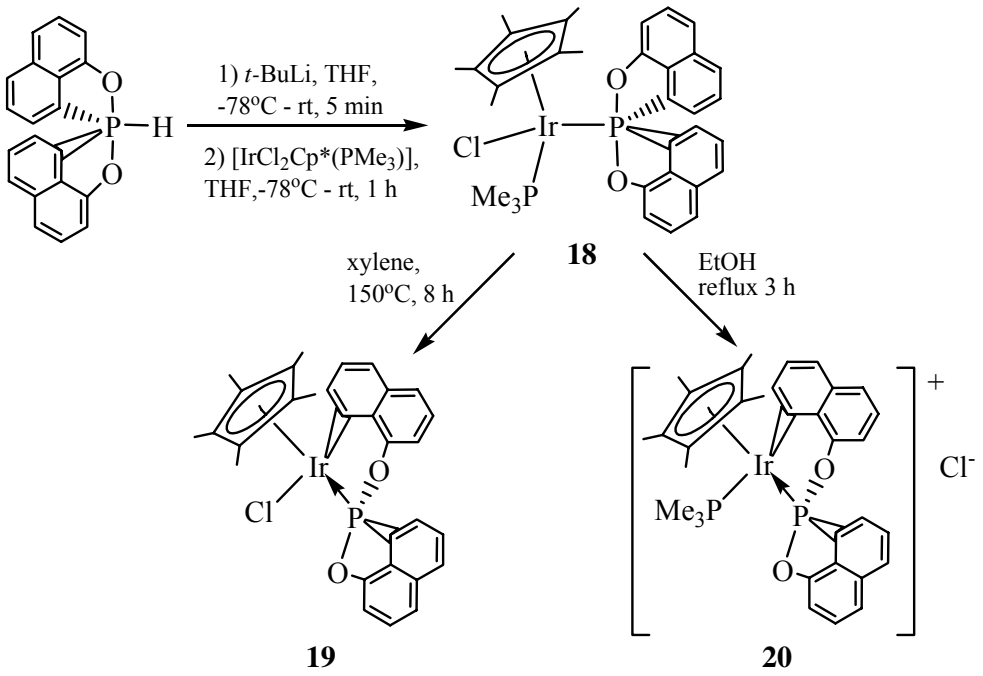

Figure 1.22: Formation of cyclic complexes **19** and **20** from an Ir(III) metallophosphorane, **18**.

1.3.1 Computational studies with metallophosphoranes proposed as intermediates

Many of the metallophosphoranes which have been proposed within reaction mechanisms are transient intermediate species, and as such cannot be isolated or characterised. For this reason, computational modelling is well suited to investigate the feasibility and possible structures of species that are difficult to study experimentally. To date there have been several papers published by Macgregor and co-workers and Braga *et al.* to this end.

The first such study was published by Macgregor and Neave in 2004.[48] They were using computational methods to study why CO inserts into the Pt-OMe bond in [PtMe(OMe)(dppe)],[49] while conversely CO inserts into the Ni-Me bond in [NiMe(O-*p*-C_6H_4CN)(bpy)][50] (dppe = 1,2-bis(diphenylphosphino)ethane, bpy = 2,2'-bipyridine). Whilst looking for an isomerisation pathway to link structures **21** and **23** (see Figure 1.23), thus linking two accessible parts of the mechanism together, they came across a competitive route via a metallophosphorane intermediate structure, **22**. Formation of **22** involves the chelating ligand changing from mono- to bidentate, and migration of OMe onto the previously unbound phosphorus. To complete the isomerisation, the OMe transfers back to the platinum, displacing one arm of the chelating ligand. This

mechanism via a metallophosphorane species was an unexpected novel isomerisation route.

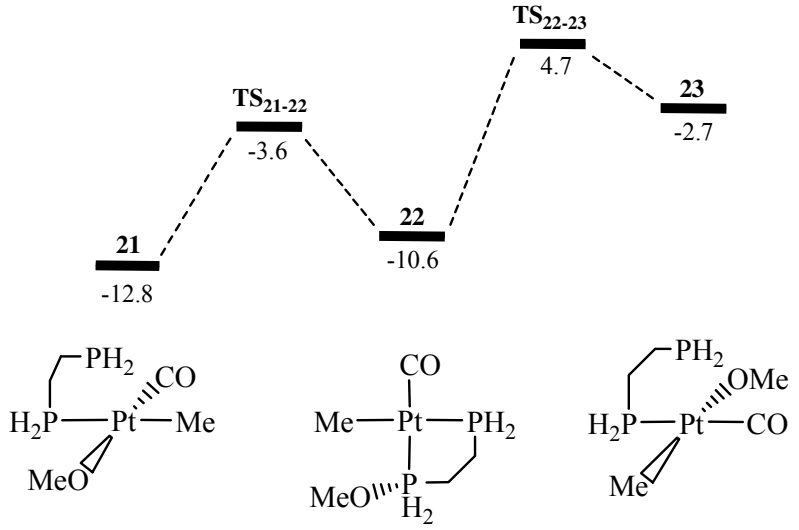

Figure 1.23: Computed isomerisation pathway between structures **21** and **23**, via metallophosphorane **22**. Energies in kcal/mol, relative to [PtCO($H_2CH_2CH_2PH_2$)-Me(OMe)] + free CO set to zero.

In 2004, Grushin and Marshall[51] published details of some unexpected reactivity of the fluoro analogue of Wilkinson's catalyst, [RhF(PPh_3)$_3$]. They discovered that [RhF(PPh_3)$_3$] can cleave the C-Cl bond in chlorobenzene, under mild conditions (see Figure 1.24), while Wilkinson's catalyst, [RhCl(PPh_3)$_3$], is unreactive, even at higher temperatures.[52]

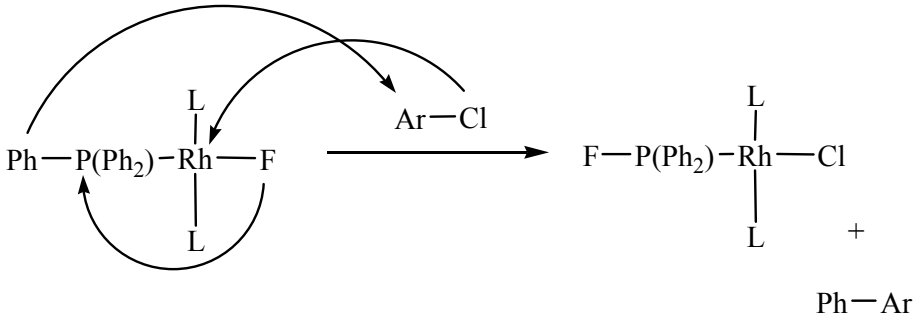

L = PPh_3; Ar = Ph, *p*-tol

Figure 1.24: Cleavage of the C-Cl bond in ArCl by [RhF(PPh_3)$_3$], accompanied by Ph/F exchange.

The mechanism of the facile exchange of the Rh-bound fluoride with a phosphine phenyl group was unknown, however it was proposed that it may occur by fluoride

transferring onto a PPh_3 to create a metallophosphorane, followed by transfer of a phenyl group onto rhodium, as shown in Figure 1.25. They observed that addition of excess PPh_3 did not decelerate the reaction, so concluded that the mechanism does not require the dissociation of a phosphine ligand.

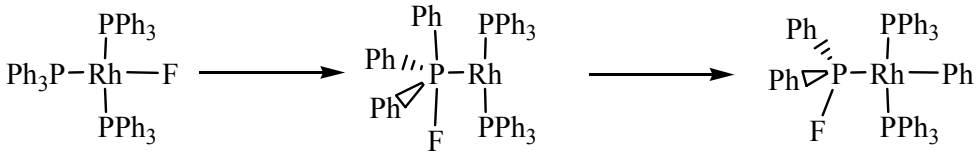

Figure 1.25: A proposed mechanism for Ph/F exchange in $[RhF(PPh_3)_3]$ via a metallophosphorane species.

To investigate possible mechanisms for this F/Ph exchange, Macgregor and co-workers carried out density functional calculations firstly on a small model system,[53] then on the full experimental system.[54] The initial computational studies were performed on a model system, $[RhF(PPhH_2)(PH_3)_2]$, where hydrogens replace all phenyl groups except the phenyl which is exchanging. They compared the relative accessibility of two possible pathways for F/Ph exchange, as shown in Figure 1.26.

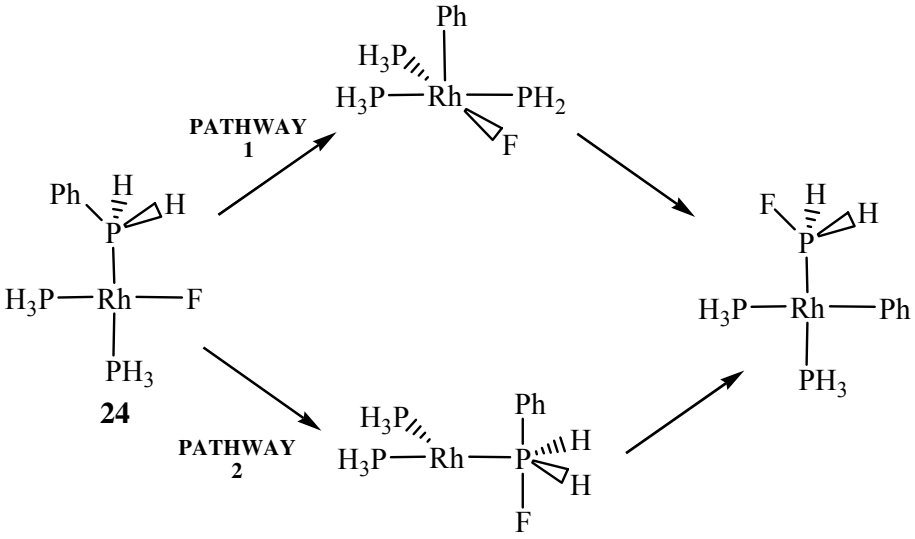

Figure 1.26: The two pathways investigated for Ph/F exchange in $[RhF(PH_3)_2(PH_2Ph)]$.

Pathway **1** proceeds via oxidative addition of the phosphine phenyl group to rhodium, and calculations were performed on both *cis* (Pathway **1a**) and *trans* (Pathway **1b**) isomers of **24**. Pathway **2** has an initial step of attack of the fluoride onto PH_2Ph, which can form two different isomers of the metallophosphorane intermediate (Pathway **2a**:

T_{PH_3}, Pathway **2b**: T_{PFH_2Ph}). They found that Pathways **1a**, **1b** and **2b** all have similar activation barriers (31.1, 30.0 and 31.0 kcal/mol respectively) while the highest barrier in Pathway **2a** was less accessible (36.9 kcal/mol) with respect to *cis*-**24**.

Macgregor and Wondimagegn[54] proceeded to compute the mechanisms for the full experimental system, $[RhF(PPh_3)_3]$, using the DF/HF ONIOM method within *Gaussian 03*.[55] With this system, both of the activation barriers in Pathway **1** increased (**1a** = 34.3, **1b** = 34.9 kcal/mol), while both of the barriers in Pathway **2** decreased (**2a** = 27.5, **2b** = 22.3 kcal/mol). Pathway **2b** has the lowest activation barrier, and this value is very close to the experimentally determined activation enthalpy of 22.0 ± 1.2 kcal/mol.[53]

A further computational study where a metallophosphorane was proposed as an intermediate was published by Braga *et al*. in 2005.[56] They were investigating the role of the base, in this case OH^-, in a Suzuki-Miyaura cross-coupling reaction between a palladium complex and an organoboronic acid. In one of the reaction pathways investigated, Path B, the hydroxyl makes an intermolecular attack on a palladium-bound phosphine, before migrating onto palladium and displacing bromide, in Path B' (see Figure 1.27). They found this pathway to be energetically competitive to the other possibilities investigated, but concluded that it was unlikely as no oxidised phosphine products were observed, as in Path B".

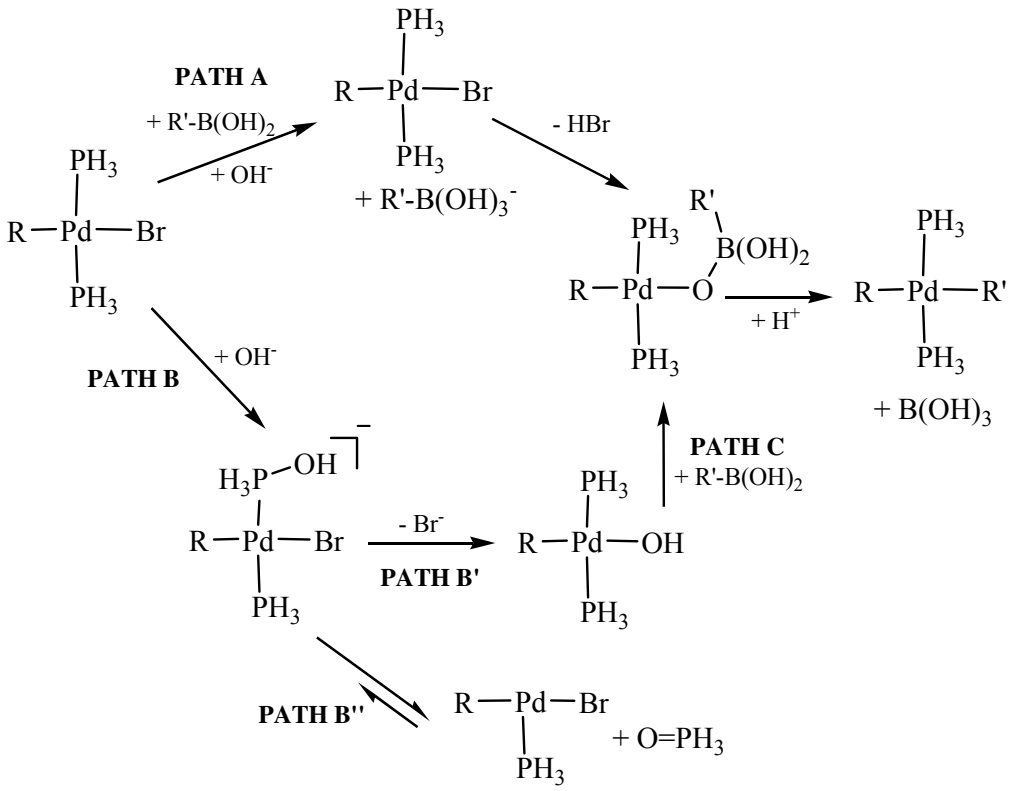

Figure 1.27: Intermolecular attack of OH^- on *trans*-[PdBr(R)$(PH_3)_2$] followed by displacement of Br^- (Path B') as a step of a proposed mechanism in a Suzuki-Miyaura cross-coupling reaction.

A recent paper by Macgregor and Erhardt[57] investigates possible mechanisms for C-F and P-C bond activations in the reaction between C_6F_6 and [IrMe$(PEt_3)_3$]. This reaction produces *trans*-[Ir$(C_6F_5)((PEt_3)_2(PEt_2F)]$, C_2H_4 and CH_4 when conducted at 60ºC, as shown in Equation 1.1.[58]

$$[Ir(Me)(PEt_3)_3] + C_6F_6 \xrightarrow[-\ CH_4]{-\ C_2H_4} \textit{trans}\text{-}[Ir(C_6F_5)(PEt_3)_2(PEt_2F)] \qquad \textbf{(1.1)}$$

A mechanism was proposed in which C-F activation proceeds via an initial step through a novel 4-centred transition state, leading to a metallophosphorane intermediate (see Figure 1.28). This pathway transpired to be more accessible than an alternative pathway computed, which involves the oxidative addition of C_6F_6 to iridium, forming an Ir(III) intermediate.

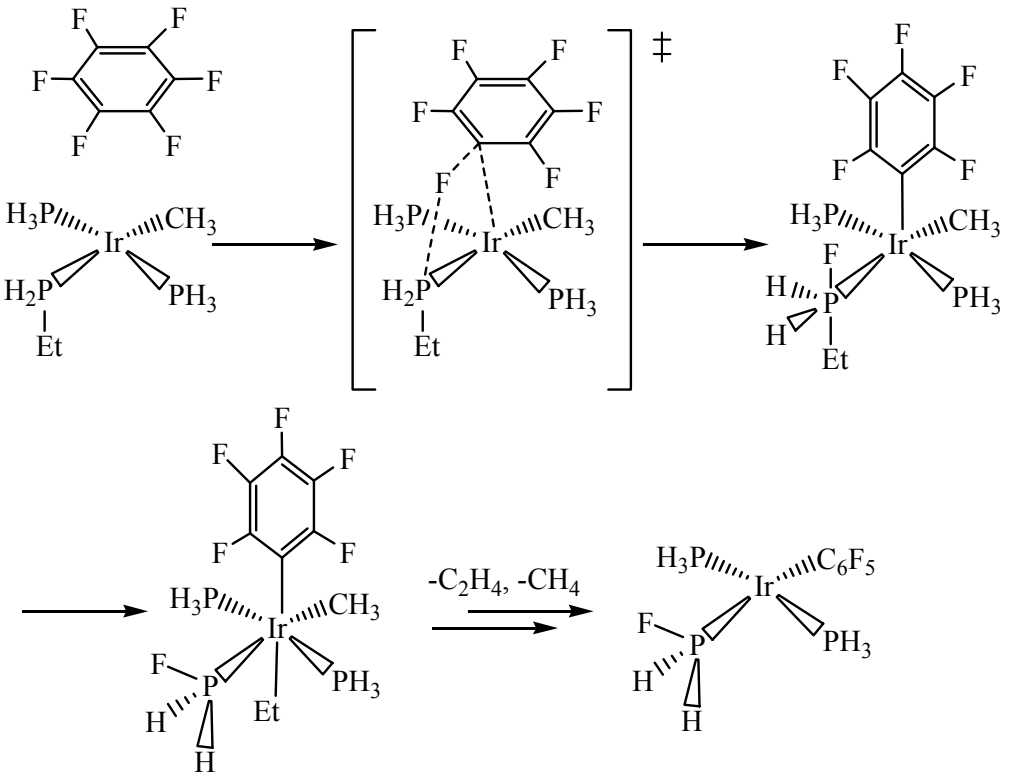

Figure 1.28: Proposed mechanism for reaction between C_6F_6 and the model complex $[IrMe(PH_2Et)(PH_3)_2]$ via a 4-centred transition state.

Another example of a mechanism involving phosphine-assisted C-F activation via a metallophosphorane intermediate was proposed for the reaction of pentafluoropyridine with $[Pt(PR_3)_2]$ (R = Cy, ^{i}Pr).[59] The mechanism was investigated using a model system, namely $[Pt(PH_3)(PH_2Me)]$. Figure 1.29 shows one of the mechanisms that was computed for the initial step, and as with the iridium complex discussed above, the reaction proceeds via a 4-centred transition state, and leads to a metallophosphorane intermediate species. Methyl is then transferred from phosphorus to platinum to form the experimentally-observed product.

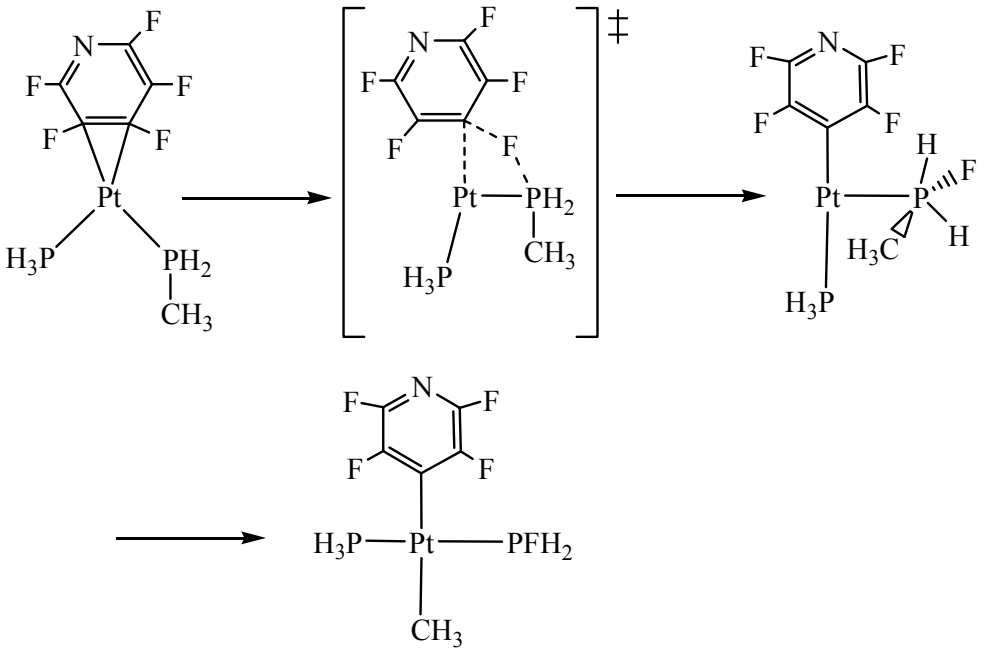

Figure 1.29: Part of a proposed mechanism for the reaction between C_5F_5N and the model complex $[Pt(PH_3)(PH_2Me)]$ via a 4-centred transition state.

1.3.2 Overview

It has been shown thus far that a range of different metallophosphoranes have been synthesised and characterised over the last three decades, and some of these species have been identified as intermediates in reaction pathways. The work in this thesis focuses on two specific types of reaction where metallophosphoranes may be involved as intermediate species. The first reaction, which is investigated in Chapter 4, is the hydroxide-induced disproportionation of a Pd(II) phosphine species. The relevant background literature to this reaction is discussed in the following section in this chapter. Chapters 5 and 6 focus on aryl/ aryl and alkyl/aryl exchange reactions in Pd(II) phosphine complexes respectively. The literature surrounding these types of reactions is reviewed in Section 1.5 of this chapter.

1.4 Metallophosphoranes in disproportionation reactions

In this context, disproportionation is observed when palladium is reduced from Pd(II) to Pd(0), normally to yield a catalytically active species, while phosphorus is oxidised from P(III) to P(V), normally forming phosphine oxide. The following reactions feature this redox chemistry and also may feature metallophosphorane species either as intermediates or transition state structures.

A novel reaction involving the reduction of Pd(II) phosphines in the presence of fluoride was published by Mason and Verkade[60] in 1992. They observed the unexpected formation of $[Pd(dppp)_2]$ (dppp = 1,3-bis(diphenylphosphino)propane) whilst trying to synthesise $[Pd(dppp)_2]^{2+}$, as shown in Equation 1.2. None of the usual reagents which may be expected to reduce Pd(II) phosphine complexes, such as

$$Pd(BF_4)_2.4CH_3CN + 2\ dppp \longrightarrow [Pd(dppp)_2][BF_4]_2 + [Pd(dppp)_2] \quad \textbf{(1.2)}$$

$NaBH_4$[61,62] or KOH/phosphine,[63,64] were present. There was no precedent for this type of reaction found in the literature, and the only reagent present that could be responsible for this reaction was thought to be tetrafluoroborate, which can act as a fluoride source to TM-complexes.[65,66] To test this idea, they added a source of fluoride to a range of solutions of Pd(II) phosphines complexes, and as anticipated the formation of Pd(0) species was observed. The reaction mechanism proposed for this fluoride-induced reduction of palladium is shown in Figure 1.30.

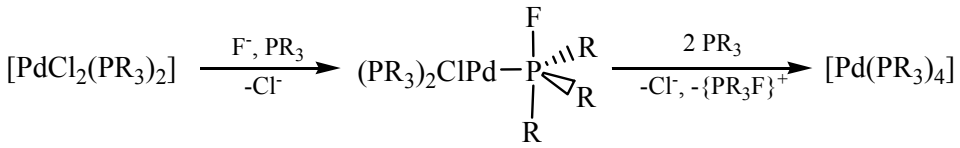

Figure 1.30: Mechanism proposed by Mason and Verkade for the fluoride induced reduction of $[PdCl_2(PR_3)_2]$.

It was suggested that a metallophosphorane intermediate is formed either by direct nucleophilic attack of the fluoride on a phosphine, or else the fluoride initially coordinating to the palladium then migrating onto the phosphorus. The reduction of Pd(II) then occurs through the loss of a fluorophosphonium cation, $[PR_3F]^+$, and chloride to yield the Pd(0) product. $[PR_3F]^+$ then either reacts with fluoride to produce the phosphorane PF_2R_3, or with water to produce phosphine oxide.

Mason and Verkade were confident that the presence of fluoride is necessary to reduce the Pd(II), as the reaction of $[PdCl_2]$ with PPh_3 with added water but no source of fluoride only produced $[PdCl_2(PPh_3)_2]$. It was attempted to perform the reaction in anhydrous conditions, and as these were approached, the yield of phosphorane product was increased while the yield of phosphine oxide decreased. A competition experiment was used to show that is the phosphorus coordinated to palladium which is oxidised (Equation 1.3). The fact that no $O{=}PPh_3$ or PF_2PPh_3 was formed shows that only coordinated phosphines were oxidised.

$$[PdCl_2] + 5\ PPh_3 + 5\ dppe \xrightarrow{DMSO} [Pd(dppe)_2]Cl_2$$

$$\xrightarrow{n\text{-}Bu_4NF.3H_2O} [Pd(dppe)_2] + O{=}PPh_2(CH_2CH_2PPh_2) + PF_2Ph_2(CH_2CH_2PPh_2) \quad \textbf{(1.3)}$$

It was possible to do the same disproportionation reaction with analogous Pt(II) phosphine complexes, but with a lower yield of Pt(0) phosphine than seen with palladium. However, the same redox reaction was not possible with nickel complexes.

Also in 1992 Amatore *et al*.[67] published details of a disproportionation reaction when $[Pd^{II}(OAc)_2]$ reacts with triphenylphosphine to form a palladium(0) species and $O{=}PPh_3$. Initially $[Pd(OAc)_2(PPh_3)_2]$ is formed, and this complex has been detected and identified by its reduction peak in cyclic voltammetry. From this point $[AcO\text{-}PPh_3]^+$ was lost, to yield a Pd(0) species, which in the presence of excess phosphine can be identified as $[Pd(OAc)(PPh_3)_3]^-$.[68] Through kinetic experiments it was proved that the formation of the Pd(0) species was first order in Pd(II), and there was also evidence for formation of an intermediate. Thus, Amatore *et al*. proposed the reaction mechanism shown in Figure 1.31.

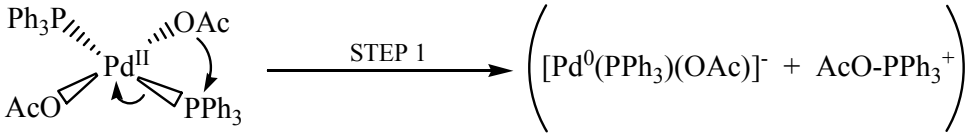

$$\xrightarrow[+\ 2PPh_3,\ H_2O,\ H^+]{STEP\ 2} [Pd^0(PPh_3)_3(OAc)]^- + O{=}PPh_3 + AcOH$$

Figure 1.31: Mechanism proposed by Amatore *et al.* for disproportionation of $[Pd(OAc)_2(PPh_3)_2]$ in presence of excess PPh_3.

They demonstrated that Step 1 is an intramolecular disproportionation and is the rate-determining step in the overall reaction. This intramolecular attack of an acetate ligand on a coordinated phosphine bears strong similarities to the mechanism proposed by Mason and Verkade[60] with a fluoride attacking a phosphine. The disproportionation of $[Pd(OAc)_2(PR_3)_2]$ was performed with a range of different para-substituted triarylphosphines groups, and it was discovered that it is easier and faster to reduce the Pd(II) when R is para-substituted with an electron-withdrawing group. Presumably the reduced electron density on the phosphorus makes it more susceptible to attack by the acetate.

Amatore *et al*. also reported that this disproportionation reaction can be accomplished with a variety of oxygen-containing ligands, including $CF_3CO_2^-$ and Acac (Acac = MeC(O)CHC(O)Me). Therefore, the results published by several groups suggest that the reduction of Pd(II) to Pd(0) by triphenylphosphine is a general reaction which can occur with a variety of oxygen-containing ligands such as OAc, $CF_3CO_2^-$,[69] Acac, NO_3 and oxide.[70]

It has also been found that hydroxide can induce a disproportionation reaction in Pd(II) phosphine complexes. Grushin and Alper published a detailed paper on the investigation of such reactions in 1993.[71] They were studying the biphasic carbonylation of aryl halides catalysed by $[PdCl_2L_2]$ (L = tertiary phosphine), and were particularly interested in how the Pd(II) species converts to a catalytically active Pd(0) species. They believe that OH^- induces the reduction of Pd(II), and proposed two possible reaction mechanisms, as shown in Figure 1.32.

Path A proceeds via an external nucleophilic attack of OH^- on a phosphine followed by the loss of phosphine oxide, then Cl^- and HCl to form a Pd(0) species. In Path B OH^- initially coordinates to palladium, substituting a chloride, the performs an intramolecular attack on the phosphine. This is followed by loss of phosphine oxide and HCl to yield the Pd(0) complex.

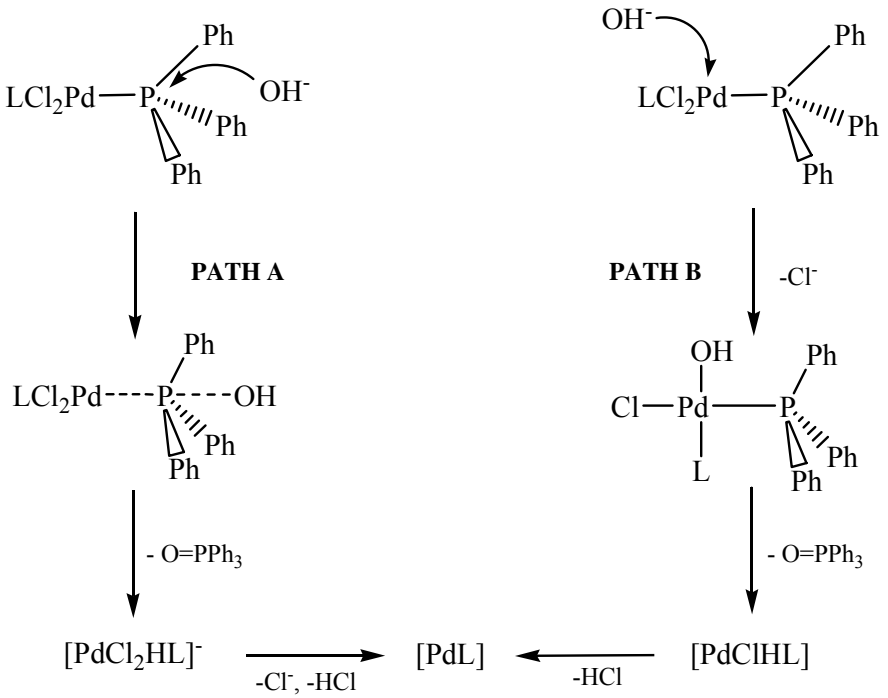

Figure 1.32: Two possible pathways proposed by Grushin and Alper for hydroxide-induced disproportionation of $[PdCl_2L_2]$.

By using chiral phosphines, in this case L = (R)-benzylmethylphenylphosphine, and examining the stereochemistry of the phosphine oxide produced, it was possible to gain an important insight into the reaction mechanism. It was found that the reaction always proceeded with retention of configuration at the chiral phosphorus which was oxidised to phosphine oxide, proving that OH^- performs an intramolecular attack on phosphorus, consistent with Path B.

1.5 Aryl/aryl and alkyl/aryl exchange reactions

1.5.1 Aryl/aryl exchange

Palladium catalysed cross coupling reactions are very important for a range of organic synthetic applications, especially in the production of pharmaceuticals, but more fundamentally as a way of forming carbon-carbon bonds. For example, palladium phosphine complexes are used as catalysts in the Stille cross coupling reaction. A general outline for the catalytic cycle[72] is shown in Figure 1.33.

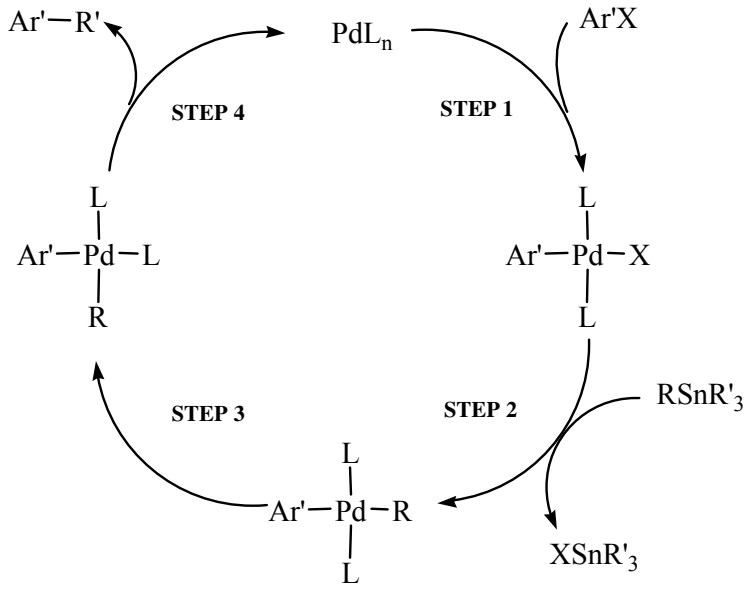

Figure 1.33: Mechanism of palladium-catalysed direct coupling in the Stille reaction.

However, the use of these catalysts often results in the formation of unwanted side products. These side products seem to be created by aryl/aryl (Ar/Ar') scrambling at some point in the catalytic cycle. It is possible that exchange could occur in [PdAr'(R)L_2] (L=PAr_3), formed in Step 2 of the cycle.

An example of this problem was encountered by Chenard *et al.*[73] when they reacted 6-methoxy-2-(trimethylstannyl)naphthalene with *p*-anisyl bromide with a [Pd(PPh_3)$_4$] catalyst (see Figure 1.34). The desired methoxy-substituted product was produced in a yield of 21.9% in DMF at 105ºC, while the unwanted phenyl biaryl was the major product, with a yield of 54.8%. It was proposed that this mixture of products arose due to exchange between a phenyl group on triphenylphosphine and the aryl from the aryl bromide, when attached to the palladium centre. This reaction is a clear example of what a problem unwanted Ar/Ar' scrambling can be.

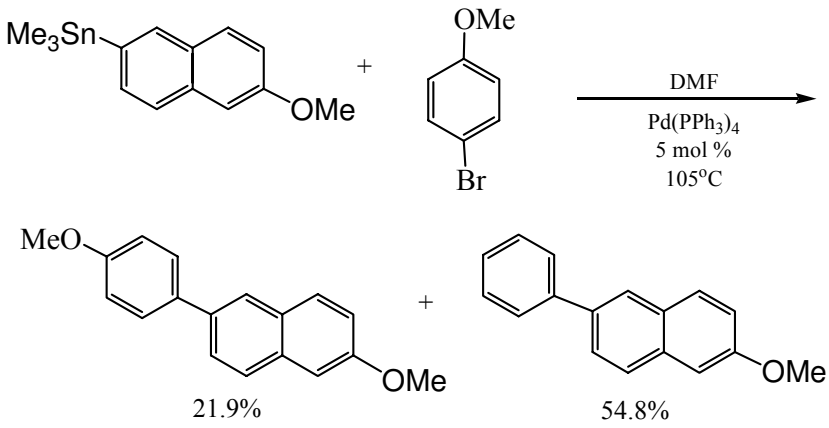

Figure 1.34: The Stille reaction can lead to a mixture of products when catalysed by $[Pd(PPh_3)_4]$.

Similar unwanted side products have been observed in a wide range of reactions, including Suzuki[74] and Heck[75] couplings, amination,[76] amidation,[77] and cyanation.[78] Interest in this area has grown considerably over the last 20 years, and some detailed experimental work has been undertaken to try to elucidate the mechanism by which these aryl exchange reactions are occurring.[73,79,80] Insights into reaction mechanisms have led to the tailoring of catalysts and reaction conditions in an attempt to inhibit unwanted scrambling. On the other hand, some chemists have exploited the tendency for exchange to their advantage, as a source of aryl groups in their reactions.

A range of different possible exchange mechanisms have been proposed, as summarised by Macgregor[81] and shown in Figure 1.35. These include (a) the oxidative addition across a P-R bond followed by reductive elimination, (b) nucleophilic attack on the phosphine, either by an external nucleophile or a group coordinated to the metal, (c) attack of the metal-bound aryl group on the phosphine, coupled by the breaking of the M-P bond to form an ion pair or salt and (d) the more novel possibility of a metallophosphorane intermediate, featuring a penta-coordinated phosphorus.

(a) Oxidative addition / reductive elimination

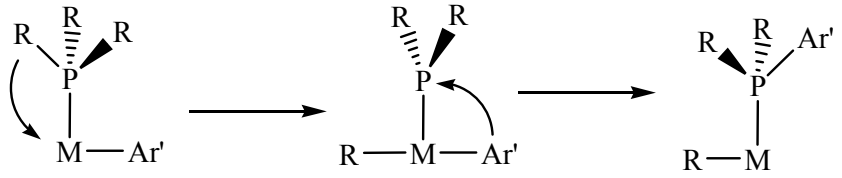

(b) Nucleophilic attack (internal or external)

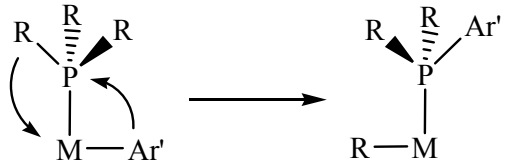

(c) Phosphonium salt formation

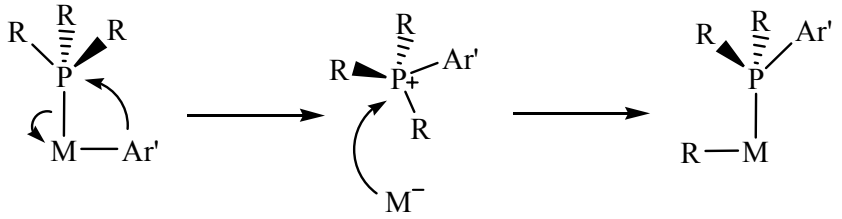

(d) Metallophosphorane formation

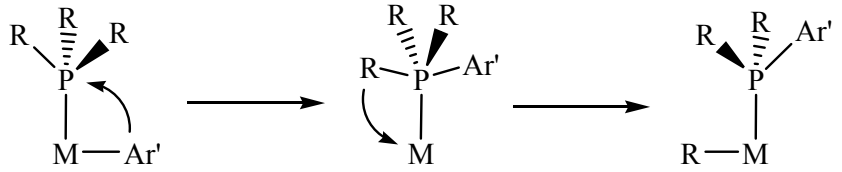

Figure 1.35: Possible mechanisms for P-R/M-Ar' exchange.

1.5.2 Examples of aryl/aryl exchange

Bryant and Abatjoglou observed aryl interchange in their studies of rhodium-catalysed hydroformylation.[82] This led them to examine whether the catalyst $[RhH(CO)(PPh_3)_3]$ would cause phenyl/*p*-tolyl scrambling between triphenylphosphine and tri-*p*-tolylphosphine, which was indeed observed.[83] They experimented with a range of rhodium catalysts, and found that the rate of aryl scrambling was higher with mononuclear complexes, such as $[RhCl(PPh_3)_3]$, than with clusters such as $[Rh_6(CO)_{16}]$. They propose that clusters need higher temperatures to facilitate the breakdown into the more reactive mononuclear compounds. It was also reported aryl group interchange between triphenylphosphine and tri-*p*-tolylphosphine is catalysed by other transition metal complexes, including $[Co_2(CO)_8]$, $[Os_3(CO)_{12}]$, $[Ni(CO)_2(PPh_3)_2]$ and

[$Pd(PPh_3)_4$]. Oxidative addition (as seen in Figure 1.35(a)) was suggested as a possible reaction mechanism.

Goel reported the palladium catalysed cleavage of P-C bonds in aryl phosphines.[84] He observed aryl/*p*-tolyl scrambling between two different triarylphosphines, but this time with [$Pd(OAc)_2$] as the catalyst.[85] Goel used *para*-substituted aryl groups to gain insight into the mechanism of the exchange process. The fact that only 4,4'-dimethyl biphenyl was produced on heating [$Pd(OAc)_2$] with P(*p*-$CH_3C_6H_4)_3$ in benzene ruled out the possibility of a mechanism involving *ortho*-metallation, as shown in Figure 1.36. He found that electron-withdrawing groups (e.g. Cl) in a *para* position on the aryls increased the rates of exchange, leading him to suggest a mechanism involving a nucleophilic attack on a coordinated phosphine. Goel also proposes the idea of a radical mechanism, but without any experimental evidence to support these possibilities.

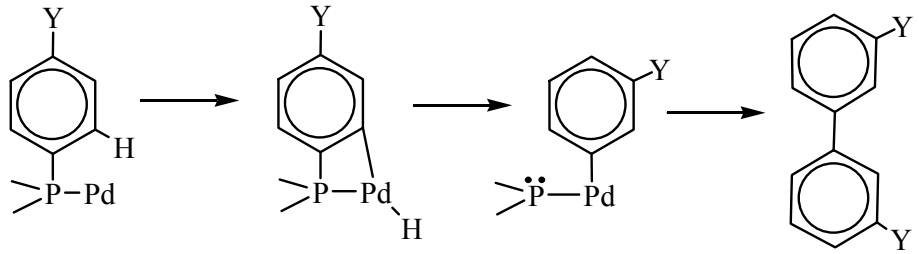

Figure 1.36: The result of an *ortho*-metallation mechanism in a cross coupling reaction.

1.5.3 Mechanistic studies of aryl/aryl exchange

A detailed study of palladium catalysed Ar/Ar' exchange was published by Cheng and Kong.[86] This was the first example where the reactants and products of exchange were well-characterised transition metal complexes, rather than observations of scrambled organic products from a catalysed reaction. They conducted studies on [PdI(*p*-$XC_6H_4)(PPh_3)_2$] (X = Me) and observed regiospecific exchange between a phosphine phenyl group and the palladium-bound aryl group. The exchange process was followed using ^{1}H NMR, and when equilibrium was reached at 60ºC, the ratio of complexes containing P-tolyl to those containing Pd-tolyl was 90:10. There was also evidence that intermolecular phosphine scrambling led to a mixture of products (Figure 1.37).

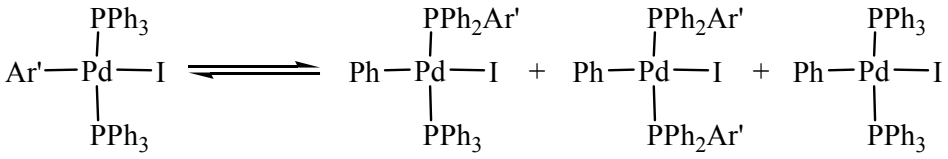

Figure 1.37: Ar/Ar' scrambling observed in palladium phosphine complexes.

Features of the ^{1}H NMR spectrum suggested that further exchange could also occur, to produce PPh(*p*-$CH_3C_6H_4$)$_2$ complexes. When X = methoxy, the equilibrium reactant to product ratio moved to favour product formation (96:4), suggesting that an electron-donating group moves the equilibrium to the right. By using deuterium labelling, Cheng and Kong confirmed that phenyl/phenyl exchange does occur in [PdI(Ph)(PC_6D_5)$_2$], with a product to reactant equilibrium ratio of 6.3:1. It was discovered that addition of 1 equivalent of excess PPh_3 to the reaction almost completely inhibited exchange. This led to the conclusion that the exchange reaction requires initial phosphine dissociation, and proceeds via a 3-coordinate intermediate structure. They postulate that oxidative addition across a P-C bond could occur, leading to a Pd(IV) intermediate. Reductive elimination (as shown in Figure 1.35(a)) and reassociation of phosphine would then lead to formation of an exchange product.

Mechanistic studies on the Ar/Ar' exchange in [PdI(Ar')(PAr_3)$_2$] complexes were carried out by Novak *et al*.[80] They found that the addition of excess halide slightly inhibited the rate of exchange, and excess phosphine caused much stronger inhibition. This suggests that halide and phosphine dissociation may be involved in the exchange mechanism. They investigated the effect of a wide range of substituted aryls on the Ar/Ar' scrambling. Tests varying the *para* substituent on either Ar' or the Ar's yielded the same result: electron-donating groups (eg Me) accelerate aryl exchange while electron withdrawing-groups (eg F) inhibit it, sometimes completely. Other groups have also reported this substituent effect.[73,74,86] Additionally, Novak *et al*. observed that the position of the equilibrium was moved to the right by electron-donating substituents on the palladium-bound aryl, as reported by Cheng and Kong.[86] If the exchange mechanism does involve a phosphonium cation (as shown in Figure 1.35(c)), electron-donating substituents would also have the effect of stabilising the positive charge on the cation. The mechanism proposed is shown in Figure 1.38 and features a phosphonium salt intermediate and the possibility of exchange with or without phosphine dissociation.

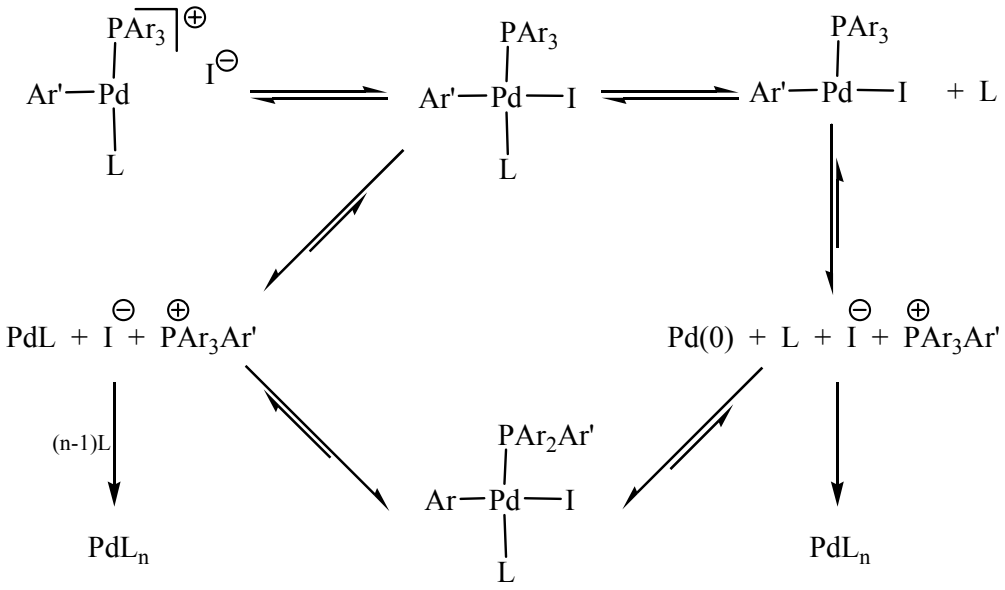

Figure 1.38: Mechanisms proposed by Novak *et al.* for Ar/Ar' exchange via phosphonium salt formation.

To investigate whether a phosphonium salt could enter into the catalytic cycle of the Stille reaction (seen in Figure 1.33), Chenard *et al.*[73] reacted 6-methoxy-2-(trimethylstannyl)naphthalene with tetraphenylphosphonium bromide under the conditions outlined in Figure 1.39.

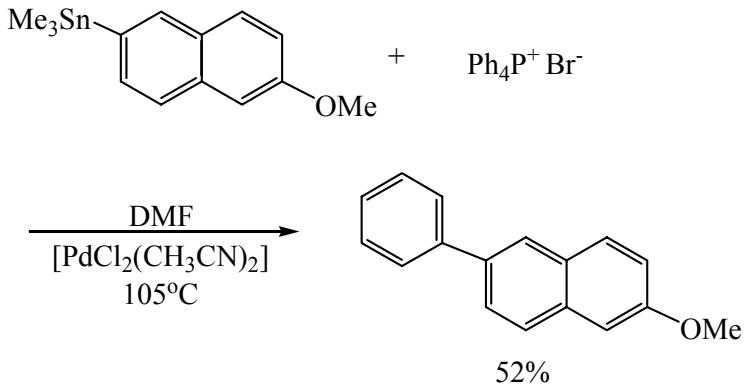

Figure 1.39: Phosphonium salt is able to enter into the catalytic cycle of the Stille reaction.

This conclusively showed that a phosphonium salt could enter into the process without terminating the reaction. Yamamoto *et al.*[87] showed the oxidative addition of a phosphonium salt to a Pd(0) species, as shown in Figure 1.40.

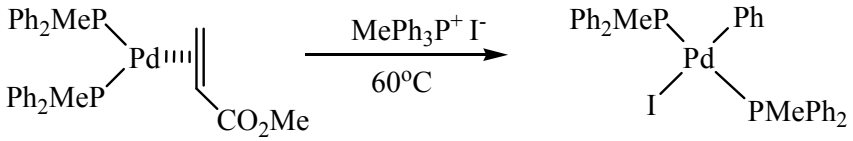

Figure 1.40: Oxidative addition of a phosphonium salt to a Pd(0) centre.

The solvent used can also affect the efficiency of the exchange process. Chenard *et al.*[73] found that exchange decreased in less polar solvents. This suggests that there may be charged species being produced during the reaction. Altogether there is strong evidence to support a reaction mechanism via a phosphonium salt mechanism.

An extensive study of Ar/Ar' exchange in $[PdX(C_6D_5)(PPh_3)_2]$ (X = Cl, Br, I, F) was published by Grushin in 2000.[79] He found that the rate of exchange in these complexes was highly dependent on the halide present. In benzene at 75ºC the rate constant ratio of $k_I:k_{Br}:k_{Cl}$ was 100:4:1. This was believed to be due to the relative ease of phosphine dissociation from these complexes, with the order Cl < Br < I, based on Pd-P bond lengths from crystallographic data. It was found that addition of excess phosphine strongly inhibited exchange, as seen by Novak *et al.*[80] and Cheng and Kong,[86] supporting the idea of phosphine dissociation being a key step. A deceleration in the rate of exchange was observed on the addition of excess halide too, but to a lesser degree than with excess phosphine, also seen by Novak *et al.*[80] However, Grushin suggested that halide dissociation is unlikely to be part of the mechanism with the relatively mild reaction conditions and a benzene solvent. The proposed mechanism is shown in Figure 1.41. It features initial phosphine dissociation, followed by reversible reductive elimination of a phosphonium cation to form a tight ion pair. The aryl interchange can occur if the P-Ar bond undergoes oxidative addition to Pd, otherwise the reactant is reformed.

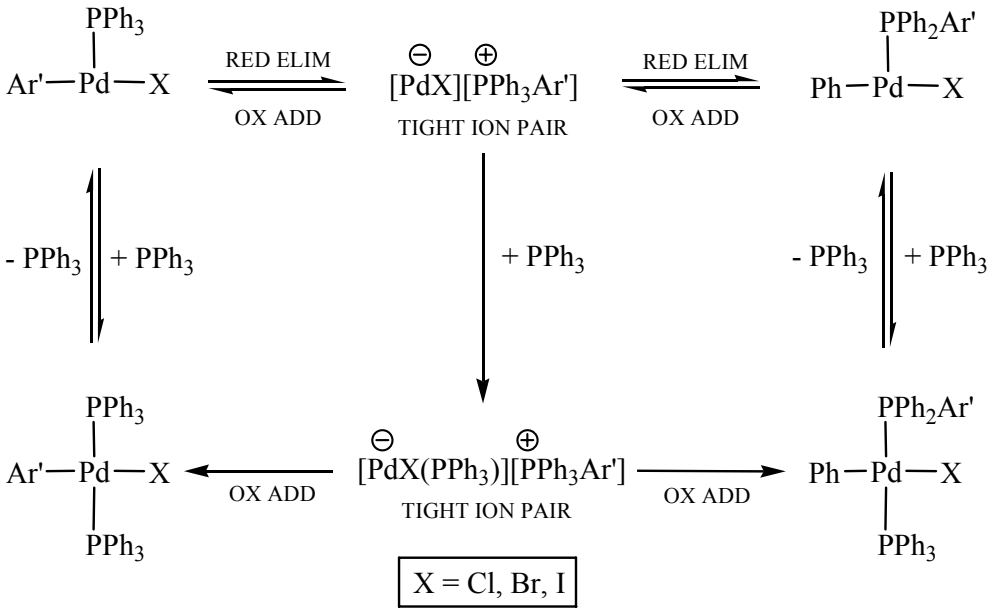

Figure 1.41: Proposed reaction mechanism for Ar/Ar' exchange involving phosphine dissociation and the formation of tight ion pairs.

Unwanted Ar/Ar' scrambling was encountered by Hartwig and Barañano whilst forming aryl sulfides via reductive elimination from a [Pd(dppe)] species (dppe = $Ph_2P(CH_2)_2PPh_2$).[88] Exchange of Pd-Ar' and P-Ph was found to be competitive with the desired C-S forming reductive elimination. Consistent with other research into Ar/Ar' interchange, it was found that the addition of excess phosphine could effectively inhibit the exchange process. This could also be achieved with use of other trapping agents such as PhCCPh or ArI.

Research has led to the discovery of a range of different ways to suppress unwanted Ar/Ar' exchange. A very effective way is to add excess phosphine to the reaction.[79,80] Addition of excess halide and the use of bulkier groups on the triarylphosphines can also reduce the rate of exchange.[74,80,89] Electron-withdrawing groups on both the metal-bound and phosphorus-bound aryls can reduce exchange.[73,74,80] Reduction in the amount of catalyst used can also be inhibiting.[74,79] Alternative catalysts have also been investigated, including a $NiCl_2/PPh_3$ catalyst for cross coupling,[90] which do not appear to suffer from unwanted Ar/Ar' exchange as many palladium/phosphine complexes do.

Some chemists are using Ar/Ar' exchange reactions to their advantage in synthesis. As Yamamoto *et al*.[87] suggested, phosphonium salts can act as a source of aryl groups to a reaction. De la Torres *et al*.[91] used $[PdCl_2(PPh_3)_2]$ as a catalyst in a reaction between tri(tert-butyl)iodophthalocyaninate zinc (II) (ZnPcI) with PPh_3 in DMF at 100ºC to form R_4P^+, as shown in Figure 1.42. These Pc-phosphonium salts are of interest as they can be used to make materials with non-linear optical properties. The fact that two different phosphonium salts are formed suggests that Ar/Ar' exchange is occurring at the palladium catalyst.

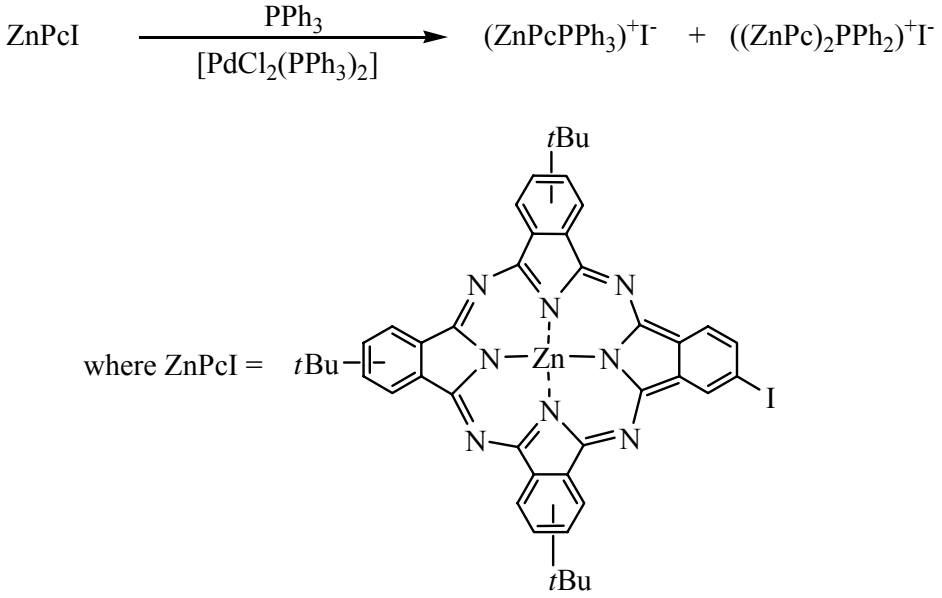

Figure 1.42: A mixture of phosphonium salts were formed in the palladium-catalysed reaction of ZnPcI with PPh_3.

1.5.4 Alkyl/aryl Exchange

Examples of alkyl/aryl scrambling have been observed, but seem to be less commonplace than Ar/Ar' exchange. There has been considerably less research published on this type of exchange, and there is only one detailed mechanistic study to date.

An early case of alkyl/aryl exchange was published by Smith and Green in 1971.[92] They observed a mixture of phosphine and aryl products in a reaction between $[NiCl_2(PPh_3)]$ and methyl magnesium bromide at room temperature (see Equation 1.4). They proposed that the reaction may proceed via a metallophosphorane intermediate, $[Ni(Me)(MgBr)(PMePh_3)]$, as shown in Figure 1.35(d).

$$[NiCl_2(PPh_3)_2] \xrightarrow[\text{ii) } H_2O]{\text{i) MeMgBr}} \begin{matrix} PhH + PhMe + Ph_2 \\ + PPh_2Me + PPhMe_2 \end{matrix} \qquad \textbf{(1.4)}$$

A similar mixture of products was produced by the decomposition of $[Co(Me)(PPh_3)_3]$ at 0ºC in THF.[93] Schumann *et al*. observed this in a range of $[Co(R)L_3]$ (R = Me, Ph, L = PPh_2Me, $PPhMe_2$) complexes,[94] with decomposition yielding products including biphenyl and rearranged phosphines such as PPh_3 and PPh_2Me.

Rhodium complexes have also been identified as catalysts which can cause alkyl/aryl interchange in phosphines.[82] Specifically, $[Rh(H)(CO)(PPh_3)_3]$ catalyses scrambling between triphenylphosphine and propene under hydrogenation conditions (see Equation 1.5).

$$PPh_3 + H_2 + C_3H_6 \xrightarrow[130^oC]{[Rh(H)CO(PPh_3)_3]} PPh_2(C_3H_7) + PhH \qquad \textbf{(1.5)}$$

This reaction also occurs, though more slowly, during the low-pressure hydroformylation of propene. The mechanism proposed for the reaction in Equation 1.4 is shown in Figure 1.43. It features the reversible oxidative addition of a P-C bond in PPh_3 to the rhodium centre, insertion of C_3H_6 into a Rh-H bond, and reductive elimination of the scrambled phosphine. Interestingly, alkyl/aryl exchange does not occur under these conditions with $[RhCl(PPh_3)_3]$ or $[RhCl(CO)(PPh_3)_2]$. However, both of these complexes undergo Ar/Ar' exchange,[83] suggesting that exchange is more accessible for an aryl group.

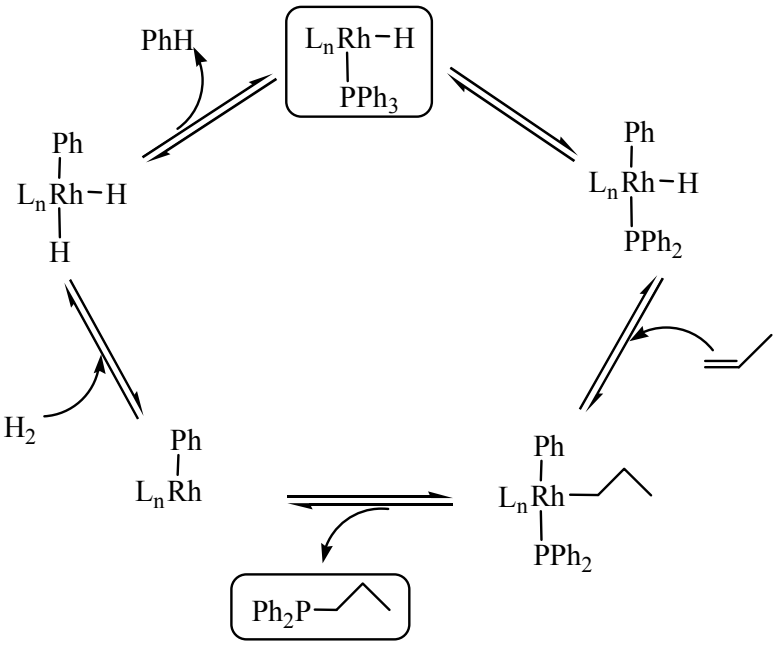

Figure 1.43: Proposed mechanism for alkyl/aryl scrambling in a rhodium-catalysed propene hydrogenation reaction.

The only detailed study of alkyl/aryl exchange published to date was carried out by Norton *et al.*[95] on *trans*-[PdI(Me)(PAr_3)$_2$] (Ar = C_6H_5). They observed not only methyl/phenyl scrambling in C_6D_6 at 50ºC, but also phosphine interchange. The first step in the reaction is the irreversible exchange between the palladium-bound methyl and a phosphine phenyl, to form complex **25** (see Figure 1.44). The irreversibility of this exchange was explained by the comparative bond strengths, favouring a Pd-Ph bond over a weaker Pd-Me bond. When equilibrium is reached, only complexes **25**, **26** and **27** are present, as characterised by $^{31}P\{^1H\}$ NMR. When Ar = C_6H_4D, an equilibrium mixture of complexes **25**, **26** and **27** was produced in benzene, with all of the deuteriums remaining in *para* positions. When *trans*-[PdI(Me)(PAr_3)$_2$] (Ar = C_6D_5) was added to [$PMePh_3$]OTf in CD_2Cl_2 at 36ºC, none of the unlabelled phenyls from [$PMePh_3$]$^+$ exchanged with the deuterated phenyls in the palladium complex. This rules

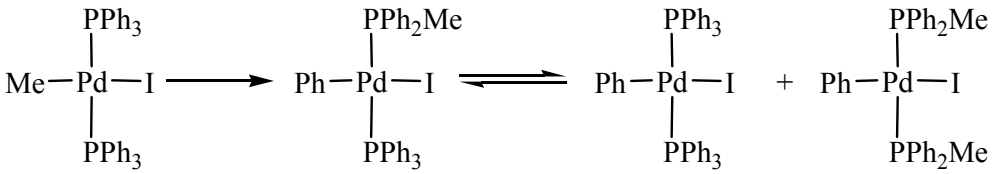

Figure 1.44: Methyl/phenyl exchange in a palladium phosphine complex in C_6D_6 at 50ºC.

out the possibility of a mechanism involving the formation of a phosphonium cationic intermediate, as proposed for Ar/Ar' exchange. Another fundamental difference in mechanism was revealed by the fact that the rate of exchange is completely unaffected by the addition of excess phosphine, suggesting that phosphine dissociation is not necessary. These findings suggest that the mechanism of alkyl/aryl exchange is different to that of Ar/Ar' exchange, but it is not clear why this is the case.

1.6 Thesis overview

The aim of the work detailed in this thesis was to investigate the possibility of metallophosphoranes being intermediate species in TM-phosphine reaction pathways. All of the work was carried out using either density functional (DF) or DF/Hartree-Fock ONIOM methods, which are explained in more detail in Chapters 2 and 7.

Chapter 3 contains general studies carried out on simple model systems, to give an insight into the ease of forming metallophosphorane intermediates in TM-phosphine complexes with the general formula $[M(X)(PH_3)(PR_3)]$, where M = Pd, Pt or Ni, X = F, OH, NH_2, Cl, Me or Ph, and R = H, F or Me. After the intermediate was formed, the reaction then proceeded to give an X/R exchange product. This work provided insight into what conditions favour the formation of metallophosphorane intermediates.

Chapters 4, 5 and 6 focus on three specific reactions where metallophosphoranes have been proposed as possible intermediate species. Chapter 4 focuses on the hydroxide-induced disproportionation of $[PdCl_2L_2]$ (L = tertiary phosphine) as published by Grushin and Alper,[71] and investigates a reaction mechanism which proceeds via an intramolecular attack of a palladium-coordinated hydroxy group on a phosphine.

Chapter 5 details the investigation of possible reaction mechanisms for phenyl/phenyl exchange in *trans*-$[PdX(Ph)(PPh_3)_2]$ (X = Cl, Br, I). This work is based on kinetic and mechanistic experimental work on $[PdX(C_6D_5)(PPh_3)_2]$ (X = Cl, Br, I, F) complexes published by Grushin.[79] In Chapter 5 four possible mechanisms are explored, comparing routes via metallophosphorane intermediates with other possible exchange mechanisms. The effect of changing the halide on the comparative accessibility of the reaction pathways is also investigated.

Chapter 6 continues the study of exchange, but looks at methyl/phenyl exchange. This work is closely linked to experimental work carried out by Norton *et al*.[95] on *trans*-[PdI(Me)(PPh_3)$_2$]. As in Chapter 5, several different mechanisms for exchange are compared, some featuring metallophosphorane intermediates. The results for methyl/phenyl exchange are compared with those for phenyl/phenyl exchange.

1.7 References

[1] Nakazawa, H.; Kubo, K.; Miyoshi, K., *Bull. Chem. Soc. Jpn*., **74**, 2255, (2001)

[2] a) Rundle, R. E., *J. Amer. Chem. Soc*., **85**, 112, (1963) b) Hach, R. J.; Rundle, R. E., *J. Amer. Chem. Soc*., **73**, 4321, (1951)

[3] Hoffmann, R.; Howell, J. M.; Muetterties, E. L., *J. Amer. Chem. Soc*., **94**, 3047, (1972)

[4] Kurimura, H.; Yamamoto, S.; Egawa, T.; Kuchitsu, K., *J. Mol. Struct*., **79**, 140, (1986)

[5] Macho, C.; Minkwitz, R.; Rohmann, J.; Steger, B.; Wölfel, V.; Oberhammer, H., *Inorg. Chem*., **25**, 2828, (1986)

[6] Holmes, R. R.; Carter, R. P.; Peterson, G. E., *Inorg. Chem*., **3**, 1748, (1964)

[7] Christen, D.; Kadel, J.; Liedtke, A.; Minkwitz, R.; Oberhammer, H., *J. Phys. Chem.,* **93**, 6672, (1989)

[8] Bartell, L. S.; Hansen, K. W., *Inorg. Chem*., **4**, 1777, (1965)

[9] Albright, T.A.; Burdett, J. K.; Whangbo, M.-H., *Orbital Interactions in Chemistry*, John Wiley and Sons, New York, (1985)

[10] Muetterties, E. L.; Mahler, W.; Schmutzler, R., *Inorg. Chem*., **2**, 613, (1963)

[11] Muetterties, E. L.; Mahler, W.; Packer, K. J.; Schmutzler, R., *Inorg. Che*m., **3**, 1298, (1964)

[12] Emsley, J.; Hall, D., *The Chemistry of Phosphorus*, Harper & Row Ltd, London, (1976)

[13] Dillon, K. B., *Chem. Rev*., **94**, 1441, (1994)

[14] a) Peake, S. C.; Schmutzler, R., *Chem. Commun*., 1662, (1968) b) Peake, S. C.; Schmutzler, R., *J. Chem. Soc. A*., 1049, (1970)

[15] Muetterties, E. L.; Meakin, P.; Hoffmann, R., *J. Amer. Chem. Soc*., **94**, 5674, (1972)

[16] a) Allen, F. H., *Acta Cryst*., **B58**, 380, (2002) b) Bruno, I. J.; Cole, J. C.; Edgington, P. R.; Kessler, M.; Macrae, C. F.; McCabe, P.; Pearson J.; Taylor, R., *Acta Cryst.*, B**58**, 389, (2002)

[17] Kubo, K.; Nakazawa, H.; Mizuta, T.; Miyoshi, K., *Organometallics*, **17**, 3522, (1998)

[18] Wachter, J.; Mentzen, B. F.; Riess, J. G., *Angew. Chem. Int. Ed. Engl*., **20**, 284, (1981)

[19] Shaw, R. A., *Phosphorus Sulfur*, **4**, 701, (1978)

[20] McPhail, A. T.; Knop, G. R.; Roberson, C. G.; Sim, G. A., *J. Chem. Soc. (A),* 205, (1971)

[21] Jeanneaux, F.; Grand, A.; Riess, J. G., *J. Am. Chem. Soc*., **103**, 4272, (1981)

[22] Dupart, J-M.; Grand, A.; Pace, S.; Riess, J. G., *J. Am. Chem. Soc*., **10**4, 2316, (1982)

[23] Lattman, M.; Anad, B. N.; Garrett, D. R.; Whitener, M. A., *Inorg. Chim. Acta*, **76**, L139, (1983)

[24] Lattman, M.;Morse, S. A.; Cowley, A. H.; Lasch, J. G.; Norman, N. C., *Inorg. Chem*., **24**, 1364, (1985)

[25] (comparing a metal-P(III) to a metal-P(IV) bond) Towle, D. K.; Landon, S. J.; Brill, T. B.; Tulip, T. H., *Organometallics,* **1**, 295, (1982)

[26] Lattman, M.; Burns, E. G.; Chopra, S. K.; Cowley, A. H.; Arif, A. M., *Inorg. Chem*., **26**, 1926, (1987)

[27] Khasnis, D. V.; Lattman, M.; Siriwardane, U., *Inorg. Chem*., **28**, 681, (1989)

[28] Lattman, M.; Olmstead, M. M.; Power, P. P.; Rankin, D. W. H.; Robertson, H. E., *Inorg. Chem*., **27**, 3012, (1988)

[29] De Meester, P.; Lattman, M.; Chu, S. S. C. *Acta Crystallogr., Sect. C: Cryst. Struct. Commun.*, **43**, 162, (1987)

[30] Khasnis, D. V.; Lattman, M.; Siriwardane, U., *Inorg. Chem*., **28**, 2594, (1989)

[31] Khasnis, D. V.; Lattman, M.; Siriwardane, U.; Zhang, H., *Organometallics*, **11** 2074, (1992)

[32] Khasnis, D. V.; Burton, J. M.; Zhang, H.; Lattman, M., *Organometallics*, **11**, 3745, (1992)

[33] Ebsworth, E. A. V.; McManus, N. T.; Pilkington, N. J.; Rankin, D. W. H., *Chem. Commun*., 484, (1983)

[34] Blake, A. J.; Cockman, R. W.; Ebsworth, E. A. V.; Henderson, S. G. D.; Holloway, J. H.; Pilkington, N. J.; Rankin, D. W. H., *Phosphorus Sulfur*, **30**, 143, (1987)

[35] Kubo, K.; Bansho, K.; Nakazawa, H.; Miyoshi, K., *Organometallics*, **18**, 4311, (1999)

[36] Nakazawa, H.; Kubo, K.; Miyoshi, K., *J. Amer. Chem. Soc*., **115**, 5863, (1993)

[37] a) Nakazawa, H.; Kawamura, K.; Kubo, K.; Miyoshi, K., *Organometallics*, **18**, 2961, (1999) b) Nakazawa, H.; Nakazawa, K.; Ogawa, T.; Miyoshi, K., *J. Organomet. Chem.*, **646**, 204, (2002)

[38] Toyota, K.; Yamamoto, Y.; Akiba, K., *J. Chem. Res*., **6**, 386, (1999)

[39] Toyota, K.; Yamamoto, Y.; Akiba, K., *J. Organomet. Chem*., **586**, 171, (1999)

[40] Kajiyama, K.; Miyamoto, T. K.; Sawano, K., *Inorg. Chem*., **45**, 502, (2006)

[41] Mikhel, I. S.; Bondarev, O. G.; Tsarev, V. N.; Grintselev-Knyazev, G. V.; Lyssenko, K. A.; Davankov, V. A.; Gavrilov, K. N., *Organometallics*, **22**, 925, (2003)

[42] Riess, J. G.; Vierling, P., *J. Am. Chem. Soc*., **106**, 2432, (1984)

[43] Riess, J. G.; Vierling, P.; Grand, A., *Inorg. Chem*., **25**, 4144, (1986)

[44] Nakazawa, H.; Kubo, K.; Kai, C.; Miyoshi, K., *J. Organomet. Chem*., **429**, C42, (1992)

[45] Nakazawa, H.; Kubo, K.; Miyoshi, K., *J. Amer. Chem. Soc*., **115**, 5863, (1993)

[46] Nakazawa, H.; Kubo, K.; Tanisaki, K.; Kawamura, K.; Miyoshi, K., *Inorg. Chim. Acta*, **222**, 123, (1994)

[47] Kajiyama, K.; Nakamoto, A.; Miyazawa, S.; Miyamoto, T. K., *Chem. Lett*., **32**, 4, 332, (2003)

[48] Macgregor, S. A.; Neave, G. W., *Organometallics*, **23**, 891, (2004)

[49] Bryndza, H. E., *Organometallics*, **4**, 1686, (1985)

[50] Komiya, S.; Akai, Y.; Tanaka, K.; Yamamoto, T.; Yamamoto, A., *Organometallics*, **4**, 1130, (1985)

[51] Grushin, V. V.; Marshall, W. J., *J. Amer. Chem. Soc*., **126**, 3068, (2004)

[52] Fawcett, J.; Holloway, J. H.; Saunders, G. C., *Inorg. Chim. Acta*, **202**, 111, (1992)

[53] Macgregor, S. A.; Roe, D. C.; Marshall, W. J.; Bloch, K. M.; Bakhmutov, V. I.; Grushin, V. V., *J. Amer. Chem. Soc*., **127**, 15304, (2005)

[54] Macgregor, S.A.; Wondimagegn, T., *Organometallics*, **26**, 1143, (2007)

[55] Frisch, M. J.; Trucks, G. W.; Schlegel, H. B.; Scuseria, G. E.; Robb, M. A.; Cheeseman, J. R.; Montgomery, Jr., J. A.; Vreven, T.; Kudin, K. N.; Burant, J. C.; Millam, J. M.; Iyengar, S. S.; Tomasi, J.; Barone, V.; Mennucci, B.; Cossi, M.; Scalmani, G.; Rega, N.; Petersson, G. A.; Nakatsuji, H.; Hada, M.; Ehara, M.; Toyota, K.; Fukuda, R.; Hasegawa, J.; Ishida, M.; Nakajima, T.; Honda, Y.; Kitao, O.; Nakai, H.; Klene, M.; Li, X.; Knox, J. E.; Hratchian, H. P.; Cross, J. B.; Bakken, V.; Adamo, C.; Jaramillo, J.; Gomperts, R.; Stratmann, R. E.; Yazyev, O.; Austin, A. J.; Cammi, R.; Pomelli, C.; Ochterski, J. W.; Ayala, P. Y.; Morokuma, K.; Voth, G.

A.; Salvador, P.; Dannenberg, J. J.; Zakrzewski, V. G.; Dapprich, S.; Daniels, A. D.; Strain, M. C.; Farkas, O.; Malick, D. K.; Rabuck, A. D.; Raghavachari, K.; Foresman, J. B.; Ortiz, J. V.; Cui, Q.; Baboul, A. G.; Clifford, S.; Cioslowski, J.; Stefanov, B. B.; Liu, G.; Liashenko, A.; Piskorz, P.; Komaromi, I.; Martin, R. L.; Fox, D. J.; Keith, T.; Al-Laham, M. A.; Peng, C. Y.; Nanayakkara, A.; Challacombe, M.; Gill, P. M. W.; Johnson, B.; Chen, W.; Wong, M. W.; Gonzalez, C.; and Pople, J. A.; *Gaussian 03* (Gaussian, Inc., Wallingford CT, 2004)

[56] Braga, A. A. C.; Morgon, N. H.; Ujaque, G.; Maseras, F., *J. Amer. Chem. Soc*., **127**, 25, 9298, (2005)

[57] Erhardt, S.; Macgregor, S. A., *J. Am. Chem. Soc*., **130**, 46, 15490, (2008)

[58] Blum, O.; Frolow, F.; Milstein, D., *Chem. Commun*., 258, (1991)

[59] Flores, A. N.; Erhardt, S.; Jasim, N. A.; Perutz, R. N.; Macgregor, S. A.; McGrady, J. E.; Whitwood, A. C., *J. Am. Chem. Soc*., **130**, 46, 15499, (2008)

[60] Mason, M. R.; Verkade, J. G., *Organometallics*, **11**, 2212, (1992)

[61] Chatt, J.; Hart, F. A.; Watson, H. R., *J. Chem. Soc*., 2537, (1962)

[62] Clark, H. C.; Kapoor, P. N.; McMahon, I. J., *J. Organomet. Chem*., **265**, 107, (1984)

[63] Laing, K. R.; Robinson, S. D.; Uttley, M. F., *J. Chem. Soc., Dalton Trans*., 1205, (1974)

[64] Hartley, F. R., *The Chemistry of Platinum and Palladium*, John Wiley and Sons, New York, p 28-29, 51, (1973)

[65] Thomas, B. J.; Mitchell, J. F.; Theopold, K. H.; Leary, J. A., *J. Organomet. Chem*., **348**, 333, (1988)

[66] Jordan, R. F.; Dasher, W. E.; Echols, S. F., *J. Am. Chem. Soc*., **108**, 1718, (1986)

[67] Amatore, C.; Jutland, A; M'Barki, M. A., *Organometallics*, **11**, 3009, (1992)

[68] Amatore, C.; Carré, E.; Jutland, A; M'Barki, M. A., *Organometallics*, **14**, 1818, (1995)

[69] Amatore, C.; Jutand, A.; Lemaître, F.; Ricard, J. L.; Kozuch, S.; Shaik, S., *J. Organomet. Chem.*, **689**, 3728, (2004)

[70] Malatesta, L.; Angoletta, M. J., *J. Chem. Soc*., 1186, (1957)

[71] Grushin, V. V.; Alper, H., *Organometallics*, **12**, 1890, (1993)

[72] Stille, J. K., *Angew. Chem., Int. Ed. Engl*., **25**, 508, (1986)

[73] Segelstein, B. E.; Butler, T. W.; Chenard, B. L., *J. Org. Chem*., **60**, 12, (1995)

[74] O'Keefe, D. F.; Dannock, M. C.; Marcuccio, S. M., *Tetrahedron Lett*., **33**, 6679, (1992)

[75] Björkman, M.; Långström, B., *J. Chem. Soc., Perkin Trans*., **1**, 3031, (2000)

[76] Hamann, B. C.; Hartwig, J. F., *J. Am. Chem. Soc*., **120**, 3694, (1998)

[77] Yin, J.; Buchwald, S. L., *Org. Lett*., **2**, 1101, (2000)

[78] Sundermeier, M.; Zapf, A.; Beller, M.; Sans, J., *Tetrahedron Letters*, **42**, 6707, (2001)

[79] Grushin, V. V., *Organometallics*, **19**, 1888, (2000)

[80] Goodson, F. E.; Wallow, T. I.; Novak, B. M., *J. Am. Chem. Soc.*, **119**, 12441, (1997)

[81] Macgregor, S. A., *Chem. Soc. Rev*., **36**, 67, (2007)

[82] Abatjoglou, A. G.; Billig, E.; Bryant, D. R., *Organometallics*, **3**, 923, (1984)

[83] Abatjoglou, A. G.; Bryant, D. R., *Organometallics*, **3**, 932, (1984)

[84] Goel, A. B., *Inorg. Chim. Acta*, **86**, L25, (1984)

[85] Goel, A. B., *Inorg. Chim. Acta*, **86**, L77, (1984)

[86] Kong, K-C.; Cheng, C.-H., *J. Am. Chem. Soc*., **113**, 6313, (1991)

[87] Sakamoto, M.; Shimizu, I.; Yamamoto, A., *Chem. Lett*., **24**, 1101, 1995

[88] Barañano, D.; Hartwig, J. F., *J. Am. Chem. Soc*., **117**, 2937, (1995)

[89] Herrmann, W. A.; Brossmer, C.; Oefele, K.; Beller, M.; Fischer, H., *J. Mol. Catal. A: Chem*., **103**, 133, (1995)

[90] Inada, K.; Miyaura, N., *Tetrahedron*, **56**, 8657, (2000)

[91] de la Torre, G.; Gouloumis, A.; Vazquez, P.; Torres, T., *Angew. Chem., Int. Ed. Engl*., **40**, 2895, (2001)

[92] Green, M. L. H.; Smith, M. J.; Felkin, H.; Swierczewski, G., *J. Chem. Soc. D*., 158, (1971)

[93] Nussbaum, S.; Michman, M., *J. Organomet. Chem*., **182**, 555, (1979)

[94] Mohtachemi, R.; Kannert, G.; Schumann, H.; Chocron, S.; Michman, M., *J., Organomet. Chem*., **310**, 107, (1986)

[95] Morita, D. K.; Stille, J. K.; Norton, J. R., *J. Am. Chem. Soc*., **117**, 8576, (1995)

Chapter 2: Computational Details

This chapter contains technical information about the calculations within this thesis, along with the functionals and basis sets chosen. A more comprehensive discussion of the methodologies involved can be found in Chapter 7.

2.1 Calculation details

The results in this thesis were produced by running calculations using the *Gaussian 98*[1] and *Gaussian 03*[2] packages. The following details apply to all of the calculations performed, except for those calculated using the ONIOM method[3] which is discussed below. The functional used was the exchange functional of Becke[4] with the correlation functional of Perdew.[5] Nickel, palladium, platinum, chlorine, bromine, iodine and phosphorus were represented by the relativistic core potential of the Stuttgart group[6] and the associated basis sets (SDD), with an added polarisation function on phosphorus, chlorine, bromine and iodine.[7] The basis set 6-31G(d,p)[8] was used to represent the nitrogen, carbon, oxygen, fluorine and hydrogen atoms.

For the calculations performed using the ONIOM method within *Gaussian 03*, the following functionals and basis sets were used. On the 'high' model, BP86 and the basis sets described in the previous paragraph were used. However, the Hartree-Fock approximation was used to calculate at the 'low' level within ONIOM. Palladium, phosphorus, chlorine, bromine and iodine were represented by LANL2DZ[9] and all other atoms were described using 6-31G.

The term 'transition state' should be more clearly defined in relation to this project. In order to locate a transition state, a scan was initially performed, beginning from a chosen optimized species and varying a parameter (normally a bond length, atomic distance or angle) in a stepwise manner. A transition state optimisation was then started from the geometry corresponding to the energy highpoint of the scan. The transition state was then characterised by having one imaginary frequency. Intrinsic reaction co-ordinate (IRC) calculations were also run, which involve optimising a series of geometries down both

directions in the potential energy curve to find local minima, i.e. the reactant and product directly linking to the transition state. It is not possible within *Gaussian 03* to perform IRC calculations when using ONIOM, therefore an alternative method, named pseudo-IRC (PIRC) calculations, was used instead. In these cases the transition state geometry would be slightly displaced by lengthening and shortening the bond corresponding to the negative frequency. From these geometries normal optimizations was then run to determine the local minima.

All energies reported in this thesis are enthalpies which include a zero-point energy correction, unless otherwise stated. These values were obtained from frequency calculations performed on optimized stationary points. When relevant to the discussion, free energy data have been given, and these also came from frequency calculations. In some cases the effect of solvation has been investigated using polarisable continuum model (PCM)[10] calculations (radii=UFF). These produce a correction value which can be added to the electronic energy associated with the gas-phase result. The enthalpy and/or free energy contributions derived from the gas phase calculation can then also be included.

All complexes investigated have a C_1 point group unless otherwise stated.

2.2 References

[1] Frisch, M. J.; Trucks, G. W.; Schlegel, H. B.; Scuseria, G. E.; Robb, M. A.; Cheeseman, J. R.; Zakrzewski, V. G.; Montgomery Jr., J. A.; Stratmann, R. E.; Burant, J. C.; Dapprich, S.; Millam, J. M.; Daniels, A. D.; Kudin, K. N.; Strain, M. C.; Farkas, Ö.; Tomasi, J.; Barone, V.; Cossi, M.; Cammi, R.; Mennucci, B.; Pomelli, C.; Adamo, C.; Clifford, S.; Ochterski, J.; Petersson, G. A.; Ayala, P. Y.; Cui, Q.; Morokuma, K.; Salvador, P.; Dannenberg, J. J.; Malick, D. K.; Rabuck, A. D.; Raghavachari, K.; Foresman, J. B.; Cioslowski, J.; Ortiz, J. V.; Baboul, A. G.; Stefanov, B. B.; Liu, A.; Liashenko, G.; Piskorz, P.; Komáromi, I.; Gomperts, R.; Martin, R. L.; Fox, D. J.; Keith, T.; Al-Laham, M. A.; Peng, C. Y.; Nanayakkara, A.; Challacombe, M.; Gill, P. M. W.;

Johnson, B.; Chen, W.; Wong, M. W.; Andres, J. L.; Gonzalez, C.; Head-Gordon, M.; Replogle, E. S.; Pople, J. A., *Gaussian 98* (Gaussian, Inc., Pittsburgh, PA, 1998)

[2] Frisch, M. J.; Trucks, G. W.; Schlegel, H. B.; Scuseria, G. E.; Robb, M. A.; Cheeseman, J. R.; Montgomery, Jr., J. A.; Vreven, T.; Kudin, K. N.; Burant, J. C.; Millam, J. M.; Iyengar, S. S.; Tomasi, J.; Barone, V.; Mennucci, B.; Cossi, M.; Scalmani, G.; Rega, N.; Petersson, G. A.; Nakatsuji, H.; Hada, M.; Ehara, M.; Toyota, K.; Fukuda, R.; Hasegawa, J.; Ishida, M.; Nakajima, T.; Honda, Y.; Kitao, O.; Nakai, H.; Klene, M.; Li, X.; Knox, J. E.; Hratchian, H. P.; Cross, J. B.; Bakken, V.; Adamo, C.; Jaramillo, J.; Gomperts, R.; Stratmann, R. E.; Yazyev, O.; Austin, A. J.; Cammi, R.; Pomelli, C.; Ochterski, J. W.; Ayala, P. Y.; Morokuma, K.; Voth, G. A.; Salvador, P.; Dannenberg, J. J.; Zakrzewski, V. G.; Dapprich, S.; Daniels, A. D.; Strain, M. C.; Farkas, O.; Malick, D. K.; Rabuck, A. D.; Raghavachari, K.; Foresman, J. B.; Ortiz, J. V.; Cui, Q.; Baboul, A. G.; Clifford, S.; Cioslowski, J.; Stefanov, B. B.; Liu, G.; Liashenko, A.; Piskorz, P.; Komaromi, I.; Martin, R. L.; Fox, D. J.; Keith, T.; Al-Laham, M. A.; Peng, C. Y.; Nanayakkara, A.; Challacombe, M.; Gill, P. M. W.; Johnson, B.; Chen, W.; Wong, M. W.; Gonzalez, C.; and Pople, J. A.; *Gaussian 03* (Gaussian, Inc., Wallingford CT, 2004)

[3] a) Maseras, F.; Morokuma, K., *J. Comp. Chem.* **16**, 1170 (1995) b) Humbel, S.; Sieber, S.; Morokuma, K., *J. Chem. Phys.* **105**, 1959 (1996) c) Matsubara, T.; Sieber, S.; Morokuma, K., *Int. J. Quant. Chem.* **60**, 1101 (1996) d) Svensson, M.; Humbel, S.; Froese, R. D. J.; Matsubara, T.; Sieber, S.; Morokuma, K., *J. Phys. Chem.* **100**, 19357 (1996) e) Svensson, M.; Humbel, S.; Morokuma, K., *J. Chem. Phys.* **105**, 3654 (1996) f) Dapprich, S.; Komáromi, I.; Byun, K. S.; Morokuma, K.; Frisch, M. J., *J. Mol. Struct. (Theochem)* **462**, 1 (1999) g) Vreven, T.; Morokuma, K., *J. Comp. Chem.* **21**, 1419 (2000)

[4] Becke, A. D., *J. Chem. Phys.,* **84**, 4524, (1986)

[5] Perdew, J. P., *Phys. Rev. B,* **33**, 8822, (1986)

[6] Perdew, J. P.; Wang, Y. *Phys. Chem Rev. B,* **45***,* 13244, (1992)

[7] Hollwarth, A.; Bohme, M.; Dapprich, S.; Ehlers, A. W.; Gobbi, A.; Jonas, V.; Kohler, K. F.; Stegman, R.; Veldkamp, A.; Frenking, G., *Chem. Phys. Lett.,* **208**, 237, (1993)

[8] a) Ditchfield, R.; Hehre, W. J.; Pople, J. A., *J. Chem. Phys.* **54**, 724, (1971) b) Hehre, W. J.; Ditchfield, R.; Pople, J. A., *J. Chem. Phys.* **56**, 2257, (1972) c) Hariharan P. C.; Pople, J. A., *Mol. Phys.* **27**, 209, (1974) d) Gordon, M. S., *Chem. Phys. Lett.* **76**, 163, (1980) e) Hariharan P. C.; Pople, J. A., *Theo. Chim. Acta* **28**, 213, (1973) f) Blaudeau, J.-P.; McGrath, M. P.; Curtiss, L. A.; Radom, L., *J. Chem. Phys.* **107**, 5016, (1997) g) Francl, M. M.; Pietro, W. J.; Hehre, W. J.; Binkley, J. S.; DeFrees, D. J.; Pople, J. A.; Gordon, M. S., *J. Chem. Phys.* **77**, 3654, (1982) h) Binning Jr. R. C.; Curtiss, L. A., *J. Comp. Chem.* **11**, 1206, (1990) i) Rassolov, V. A.; Pople, J. A.; Ratner, M. A.; Windus, T. L., *J. Chem. Phys.* **109**, 1223, (1998) j) Rassolov, V. A.; Ratner, M. A.; Pople, J. A.; Redfern, P. C.; Curtiss, L. A., *J. Comp. Chem.* **22**, 976, (2001)

[9] a) Dunning Jr. T. H.; Hay, P. J., *Modern Theoretical Chemistry*, Ed. H. F. Schaefer III, Vol. 3, Plenum, New York, 1-28, (1976) b) Rappé A. K.; Goddard III, W. A., *J. Phys. Chem.* **95**, 3358, (1991) c) Segal G.; Pople, J., *J. Chem. Phys.* **44**, 3289, (1966) d) Pople, J. A.; Beveridge, D.; Dobosh, P., *J. Chem. Phys.* **47**, 2026, (1967)

[10] Miertuš, S.; Scrocco, E.; Tomasi, J., *Chem. Phys.*, **55**, 117-29, (1981)

Chapter 3: Study of X/R exchange in *trans*-[M(Cl)X(PH_3)(PR_3)] species (M = Pd, Ni, Pt; X = F, OH, NH_2, Me, Ph, Cl; R = H, F, Me)

3.1 Overview

The aim of this chapter is to look at metallophosphorane formation and subsequent X/R exchange in the model system *trans*-[M(Cl)X(PH_3)(PR_3)]. The effect of changing the X group (X = F, OH, NH_2, Me, Ph, Cl), the nature of the active phosphine (R = H, F, Me) and the metal centre (M = Pd, Ni, Pt) on the exchange profile and structures will be investigated. However, to begin with, the discussion of site preferences in phosphorane structures, which began in Chapter 1, will be continued and explored through some simple calculations.

3.2 Calculations exploring site preferences in PH_4R

Calculations were performed on a range of simple PH_4R molecules to see whether the literature results for phosphorane site preference could be reproduced. The R groups that were chosen range from electronegative halogens to more electron donating hydrocarbon groups. The results are shown in Table 3.1. It was found that not all of the

R	Energy / a.u.		ΔE / kcalmol^{-1}
	$PH_4R_{(ax)}$	$PH_4R_{(eq)}$	
F	-108.76356	-108.75466	-5.6
Cl	-23.96222	-23.94905	-8.3
OH	-84.72837	-84.73359	3.3
NH_2	-64.84458	-64.85686	7.7
CH_3	-48.78382	-48.79147	4.8
C_6H_5	-240.52020	-240.52773	4.7

Table 3.1: Comparison of optimised energies of PH_4R, with the R group in either an axial or equatorial position. Blue = C_s symmetry imposed to prevent isomerisation, red = bond angles fixed.

molecules could form stable isomers with the R group in both axial and equatorial positions in the molecule. For instance, when fluorine or chlorine were placed in equatorial positions in PH_4R, both molecules isomerised to the axial isomer when optimised. This clearly indicates that the electronegative halogens prefer axial sites in the TBP, which is in line with the experimental observations, as discussed in Chapter 1. To obtain energy values for the equatorial isomers for comparison, it was necessary to impose C_s symmetry on some of the molecules, which made optimisation without

isomerisation possible. The ΔE values are negative for molecules containing either halogen, further supporting the axial preference. Hydroxy and methyl were the only two R groups which formed stable structures for both the axial and equatorial isomers without symmetry constraints. The ΔE values are both positive, indicating that both R groups form more stable molecules with R in an equatorial position. This is not a surprising preference for methyl, as its electron-donating ability suggests it would prefer an equatorial site. However, the oxygen in hydroxy is relatively electronegative, so it must be its ability to engage in π-bonding which leads it to be more stable in an equatorial position. The amido and phenyl R groups isomerised from an axial position when optimised, and only formed stable molecules with R in an equatorial position. It was necessary to fix two angles in both axial isomers to hold the R groups in position to obtain energy values for comparison. The ΔE values also support the equatorial preference. This result is also consistent with experimental findings, and is possibly due to the amido group having a lone pair available for π-bonding that is not so tightly held as in the halides. The phenyl group is bulky and has a π-system, so would also be expected to prefer an equatorial site.

In summary, these calculations have reproduced the trend seen experimentally, that only strongly electronegative groups will prefer to be in the axial sites of a TBP phosphorane.

3.3 Site preferences of the metal fragments in metallophosphoranes

All metallophosphoranes with published crystallographically determined structures have the transition metal fragment in an equatorial position with respect to the TBP pentacoordinated phosphorus.[1,2] Two crystallographically characterised metallophosphoranes were chosen,[2m,v] and simplified models of each were constructed and optimised, to see whether this equatorial preference would be reproduced by calculations. The crystallographically determined structures and the calculated model structures are shown in Figure 3.3. The model structures were set up with starting geometries where the metal was at equatorial and axial positions. In each case the axial isomer was not stable, and isomerised to the equatorial structure. This supports the experimental evidence that the metal is always observed in an equatorial position. Since the metal fragment is normally bulky and less electronegative than other substituents, it is logical that it would prefer an equatorial position.

The trend of axial bonds being longer than equatorial bonds around a TBP phosphorus is seen in all four structures. In addition, in each structure the phosphorane M-P bond is shorter than the phosphine M-P bond, a trend which is common with these types of complex.[3] Although the correct trend was reproduced in the model systems calculated, the TBP bonds and the M-P1 bonds were overestimated.

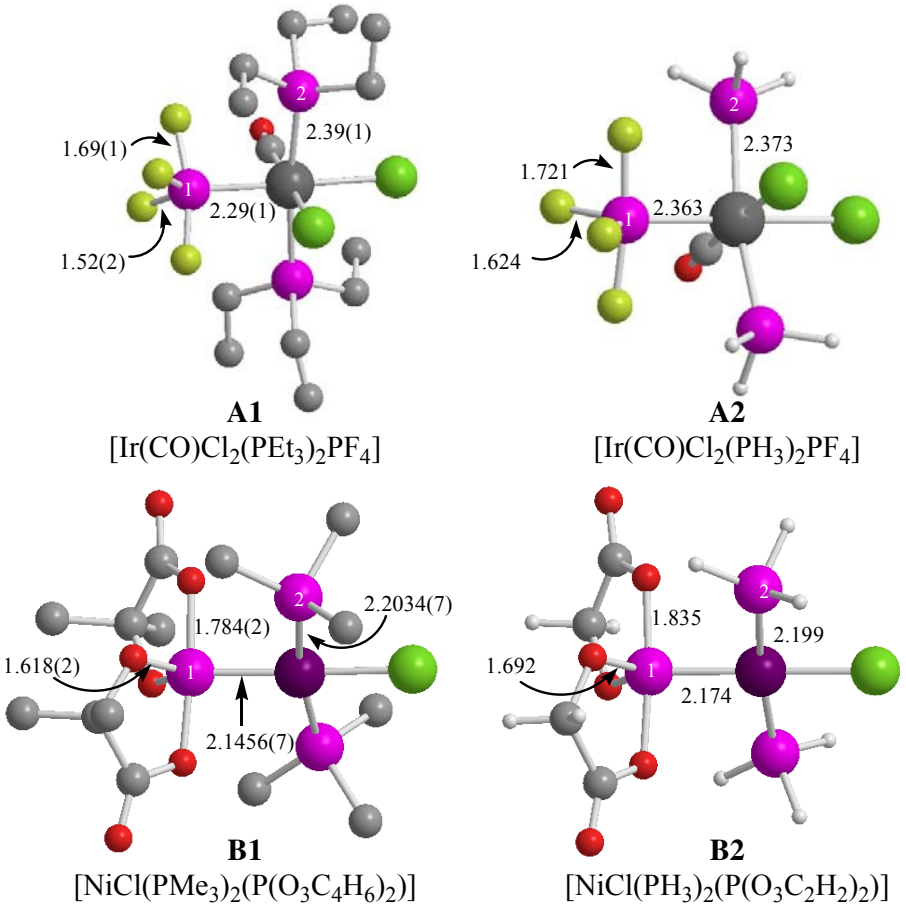

Figure 3.1: Metallophosphorane structures determined by X-ray crystallography: **A1**[2m] and **B1**[2v]. Optimised model structures: **A2** and **B2**.

3.4 Model system: *trans*-[M(Cl)X(PH_3)(PR_3)] (M = Pd, Ni, Pt; X = F, OH, NH_2, Me, Ph, Cl; R = H, F, Me)

The aim of the work described in this thesis was to investigate the possibility of metallophosphoranes being involved, as intermediates or transition states, in Pd(II) phosphine disproportionation and exchange reactions. Before specific experimental systems were looked at in detail, it was decided that it would be useful to look at the formation of metallophosphorane species by the intramolecular attack of an X ligand on a coordinated phosphine, the structures of the resulting complexes, and the transfer of R (normally H) back to the metal to complete the exchange reaction, as shown in Figure 3.2. A range of calculations were performed on a model system which is a simplified version of the experimental species. The basic model system used was *trans*-[M(Cl)X(PH_3)(PR_3)], where the metal (M), the ligand attacking the phosphine (X) and

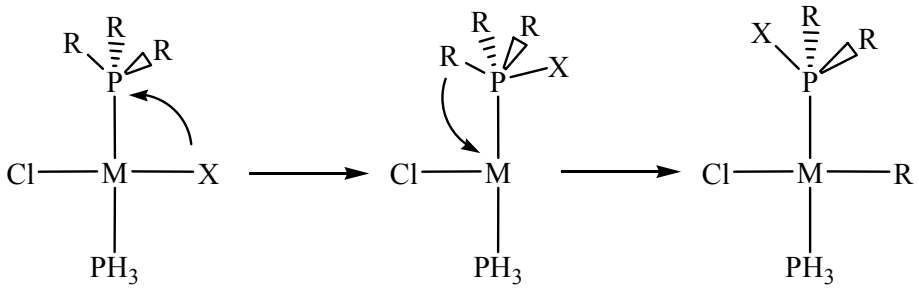

Figure 3.2: X/R exchange pathway in *trans*-[M(Cl)X(PH_3)(PR_3)].

the active phosphine (PR_3) were varied as shown in Figure 3.3. The following sections describe the results of changing these three variables. The defaults of M = Pd, R = H and X = OH were used so that only one variable at a time was changed. These were chosen as they make up a model system for *trans*-[Pd(Cl)(OH)(PPh_3)$_2$], which is an important intermediate in the hydroxide-induced disproportionation reaction published by Grushin and Alper,[4] which is investigated in detail in Chapter 4. All of the following calculations were done using density functional methods as described in Chapter 2.

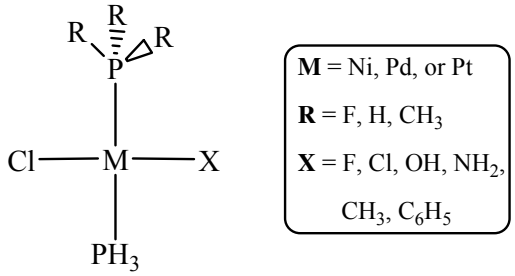

Figure 3.3: Structure of *trans*-[M(Cl)X(PH_3)(PR_3)].

3.5 Changing the X ligand: *trans*-[M(Cl)X(PH_3)$_2$] (X = F, OH, NH_2, Me, Ph, Cl) F/H exchange in *trans*-[Pd(Cl)F(PH_3)$_2$]

3.5.1 F-transfer from Pd onto PH_3

The first reaction investigated was metallophosphorane formation from **1a** (E = 0.0 kcal/mol), *trans*-[Pd(Cl)F(PH_3)$_2$]. This is a simple model of a possible precursor in the formation of [Pd(Cl)(PPh_3F)(PPh_3)$_2$], which was proposed as an intermediate in the fluoride-induced reduction of palladium(II) by Mason and Verkade.[5]

The first attempt at forming a metallophosphorane from reactant **1a** was made by decreasing the F···P1 distance as shown in Figure 3.4 (**A**). However, the energy was found to only increase as the F···P1 distance decreased, and optimisation without any geometric constraints led back to **1a**. Therefore, the F···P1 distance was fixed at 1.9 Å, which is somewhat longer than the predicted P-F bond length of 1.59 Å (for an axial P-F bond in PF_5).[3] Stepwise rotation around the Pd-P1 bond was performed to move fluoride out of the metal coordination plane (shown in Figure 3.4 (**B**)), but this was also unsuccessful at yielding a stable metallophosphorane. It was finally discovered that it was necessary to open the Cl-Pd-P2 angle in conjunction with the shortening of the P1···F distance to lead to a metallophosphorane, as shown in Figure 3.4 (**C**). The isomerisation results in there no longer being a vacant site cis to {PH_3F}, which seems to prevent the fluoride from transferring back to the metal.

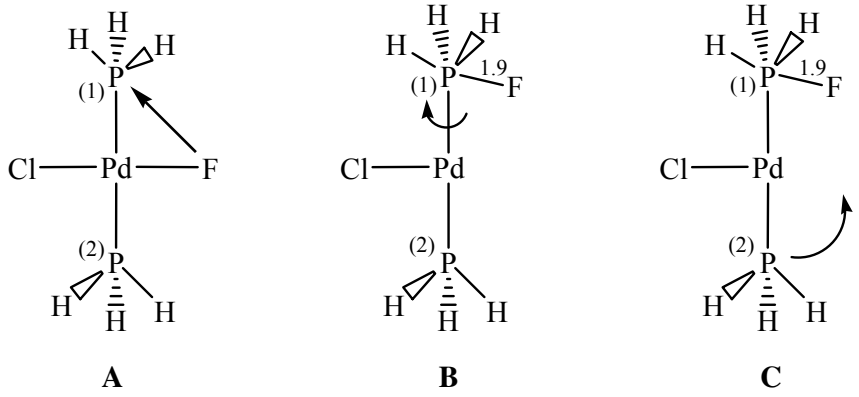

Figure 3.4: Attempts to form a metallophosphorane by attack of F on P1 in **1a**.

The geometry from the highest energy point of a scan that reduced the Cl-Pd-P2 angle was used as a starting point for a transition state calculation. This led to the discovery of **TS_{1a-1b}** (E = 29.0 kcal/mol). IRC calculations confirmed that this transition state links **1a** to a metallophosphorane intermediate, **1b** (E = 16.8 kcal/mol).

The structures of **1a**, $\mathbf{TS_{1a\text{-}1b}}$ and **1b** are shown in Figure 3.5, and some key bond lengths and interatomic distances are shown in Table 3.2. In the progression from **1a** to **1b**, the Pd-F bond is broken and an F-P1 bond is formed. This bond formation and cleavage is almost complete in $\mathbf{TS_{1a\text{-}1b}}$. The geometry around P1 is seen to change from tetrahedral in **1a** (average H-P1-Pd = 117.8º) to trigonal bipyramidal in **1b** (F-P1-H_{ax} = 172.5º, F-P1-Pd = 86.2º, average equatorial angle = 119.9º). This causes the lengthening of the axial P1-H1 bond (**1a** = 1.429 Å, **1b** = 1.465), while the equatorial P-H bond lengths are unchanged or shortened (**1a** = 1.430, 1.431 Å, **1b** = 1.425, 1.430 Å). This trend is consistent with the observations made earlier in the chapter on PH_4X molecules. There is also rotation around the P1-Pd bond as the metallophosphorane is formed, which causes the fluoride to move out of the metal coordination plane (F-P1-Pd-Cl: **1a** = 180.0º, $\mathbf{TS_{1a\text{-}1b}}$ = 165.9º, **1b** = 118.4º). In metallophosphorane **1b** the fluoride is in an axial site and the palladium in an equatorial site around P1, which is consistent with the trends discussed earlier in this chapter and in Chapter 1.

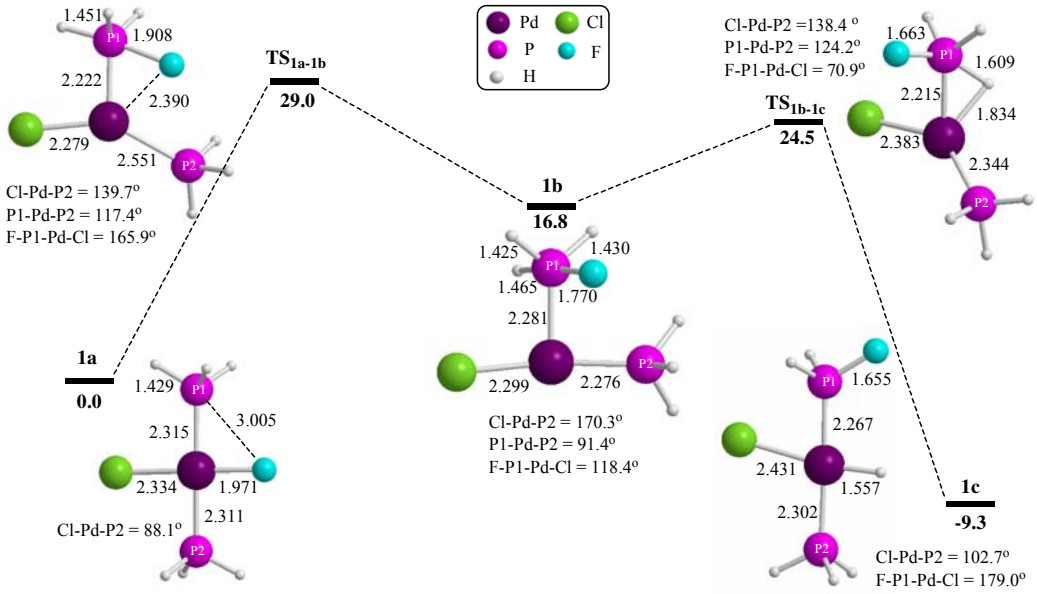

Figure 3.5: Profile for F/H exchange in *trans*-[Pd(Cl)F(PH_3)$_2$]. Energies in kcal/mol, bond lengths in Å.

	Bond Length or Atomic Distance / Å					
	Pd-F	F-P1	Pd-Cl	Pd-P2	Pd-P1	P1-H1
1a	1.971	3.005	2.334	2.311	2.315	1.429
TS_{1a-1b}	2.390	1.908	2.279	2.551	2.222	1.451
1b	2.793	1.770	2.299	2.276	2.281	1.465

Table 3.2: Selected computed bond lengths and distances in **1a**, **TS_{1a-1b}** and **1b**.

The isomerisation which occurs in the formation of **1b** was found to be essential to create a stable metallophosphorane structure. It is likely that the $\{PH_3F^-\}$ ligand has a stronger trans influence than either chloride or phosphine, leading it to prefer the position trans to the vacant site.[6] The changes that occur in the Pd-Cl bond length are probably initially due to the difference between the trans influences of fluoride in **1a** (Pd-Cl = 2.334 Å) and a partial vacant site in **TS_{1a-1b}** (Pd-Cl = 2.279 Å). **1b** (Pd-Cl = 2.299 Å) is not directly comparable as the complex has changed from being 4- to 3-coordinate, a phenomenon which is investigated further in Chapter 5. Conversely, the Pd-P2 bond lengthens considerably in the formation of the transition state (by 0.24 Å), as the phosphine moves away from its position trans to P1 in **1a**, and the Cl-Pd-P2 angle opens by 51.6º to create a Y-shaped geometry around the metal in **TS_{1a-1b}**. The Pd-P2 bond shortens again when T-shaped **1b** is formed. The Y-shaped geometry around palladium and the lengthening of the Pd-P2 bond observed in **TS_{1a-1b}** can be explained by consideration of the molecular orbitals involved in the bonding.

In **TS_{1a-1b}** the Pd-F bond has broken and the P-F bond has largely formed, so the structure could be considered as a $14e^-$ d^8-ML_3 species, and a geometric isomer of **1b** (T_{PH_3F}). The orbital interactions for $14e^-$ d^8-ML_3 $[MCl(PH_3)(PH_3F)]$ isomerising between T_{Cl} and T_{PH_3F} forms of complex were investigated. Firstly, the preference of **TS_{1a-1b}** to be Y-shaped rather than trigonal planar will be discussed, then the reason for the lengthening of the Pd-P2 bond will be investigated.

Figure 3.6 shows two possible isomerisation pathways: (i) via a Y-shaped TS or (ii) via a trigonal planar transition state structure. The geometry preference for **TS_{1a-1b}** is explained in Figure 3.7.

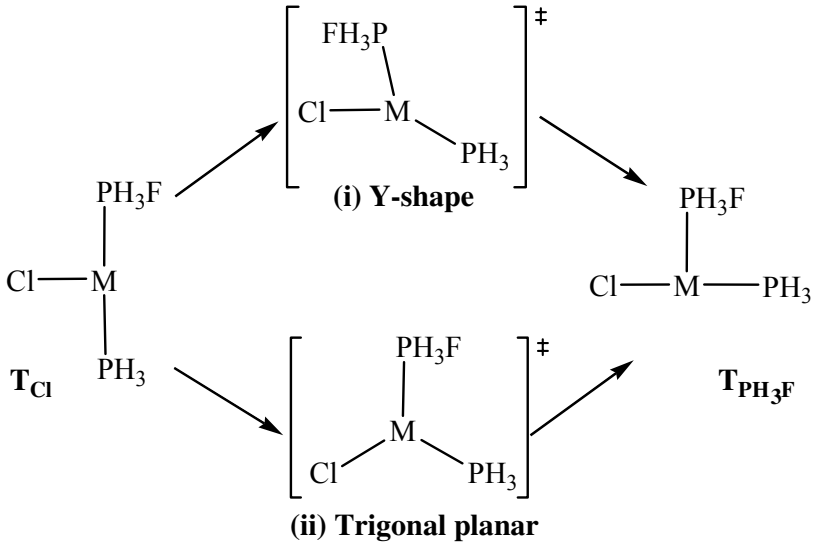

Figure 3.6: The possible transition state geometries when isomerising between T_{Cl} and T_{PH_3F} forms of $[MCl(PH_3)(PH_3F)]$.

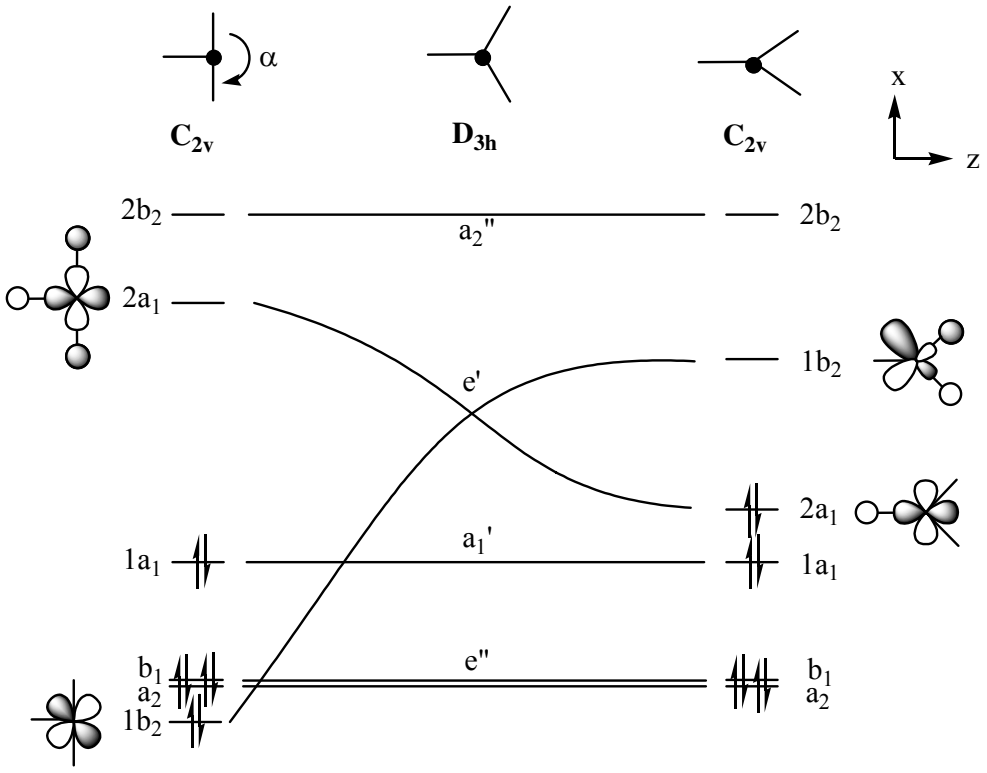

Figure 3.7: Walsh diagram of the reduction of an L-M-L angle (α) in a $14e^-$ d^8-ML_3 complex.

As the geometry changes from a C_{2v} T-shape to D_{3h} trigonal planar, the $2a_1$ orbital is stabilised by removal of the antibonding interactions with two of the ligands. At the same time the b_2 orbital is destabilised as it gains two antibonding ligand interactions when angle α is reduced. The $2a_1$ and b_2 orbitals become a degenerate e' set when the L-M-L angles are all 120º. Since these are 14-electron complexes, the e' set of orbitals would be half-filled. This would cause Jahn-Teller distortion either back to a T-shape, or alternatively to a Y-shaped geometry via a further closing of the α angle, to maintain the existing singlet spin state and remove the degeneracy, or else the system would have a triplet spin state.[7] Therefore, this $14e^-$ d^8-ML_3 species will avoid having a D_{3h} geometry, instead preferring T-shape or Y-shape geometries. In the present case where X = F, the minima are T-shaped and the transition state is Y-shaped.

The reason for the long Pd-P bond seen in Y-shaped **$TS_{1a\text{-}1b}$** can be explained by focusing on the b_2 orbital, as shown in Figure 3.8. This relates to the metal d_{xz} orbital, which is non-bonding with all three ligands when the complex has a C_{2v} T-shaped geometry, as shown on the left hand side of the diagram. However, when the complex is C_{2v} Y-shaped, as in **$TS_{1a\text{-}1b}$**, there is an antibonding interaction between the metal d_{xz} orbital and the phosphine ligand. This causes the lengthening and weakening of the Pd-P σ-bond.

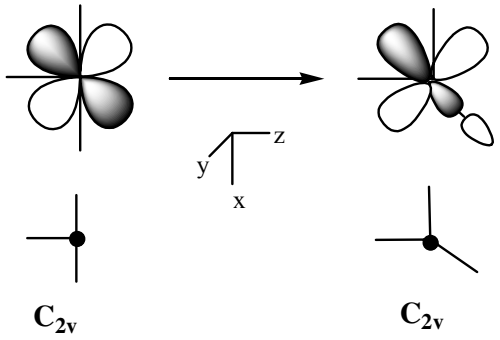

Figure 3.8: The interaction between the metal b_2 orbital and ligands in the isomerisation from a T-shaped to a Y-shaped $14e^-$ d^8-ML_3 complex.

Further calculations were carried out on a model d^8-ML_3 system in order to investigate the particular orbitals affected by the isomerisation taking place from **1a** to **1b**. In [Pd(Cl)(PH_3F)(PH_3)], the PH_3F ligand was replaced by methyl, an alternative one-electron-donor ligand, to increase the symmetry of the complex to C_s, thus allowing the orbitals to be seen more clearly. Figure 3.9 shows the frontier molecular orbitals and their computed energies.

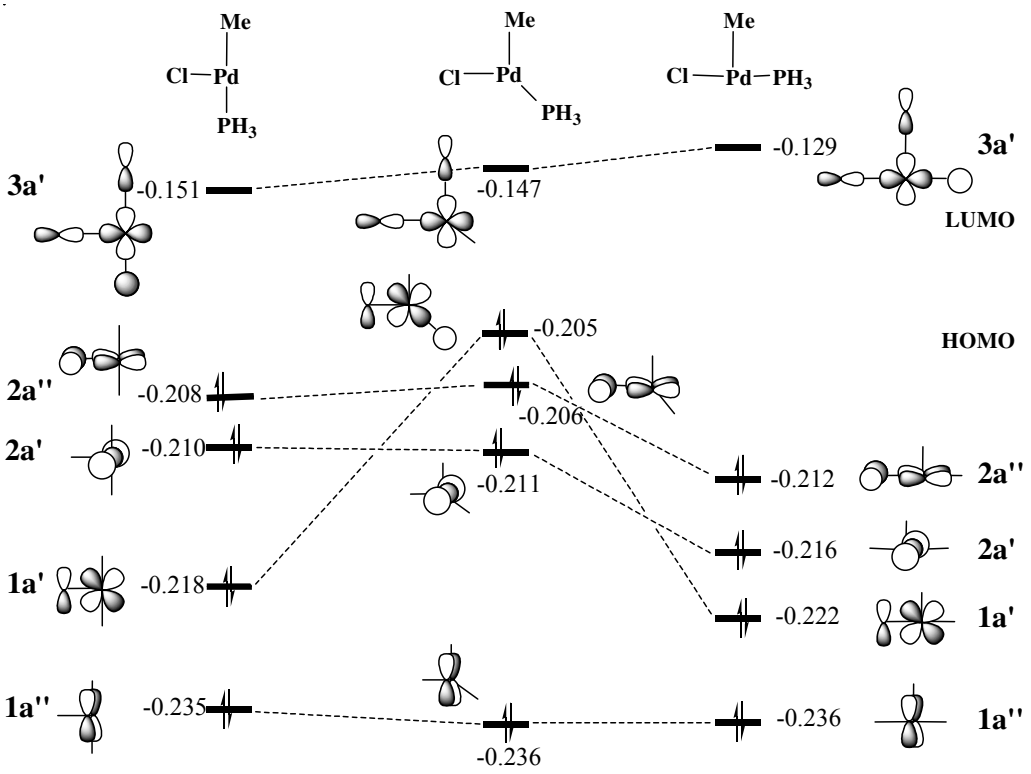

Figure 3.9: Evolution of the frontier molecular orbitals for the isomerisation of T_{Cl}-[Pd(Cl)(Me)(PH_3)] via a Y-shaped TS, to T_{Me}-[Pd(Cl)(Me)(PH_3)]. Energy in atomic units.

Only the 1a' orbital, equivalent to the d_{xz} orbital in Figure 3.8, experiences a significant change in energy between the three structures investigated. In the T_{Cl} geometry on the left the energy of 1a' is –0.218 a.u. As the Cl-Pd-PH_3 angle is opened to 135º, the antibonding interaction between the phosphine and the metal d_{xz} orbital is activated, raising the orbital energy to –0.205 a.u. in the Y-shaped transition state. When the Cl-Pd-P angle is opened further to 180º to form the T_{Me} isomer, shown on the right hand side of the diagram, the P-Pd antibonding interaction is removed and the 1a' orbital stabilises to –0.222 a.u. This confirms that the effect predicted in Figure 3.8 for the b_2 orbital of a C_{2v} complex is indeed the cause of the lengthening seen in the Pd-P bond in the palladium complex being investigated.

3.5.2 H-transfer from P to Pd

To complete the exchange, it was necessary to transfer H1, the axial hydrogen in {PH_3F}, to palladium. Shortening of the Pd···H1 distance from **1b** led to the required transfer, with a relatively small activation barrier of 7.7 kcal/mol. Thus the exchange product, [Pd(Cl)H(PH_2F)(PH_3)], **1c** (E = -9.3 kcal/mol) was formed via $\mathbf{TS_{1b\text{-}1c}}$ (E = 24.5 kcal/mol). Their structures are also in Figure 3.5 and selected bond lengths and inter-atomic distances are shown in Table 3.3.

	Bond Length or Atomic Distance / Å					
	Pd-H1	H1-P1	Pd-Cl	Pd-P2	Pd-P1	P1-F
1b	2.638	1.465	2.299	2.276	2.281	1.770
$\mathbf{TS_{1b\text{-}1c}}$	1.834	1.609	2.383	2.344	2.215	1.663
1c	1.557	2.880	2.431	2.302	2.267	1.655

Table 3.3: Selected computed bond lengths and distances in **1b**, $\mathbf{TS_{1b\text{-}1c}}$ and **1c**.

This process involves the reversal of many of the changes which occurred in the formation of **1b**. As the P1-H1 bond starts to break, the Pd-H1 bond starts to form in $\mathbf{TS_{1b\text{-}1c}}$, a process which is completed in **1c**. The Pd-P2 bond lengthens to 2.344 Å in $\mathbf{TS_{1b\text{-}1c}}$, for the reasons discussed previously, then shortens to 2.302 Å in **1b** as the Cl-Pd-P2 angle closes (Cl-Pd-P2: **1b** = 170.3º, $\mathbf{TS_{1b\text{-}1c}}$ = 138.4º, **1c** = 102.7º) and P2 returns to its previous position trans to P1. In **1c** both F and H1 lie in the metal coordination plane (F-P1-Pd-Cl = 179.0º, H1-P1-Pd-Cl = 179.0º).

Comparison of structures **1a** and **1c** shows that hydride has a much stronger trans influence than fluoride (Pd-Cl: **1a** = 2.334 Å, **1c** = 2.431 Å). Also, the Pd-P1 is shorter with the {PH_2F} ligand in **1c** than for PH_3 in **1a**. The electron-withdrawing effect of the fluoride in PH_2F makes the phosphine a better π-acceptor and results in the shortening of Pd-P1 by 0.05 Å.

3.6 OH/H exchange in *trans*-[Pd(Cl)OH(PH_3)$_2$]

3.6.1 OH-transfer from Pd onto PH_3

trans-[Pd(Cl)(OH)(PH_3)$_2$], **2a**, was the second molecule studied, and as mentioned in Chapter 1, it is an important complex as it is a model system for *trans*-[Pd(Cl)(OH)(PPh_3)$_2$], a key intermediate in a hydroxide-induced disproportionation reaction.[4]

The process of forming a metallophosphorane was the same as that described in the case of the fluoride analogue. No assumptions were made as to whether the isomerisation seen with fluoride would occur here, but it was found to be essential to allow the formation of a metallophosphorane intermediate.

By shortening the P1···O distance to 1.9 Å, then opening up the Cl-Pd-P2 angle in a stepwise manner, a transition state was found at the energy highpoint, which led to a metallophosphorane intermediate. The structures of **TS_{2a-2b}** (E = 28.3 kcal/mol) and metallophosphorane **2b** (E = 14.1 kcal/mol) can be seen in Figure 3.10, with key bond lengths shown in Table 3.4.

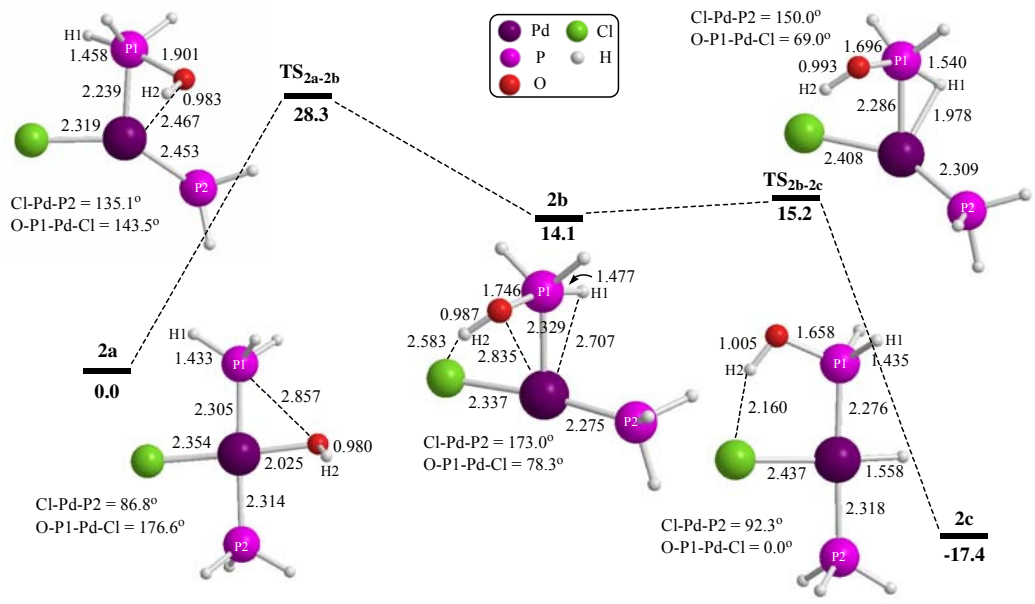

Figure 3.10: Profile for OH/H exchange in *trans*-[Pd(Cl)OH(PH_3)$_2$]. Energies in kcal/mol, bond lengths in Å.

	Bond Length or Atomic Distance / Å					
	Pd-O	O-P1	Pd-Cl	Pd-P2	Pd-P1	P1-H1
2a	2.025	2.857	2.354	2.314	2.305	1.433
$\mathbf{TS_{2a\text{-}2b}}$	2.467	1.901	2.319	2.453	2.239	1.458
2b	2.835	1.746	2.337	2.275	2.329	1.477

Table 3.4: Selected computed bond lengths and distances in **2a**, $\mathbf{TS_{2a\text{-}2b}}$ and **2b**.

It can be seen that the same geometric changes occur here during metallophosphorane formation as happened in the fluoride analogue. The most important changes to note are the cleavage of the Pd-O bond, formation of an O-P1 bond, the opening of the Cl-Pd-P2 angle (Cl-Pd-P2: **2a** = 86.8º, $\mathbf{TS_{2a\text{-}2b}}$ = 135.1º, **2b** = 173.0º) and the change in geometry around palladium and P1. The P1-O bond length of 1.746 Å is within the typical range for a P-O single bond in a metallophosphorane.[8] In **2a**, as in **1a**, the X group lies in the metal coordination plane (O-P1-Pd-Cl = 176.5º). As the P1-O bond forms in $\mathbf{TS_{2a\text{-}2b}}$, rotation around Pd-P1 causes the hydroxide to move out of the plane, reaching an approximately perpendicular position in **2b** (O-P1-Pd-Cl = 78.3º). A geometric feature that is not present in the fluoride system is the different orientations possible due to the location of the hydroxide hydrogen. In **2a** the H-O-Pd-Cl torsion angle is 163.7º, reducing to 62.1º in $\mathbf{TS_{2a\text{-}2b}}$, and further reducing to 29.2º in **2b**. This is coupled with a short Pd···H2 distance in $\mathbf{TS_{2a\text{-}2b}}$ (2.621 Å) and a short Cl···H2 distance in **2b**, both of which may be stabilising interactions.

The main difference between the fluoride and hydroxide pathways is the position of the X groups and the relative energies, which may be related issues. The hydroxide system has a slightly lower activation energy (by -0.7 kcal/mol) and a relatively more stable metallophosphorane (by 2.7 kcal/mol) than the fluoride analogue. The relative stability of the hydroxide pathway may be because a hydroxide hydrogen has the ability to form an interaction with palladium or chloride, an ability which fluoride does not possess. To investigate this possibility, calculations were performed on alternative structures where these interactions are removed by changing the position of the hydroxide hydrogen, H2, by rotation around P1-O by 180º, then transition state calculations were run. This led to the location of an alternative transition state structure, $\mathbf{TS'_{2a\text{-}2b}}$ (E = 30.3 kcal/mol). Once optimised, the H2 has repositioned from H2-O-Pd-Cl = 62.1º in $\mathbf{TS_{2a\text{-}2b}}$ to 164.1º in $\mathbf{TS'_{2a\text{-}2b}}$ and the H2···Pd distance has increased from 2.621 Å to

2.770 Å. The structure of this new transition state is shown in Figure 3.11, with the data for $\mathbf{TS_{2a\text{-}2b}}$ shown in parenthesis for comparison.

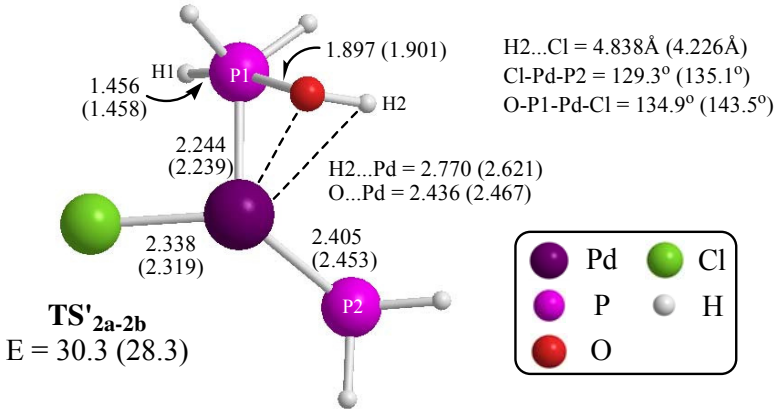

Figure 3.11: Structure of alternative transition state $\mathbf{TS'_{2a\text{-}2b}}$. Data for $\mathbf{TS_{2a\text{-}2b}}$ is shown in parenthesis. Energies in kcal/mol, distances in Å.

$\mathbf{TS'_{2a\text{-}2b}}$ links the same 4-coordinate reactant to metallophosphorane **2b**, but is 2 kcal/mol higher in energy than $\mathbf{TS_{2a\text{-}2b}}$. The effect of rotating the hydroxide group around the O-P1 bond is even more pronounced with the metallophosphorane structure, **2b**. A new geometry was optimised with a constraint to hold the alternative hydroxide orientation at 180º with respect to **2b**, and was found to be 8.7 kcal/mol less stable (SCF energy) than **2b**. Geometric constraints can make the energy artificially higher, but not by so much as to negate the effect being investigated.

These results seem to suggest that there are indeed stabilising interaction between H2 and palladium or chloride in $\mathbf{TS_{2a\text{-}2b}}$ and **2b** respectively. This may explain why the hydroxide metallophosphorane, **2b**, is more accessible than the fluoride analogue, **1b**.

3.6.2 H-transfer from P to Pd

To complete the profile H1 must break its bond to P1 and transfer onto palladium, to form exchange product **2c**, [PdCl(H)(PH_3)(PH_2OH)] (E = -17.4 kcal/mol). This was achieved by shortening the Pd···H1 distance from 2.707 Å in **2b** in a stepwise manner, and seeking a transition state at the energy highpoint. The structures of $\mathbf{TS_{2b\text{-}2c}}$ (E = 15.2 kcal/mol) and **2c** are shown in Figure 3.10 with key bond lengths in Table 3.5. The same structural changes occurred in the formation of product **2c** as were seen in the formation of **1c**. Comparison of the two analogous transition states, $\mathbf{TS_{1b\text{-}1c}}$ and $\mathbf{TS_{2b\text{-}2c}}$, shows that the transition state is much more easily formed in the hydroxide system, with

	Bond Length or Atomic Distance / Å					
	Pd-H1	H1-P1	Pd-Cl	Pd-P2	Pd-P1	P1-O
2b	2.523	1.477	2.337	2.275	2.329	1.746
TS_{2b-2c}	1.978	1.540	2.408	2.309	2.286	1.696
2c	1.558	2.690	2.437	2.318	2.276	1.658

Table 3.5: Selected computed bond lengths and distances in **2b**, **TS_{2b-2c}** and **2c**.

an activation energy of 1.1 kcal/mol from **2b**, compared to 7.7 kcal/mol from **1b**. H-transfer from **2b** may be assisted by the orientation of the {PH_3OH} group. In **2b** the O-P1-Pd-Cl torsion angle is 78.3º, meaning that H1 is close to the site to which it will transfer. However, in **1b** the F-P1-Pd-Cl angle is 118.4º, so the hydrogen has further to travel to reach the destination site in the metal coordination plane. **TS_{2b-2c}** is also earlier, with P1···H1 and Pd-P2 being shorter, Pd···H1 and Pd-P1 being longer, and a wider Cl-Pd-P2 angle of 150.0º compared to 138.4º in **TS_{1b-1c}**.

The main structural difference between the exchange products **1c** and **2c** is the orientation of the X group. In **1c** the fluoride has an F-P1-Pd-Cl torsion angle of 179.0º, which keeps the two halogen groups as far away from each other as possible. This means that a rotation must occur to deliver H1 onto palladium. However, in **2c** the O-P1-Pd-Cl angle is 0.0º, presumably due to the intramolecular hydrogen-bonding-type interaction between the chloride and H1, so it is already in a good orientation to transfer H1. A similar test as described earlier was performed on structure **2c** to see whether this interaction was stabilising the structure, by removing the H1···Cl interaction to see whether the product became less stable. The {PH_2OH} group was rotated around the P1-Pd bond by 180º and then allowed to optimise without constraint. The alternative minimum structure identified was found to be 10.8 kcal/mol less stable than **2c**, supporting the theory that the Cl···H1 interaction stabilises **2c**.

3.7 NH_2/H exchange in *trans*-[Pd(Cl)NH_2(PH_3)$_2$]

3.7.1 NH_2-transfer from Pd onto PH_3

The next X group to be investigated was the amido group, NH_2. Despite being another small, relatively electronegative ligand, NH_2 showed some very different behaviour from the hydroxide and fluoride analogous systems. In fact, NH_2 also behaved differently in the studies discussed at the beginning of the chapter, as it preferred to occupy an equatorial site in {PH_4R}, while fluoride preferred axial sites. All the structures with their corresponding energies are shown in Figure 3.12 and key bond lengths and distances are shown in Table 3.6.

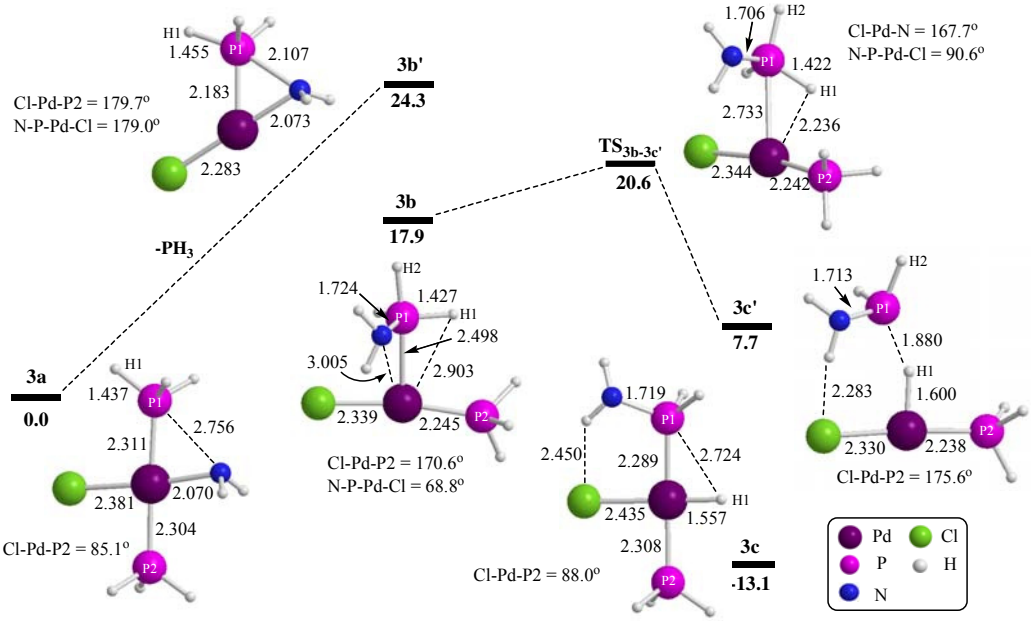

Figure 3.12: Profile for NH_2/H exchange in *trans*-[PdCl(NH_2)(PH_3)$_2$]. Energies in kcal/mol, bond lengths in Å.

The reactant, *trans*-[PdCl(NH_2)(PH_3)$_2$], **3a** (0.0 kcal/mol) was found to have a square planar geometry similar to the other reactants. The amido ligand exerts a stronger trans influence than the other X groups so far, with a trans Pd-Cl bond of 2.381 Å, almost 0.03 Å longer than in **2a**.

	Bond Length or Atomic Distance / Å						
	Pd-N	N-P1	Pd-Cl	Pd-P2	Pd-P1	P1-H1	Pd-H1
3a	2.070	2.756	2.381	2.304	2.311	1.437	-
3b'	2.073	2.107	2.283	-	2.183	1.455	-
3b	3.005	1.724	2.339	2.245	2.498	1.427	2.903
$TS_{3b-3c'}$	-	1.706	2.334	2.242	2.733	1.442	2.236
3c'	-	1.713	2.330	2.238	-	1.880	1.600
3c	-	1.719	2.435	2.308	2.289	2.724	1.557

Table 3.6: Selected calculated bond lengths and distances in structures from the NH_2/H exchange profile.

The methods previously described were employed to locate a transition state leading forward towards a metallophosphorane intermediate. However, it was not possible to find such a transition state, as the Pd-N bond would not break, even when the complex was forced to isomerise by opening the Cl-Pd-P2 angle. Instead, an N-Pd-P metallacycle was formed, and the spectator phosphine dissociated, forming structure **3b'** (E = 24.3 kcal/mol). No transition state was located for this process as the energy just rose as the Pd□P2 distance increased from 2.304 Å in **3a**. The geometry around the metal in **3b'** is a distorted 3-coordinate T-shape. In this case no isomerision was required between reactant and transition state, as the phosphine leaving created a vacant site opposite P1. The N□P1 distance shortened to 2.107 Å in **3b'** but the N-Pd bond remained intact, lengthening only by 0.003 Å.

Nitrogen has the ability to form a metallacycle because even after making a bond to P1, it has another lone pair to maintain the bond to the palladium. This type of Pd-P-N metallacycle has been seen in other metallophosphorane structures characterised experimentally. For example, Figure 3.13 shows the structure of [(η^2-cyclenP)PtClPPh_3] which was determined by Lattman *et al.*[9] using X-ray crystallography. This structure features a Pt-P-N metallacycle where the phosphorus is also pentacoordinated. The P1-N1 bond is shorter than P1-N in **3b'**; this difference may be due to the different axial substituent of N as opposed to H1 in **3b'**. One further difference is that there is a long Pt-Cl bond (2.440(4) Å) in [(η^2-cyclenP)PtClPPh_3]. Lattman suggests that this may be due to steric and/or electronic effects caused by the distortion from a square planar geometry within the metallacycle. Conversely, in **3b'** the Pd-Cl bond is quite short compared to the other structures in the profile (2.283 Å). This may be because the nitrogen has a reduced trans influence when it is part of a

metallacycle. It is not clear why the phosphine dissociates upon formation of the metallacycle in the model system, but is stable with the triphenylphosphine attached in this experimental system. It may be due to the strong trans influence of the {η^2-cyclenP} ligand.

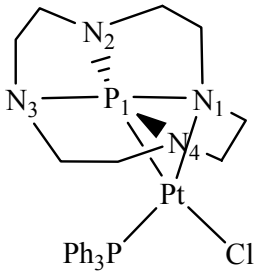

Angle	Angle / ^{o}
Cl-Pt-P1	148.1(1)
Cl-Pt-P2	100.7(1)
Cl-Pt-N1	97.6(3)
P1-Pt-P2	110.3(1)
P1-Pt-N1	51.0(3)
P2-Pt-N1	161.2(3)

Bond	Bond Length / Å
Pt-Cl	2.440(4)
Pt-P1	2.223(3)
Pt-P2	2.214(3)
Pt-N1	2.120(10)
P1-N1	1.872(11)
P1-N2	1.694(11)
P1-N3	1.698(11)
P1-N4	1.676(11)

Figure 3.13: Structure of [(η^2-cyclenP)PtClPPh$_3$] with selected bond lengths and angles.

Although a pathway was not found for transfer of the amido group from palladium to P1, it was possible to find a metallophosphorane structure which was similar to those seen with the other X groups. It was located by substituting the hydroxide group in **2b** with the amido group and optimising without constraints. The comparative energy of the minimum structure found, **3b** (E = 17.9 kcal/mol), is higher than the fluoride analogue (**1b** E = 16.8 kcal/mol) and the hydroxide analogue (**2b** E = 14.1 kcal/mol). The main structural difference between this amido metallophosphorane and **1b** and **2b** is the arrangement at P1. In **3b** P1 has a distorted trigonal bipyramidal geometry, with palladium in an axial position and NH_2 in an equatorial position, the opposite from in **1b** and **2b**. This is consistent with the findings in Section 3.2, where $PH_4(NH_2)$ with NH_2 in an axial position isomerised to the preferred equatorial isomer. The Pd-P1-H2 angle is 174.2º and N, H1 and H3 are coplanar with P1 (sum of equatorial angles around P1 is 359.1º). The Pd-P1 bond is long in **3b** at 2.498 Å. This may be because it is in an axial position on P1, rather than its usual equatorial position (Pd-P1: **1b** = 2.281 Å, **2b** = 2.329 Å). Axial bonds are normally longer than equatorial bonds in PF_5 and other phosphorus (V) halides, as discussed in Chapter 1. This effect is also exhibited in the difference between the P1-H bond lengths in **3b**: P1-H_{ax} = 1.468 Å, P1-H_{eq} = 1.427 Å and 1.439 Å.

3.7.2 H-transfer from P to Pd

Starting from **3b**, the Pd···H1 distance was reduced stepwise to facilitate the transfer of H1 from P1 onto palladium. A transition state, $\mathbf{TS_{3b\text{-}3c'}}$ (E = 20.6 kcal/mol), was found close to the energy highpoint in the scan. It is evident from the structure of $\mathbf{TS_{3b\text{-}3c'}}$ that this part of the profile is different from the fluoride and hydroxide systems. Firstly, the Pd···P1 distance is very long in $\mathbf{TS_{3b\text{-}3c'}}$ at 2.733 Å, compared to less than 2.3 Å in both $\mathbf{TS_{1b\text{-}1c}}$ and $\mathbf{TS_{2b\text{-}2c}}$. The geometry around P1 has also altered to a distorted tetrahedron, with the three N-P1-H angles in the range of 97-121º. The lengthening usually seen in the Pd-P2 bond in all the transition states so far is not present either, with Pd-P2 actually shortening by 0.003 Å from **3b**. There is only a small change in the Cl-Pd-P2 angle, which reduces by 2.9º from **3b**, which is much less than the change seen in the other systems.

It seems that although H1 is breaking its bond to P1 and forming a bond to palladium, the isomerisation around palladium that normally accompanies this is not present here. Instead, as H1 is transferring to palladium, the Pd-P1 bond is breaking, resulting in the dissociation of $\{PH_2NH_2\}$. Indeed, an IRC calculation confirmed that $\mathbf{TS_{3b\text{-}3c'}}$ leads to a structure where the Pd-P1 bond has broken and $\{PH_2NH_2\}$ has dissociated, to form structure **3c'** (E = 7.7 kcal/mol). The palladium now has a 3-coordinate T-shaped geometry with H1 trans to a vacant site. The Pd-Cl and Pd-P2 bonds are both slightly shorter than in **3b**, where the chloride and phosphine groups also lie trans to each other, possibly because there is less steric crowding around the palladium in **3c'** and the complex is 3- rather than 4-coordinate. The free $\{PH_2NH_2\}$ fragment has a trigonal pyramidal structure, with the three angles in the range of 97-111º. There is an interaction between P1 and H1 (1.880 Å) and between an amido hydrogen and the chloride (2.283 Å).

Although it was not possible to link it into the reaction profile, a 4-coordinate square planar product analogous to **1c** and **2c** was constructed by substituting the X group in **1c** with the amido group. The structure, **3c** (E = -13.1 kcal/mol), was optimised, but a transition state to link to a metallophosphorane species was not found. The structure was similar to that of **2c**, with a hydrogen-bonding interaction between an NH_2 hydrogen and chloride (2.450 Å), keeping the amido group on the same side of the molecule as the chloride (N-P1-Pd-Cl = 31.0º). This product is considerably more thermodynamically favourable than product **3c'**.

3.8 Me/H exchange in *trans*-[Pd(Cl)Me(PH_3)$_2$]

3.8.1 Me-transfer from Pd onto PH_3

It was of interest to investigate how the properties of the reaction profile would be affected by a hydrocarbyl X group, the simplest example of which being methyl. These systems are particularly relevant to the work discussed in Chapters 5 and 6, which look at methyl and phenyl exchange processes. The structures and energies for the profile when X = Me are shown in Figure 3.14, with bond lengths and distances in Table 3.7 below.

	Bond Length or Atomic Distance / Å						
	Pd-C1	C1-P1	Pd-Cl	Pd-P2	Pd-P1	P1-H1	Pd-H1
4a	2.076	3.166	2.431	2.299	2.305	1.430	-
TS_{4a-5b}	2.435	2.110	2.405	2.350	2.229	1.450	-
4b	3.036	1.910	2.367	2.254	2.383	1.467	2.421
TS_{4b-4c}	-	1.892	2.395	2.270	2.343	1.497	2.085
4c	-	1.863	2.417	2.302	2.292	2.760	1.561

Table 3.7: Selected calculated bond lengths and distances in structures from the Me/H exchange profile.

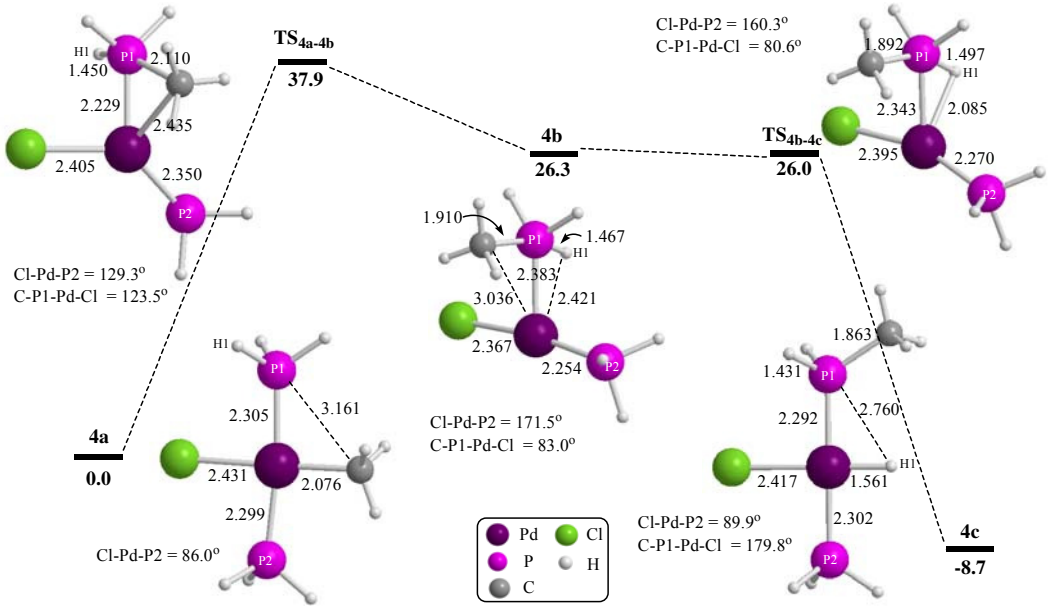

Figure 3.14: Profile for Me/H exchange in *trans*-[PdCl(Me)(PH_3)$_2$]. Energies in kcal/mol, bond lengths in Å.

The reactant, **4a**, *trans*-[PdCl(CH_3)(PH_3)$_2$] (set to 0.0 kcal/mol), was optimised and found to have a similar structure to the other reactants. The Pd-Cl bond is very long at 2.413 Å, indicating that methyl exerts a strong trans influence.

The standard method was used to locate a methyl-transfer transition state, **TS$_{4a-4b}$** (E = 37.9 kcal/mol), and IRC calculations confirmed that it leads to a metallophosphorane intermediate, **4b** (E = 26.3 kcal/mol). In geometric terms, **TS$_{4a-4b}$** seems to be earlier than the analogous structures from the fluoride and hydroxide pathways. This is exhibited by a longer P1···C distance of 2.110 Å (P1···F in **TS$_{1a-1b}$** = 1.908 Å) and a small Cl-Pd-P2 angle of 129.3º. **TS$_{4a-4b}$** also has a relatively long Pd-Cl bond (2.405 Å) and a short Pd-P2 bond (2.350 Å). Despite this, the activation energy is high at 37.9 kcal/mol. The comparative energy of **4b** is also considerably higher than the metallophosphoranes in the other systems investigated; the structure of **4b**, however, is similar to **1b**. The methyl group lies almost perpendicular to the metal coordination plane (C-P1-Pd-Cl = 83.0º), as there is no evidence for any stabilising interaction with the chloride, in contrast to the hydroxide and amido groups. The Pd-P1 bond is slightly longer than in the other metallophosphoranes in the series: for example it is 0.1 Å longer than in **1b**.

3.8.2 H-transfer from P to Pd

The pathway to the exchange product *trans*-[PdCl(H)(PH_3)(PH_2CH_3)], **4c** (E = -8.7 kcal/mol), was found by decreasing the Pd···H1 distance. An extremely early transition state was located, **TS$_{4b-4c}$** (E = 26.0 kcal/mol), the structure of which only shows small geometric changes from the structure of **4b**. In this case the transition state energy is actually lower than one of the minima it links to. This effect is often seen when a destabilising zero-point energy correction is made to SCF energies. If the pure electronic SCF energies of **4b** and **TS$_{4b-4c}$** are compared, the transition state is the less stable by 0.5 kcal/mol. However, when the zero-point energy correction is applied, the relative energy of the transition state is destabilised by less than that of **4b**, resulting in **TS$_{4b-4c}$** being 0.3 kcal/mol more stable than **4b**. This happens because a transition state, as a turning point with one imaginary frequency, is considered in a frequency calculation by the Gaussian program to have one less vibrational mode than a minimum (with 3N-7 rather than 3N-6 vibrational modes). If a minimum and a transition state are close in energy, this difference in the degree of destabilisation can lead to the transition state having a lower energy than the minimum. In this case, this results in there being

effectively no barrier for the H-transfer, meaning that Me/H exchange is a concerted reaction.

The structure of exchange product **4c** is very similar to the other products seen before. The methyl group lies almost 180º from chloride (C-P1-Pd-Cl = 179.8º), as seen in analogous fluoride complex **1c**, presumably for steric reasons. This Me/H exchange reaction is thermodynamically favourable by 8.7 kcal/mol.

3.9 Ph/H exchange in *trans*-[Pd(Cl)Ph(PH_3)$_2$]

3.9.1 Ph-transfer from Pd onto PH_3

The next variation of the X group to be investigated was phenyl. The structures and energies for the phenyl system are shown in Figure 3.15 with bond lengths and distances in Table 3.8.

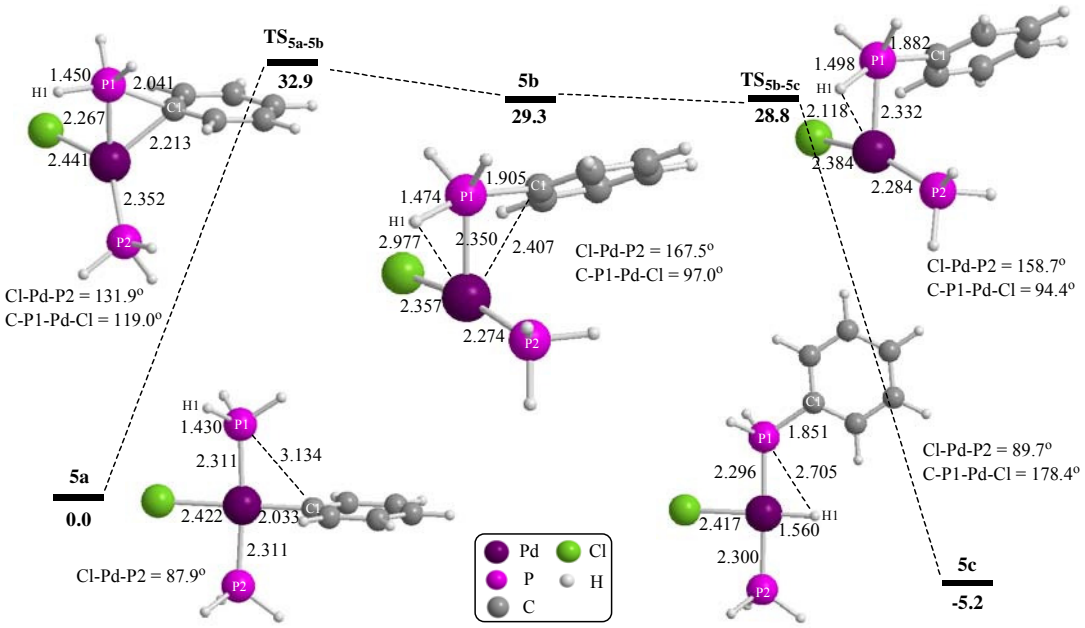

Figure 3.15: Profile for Ph/H exchange in *trans*-[PdCl(Ph)(PH_3)$_2$]. Energies in kcal/mol, bond lengths in Å.

	Bond Length or Atomic Distance / Å						
	Pd-C1	C1-P1	Pd-Cl	Pd-P2	Pd-P1	P1-H1	Pd-H1
5a	2.033	3.134	2.422	2.311	2.311	1.430	-
TS_{5a-5b}	2.213	2.041	2.441	2.352	2.267	1.450	-
5b	2.407	1.905	2.357	2.274	2.350	1.474	2.977
TS_{5b-5c}	-	1.882	2.384	2.284	2.332	1.498	2.118
5c	-	1.851	2.417	2.300	2.296	2.705	1.560

Table 3.8: Selected calculated bond lengths and distances in structures from the Ph/H exchange profile.

The reactant structure *trans*-[PdCl(C_6H_5)(PH_3)$_2$], **5a** (E = 0.0 kcal/mol), was optimised and found to have a square planar structure similar to the other reactants. Phenyl appears to have a strong trans influence, exceeded only by methyl in the series of reactants investigated. A transition state, **TS_{5a-5b}** (E = 32.9 kcal/mol), was identified to lead from **5a** to a metallophosphorane structure. It has structural features suggestive of an early transition state (P1-C = 2.041 Å), coupled with a high activation barrier – as was the case with the methyl system. The Cl-Pd-P2 angle in **TS_{5a-5b}** is small at 131.9º (compared to 139.7º in **TS_{1a-1b}**); the Pd-Cl bond has not shortened much towards its eventual length in **5b**, and Pd-P2 has not lengthened as much as in other analogous transition states. However, the phenyl group has rotated completely out of the metal coordination plane (C1-P1-Pd-Cl = 119.0º). The phenyl ring adopts an orientation perpendicular to the metal coordination plane in **TS_{5a-5b}**, as predicted by Hoffmann *et al.*[10]

3.9.2 H-transfer from P to Pd

The pathway continues with **TS_{5b-5c}** (E = 28.8 kcal/mol), which was located using the method previously described. As seen in the analogous Me/H exchange reaction, the second transition state is only slightly geometrically different to its corresponding metallophosphorane, and its energy is slightly lower - in this case E_a = -0.5 kcal/mol. This makes the formation of exchange product **5c**, *trans*-[PdCl(H)($H_2PC_6H_5$)(PH_3)] (E = -5.2 kcal/mol), a concerted process. Complex **5c** has a C1-P1-Pd-Cl torsion angle of 178.4º, meaning the chloride and phenyl group lie on opposite sides of the molecule, as seen with the analogous fluoride and methyl exchange products, **1c** and **4c**.

3.10 Summary of the effect of changing the X ligand on X/H exchange

Before going on to look at the ways in which changing the metal or the nature of the phosphine affects metallophosphorane formation and subsequent exchange, the results from varying the X ligand will be summarised. Table 3.9 shows the comparative energies of the five structures which are common to each reaction pathway, for each variation of the X ligand.

	Energy / kcal/mol				
X	**Reactant a**	**TS_{a-b}**	**Metallo-phosphorane b**	**TS_{b-c}**	**Exchange Product c**
F (1)	0	29.0	16.8	24.5	-9.3
OH (2)	0	28.3	14.1	15.2	-17.4
NH_2 (3)	0	-	17.9	-	-13.1
CH_3 (4)	0	37.9	26.3	26.0	-8.7
C_6H_5 (5)	0	32.9	29.3	28.8	-5.2

Table 3.9: Comparison of the comparative energies from X/H exchange in *trans*-$[PdCl(X)(PPh_3)_2]$, varying the X ligand.

Focusing first on the transition states which link structures **a** and **b**, with the activation energy E_a1, the more electronegative X groups have a lower activation energy than the less electron-withdrawing X groups. Since $\mathbf{TS_{a-b}}$ essentially features an intramolecular nucleophilic attack of the X group on a phosphine, it is logical that the process would be easier with more electronegative X groups as they make better nucleophiles. With this in mind, $\mathbf{TS_{2a-2b}}$ should be higher than $\mathbf{TS_{1a-1b}}$ due to electronegativity, however, as discussed earlier in the chapter, there seems to be intermolecular stabilisation occurring when X = hydroxyl.

Calculations were performed on a range of model molecules to obtain relative bond interaction (BI) energies for the bonds formed and broken in the exchange reaction profiles. The model molecules that were used are shown in Figure 3.16, with the relevant bonds highlighted by a dashed line. Molecule **ii** models the phosphorane part of the metallophosphorane intermediate structures (**b**), with a hydrogen atom in place of the palladium fragment. In each case, the energies of the two fragments were taken without allowing relaxation to occur, and compared to the optimised energy of the parent molecule.

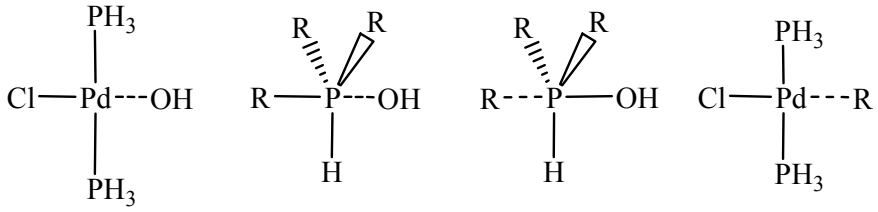

Figure 3.16: The model systems used to obtain BI energies (of dashed bonds) for OH/R exchange profiles.

$TS_{a\text{-}b}$ involves breaking a Pd-X bond and forming a P-X bond. Therefore, differences in BI energies will also play a role in the accessibility of these transition states. Table 3.10 shows calculated Pd-X and P-X BI energies for three of the X groups that were studied.

X	BI / $kcalmol^{-1}$ Pd-X[i]	P-X[ii]	ΔBI	E_a 1 ($TS_{a\text{-}b}$)	E of b
F (1)	100.5	129.8	29.3	29.0	16.8
OH (2)	74.8	97.7	22.9	28.3	14.1
Me (4)	66.0	68.5	2.5	37.9	26.3

Table 3.10: Comparison of BI energies for metallophosphorane formation, the initial step in X/H exchange in *trans*-$[PdCl(X)(PPh_3)_2]$, when X = F, OH, or Me.

If the profiles for F/H exchange and Me/H exchange are compared, it can be seen that the greater value of ΔBI when X = F results in a lower activation barrier and a more comparatively stable metallophosphorane species (**1b**) being formed. However, the analogous hydroxide system does not fit in with this trend. As the ΔBI value for X = OH is lower than when X = F, **$TS_{2a\text{-}2b}$** should be comparatively higher than **$TS_{1a\text{-}1b}$**, and **2b** should be less comparatively stable than **1b**. In fact, the reverse is true. This anomaly can be attributed to the stabilising interactions present in **$TS_{2a\text{-}2b}$** and **2b**, as discussed earlier in the chapter.

It is also worth noting that the barrier for transferring methyl onto PH_3 was calculated to be 5 kcal/mol higher than for the same process with phenyl. An earlier computational study by Hoffman *et al.*[10] using extended Hückel calculations on $[PdH_3(PH_2R)]^-$ (R = Me, Ph) investigated the relative barriers for transferring the R group from phosphorus to palladium. The absolute values are not helpful for comparison as they had

constraints on the geometries during the transfer, which was formally an oxidative addition. However, the overall result is relevant, that it is easier to transfer a phenyl group than a methyl. The process would also be expected to be more accessible with phenyl as it has a π-system that is able to strengthen the bonding interactions in the transition state by simultaneously interacting with the atoms it is transferring from and to, lowering the activation barrier.

The trend in the relative stabilities of the metallophosphorane structures follows the same trend as for ΔE_a1. This can partly be attributed to the ΔBI values discussed previously. Another factor could be the more electron-withdrawing X groups making the PH_3X ligand a better π-acceptor, which may be stabilising the intermediate species. There is evidence for this in the Pd-P1 bond lengths shown in Table 3.11. The increased π-back donation from the palladium shortens the Pd-P1 bond. This effect was discussed in Chapter 1, when comparing the Fe-P bond lengths in $[FeCp\{P(OC_6H_4NMe)_2\}(CO)_2]$ to $[FeCp\{P(OC_6H_4NMe)(OC_6H_4O)\}(CO)_2]$. The X-ray data showed that the Fe-P bond is shorter in the second complex (2.272(1) Å cf. 2.291(1) Å),[11] which has a more electron-poor phosphorus, making it a better π-acceptor. The exception to this trend is **3b** (X = NH_2), but in this case the palladium is in an axial site on P1, and as discussed earlier in the chapter, axial bonds in a TBP are longer than equatorial bonds.

X	**Pd-P1 Length / Å Metallophosphorane b**
F (1)	2.281
OH (2)	2.329
Ph (5)	2.350
Me (4)	2.383
NH_2 (3)	2.498

Table 3.11: Pd-P1 bond lengths (Å) in structure **b** when varying the X ligand.

The most comparatively stable metallophosphorane is seen when the X group is hydroxide. As demonstrated earlier, this structure can obtain extra stability by the hydroxide group forming a hydrogen-bonding-type interaction with chloride.

The second activation energy, E_a2, is smallest when the X group is methyl or phenyl, as shown in Table 3.12. In both of these cases $\mathbf{TS_{b\text{-}c}}$ is actually slightly lower in energy

than the preceding metallophosphorane structure due to the inclusion of zero point energy corrections on extremely small activation barriers. The process of H-transfer from {PH_3X} to palladium involves breaking a P-H bond and forming a Pd-H bond. Since the Pd-H bond formed is approximately the same in each case (all 1.56 Å), the nature of the {PH_3X} group and the ease of breaking the P-H bond are
the key to ΔE_a2. There is no obvious link between the P-H1 bond lengths in the metallophosphorane structures (X = F < CH_3 < C_6H_5 < OH) and the ease of breaking P-H1. It is possible that it is simply the greater electronegativity of fluoride and hydroxide which make the P-H1 bond harder to break than with methyl or phenyl as the X group. In general, it is easier to transfer a hydrogen than it is to transfer any of the X groups.

X	**E_a 2** / kcal/mol
F (1)	7.6
OH (2)	1.1
NH_2 (3)	-
Me (4)	-0.4
Ph (5)	-0.6

Table 3.12: Activation energy E_a2 (kcal/mol) for H-transfer from P to Pd.

The final energies to be analysed are the comparative stabilities of the exchange products, which all have the structure [PdCl(H)(PH_2X)(PH_3)] (*trans*-phosphine). Their energies are shown again in Table 3.13 alongside the Pd-P1 bond lengths for the different variations of X. The products with the more electronegative X groups - fluoride, hydroxide and amido - are more thermodynamically favourable than methyl and phenyl. However, the hydrogen-bonding-type interaction in products **2c** (Cl···H(O) = 2.160 Å) and **3c** (Cl···H(N) = 2.450 Å) seem to cause these two structures to be further stabilised.

As was seen with the metallophosphorane Pd-P1 bond lengths, shorter bonds are observed in the exchange products with more electronegative X groups. Hence Pd-P1 is longer when X is a hydrocarbyl group. Since all these structures have the same groups cis and trans to the PH_2X phosphine in the [PdCl(H)(PH_3)(PH_2X)] products, it can only be the nature of the X group that is affecting the Pd-P1 bond length.

X	Pd-P1 Length / Å Product c	Energy of c / kcal/mol
F (1)	2.267	-9.3
OH (2)	2.276	-17.4
NH_2 (3)	2.289	-13.1
Me (4)	2.292	-8.7
Ph (5)	2.296	-5.2

Table 3.13: The Pd-P1 bond lengths and relative energies in the exchange product structures, when varying the X ligand in [PdCl(H)(PH_3)(PH_2X)] (*trans*-PR_3).

It is surprising that the Pd-P1 bond is longer in **5c** than in **4c**, as $P(C_6H_5)_3$ would be expected to have a stronger π-acceptor ability than $P(CH_3)_3$.[12,13] However, the difference between the Pd-P1 in the methyl and phenyl systems is very small, and it is possible that the order would reverse with PX_3 rather than PH_2X.

To conclude, it is easier to form a metallophosphorane structure with a more electronegative X group. The resultant metallophosphoranes are more comparatively stable with electronegative X groups rather than hydrocarbyl groups. The activation energy is smaller for the H-transfer step than for metallophosphorane formation in all cases. The electronegative X groups also lead to the most thermodynamically favourable exchange products. Intramolecular interactions can lower the comparative energies of both minimum and transition state structures.

3.11 Cl/H exchange in *trans*-[Pd(Cl)$_2$(PH$_3$)$_2$]

3.11.1 Cl-transfer from Pd onto PH$_3$

One further variation of the X group was investigated: chloride. It was of interest to discover whether a larger, less electronegative halide would behave similarly to the smaller, harder halide, fluoride. Chloride was found to behave quite differently to fluoride, and in fact to all the other X groups investigated, which is why it has not been included in the general comparison.

The reactant, *trans*-[PdCl$_2$(PH$_3$)$_2$], was optimised, and is shown along with the Cl/H exchange profile in Figure 3.17. Table 3.14 shows key bond lengths and distances for all the species involved.

The structure of reactant **6a** (energy set to 0.0 kcal/mol) is very similar to the fluoride analogue, **1a**. Chloride and fluoride exert an almost identical trans influence, with the trans Pd-Cl bond being only 0.001 Å longer in **6a** than in **1a**. The transition state, **TS$_{6a-}$**

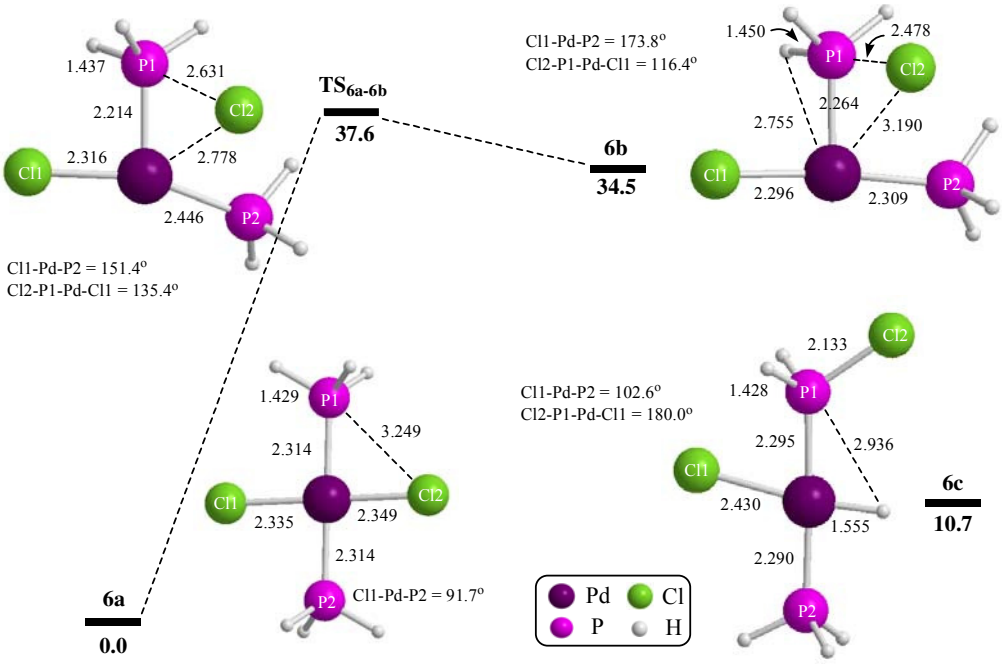

Figure 3.17: Profile for Cl/H exchange in *trans*-[PdCl(Cl)(PH$_3$)$_2$]. Energies in kcal/mol, bond lengths in Å.

	Bond Length or Atomic Distance / Å						
	Pd-Cl2	Cl2-P1	Pd-Cl1	Pd-P2	Pd-P1	P1-H1	Pd-H1
6a	2.349	3.249	2.335	2.314	2.314	1.429	-
TS_{6a-6b}	2.778	2.631	2.316	2.446	2.214	1.437	-
6b	3.190	2.478	2.296	2.309	2.264	1.450	2.755
6c	-	2.133	2.430	2.290	2.295	2.936	1.555

Table 3.14: Selected calculated bond lengths and distances in structures from the Cl/H exchange profile.

6b (E = 37.6 kcal/mol), was found in the standard way, but structural differences to the other X group profiles became apparent. **TS_{6a-6b}** displays a much later geometry than **TS_{1a-1b}**, with a large Cl1-Pd-P2 angle of 151.4º and a long Pd···Cl2 distance. The activation barrier is 8.6 kcal/mol higher than at **TS_{1a-1b}**.

Despite the long Pd···Cl2 distance, the P1···Cl2 distance is also unusually long, at 2.631 Å. This compares with the experimentally determined axial P-Cl bond length in PCl_5 of 2.127(3) Å.[14] **TS_{6a-6b}** was found to lead to an intermediate species, **6b** (E = 34.5 kcal/mol). This structure also features an extremely long P1···Cl2 distance of 2.478 Å. The P1-H1 bond is shorter than in the hydroxide and fluoride systems, probably due to the weak P1□Cl2 interaction trans to it. This structure could be considered as a tight ion pair between $[PdCl(PH_3)_2]^+$ and Cl^-. Whatever the description, **6b** is the most thermodynamically unfavourable intermediate seen so far in this series.

3.11.2 H-transfer from P to Pd

The Pd···H1 distance was reduced in the standard way in order to find a pathway linking species **6b** with the exchange product **6c** (E = 10.7 kcal/mol), *trans*-$[PdCl(H)(PH_3)(PH_2Cl)]$. However, all attempts to locate a transition state were unsuccessful. As seen before, as the Pd···H1 distance was shortened, the Cl1-Pd-P2 angle also started to reduce. The difference in this case was that as a vacant site became available, Cl2 would always form a bond to the palladium before H1 was able to, as the chloride is so loosely bound to P1. Exchange product **6c** (E = 10.7 kcal/mol) was optimised for comparison, and was found to have a similar structure to the fluoride product, **1c**. The Cl2-P1-Pd-Cl1 torsion angle is 180.0º, so the two halides are as far away from each other as possible, as seen in **1c**. An important difference is that **6c** is the first exchange product that is less stable than its corresponding reactant, at +10.7 kcal/mol.

Overall, Cl/H exchange from *trans*-[$PdCl_2(PH_3)_2$] does not occur through a similar mechanism to the other variations of the X group investigated. Species **6b** is difficult to form and is relatively unstable, with its very long P□Cl2 distance casting doubt over its true nature. H-transfer from **6b** was also problematic, resulting in the conclusion that X = Cl cannot be compared to exchange with the other X groups.

3.12 Changing the nature of the phosphine: *trans*-[Pd(Cl)(OH)(PH_3)(PR_3)] (R = F, Me)

The next aspect of the model system *trans*-[M(Cl)X(PR_3)(PH_3)] to be investigated was the effect of varying the R group in the active phosphine. To allow a direct comparison, X will be hydroxyl and M will be palladium, so that only the R group is varied. R = H has already been analysed in section 3.6; this will be compared with R = F and R = CH_3. The results will be presented for these two new exchange profiles, followed by a more general discussion of the effect of changing the nature of the active phosphine in these types of systems.

3.13 OH/F exchange in *trans*-[Pd(Cl)OH(PH_3)(PF_3)]

3.13.1 OH-transfer from Pd onto PF_3

The structures and energies of the profile for OH/F exchange will be compared to the OH/H exchange profile described earlier in the chapter. Selected bond lengths and distances are shown in Table 3.15; structures and the energy profile are displayed in Figure 3.18.

	Bond Length or Atomic Distance / Å						
	Pd-O	O-P1	Pd-Cl	Pd-P2	Pd-P1	P1-F1	Pd-F1
7a	2.100	2.065	2.312	2.347	2.252	1.639	-
TS7a-7b	2.479	1.787	2.288	2.500	2.196	1.647	-
7b	2.847	1.686	2.312	2.292	2.273	1.709	2.782
TS7b-7c	-	1.659	2.319	2.501	2.229	1.764	2.391
7c	-	1.623	2.356	2.332	2.279	3.062	1.958

Table 3.15: Selected calculated bond lengths and distances in structures from the OH/F exchange profile.

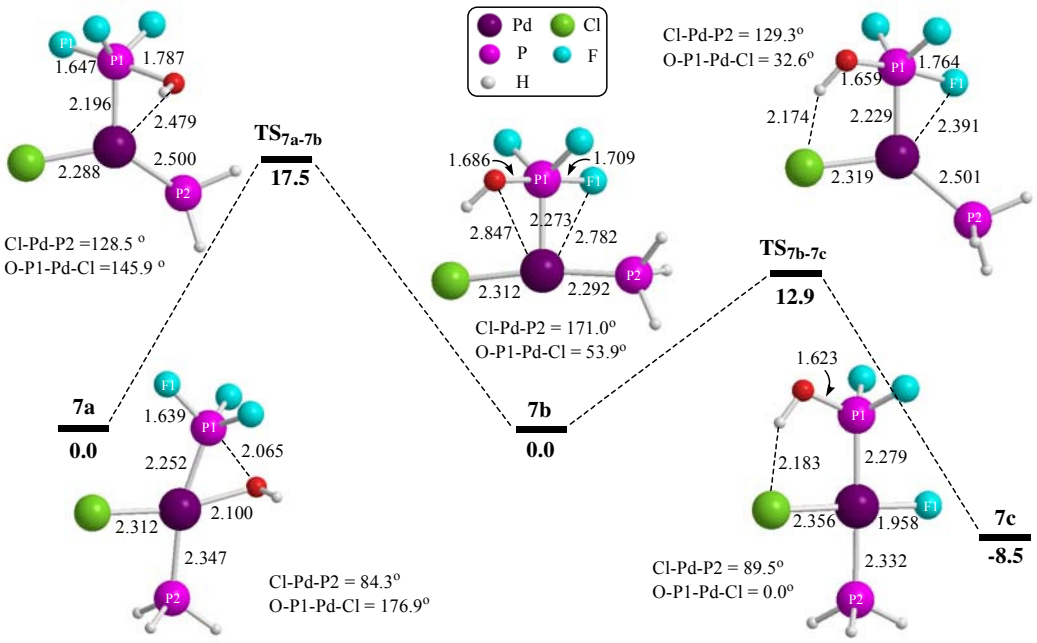

Figure 3.18: Profile for OH/F exchange in *trans*-[PdCl(OH)(PH_3)(PF_3)]. Energies in kcal/mol, bond lengths in Å.

The reactant structure *trans*-[Pd(Cl)OH(PF_3)(PH_3)], **7a** (set to 0.0 kcal/mol), was optimised. The structure is considerably distorted from a square planar geometry with a short O···P1 distance of 2.065 Å and a small P1-Pd-O angle of 56.5º. This O···P1 interaction may be the cause of the longer O-Pd bond observed (O-Pd: **7a** = 2.100 Å, **2a** = 2.025 Å). This in turn may disrupt the trans influence that the hydroxyl has on the chloride, leading to a shorter Pd-Cl bond (Pd-Cl: **7a** = 2.312 Å, **2a** = 2.354 Å). The Pd-P1 bond (2.252 Å) is shorter than the Pd-P2 bond (2.347 Å), due to the non-equivalence of the two phosphine ligands. This can be attributed to the better π-acceptor ability of PF_3 compared to PH_3. Generally, when the R group on a phosphine is more electronegative, the empty σ*-orbital on the phosphorus that is able to accept electron density from the metal becomes more stable. This allows better orbital overlap and a smaller energy mismatch with the donating dπ-orbital on the metal. Stronger π-back donation from the palladium leads to a shorter Pd-P bond. In some cases the σ-donating ability of the phosphine can also be an important factor affecting the Pd-P bond length. However, with electron-withdrawing fluorides on the phosphorus in this system, the σ-donating ability of the phosphorus to the metal should be reduced compared to PH_3. It therefore seems likely that π-effects are dominant in this particular case.

A transition state for OH-transfer was located using the method developed earlier in the chapter, namely by reducing the O···P1 distance, then opening the Cl-Pd-P2 angle in a scan. The transition state, **TS_{7a-7b}** (E = 17.5 kcal/mol), was found near the energy highpoint. This activation energy of 17.5 kcal/mol is extremely low, because P1 is very susceptible to nucleophilic attack as the fluorines withdraw electron density from the phosphorus. The O···P1 distance (1.787 Å) is much shorter than in **TS_{2a-2b}** (1.901 Å), and the Pd-P1 bond is also shorter in **TS_{7a-7b}** (2.196 Å) than in **TS_{2a-2b}** (2.239 Å), presumably due to the π-donation effects discussed above. The Pd-P2 bond, however, is long (Pd-P2: **TS_{7a-7b}** = 2.500 Å, **TS_{2a-2b}** = 2.453 Å).

IRC calculations showed that **TS_{7a-7b}** leads to a metallophosphorane intermediate, **7b** (E = 0.0 kcal/mol). This is by far the most stable metallophosphorane seen so far in this study. This stability may arise from π-back donation from palladium to P1. The case for good π-back donation is supported by the short Pd-P1 bond (2.273 Å) seen in **7b** compared to in **2b** (2.329 Å). The O-P1 bond is also shorter (O-P1: **7b** = 1.686 Å, **2b** = 1.746 Å), presumably due to the presence of the fluorine substituents on P1. There is a short Cl···H(O) interaction that causes the O-P1-Pd-Cl torsion angle to be small at 53.9º (24.4º less than in **2b**).

3.13.2 F-transfer from P to Pd

A transition state for the transfer of F1 from P1 onto palladium was found by shortening the Pd···F1 distance in a scan. **TS_{7b-7c}** (E = 12.9 kcal/mol) was found near the energy highpoint. While E_a1 is comparatively small in this profile, a high activation barrier of 12.9 kcal/mol is seen in the second stage of the exchange reaction. This barrier is more than ten times larger than the equivalent barrier in the R = H system at **TS_{2b-2c}**. This may be due to the strong P1-F1 bond which has to be broken. Consistent with the trend thus far, the Pd-P1 bond (2.229 Å) is shorter than in **TS_{2b-2c}** (2.286 Å). As in **TS_{7a-7b}** the Pd-P2 bond is long (2.501 Å) and the Cl-Pd-P2 angle is small at 129.3º. This results in P2 having a weak trans influence on the chloride, leading to a shorter Pd-Cl bond (2.319 Å) than in **TS_{2b-2c}** (2.408 Å).

TS_{7b-7c} leads forwards to exchange product *trans*-[PdCl(F)(PH_3)(PF_2OH)], **7c** (E = -8.5 kcal/mol). The structure of **7c** is very similar to the structure of **2c**. Surprisingly, the Pd-P1 bond is longer in **7c** than in **2c** (2.276 Å). **7c** has a shorter Pd-Cl bond (2.356 Å)

than **2c** (2.437 Å), indicating once again that hydride exerts a stronger trans influence than fluoride.

3.14 OH/Me exchange in *trans*-[Pd(Cl)OH(PH_3)(PMe_3)]

3.14.1 OH-transfer from Pd onto PMe_3

The third variation in the type of active phosphine which was investigated was R = CH_3, to see the effect that electron donating substituents on the phosphine would have on the reaction profile. Perhaps unsurprisingly, the profile for OH/Me exchange was found to be more similar to OH/H exchange than OH/F exchange. The structures and energies for this profile are shown in Figure 3.19 and selected bond lengths are in Table 3.16.

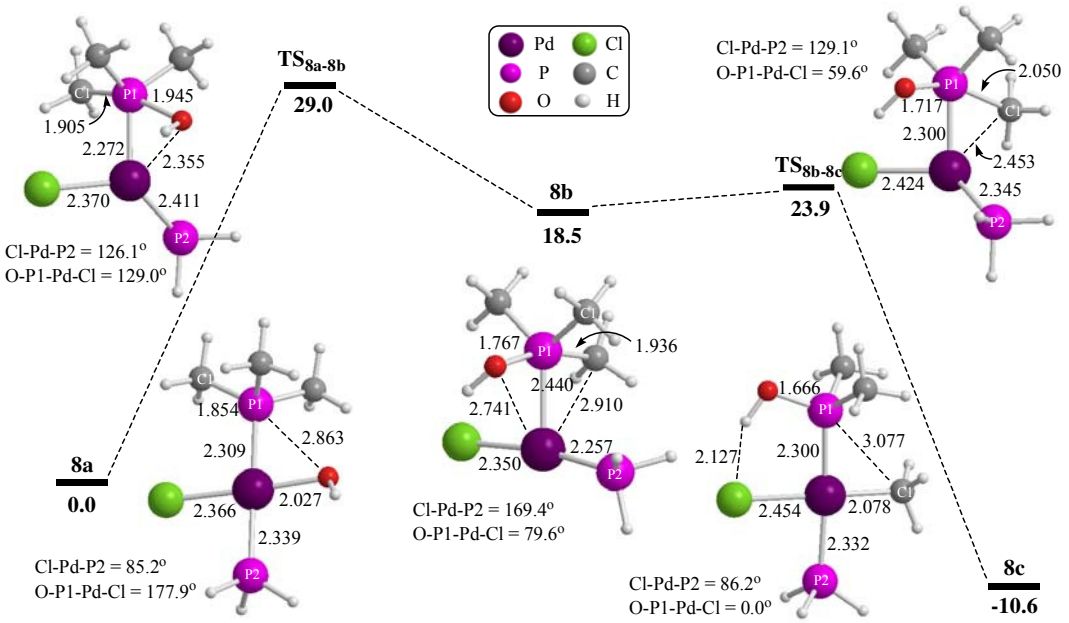

Figure 3.19: Profile for OH/Me exchange in *trans*-[PdCl(OH)(PH_3)(PMe_3)]. Energies in kcal/mol, bond lengths in Å.

Reactant *trans*-[PdCl(OH)(PMe_3)(PH_3)], **8a** (set to E = 0.0 kcal/mol) was optimised and found to be structurally very similar to reactant **2a**. The change in the nature of the phosphine has only caused a very small lengthening of 0.004 Å in the Pd-P1 bond and 0.025 Å in the Pd-P2 bond compared to **2a**. The added steric bulk on the active phosphine has little effect on the adjacent P1-Pd-Cl and P1-Pd-P2 angles, enlarging them by less than 1° each.

TS_{8a-8b} (E = 29.0 kcal/mol) was found using the standard methods, and IRC calculations confirmed that it links reactant **8a** to a metallophosphorane intermediate. Comparison

of the structures reveals that $\mathbf{TS_{8a\text{-}8b}}$ has a geometry indicative of an early transition state. For example, the hydroxyl is earlier in its transfer to P1, with a Pd···O distance 0.112 Å shorter and an O···P1 distance 0.044 Å longer than in $\mathbf{TS_{2a\text{-}2b}}$. The Cl-Pd-P2 angle is 9.0º smaller than in $\mathbf{TS_{2a\text{-}2b}}$, coupled with a smaller increase in the Pd-P2 bond length. The Pd-Cl bond has lengthened from 2.366 Å in **8a** to 2.370 Å in $\mathbf{TS_{8a\text{-}8b}}$, which seems counterintuitive, as the trans influence of hydroxyl has greatly lessened, which should shorten the Pd-Cl distance in the transition state. The activation barrier for metallophosphorane formation is 0.7 kcal/mol higher than for the same barrier in the profile where R = H. The positive inductive effect of the methyl groups will make P1 slightly more electron rich, making it less susceptible to nucleophilic attack, which may account for the slightly higher activation barrier.

	Bond Length or Atomic Distance / Å						
	Pd...O	O-P1	Pd-Cl	Pd-P2	Pd-P1	P1-C1	Pd-C1
8a	2.027	2.863	2.366	2.339	2.309	1.854	-
TS8a-8b	2.355	1.945	2.370	2.411	2.272	1.905	-
8b	2.741	1.767	2.350	2.257	2.440	1.936	2.910
TS8b-8c	-	1.717	2.424	2.345	2.300	2.050	2.453
8c	-	1.666	2.454	2.332	2.300	3.077	2.078

Table 3.16: Selected calculated bond lengths and distances in structures from the OH/Me exchange profile.

The metallophosphorane intermediate located, **8b** (E = 18.5 kcal/mol), is 4.4 kcal/mol less comparatively stable than **2b**. Nevertheless, the two compounds are structurally similar. The greatest difference is in the length of the Pd-P1 bond, which is longer in **8b** (2.440 Å) than in **2b** (2.329 Å). The connection between the Pd-P1 bond length and the electronegativity of the R groups on P1 will be discussed further in section 3.16.

3.14.2 H-transfer from P to Pd

A scan lengthening the P1···C1 distance in **8b** led to the discovery of a transition state, $\mathbf{TS_{8b\text{-}8c}}$ (E = 23.9 kcal/mol). The activation barrier for methyl transfer is 5.4 kcal/mol, higher than the barrier of 1.1 kcal/mol for the H-transfer in the OH/H exchange profile. The geometry of $\mathbf{TS_{8b\text{-}8c}}$ seems to bear features of a late transition state – with a long Pd-P2 bond (Pd-P2: $\mathbf{TS_{8b\text{-}8c}}$ = 2.345 Å, $\mathbf{TS_{2b\text{-}2c}}$ = 2.309 Å) and a small Cl-Pd-P2 angle (Cl-Pd-P2: $\mathbf{TS_{8b\text{-}8c}}$ =129.1º, $\mathbf{TS_{2b\text{-}2c}}$ = 150.0º). However, the transferring methyl group is still quite far from the palladium (Pd···C1 = 2.453 Å). It is typical for a methyl-

transfer to have a higher activation barrier than an H-transfer. This difference in barriers was studied by Low and Goddard[15] using theoretical methods to compare the reductive elimination of H_2 and CH_4 from palladium and platinum bisphosphine species. They pointed out that since a hydrogen atom's 1s orbital is spherical, it can simultaneously overlap with the two moieties to which it is forming and breaking a bond. Conversely, the sp^3 orbital of a methyl has a definite directionality, and so the methyl must change its orientation between breaking one bond and forming another. For this reason, the barrier to methyl-transfer should be considerably higher than the barrier to H-transfer.

The route forwards from $\mathbf{TS_{8b\text{-}8c}}$ to an exchange product, **8c** (E = -10.6 kcal/mol), was confirmed by IRC calculations. As with the previous systems, the exchange product formed has a square planar geometry with the two phosphine ligands trans to each other. In accordance with the other products containing a hydroxyl group, the hydroxyl lies in the metal coordination plane (O-P1-Pd-Cl = 0.0º) with an short distance between the hydroxyl hydrogen and the chloride (Cl···H(O) = 2.127 Å). All the other bond lengths in **8c** are very similar to those in **2c**, varying by less than 0.025 Å. The overall process of OH/Me exchange is thermodynamically favourable by 10.6 kcal/mol.

3.15 Summary of changing the nature of the phosphine

Varying the R group in *trans*-[PdCl(OH)(PH_3)(PR_3)] between R = H, F or CH_3 did not change the mechanism of metallophosphorane formation or OH/R exchange. However, it did affect the activation barriers and comparative stabilities of the structures, and geometric differences were also seen.

A summary of the comparative energies of the structures in each of the profiles where the R group is varied is shown in Table 3.17. The trends in the activation energies and the stability of the minima will be discussed in turn.

	Structure				
R	**a**	**$TS_{a\text{-}b}$**	**b**	**$TS_{b\text{-}c}$**	**c**
F	0.0	17.5	0.0	12.9	-8.5
H	0.0	28.3	14.1	15.2	-17.4
CH_3	0.0	29.0	18.5	23.9	-10.6

Table 3.17: Comparative energies (kcal/mol) of the five structures in each OH/R exchange profile, varying the R groups in the active phosphine.

The energies of the first activation barrier, E_a1, corresponding to the transfer of hydroxyl from palladium to phosphorus, are equivalent to the $\mathbf{TS_{a\text{-}b}}$ energies shown in Table 3.17. This step in the reaction can be considered essentially as a nucleophilic attack of hydroxy on the phosphorus in PR_3. Therefore, the accessibility of the reaction will be governed by the nucleophilicity of the attacking group and the susceptibility of the phosphorus to nucleophilic attack. In this case the attacking group, hydroxy, is common to all three profiles. The differences lie in the way that varying the R group changes the environment around the phosphorus. When R = F, the electronegative fluorine atoms withdraw electron density from P1, making it more electron poor, and thus more susceptible to nucleophilic attack by the hydroxy group. Conversely, when R = CH_3, the methyl groups' positive inductive effect push electron density onto P1, making it more electron rich and subsequently less susceptible to nucleophilic attack. When R = H, the electronegativity value is between those of the two other R groups, but closer to the value of methyl, which is reflected in the values of E_a1 when R is varied F < H < CH_3.

When progressing from the reactant structures, **a**, to the metallophosphorane intermediate species, **b**, a Pd-O bond is broken and a P-O bond is formed. The Pd-O / P-O BI energies are shown along with the comparative energies of the metallophosphorane structures in Table 3.18. An approximately equivalent Pd-O bond is broken in all three systems, however the strengths of the P-O bonds formed vary depending on the R groups attached to the phosphorus. It can be seen that the P-O bond formed when R = F is the strongest of the three, and this is consistent with the very stable metallophosphorane formed. The P-O bond is weakest when R = Me, presumably due to the more electron rich phosphorus, and this corresponds to the least stable metallophosphorane of the three.

R	BI / kcal/mol		ΔBI (P-O) - (Pd-O)	Energy of b / kcal/mol
	Pd-O[i]	P-O[ii]		
F	74.8	102.2	27.4	0.0
H	74.8	97.7	22.9	14.1
CH_3	74.8	89.2	14.4	18.5

Table 3.18: Calculated BI energies in **i**, trans-$Pd(OH)Cl(PH_3)_2$, and in **ii**, fac-$PR_3H(OH)$.

There is also a trend in these metallophosphorane structures that as the relative stability decreases, the Pd-P1 bond lengthens (Pd-P1: **7b** = 2.273 Å, **2b** = 2.329 Å, **8b** = 2.440 Å). This is likely to be similar to the effect seen in metal-phosphine bonds, where more electronegative substituents on the phosphine improve π-bonding with the metal, thus shortening the metal-phosphorus bond. This appears to stabilise the metallophosphorane structures. Indeed, the literature examples of characterised metallophosphorane structures feature electronegative heteroatoms attached to the pentacoordinated phosphorus,[2] suggesting that their presence is indeed a stabilising influence.

The barrier to formation of an exchange product, E_a2, is smaller than E_a1 in all three profiles. In E_a2 a P-R bond must be broken, so clearly a variation in R should affect the magnitude of the activation barrier. The calculated relative P-R BI energies are shown in Table 3.19. It can be seen that breaking a strong P-F bond results in a larger activation barrier than breaking a weaker P-C or P-H bond. The barrier for transferring hydrogen from phosphorus to palladium would be expected to be lower than the barrier for transferring methyl, for the reasons of directionality discussed in Section 3.14.2.

R	BI of P-R[ii] / kcal/mol	E_a2 / kcal/mol
F	121.8	12.9
H	72.7	1.1
CH_3	73.2	5.4

Table 3.19: Calculated BI energies in **ii**, fac-$PR_3H(OH)$, and values for E_a2 (kcal/mol).

The overall exchange process involves the breaking of a Pd-O and a P-R bond, and the formation of a P-O and a Pd-R bond, to form product structure **c**. The BI energies for the three profiles are shown in Table 3.20, along with the relative energies of structure **c**. Since the overall ΔBI = (bonds formed – bonds broken) and the value is positive, it equates to energy being released by the process. Indeed, all three profiles are exothermic. The greatest value for ΔBI is when R = H, and this also corresponds to the most thermodynamically favourable product, **2a** (E = -17.4 kcal/mol). Conversely, the smallest overall ΔBI value is seen for R = F, which produces the least stable product, **7a** (E = -8.5 kcal/mol).

R	BI / kcal/mol				ΔBI	E of c
	Pd-O[i]	**P-O[ii]**	**P-R[ii]**	**Pd-R[iii]**	**Overall**	**/ kcal/mol**
F	74.8	102.2	121.8	100.5	6.1	-8.5
H	74.8	97.7	72.7	76.5	26.7	-17.4
CH_3	74.8	89.2	73.2	66.0	7.2	-10.6

Table 3.20: Calculated BI energies in **i** *trans*-Pd(OH)Cl(PH_3)$_2$, **ii** *fac*-$PR_3H(OH)$ and **iii** *trans*-Pd(R)Cl(PH_3)$_2$.

As discussed in section 3.13.1, the electronegativity of the R groups in PR_3 can affect the length of a bond between the phosphorus and a metal centre. Usually stronger π-back donation from palladium to phosphorus, and thus a shorter Pd-P bond, is seen with more electronegative R groups. Indeed, this trend was seen during the work reported here, with the Pd-P1 bonds increasing in length as the electronegativity of the R group decreased F > H > CH_3. This was the case for all of the structures in the reaction profiles, apart from the exchange products, **7c**, **2c** and **8c**. In these structures the Pd-P1 bond lengths were all close in value (Pd-P1: **7c** = 2.279 Å, **2c** = 2.276 Å, **8c** = 2.300 Å). However, the effect of the electronegativity of the R group will be diluted in these structures by the exchange of one R group in the active phosphine by a hydroxy group.

To summarise, having more electronegative R groups on the active phosphine lowers E_a1 by making the active phosphine more susceptible to nucleophilic attack. However, the value of E_a2 is likely to increase, as a strong P-R bond must be broken. The most stable metallophosphorane structure is seen with electronegative R groups, but they produce a less thermodynamically stable exchange product.

3.16 Changing the metal centre: *trans*-[M(Cl)(OH)(PH_3)$_2$] (M = Ni, Pt)

The final variation to be examined in the [MClX(PH_3)(PR_3)] model system is the effect of changing the metal. To allow a direct comparison, X is hydroxide and R is hydrogen for this section. Although a wide range of main group and transition metals can be found in metallophosphoranes, this work will focus on the group 10 transition metal triad.

3.17 OH/H exchange in *trans*-[Ni(Cl)OH(PH_3)$_2$]

3.17.1 OH-transfer from Ni onto PH_3

The reactant structure, *trans*-[NiCl(OH)(PH_3)$_2$], was constructed by substituting nickel for palladium in **2a**, then optimising the structure. This new reactant, **9a** (E = 0.0 kcal/mol) has a very similar square planar structure to **2a**. The four metal-ligand bonds are 0.1-0.2 Å shorter in **9a** than in **2a**, which is consistent with the smaller metal centre. The structures and energies for the nickel profile can be seen in Figure 3.20, with key bond lengths and distances in Table 3.21.

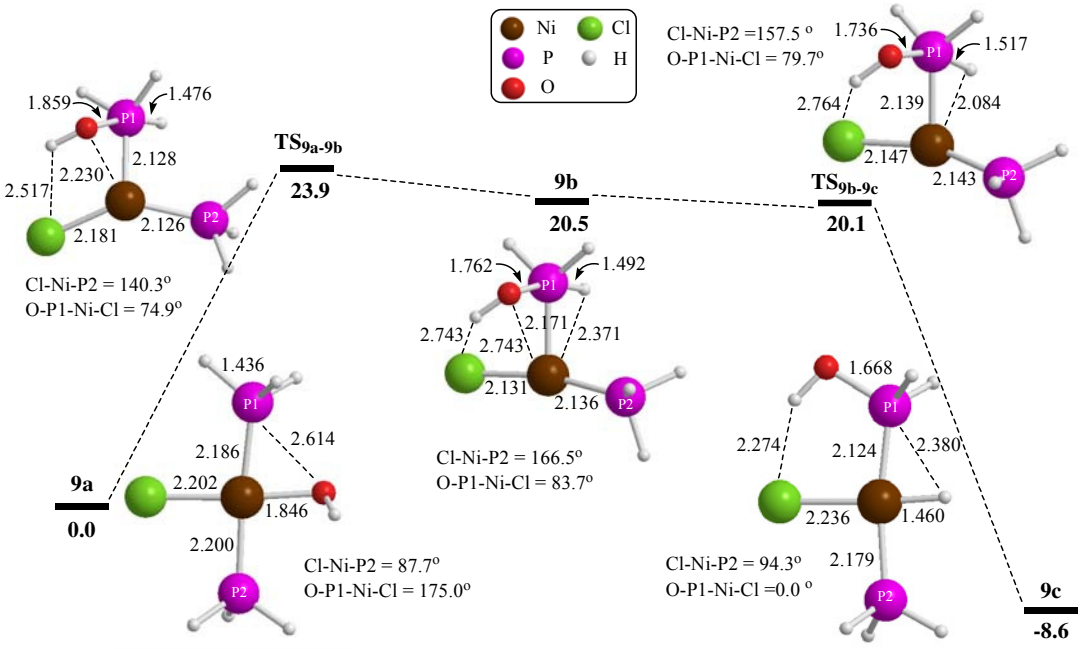

Figure 3.20: Profile for OH/H exchange in *trans*-[NiCl(OH)(PH_3)$_2$]. Energies in kcal/mol, bond lengths in Å.

The P1···O distance was shortened, followed by the opening of the Cl-Ni-P2 angle, in order to locate a transition state, **$TS_{9a\text{-}9b}$** (E = 23.9 kcal/mol), for the transfer of OH onto P1. The structure indicates that **$TS_{9a\text{-}9b}$** is a later transition state than **$TS_{2a\text{-}2b}$**, with a 5.2º larger Cl-M-P2 angle, a 0.04 Å shorter P1···O distance and a much shorter M-P2 bond (M-P2: **$TS_{9a\text{-}9b}$** = 2.126 Å, **$TS_{2a\text{-}2b}$** = 2.453 Å). The OH group lies much closer to the chloride, with an O-P1-Ni-Cl torsion angle of 74.9º (O-P1-Pd-Cl = 143.5º in **$TS_{2a\text{-}2b}$**) and a Cl···H distance of 2.517 Å.

	Bond Length or Atomic Distance / Å						
	Ni-O	O-P1	Ni-Cl	Ni-P2	Ni-P1	P1-H1	Ni-H1
9a	1.846	2.614	2.202	2.200	2.186	1.436	-
$TS_{9a\text{-}9b}$	2.230	1.859	2.181	2.126	2.128	1.476	-
9b	2.743	1.762	2.131	2.136	2.171	1.492	2.371
$TS_{9b\text{-}9c}$	-	1.736	2.147	2.143	2.139	1.517	2.084
9c	-	1.668	2.236	2.179	2.124	2.380	1.460

Table 3.21: Selected calculated bond lengths and distances in structures from the OH/H exchange profile (M = Ni).

The activation energy for the transfer of OH from Ni onto P1 is 4.4 kcal/mol lower than in the equivalent profile where M = Pd. The energy required to break a Ni-O bond (74.3 kcal/mol)[16] is very similar to a Pd-O bond (74.8 kcal/mol)[17] so that cannot be the cause of the difference in barriers. The Cl···H interaction in **$TS_{9a\text{-}9b}$** may lead to extra stabilisation. To test this theory, an alternative transition state structure was computed by substituting nickel for palladium in **$TS'_{2a\text{-}2b}$** (see Figure 3.11) and running a transition state calculation. As suspected, when the Cl···H interaction was removed, the transition state raised in energy by 5 kcal/mol.

IRC calculations confirmed that **$TS_{9a\text{-}9b}$** leads forward to a metallophosphorane intermediate, **9b** (E = 20.5 kcal/mol). **9b** appears to have a lesser H···Cl interaction than **2b**, with a 0.16 Å longer Cl···H distance and a 5.4º larger O-P1-M-Cl torsion angle. This may contribute to **9b** being comparatively less stable than **2b**. In contrast to the other metallophosphorane structures optimised so far, the M-P1 is shorter in the intermediate, **9b**, than in the reactant, **9a**. The Ni-Cl bond is **9b** is 0.071 Å shorter than in **9a** (cf. **2b** is 0.017 Å shorter than **2a**), possibly due to the smaller Cl-M-P2 angle (Cl-

M-P2: **9b** = 166.5º, **2b** = 173.0º) reducing the trans influence of the phosphine. It is not obvious why **9b** is considerably less comparatively stable than **2b**.

3.17.2 H-transfer from P to Ni

It is essentially a barrierless process to transfer hydrogen from P1 onto the nickel, with $\mathbf{TS_{9b\text{-}9c}}$ (E = 20.1 kcal/mol) lying 0.4 kcal/mol lower in energy than **9b**. It is therefore not surprising that $\mathbf{TS_{9b\text{-}9c}}$ has geometric features of an early transition state, with a short P1-H1 bond (1.517 Å) and a large Cl-Ni-P2 angle (157.5º). The H···Cl interaction seen in **9b** is still present in $\mathbf{TS_{9b\text{-}9c}}$, with an H···Cl distance of 2.764 Å and an O-P1-Ni-Cl torsion angle of 79.7º. $\mathbf{TS_{9b\text{-}9c}}$ leads forwards to an exchange product, **9c** (E = -8.6 kcal/mol). It has a slightly distorted square planar structure, with a reduced P1-M-H angle (P1-M-H: **9c** = 80.9º, **2c** = 87.0º) and a larger P1-M-Cl angle (P1-M-Cl: **9c** = 95.3º, **2c** = 90.5º) compared to the palladium system. **9b** is less thermodynamically favourable than **2c** by 8.8 kcal/mol.

3.18 OH/H exchange in *trans*-[Pt(Cl)OH(PH_3)$_2$]

3.18.1 OH-transfer from Pt onto PH_3

The reactant, *trans*-[PtCl(OH)(PH_3)$_2$], **10a** (E = 0.0 kcal/mol) was optimised first. All of the structures and energies for the platinum profile are shown in Figure 3.21, with key bond lengths in Table 3.22. The structure and bond lengths for **10a** are very similar to those in **2a**, which is not surprising as palladium and platinum have similar ionic radii ($r_{ion}(Pd^{2+})$ = 1.00 Å, $r_{ion}(Pt^{2+})$ = 0.94 Å).

The P1···O distance was shortened and fixed, followed by stepwise opening of the Cl-Pt-P2 angle, which led to the discovery of $\mathbf{TS_{10a\text{-}10b}}$ (E = 36.9 kcal/mol) at the energy highpoint. This transition state was similar to $\mathbf{TS_{2a\text{-}2b}}$ in the Cl-M-P2 angle (0.2º larger) and the O-P1-M-Cl torsion angle (2.1º larger), but also in the M-Cl distance (0.013 Å longer) and M-P1 distance (0.014 Å longer). However, the M-P2 bond is 0.062 Å shorter, despite the similar Cl-M-P2 angles. Also, the P1···O distance is 0.029 Å longer. Overall though, the structures are similar, which is why it is surprising that the activation energy in the platinum profile is 8.6 kcal/mol higher than in the palladium profile. The fact that a Pt-O bond (BI = 79.4 kcal/mol)[18] is stronger than a Pd-O bond (74.8 kcal/mol)[17] may contribute to the comparative instability of $\mathbf{TS_{10a\text{-}10b}}$.

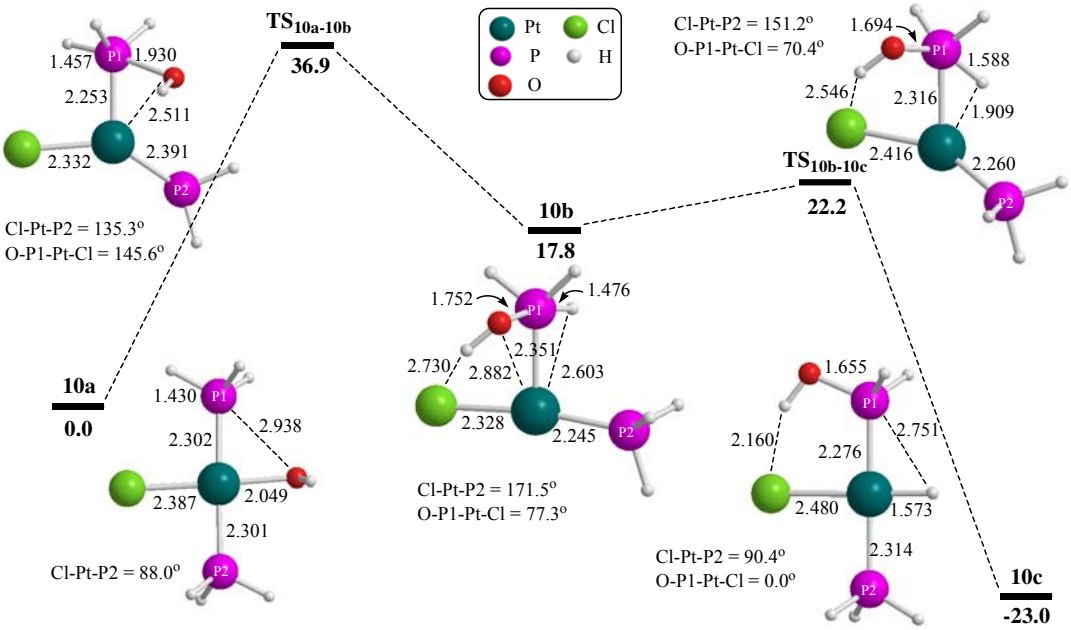

Figure 3.21: Profile for OH/H exchange in *trans*-[PtCl(OH)$(PH_3)_2$]. Energies in kcal/mol, bond lengths in Å.

	Bond Length or Atomic Distance / Å						
	Pt-O	O-P1	Pt-Cl	Pt-P2	Pt-P1	P1-H1	Pt-H1
10a	2.049	2.938	2.387	2.301	2.302	1.430	-
$TS_{10a-10b}$	2.511	1.930	2.332	2.391	2.253	1.457	-
10b	2.882	1.752	2.328	2.245	2.351	1.476	2.603
$TS_{10b-10c}$	-	1.694	2.416	2.260	2.316	1.588	1.909
10c	-	1.655	2.480	2.314	2.276	2.751	1.573

Table 3.22: Selected calculated bond lengths and distances in structures from the OH/H exchange profile (M = Pt).

IRC calculations showed that as expected, **$TS_{10a-10b}$** leads to a metallophosphorane intermediate, **10b** (E = 17.8 kcal/mol). Despite the Cl-M-P2 angle being only 1.5º smaller than in **2b**, the Cl-M and P2-M bonds are both shorter in **10b** (Cl-M: **10b** = 2.328 Å, **2b** = 2.337 Å; P2-M: **10b** = 2.245 Å, **2b** = 2.275 Å). However, the M-P1 bond is 0.022 Å longer in **10b**. The Cl···H distance is 0.147 Å longer in **10b** than in **2b**, and as this has been proven to be a stabilising interaction in other structures in this chapter, this may contribute to **10b** being 3.7 kcal/mol less comparatively stable than **2b**.

3.18.2 H-transfer from P to Pt

Shortening the Pt···H distance in **10b** led to the location of $\mathbf{TS_{10b\text{-}10c}}$ (E = 22.2 kcal/mol). Again, the structure of the transition state is similar to the analogous structure in the palladium profile, $\mathbf{TS_{2b\text{-}2c}}$. The main difference is that H1 is further on in its transfer from P1 to the metal, with a 0.048 Å longer P1···H1 distance and a 0.069 Å shorter H1···M distance than in $\mathbf{TS_{2b\text{-}2c}}$. The rest of the structure is similar, with just a 0.049 Å shorter M···P2 bond worth noting. The activation energy for H-transfer is 4.4 kcal/mol, a little larger than in the palladium profile (E_a2 = 1.1 kcal/mol), perhaps due to the slightly later transition state.

When the P1···H bond is completely broken, an exchange product, **10c** (E = -23.0 kcal/mol), is formed. This product has the same square planar structure seen in all of the previous exchange products. As expected, the hydroxy group lies in the metal coordination plane (O-P1-Pd-Cl = 0.0º) and has an H···Cl interaction at a distance of 2.160 Å. Overall, the platinum exchange process is 5.6 kcal/mol more thermodynamically favourable than for palladium.

3.19 Summary of changing the metal centre

The comparative energies for the five structures that make up the exchange profile for each group 10 metal are shown in Table 3.23. The factors affecting the differences in these energies will be discussed in turn.

	Structure				
M	**a**	**$TS_{a\text{-}b}$**	**b**	**$TS_{b\text{-}c}$**	**c**
Ni	0.0	23.9	20.5	20.1	-8.6
Pd	0.0	28.3	14.1	15.2	-17.4
Pt	0.0	36.9	17.8	22.2	-23.0

Table 3.23: Comparative energies (kcal/mol) of the five structures in each reaction profile, varying the metal centre.

Firstly, it can be seen that the initial activation energies (E_a1 = $\mathbf{TS_{a\text{-}b}}$) increase in magnitude down the triad from nickel to platinum. This process involves the breaking of the M-O bond in the reactant. Table 3.24 shows that the higher activation energies correspond to the breaking of stronger M-O bonds. Although, the Ni-O and Pd-O BI energies are very close in value, which does not explain the 4.4 kcal/mol difference in

E_a1. This may be due to a stabilising Cl□H(O) interaction in **TS_{9a-9b}** which is not present in **TS_{2a-2b}**.

M	BI M-O[iv]	E_a1
Ni	74.3	23.9
Pd	74.8	28.3
Pt	79.4	36.9

Table 3.24: Calculated BI energy (kcal/mol) in **iv** *trans*-M(OH)Cl(PH_3)$_2$ and the first activation energy for each profile.

The correlation between bond strengths and comparative stability is unclear for the metallophosphorane intermediates, **b**. As Table 3.25 shows, to form the intermediates, varying strengths of M-O bonds must be broken, but equivalent P-O bonds are formed. In fact, the nickel system has the most energy released from bond cleavage and formation, but has the least comparatively stable intermediate. Clearly other factors are at work. One such factor may be the stabilising interaction between H1 and Cl in the intermediate structures. The palladium intermediate has the shortest Cl···H distance (Cl···H: Ni **9b** = 2.743 Å, Pd **2b** = 2.583 Å, Pt **10b** = 2.730 Å), which may contribute to the fact that it is the most comparatively stable intermediate in the triad.

M	BI energies / kcal/mol			
	M-O[iv]	P-O[v]	ΔBDE	b
Ni	74.3	97.7	23.4	20.5
Pd	74.8	97.7	22.9	14.1
Pt	79.4	97.7	18.3	17.8

Table 3.25: Calculated BI energies in **iv** *trans*-M(OH)Cl(PH_3)$_2$ and **v** *fac*-$PR_3H(OH)$ and the comparative energies of the intermediate structures, **b** (kcal/mol).

The second activation energy, E_a2, requires a P-H bond in intermediate **b** to be broken, to allow H-transfer to the metal. The P-H bonds should all be of similar strengths in the three systems. In the nickel profile there is no barrier to H-transfer (E_a2 = -0.4 kcal/mol). Intermediate **9b** has a longer P-H1 bond and a shorter H1···Pd distance than in either **2b** or **10b**, which may aid the H-transfer. There is a small barrier to H-transfer

in the palladium (E_a2 = 1.1 kcal/mol) and platinum (E_a2 = 4.4 kcal/mol) systems, but the range of values is much smaller than for the first activation energy.

Finally, the comparative energies of the products, **c**, are also a measure of how thermodynamically favourable the exchange process is for each group 10 metal system. Table 3.26 shows the BI strengths of the bonds formed and broken in the exchange process, along with the overall energy released (ΔBI) and the comparative energies of the products, **c**. It can be seen that the ΔBI values are directly proportional to the increasing thermodynamic stability of the three exchange profiles. Thus, the exchange process is most thermodynamically favourable when M=Pt, mainly due to the strong Pt-H bond formed.

Overall, the highest activation barriers are seen when M = Pt, but the most thermodynamically stable product is formed.

M	BI energies / kcal/mol				ΔBI Overall	E of c / kcal/mol
	M-O[iv]	P-O[v]	P-H[v]	M-H[vi]		
Ni	74.3	97.7	72.7	67.2	17.9	-8.6
Pd	74.8	97.7	72.7	76.5	26.7	-17.4
Pt	79.4	97.7	72.7	86.4	32.0	-23.0

Table 3.26: Calculated BI energies in **iv** *trans*-$M(OH)Cl(PH_3)_2$, **v** *fac*-$PR_3H(OH)$ and **vi** *trans*-$M(R)Cl(PH_3)_2$ and the comparative energies of the product structures, **c** (kcal/mol).

3.19 References

[1] Nakazawa, H.; Kubo, K.; Miyoshi, K., *Bull. Chem. Soc. Jpn*, **74**, 2255, (2001)

[2] a) Wachter, J.; Mentzen, B.F.; Riess, J.G., *Angew.Chem.,Int.Ed.*, **20**, 284, (1981) b) Toyota, K.; Yamamoto, Y.; Akiba, K., *J. Chem. Res.*, 386, (1999) c) Jeanneaux, F.; Grand, A.; Riess, J.G., *J. Am. Chem. Soc.*, **103**, 4272, (1981) d) Dupart, J.-M.; Grand, A.; Pace, S.; Riess, J.G., J.*Am.Chem.Soc.*, **104**, 2316, (1982) e) Dupart, J.-M.; Grand, A.; Riess, J.G., *J. Am. Chem. Soc.*, **108**, 1167, (1986) f) Toyota, K.; Yamamoto, Y.; Akiba, K., *J. Organomet. Chem.*, **586**, 171, (1999) g) Lattman, M.; Morse, S.A.; Cowley, A.H.; Lasch, J.G.; Norman, N.C., *Inorg. Chem.*, **24**, 1364, (1985) h) Chopra, S.K.; Chu, S.S.C.; De Meester, P.; Geyer, D.E.; Lattman, M.; Morse, S.A.,

J. Organomet. Chem., **294**, 347, (1985) i) Lattman, M.; Chopra, S.K.; Cowley, A.H.; Arif A.M., *Organometallics*, **5**, 677, (1986) j) De Meester, P.; Lattman, M.; Chu, S.S.C., *Acta Crystallogr., Sect. C: Cryst. Struct. Com*mun., **4**3, 162, (1987) k) Burns, E.G.; Chu, S.S.C.; de Meester, P.; Lattman M., *Organometallics*, **5**, 2383, (1986) l) Lattman, M.; Burns, E.G.; Chopra, S.K.; Cowley, A.H.; Arif A.M., *Inorg. Chem*., **26**, 1926, (1987) m) Blake, A.J.; Cockman, R.W.; Ebsworth, E.A.V.; Henderson, S.G.D.; Holloway, J.H.; Pilkington, N.J.; Rankin, D.W.H., *Phosphorus and Sulfur*, **30**, 143, (1987) n) Kubo, K.; Nakazawa, H.; Mizuta, T.; Miyoshi, K., *Organometallics*, **17**, 3522, (1998) o) Kajiyama, K.; Hirai, Y.; Otsuka, T.; Yuge, H.; Miyamoto, T.K., *Chem. Lett*., 784, (2000) p) Nakazawa, H.; Kawamura, K.; Ogawa, T.; Miyoshi, K., *J. Organomet. Chem*., **646**, 204, (2002) q) Khasnis, D.V.; Lattman, M.; Siriwardane, U., *Inorg. Chem*., **28**, 681, (1989) r) Khasnis, D.V.; Lattman, M.; Siriwardane, U., *Inorg. Chem*., **28**, 2594, (1989) s) Chopra, S.K.; Martin, J.C., *Heteroat. Chem*., **2**, 71, (1991) t) Khasnis, D.V.; Lattman, M.; Siriwardane, U., *Acta Crystallogr., Sect. C: Cryst. Struct. Commun*., **45**, 1628, (1989) u) Mikhel, I.S.; Bondarev, O.G.; Tsarev, V.N.;.Grintselev-Knyazev, G.V ; Lyssenko, K.A.; Davankov, V.A.; Gavrilov, K.N., *Organometallics*, **22**, 925, (2003) v) Faw, R.; Montgomery, C.D.; Rettig, S.J.; Shurmer, B., *Inorg. Chem.*, **37**, 4136, (1998) w) Nakazawa, H.; Kawamura, K.; Kubo, K.; Miyoshi, K., *Organometallics*, **18**, 2961, (1999) x) Kajiyama, K.; Miyamoto, T.K.; Sawano, K., *Inorg. Chem*., **45**, 502, (2006) y) Berry, D.E.; Browning, J.; Bushnell, G.W.; Dixon, K.R.; Pidcock, A., *Can. J. Chem*., **67**, 48, (1989) z) Khasnis, D.V.; Lattman, M.; Siriwardane, U.; Zhang, H., *Organometallics*, **11**, 2074, (1992) aa) Khasnis, D.V.; Burton, J.M.; Zhang, Hongming; Lattman, M., *Organometallics*, **11**, 3745, (1992)

[3] Emsley, J.; Hall, D., *The Chemistry of Phosphorus*, Harper & Low Ltd, London, (1976)

[4] Grushin, V. V.; Alper, H., *Organometallics*, **12**, 1890, (1993)

[5] Mason, M. R.; Verkade, J. G., *Organometallics*, **11**, 2212, (1992)

[6] Macgregor, S. A.; Wondimagegn, T, *Organometallics*, **26**, 1143, (2007)

[7] Albright, T.A.; Burdett, J. K.; Whangbo, M-H., *Orbital Interactions in Chemistry*, John Wiley and Sons, New York, (1985)

[8] P-O_{ax} in TBP = 1.752(9) Å in $[Co(CO)_3P(o\text{-}C_6H_4O)_2(PPh_3)]$ ref 2g); P-O_{ax} in TBP = 1.811(2) Å in *trans*-$[Ni(Cl)P(C_6H_4O_3)_2(PMe_3)_2]$ ref 2v)

[9] Lattman, M.; Burns, E. G.; Chopra, S. K.; Cowley, A. H.; Arif, A. M., *Inorg. Chem*. **26**, 1926, 1987

[10] Oriz, J. V.; Havias, Z.; Hoffmann, R., *Helv. Chim. Acta*, **67**, 1 (1984)

[11] Kubo, K.; Nakazawa, H.; Mizuta, T.; Miyoshi, K., *Organometallics*, **17**, 3522, (1998)

[12] Tolman, C. A., *J. Am. Chem. Soc*., **92**, 2953, (1970)

[13] Horrocks, W. D.; Taylor R. C., *Inorg. Chem*., **2**, 723, (1963)

[14] Macho, C.; Minkwitz, R.; Rohmann, J.; Steger, B.; Wölfel, V.; Oberhammer, H., *Inorg. Chem*., **25**, 2828, (1986)

[15] Low, J. J.; Goddard, W. A. III, *J. Am. Chem. Soc*., **108**, 6115, (1986)

[16] calculated value of Ni-O BI in *trans*-[$NiCl(OH)(PH_3)_2$]

[17] calculated value of Pd-O BI in *trans*-[$PdCl(OH)(PH_3)_2$]

[18] calculated value of Pt-O BI in *trans*-[$PtCl(OH)(PH_3)_2$]

Chapter 4: Investigation of the Reaction Mechanism for the Hydroxide-Induced Disproportionation of $[PdCl_2(PPh_3)_2]$

4.1 Introduction

The focus of this chapter is on the mechanism of the hydroxide-induced disproportionation of $[PdCl_2(PPh_3)_2]$ to yield a catalytically-active Pd(0) species and triphenylphosphine oxide, as studied in detail by Grushin and Alper[1] and discussed in Chapter 1. They proposed two possible mechanisms for the reaction, shown in Figure 4.1, which differ in the way that the hydroxide attacks $[PdCl_2(PPh_3)_2]$.

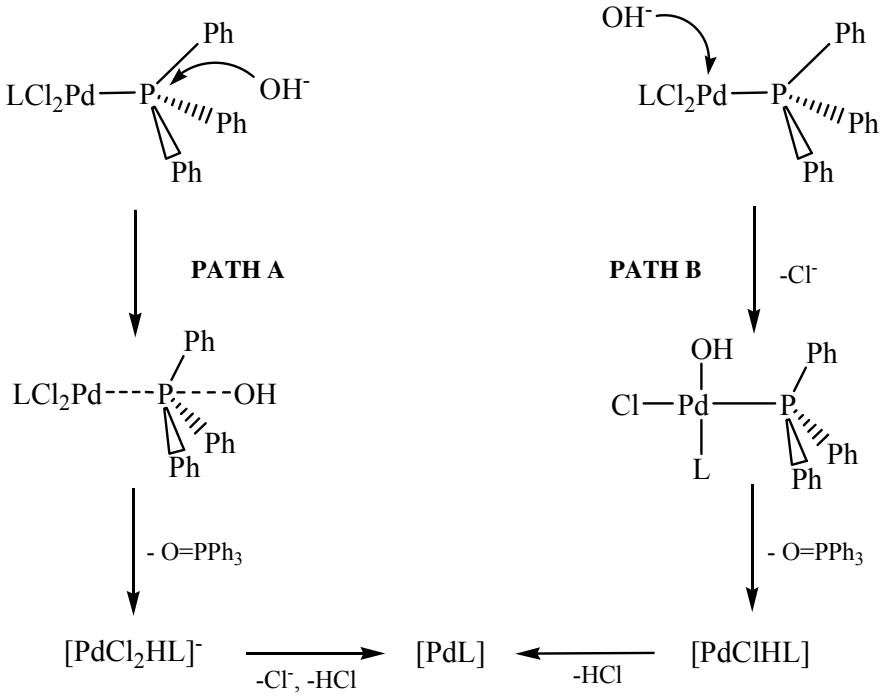

Figure 4.1: Two possible pathways proposed by Grushin and Alper for hydroxide-induced disproportionation of $[PdCl_2L_2]$, where L = PPh_3.

By using chiral phosphines and examining the stereochemistry of the phosphine oxide produced, it was observed that the reaction always proceeded with retention of configuration at the chiral phosphorus which was oxidised to phosphine oxide. This led to the conclusion that hydroxide performs an intramolecular attack on phosphorus, consistent with Path B. This mechanism is shown in Figure 4.2, broken down into three steps.

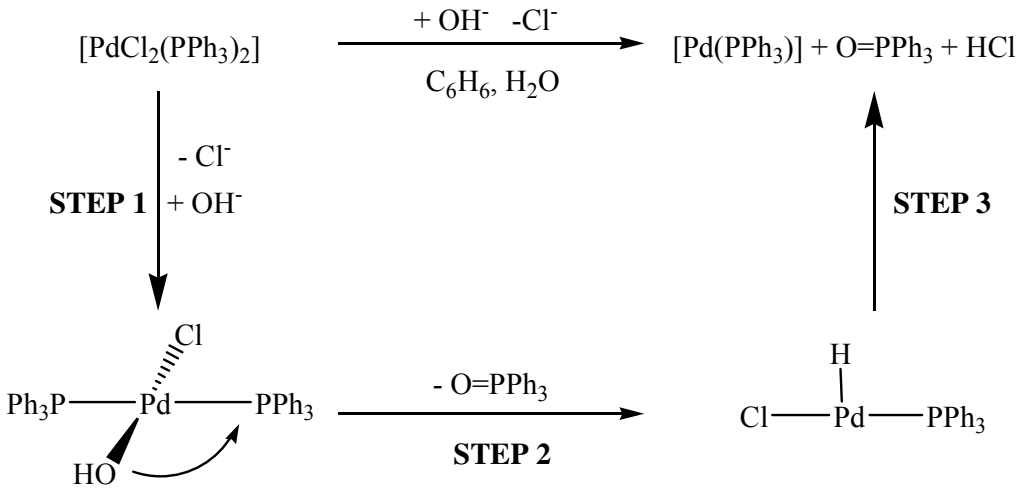

Figure 4.2: Reaction mechanism for the hydroxide-induced disproportionation of $[PdCl_2(PPh_3)_2]$ proposed by Grushin and Alper.[1]

Step 2 of the proposed mechanism presents some interesting questions as to how the mechanism could proceed. Earlier work published by Neave and Macgregor,[2] discussed in more detail in Chapter 1, suggests the novel idea that an OR^- group can attack a phosphine to produce metallophosphoranes as intermediates in certain reactions. This chapter seeks to investigate the possibility that metallophosphoranes play a role in Step 2 of the mechanism of this disproportionation reaction, as illustrated in Figure 4.3.

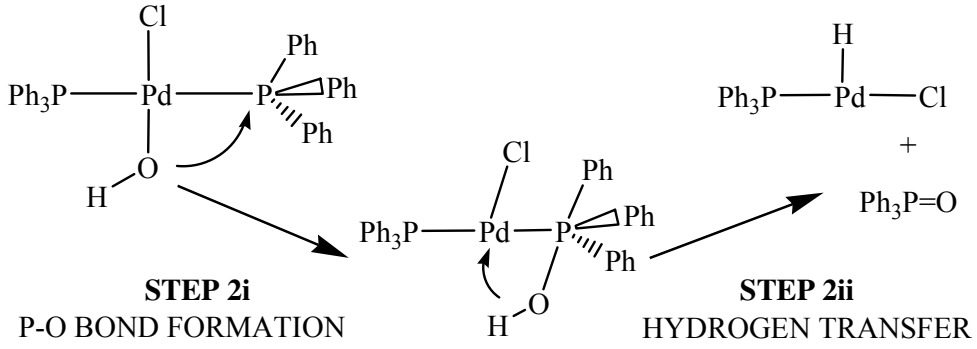

Figure 4.3: The proposal that a metallophosphorane intermediate may feature in Step 2 of the mechanism for the hydroxide-induced disproportionation of $[PdCl_2(PPh_3)_2]$.

Initially calculations were performed at full DFT level on a small model of the experimental complexes using the methods outlined in Chapter 2. In the small model the PPh_3 groups are replaced by PH_3 groups, which reduces the size of the complex

from 72 atoms down to 12 atoms. This allows the structures and mechanism to be explored in a more time efficient manner. When the small model work was complete, calculations were performed on the full experimental system using the ONIOM/HF method outlined in Chapter 2. A comparison of the results obtained for the two models will be discussed.

4.2 Small Model [PdCl(OH)(PH_3)$_2$]: P-O bond formation

Investigation of the mechanism begins after the initial displacement of a chloride group by hydroxide. As it was not possible to determine the active isomer experimentally, both the trans (**1a**) and cis (**1b**) isomers of [PdCl(OH)(PH_3)$_2$] were used as initial reactants in the small model system. All energies for the small model system are relative to the energy of **1a**, which is set to zero.

The structures of both isomers, trans **1a** (E = 0.0 kcal/mol) and cis **1b** (E = -1.6 kcal/mol), can be seen in Figure 4.4. Both Pd-P bonds are longer in **1a** than **1b**, suggesting that PH_3 has a stronger trans influence than either chloride or hydroxide. Additionally, the fact that Pd-P2 is longer than Pd-P1 in **1b**, suggests that hydroxide has a stronger trans influence than chloride. That being the case, it is surprising that the Pd-Cl bond lengths are almost identical in both isomers and that the Pd-O bond is longer in **1a**, despite being trans to chloride. It is possible that the Pd-Cl and Pd-O bonds are

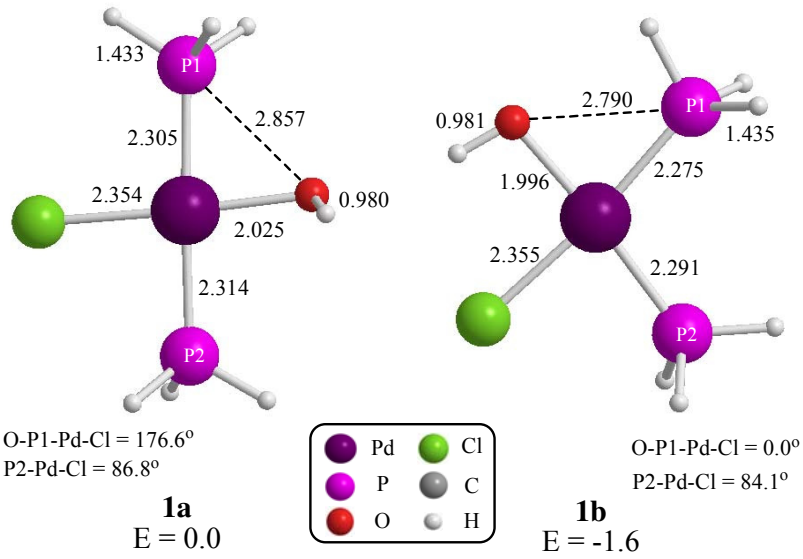

Figure 4.4: Structures of trans reactant **1a** and cis reactant **1b**. Bond lengths and distances in Å, energies in kcal/mol.

longer in **1a** than one might expect, as chloride and hydroxide are two π-donors lying trans to each other.

In **1b** the hydroxide is oriented so that the hydrogen is pointing towards the chloride, with a (O)H···Cl distance of 2.652 Å. It is possible that this intramolecular hydrogen bonding interaction contributes to **1b** being 1.6 kcal/mol more stable than **1a**.

Transition states for P-O bond formation were found from both reactants **1a** and **1b** by using the methods described in Chapter 3, and the structures are shown in Figure 4.5. The transition state from trans reactant **1a**, $\mathbf{TS_{1a\text{-}2a}}$ (E = 28.3 kcal/mol), was found to be less stable than $\mathbf{TS_{1b\text{-}2a}}$ (E = 21.8 kcal/mol), which originates from cis reactant **1b**. In $\mathbf{TS_{1a\text{-}2a}}$ the Pd-O bond breaks (Pd···O: **1a** = 2.025 Å, $\mathbf{TS_{1a\text{-}2a}}$ = 2.467 Å) as a P1-O bond is formed (P1···O: **1a** = 2.857 Å, $\mathbf{TS_{1a\text{-}2a}}$ = 1.901 Å). Equivalent bond breaking (Pd···O: **1b** = 1.996 Å, $\mathbf{TS_{1b\text{-}2a}}$ = 2.545 Å) and bond formation (P1···O: **1b** = 2.790 Å, $\mathbf{TS_{1b\text{-}2a}}$ = 1.837 Å) is seen in $\mathbf{TS_{1b\text{-}2a}}$. $\mathbf{TS_{1b\text{-}2a}}$ can be considered to be slightly later than $\mathbf{TS_{1a\text{-}2a}}$, as it has a longer Pd···O distance and a shorter P1···O distance. The hydroxyl group has started to move out of the metal coordination plane with the O-P1-Pd-Cl torsion angle decreasing from 176.6º in **1a** to 143.5º in $\mathbf{TS_{1a\text{-}2a}}$. Similarly, in $\mathbf{TS_{1b\text{-}2a}}$ the O-P1-Pd-Cl torsion angle has increased from 0.0º in **1b** to 45.8º.

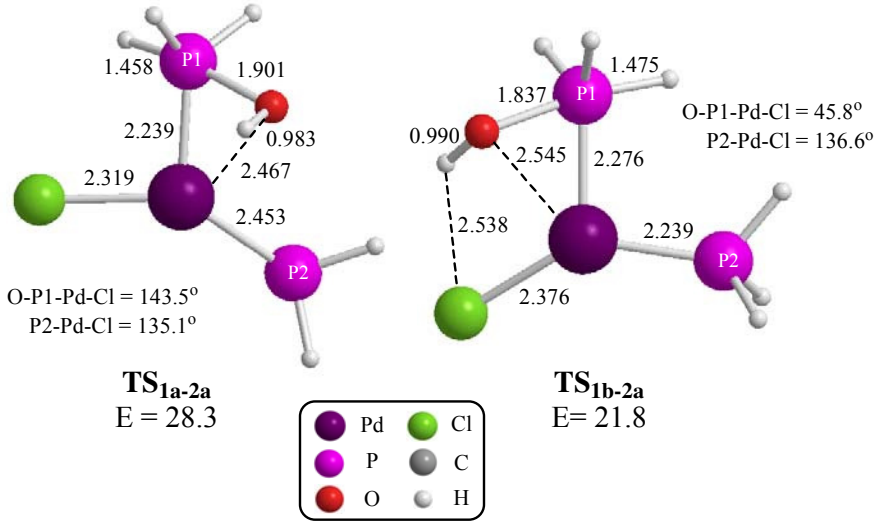

Figure 4.5: Structures of $\mathbf{TS_{1a\text{-}2a}}$ and $\mathbf{TS_{1b\text{-}2a}}$. Bond lengths and distances in Å, energies in kcal/mol.

A major difference between the two transition state structures is the orientation of the hydroxyl group, but in both cases the position is entirely consistent with the orientation in the corresponding reactant. In **TS_{1b-2a}** the hydroxyl hydrogen is pointing towards the chloride with a relatively short (O)H···Cl distance of 2.538 Å. In **TS_{1a-2a}** the (O)H···Cl distance is large at 4.226 Å, but there may be a stabilising interaction with palladium ((O)H···Pd = 2.621 Å). To investigate whether the transition states are being stabilised by interacting with chloride or palladium, the orientation of the hydroxyl hydrogens in both transition state structures was altered by rotating around the O-P1 bond by 180º, and then running new transition state calculations. When the hydrogen position is altered in **TS_{1a-2a}** (H-O-Pd-Cl = 62.1º in **TS_{1a-2a}** and 164.1º in the new geometry), the resultant transition state has a (O)H···Cl distance of 2.770 Å and is 2.0 kcal/mol less stable, presumably as any stabilising interaction with palladium has been removed. Similarly, if the hydrogen is repositioned and allowed to optimise in **TS_{1b-2a}** (H-O-Pd-Cl = 17.4º in **TS_{1b-2a}** and 81.0º in the new geometry), the alternative transition state has an increased (O)H···Pd distance of 3.564Å and is also 2.0 kcal/mol less stable, relating to the removal of any stabilising hydrogen-bonding-type interaction with the palladium. These alternative transition states will not be considered further as they are less stable than those included in the reaction profile.

In addition to the movement of the hydroxyl from palladium towards P1, in **TS_{1a-2a}** the Cl-Pd-P2 angle has increased from 86.8º in **1a** to 135.1º, and similarly in **TS_{1b-2a}** the Cl-Pd-P2 angle has increased to 136.6º. This movement is indicative of an isomerisation occurring, whereby P2 (in **TS_{1a-2a}**) and Cl (in **TS_{1b-2a}**) are moving into the sites previously occupied by the hydroxy groups, creating a vacant site opposite P1.

In both transition states a significantly elongated bond is seen between the palladium and the ligand which is changing sites. In **TS_{1a-2a}** an unusually long Pd-P2 bond is observed (Pd-P2: **1a** = 2.314 Å, **TS_{1a-2a}** = 2.453 Å), and similarly in **TS_{1b-2a}** the Pd-Cl bond is slightly elongated (Pd-Cl: **1b** = 2.355 Å, **TS_{1b-2a}** = 2.376 Å). The effect seems more pronounced for the phosphine than for chloride. As both ligands move positions, they both experience repulsion due to the close proximity of their σ-bonding electrons with filled orbitals on palladium, as shown in Figure 4.6. However, chloride is able to counter this repulsion by performing π-donation to the palladium, which stabilises the

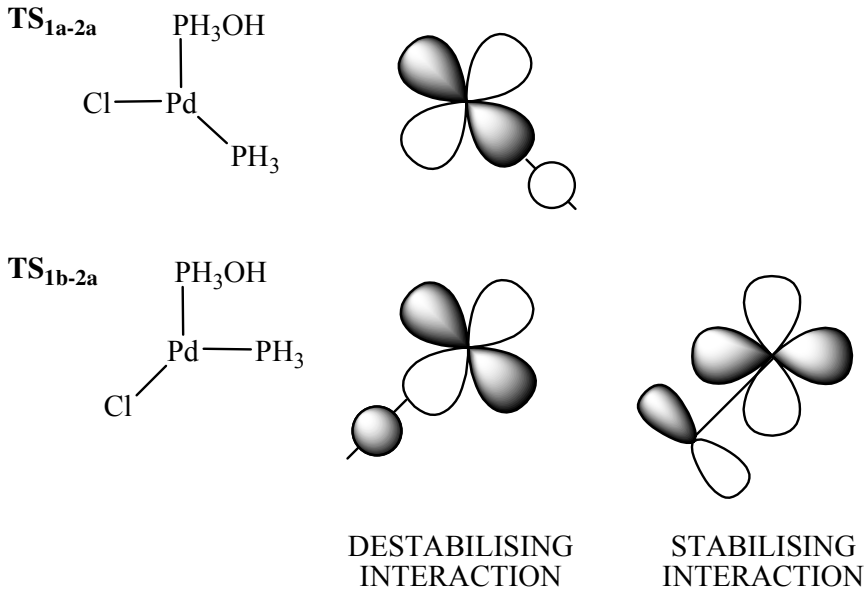

Figure 4.6: Orbital interactions in $\mathbf{TS_{1a\text{-}2a}}$ and $\mathbf{TS_{1b\text{-}2a}}$ between palladium and the ligand that is changing site.

transition state structure and shortens the Pd-Cl bond. A phosphine cannot to do this therefore the Pd-P bond remains comparatively long.

IRC calculations were performed and it transpired that both $\mathbf{TS_{1a\text{-}2a}}$ and $\mathbf{TS_{1b\text{-}2a}}$ go forwards to a common intermediate, complex **2a** (E = 14.1 kcal/mol). The structure of intermediate **2a** can be seen in more detail in Figure 4.8. This is metallophosphorane '**2b**' which was identified in Chapter 3 and the structural details of this complex were discussed in section 3.6.1.

Figure 4.7 shows the energy profile for this initial part of the reaction. The activation energy from the cis reactant, **1b**, to $\mathbf{TS_{1b\text{-}2a}}$ has the lower activation barrier at +23.4 kcal/mol. This may be due to the stabilisation of $\mathbf{TS_{1b\text{-}2a}}$ as described above.

Additionally, this P-O bond formation pathway can be considered as a novel route for cis-trans isomerisation. Starting from the trans isomer, the barrier is 28.3 kcal/mol to form metallophosphorane **2a**, then the isomerisation can continue via $\mathbf{TS_{1b\text{-}2a}}$, which has a barrier of 7.7 kcal/mol, leading to formation of the cis isomer. The highpoint for the isomerisation is $\mathbf{TS_{1a\text{-}2a}}$ at 28.3 kcal/mol.

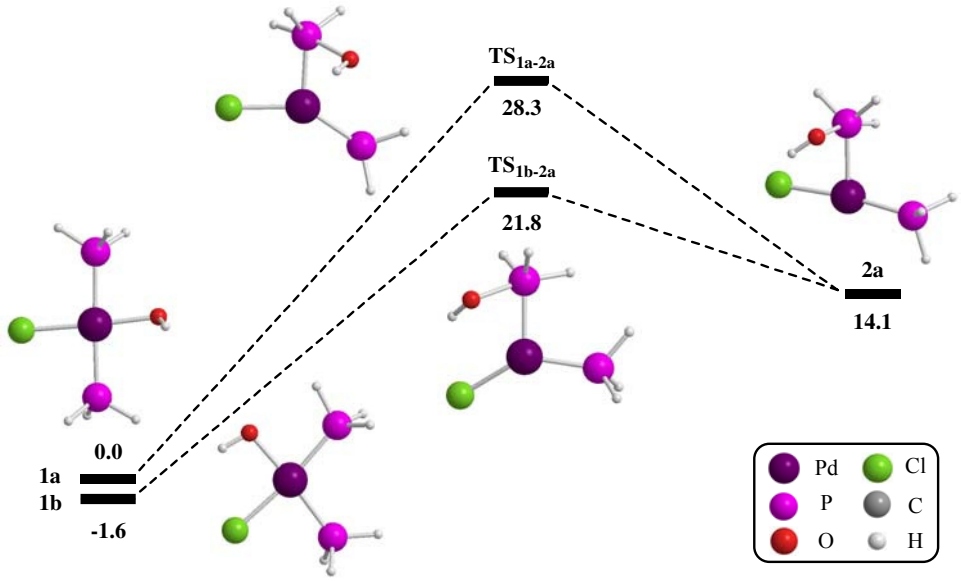

Figure 4.7: Reaction profile (kcal/mol) for P-O bond formation, from reactants **1a** and **1b** to metallophosphorane **2a**.

4.3 Small model [PdCl(OH)(PH_3)$_2$]: H-transfer and O=PH_3 formation

To reach the desired products from **2a**, the hydroxy hydrogen needs to be transferred to palladium and phosphine oxide must be produced. To achieve this, the O-H bond and the Pd-P1 bond must be broken. Therefore, the effect of shortening the Pd···H(O) distance was investigated. It was found that as the Pd···H distance was shortened in a stepwise manner, the Pd-P bond simultaneously lengthened. A transition state was found, **TS_{2a-2b}** (+15.5 kcal/mol), and IRC calculations showed that **TS_{2a-2b}** links intermediate **2a** to another minimum structure before hydrogen transfer has occurred. This is the intermediate **2b** (+15.2 kcal/mol), which is shown in Figure 4.8.

If intermediate **2b** is compared to **2a**, it can be seen that **2b** appears to be on the path towards generating phosphine oxide because the Pd-P bond has lengthened and the Pd···H(O) distance has reduced. The geometry around P1 is still trigonal bipyramidal, but has changed from having the hydroxide in an axial position and palladium equatorial in **2a**, to having the palladium axial and the hydroxide equatorial in **2b** (H_{ax}-P1-Pd = 174.2º, H_{ax}-P1-O = 88.9º). This has occurred by rearrangement of the hydrogens on P1. A precedent for a hydroxyl group occupying either an axial or equatorial position in a TBP was observed before. In Chapter 3 hydroxyl was found to be the only X group in the set investigated that had minimum structures with X in an

equatorial or an axial position in PH_4X. Other structural changes include the lengthening of the O-H bond to 0.997 Å as the hydrogen strengthens its interaction with palladium, and the shortening of the P1-O bond to 1.690 Å now that it lies equatorial to phosphorus. The small activation barrier of +1.4 kcal/mol reflects the subtlety of the geometric changes between **2a** and **2b**. The structure of $\mathbf{TS_{2a\text{-}2b}}$ is intermediate between those of **2a** and **2b**, and corresponds to rotation around the P1-O bond and isomerisation around P1. It is one of the equatorial hydrogens in **2a** that lies axial in **2b**.

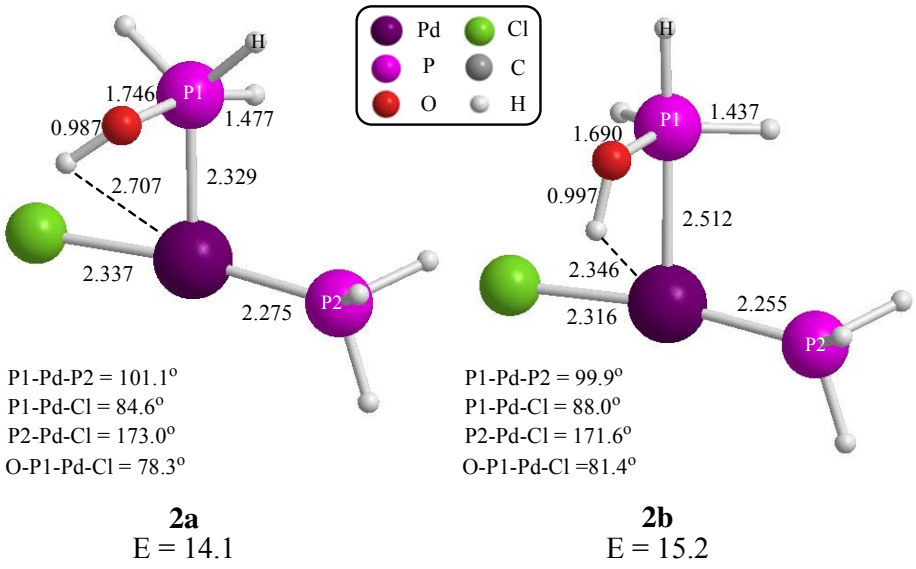

Figure 4.8: Structures of metallophosphoranes **2a** and **2b**. Bond lengths and distances in Å, energies in kcal/mol.

A further transition state, $\mathbf{TS_{2b\text{-}3}}$ (E = 15.3 kcal/mol), shown in Figure 4.9, was found by shortening the Pd···H distance from **2b** and running a transition state calculation from the energy highpoint. An IRC calculation showed that $\mathbf{TS_{2b\text{-}3}}$ leads to complex **3** (E = 12.9 kcal/mol), where the hydroxy hydrogen is bridging between the oxygen (O···H = 1.108 Å) and the palladium (Pd···H = 1.884 Å), and one of the hydrogens on P1 is interacting with chloride (H···Cl = 1.857 Å). If the structures of **2b**, $\mathbf{TS_{2b\text{-}3}}$ and **3** are compared (see Table 4.1), the P1-O bond can be seen to shorten as the O-H bond begins to break and the Pd-H bond forms.

From **3** it is an energetically uphill process, with no transition state located, to break the O···H interaction, lengthening it from 1.108 Å in **3** to yield the Pd(II) complex, **4** [PdCl(H)PH_3], and phosphine oxide, **5** (combined E = 28.9 kcal/mol).

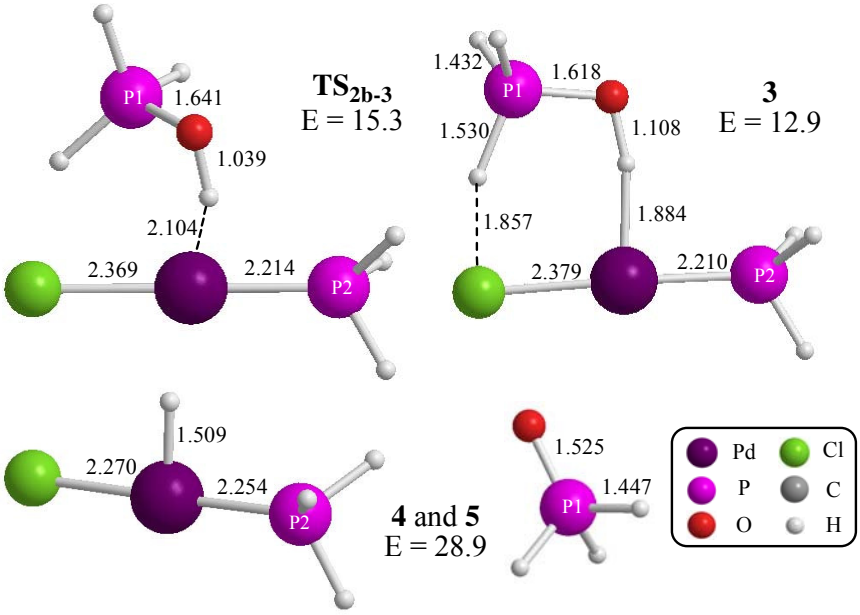

Figure 4.9: Structures of $\mathbf{TS_{2b\text{-}3}}$, intermediate **3**, and products **4** and **5**. Bond lengths and distances in Å, energies in kcal/mol.

Structure	Bond Length and distances / Å		
	Pd-H	O-H	P-O
2b	2.346	0.997	1.69
$\mathbf{TS_{2b\text{-}3}}$	2.104	1.039	1.641
3	1.884	1.108	1.618
4	1.509	-	-
5	-	-	1.525

Table 4.1: Bond lengths and distances (Å) involved in H-transfer and O=PH_3 formation in the structures of **2b**, $\mathbf{TS_{2b\text{-}3}}$, **3** and products **4** and **5**.

4.4 Small model: Overall reaction profile

The entire reaction profile using the small model can be seen in Figure 4.10. The highest energy barrier in the process is the initial formation of metallophosphorane **2a** via $\mathbf{TS_{1a\text{-}2a}}$ (+28.3 kcal/mol). If the starting point is cis reactant **1b**, the initial activation barrier is smaller, at 23.4 kcal/mol. Once **2a** has been formed, the rest of the process is relatively easy through to H-bridged product **3**, with no activation energies above 2 kcal/mol. Forming dissociated products **4** and **5** is uphill in energy, however it is important to bear in mind that these energies do not include entropy. In fact, the ΔG value for the combination of products **4** and **5** is +19.0 kcal/mol above reactant **1a**. This is still an energetically unfavourable process, but the value for free energy is almost 10 kcal/mol lower than the computed enthalpy. The other stationary points are not significantly affected by the inclusion of entropy.

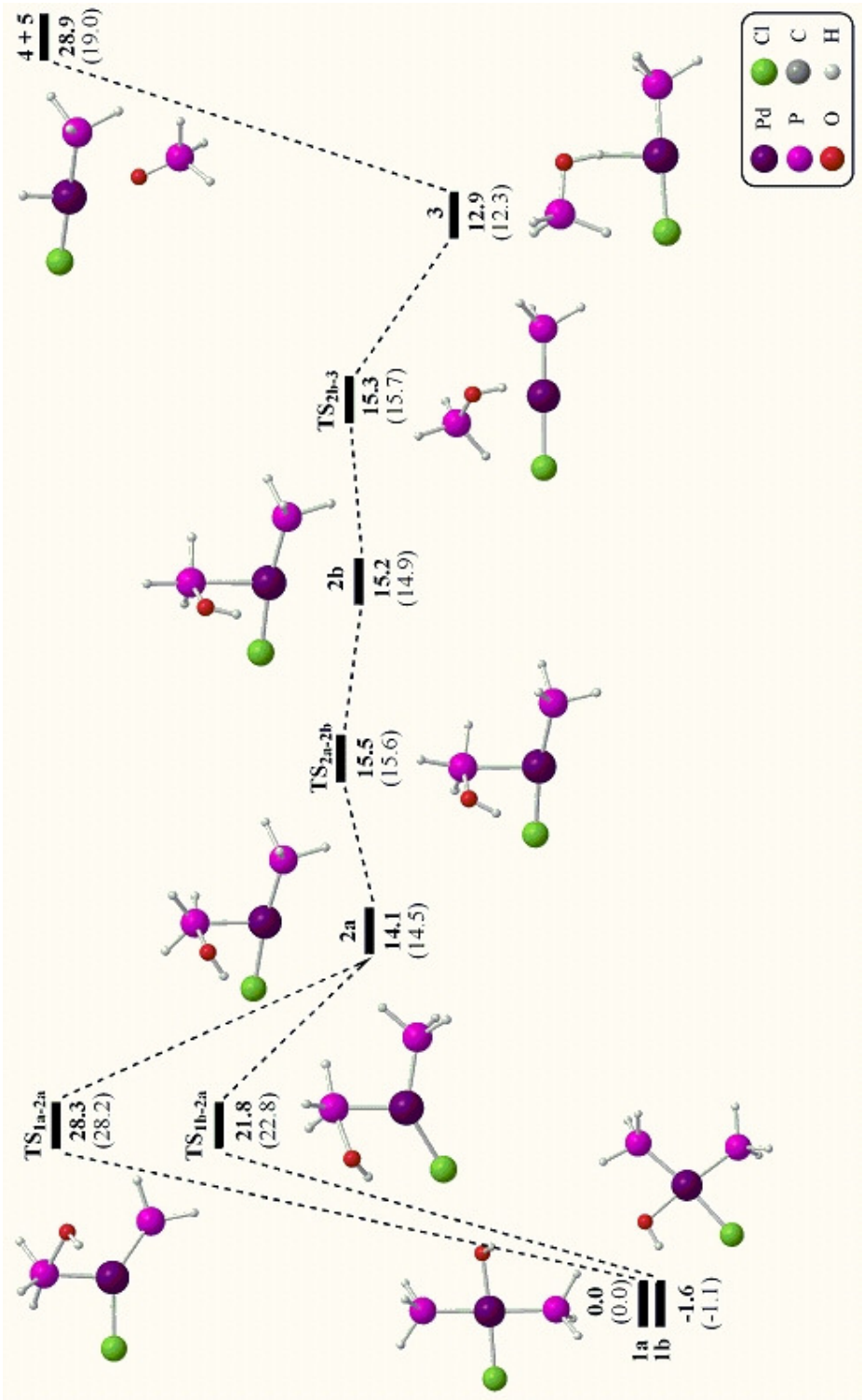

Figure 4.10: Reaction profile (kcal/mol) for the disproportionation mechanism, using the small model system, $[PdCl(OH)(PH_3)_2]$. ΔG values are shown in parenthesis.

4.5 Small Model: Natural population analysis

All of the structures were analysed by computation of the natural atomic orbital populations and the results for the charge on palladium and the key phosphorus atom (P1) are shown in Table 4.2. PH_3 and phosphine oxide have been included to show typical values for P(III) and P(V) respectively, as all the charges on P1 fall between these two extremes.

Structure	q(P1)	q(Pd)
PH_3	0.01	
trans **1a**	0.25	0.32
cis **1b**	0.23	0.32
$\mathbf{TS_{1a\text{-}2a}}$	0.70	0.21
$\mathbf{TS_{1b\text{-}2a}}$	0.70	0.19
2a	0.81	0.08
$\mathbf{TS_{2a\text{-}2b}}$	0.88	0.00
2b	0.93	-0.05
$\mathbf{TS_{2b\text{-}3}}$	1.02	-0.18
3	1.05	-0.15
4		0.14
5 $O{=}PH_3$	1.21	

Table 4.2: Computed natural atomic charges (q) on P1 and Pd for all structures from the small model disproportionation profile.

There is a clear trend of decreasing negative charge (reduced electron density) on P1 as the nature of the phosphorus gradually changes from P(III) in a phosphine ligand in **1a** (q = 0.25) and **1b** (q = 0.23), to end up as P(V) in phosphine oxide, **5** (q = 1.21). Most of the change occurs between the reactants **1a** and **1b** and the first transition states, suggesting that P1 is closer to the nature of P(V) than P(III) in the metallophosphorane structures **2a** and **2b.** This suggests that the phosphorus in a $\{PPh_3OH\}$ fragment is closer to P(V) in nature, which is contradictory to the normal view of the fragment as a phosphoranide ligand, which is formally P(III).

The negative charge on palladium increases through the reaction mechanism, concurrent with the opposite trend in q(P1), until $\mathbf{TS_{2b\text{-}3}}$ (q = -0.18), where it has its highest value of electron density when the hydroxy hydrogen is bridging between the oxygen and the palladium. When the O-H bond completely breaks and the Pd-H bond is fully formed, the charge is similar to that of **2a** (q = 0.08) in structure **4** (q = 0.14), $[PdCl(H)(PH_3)]$.

4.6 Large model system [PdCl(OH)(PPh_3)$_2$]

The HF/ONIOM method, as described in Chapter 2, was used to investigate Step 2 of the disproportionation reaction mechanism using the full experimental system, [PdCl(OH)(PPh_3)$_2$] (trans **6a** and cis **6b**). In this case, Pd, P1, P2, OH, Cl and one phenyl group on P1 were at the 'high' DFT level of calculation, with the remaining five phenyl groups at the 'low' HF level. It was necessary to have one phenyl group at the 'high' level in the calculation to allow for any possible interactions with palladium.

4.7 Large model: Overview

The discussion of the possible reaction mechanisms for the large model system will be separated into two parts. The first part of the discussion (Section 4.9) will focus on the formation of a P-O bond. At first, a pathway via a metallophosphorane intermediate was sought, similar to what was seen in the small model pathway. Such a pathway was found (A), but it was not possible to proceed forward and perform H-transfer and phosphine oxide formation from a metallophosphorane species. However, a new type of intermediate was found, where the Pd-P1 bond has broken and a phosphorus-bound phenyl engages in an η^2-interaction with palladium to form a zwitterion. Routes were found to form a zwitterion intermediate either directly from reactants **6a** and **6b** (B), or via a metallophosphorane intermediate (A-B). The second part of the discussion (Section 4.10) focuses on the transfer of the hydroxy hydrogen from oxygen onto palladium (C), producing phosphine oxide and [PdCl(H)(PPh_3)]. These pathways are depicted in Figure 4.11.

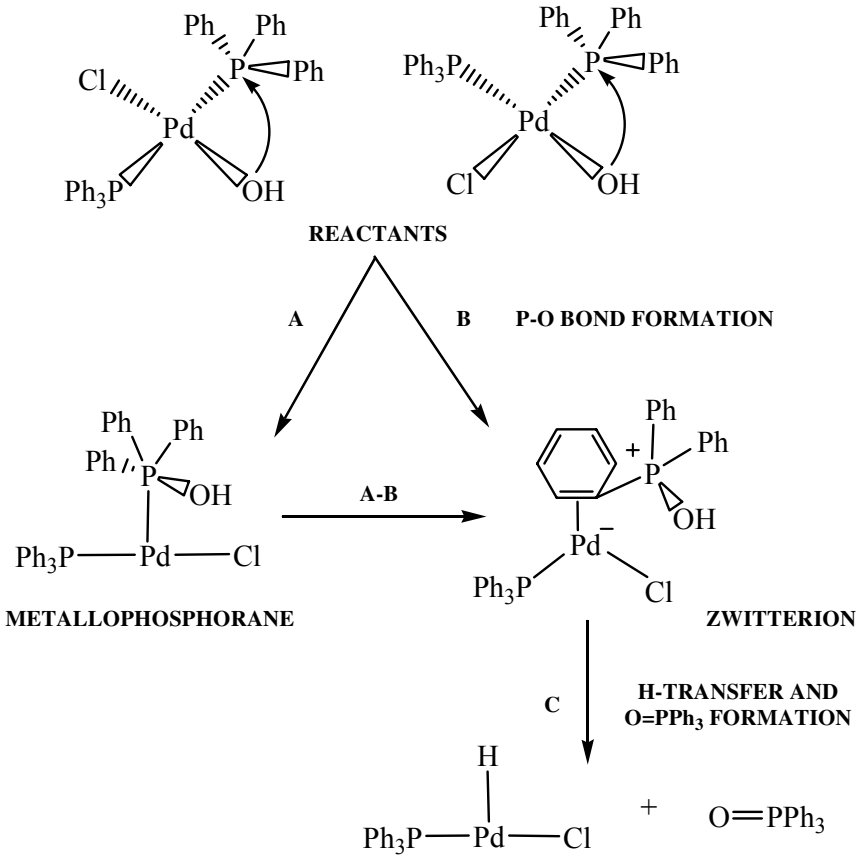

Figure 4.11: Overview of mechanistic possibilities.

4.8 Large model: Method Comparison

The first task was to generate geometries for the starting species **6a** and **6b** that were as realistic as possible. Since there was no structural data available for either isomer of $[PdCl(OH)(PPh_3)_2]$, the most closely related crystallographically determined structures were used. Therefore, *trans*-$[PdCl_2(PPh_3)_2]$[3] was used as a starting point for **6a**, and *cis*-$[Pd(H_2O)_2(PPh_3)_2]^{2+}$ [4] for **6b**. To see whether structures optimised using DF/HF ONIOM would accurately model the experimental data, a series of test calculations were performed for *trans*-$[PdCl_2(PPh_3)_2]$[3] and these were compared with results of full DFT calculations. Key bond lengths are shown in Figure 4.12.

The calculations consistently overestimate the bond lengths compared to the experimental data. One possible explanation is that the calculations model a single molecule in the gas phase as opposed to a solid crystal. This trend is not unusual, and has been observed in other computational work.[5] An exception to this is the

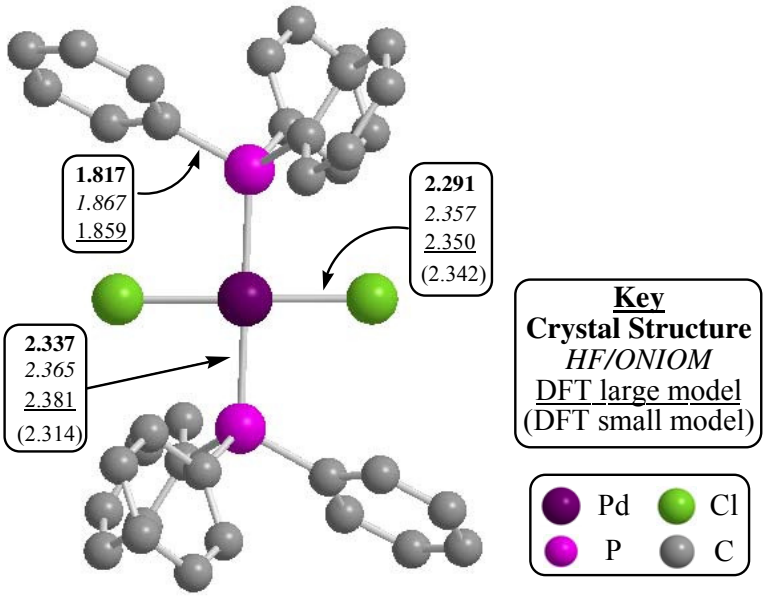

Figure 4.12: The structure of *trans*-[$PdCl_2(PPh_3)_2$] with bond lengths (Å) from the experimentally determined structure and 3 structures computed at different levels.

underestimation of the Pd-P bond lengths in the small model, but since it is a different phosphine (PH_3) it is not a direct comparison.

The maximum overestimation is the HF/ONIOM Pd-Cl bond length, which is 0.066 Å (3%) longer than in the experimentally determined structure. If the bond lengths for the HF/ONIOM and large model DFT structures are compared, the maximum difference is only 0.016 Å in the Pd-P bond lengths, which suggests that HF/ONIOM can produce structures with only a negligible difference from the DFT structures in this type of complex. Thus, HF/ONIOM should be able to produce good structural results in this type of system.

4.9 Large model: P-O bond formation

4.9.1 Pathway A

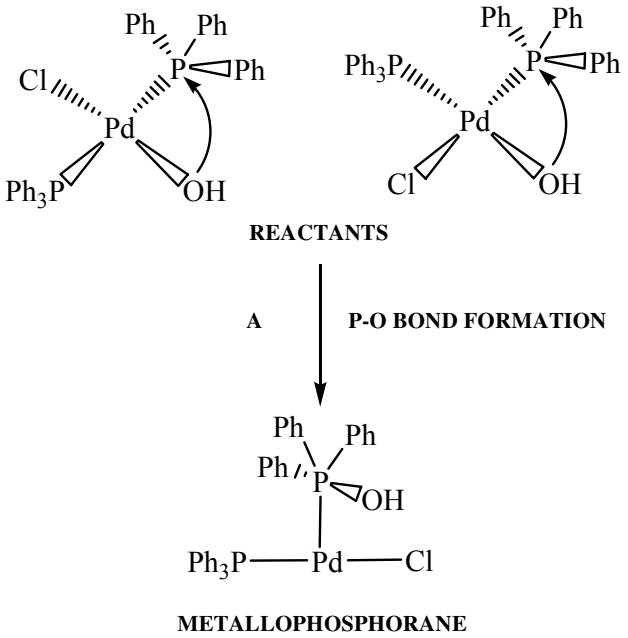

The complex *trans*-[PdCl(OH)(PPh_3)$_2$], **6a**, was constructed from crystallographic data for *trans*-[$PdCl_2(PPh_3)_2$],[3] with a chloride substituted for a hydroxy group. Similarly, *cis*-[PdCl(OH)(PPh_3)$_2$], **6b** (E = 4.0 kcal/mol), was constructed from a closely related experimental determined structure, that of *cis*-[$Pd(H_2O)_2(PPh_3)_2]^{2+}$,[4] with substitution of the water ligands. These were then optimised, and their structures can be seen in Figure 4.13. All energies for the large model system will be reported relative to the energy of **6a**. If these structures are compared to the analogous structures in the small model (Figure 4.4), the main difference is that all the bond lengths shown are longer in the large model, as was seen in section 4.8. This can be explained by the greatly increased steric bulk of the triphenylphosphine groups in the large model compared to the PH_3 groups in the small model. Similar to the trend seen in the small model, the bonds to palladium in trans isomer **6a** are longer than in cis isomer **6b**, with the exception of the Pd-Cl bond. The order of trans influence is also the same as in the small model reactants, with the phosphines exerting the strongest trans influence, and the chloride the weakest.

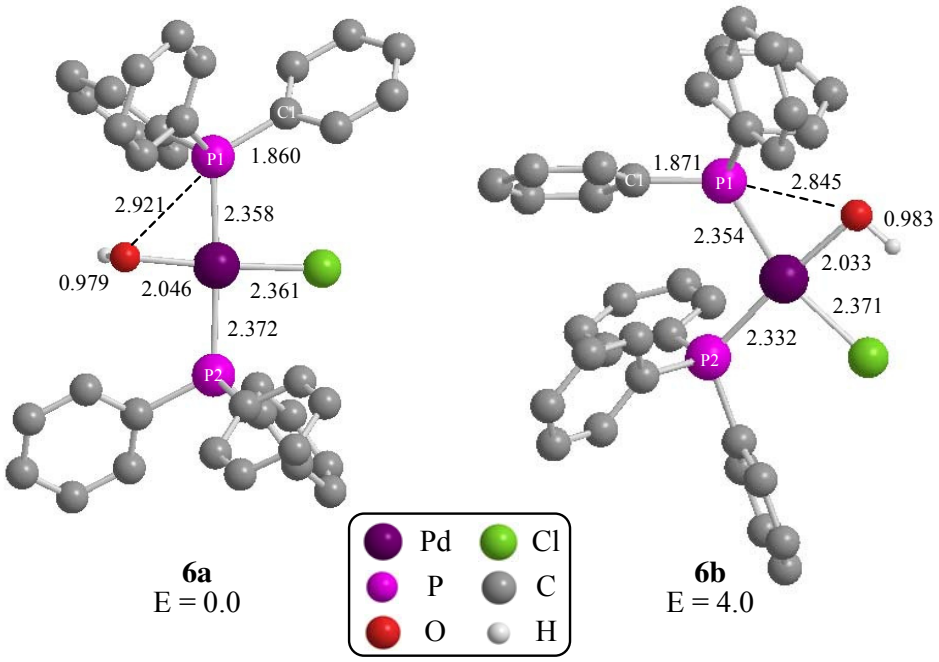

Figure 4.13: The optimised structures of **6a** and **6b**, *trans*- and *cis*-$[PdCl(OH)(PPh_3)_2]$ respectively. Bond lengths in Å, energies in kcal/mol. Phenyl hydrogens are omitted for clarity.

In the small model, where purely the electronic character of the phosphine is present, cis isomer **1b** is more stable than **1a** by 1.6 kcal/mol. Conversely, in the large model, the trans isomer, **6a**, is the more stable isomer by 4.0 kcal/mol. This can be accounted for by the close proximity of the two bulky triphenylphosphine ligands in the cis form. Although the P1-Pd-P2 angle only increases by 1.1º between **1b** and **6b**, it is likely to be a steric effect that is destabilising the cis isomer.

To progress towards P-O bond formation, the P1···O distances in **6a** and **6b** were reduced to 1.9 Å, followed by the opening of the P2-Pd-Cl angle, to yield two transition states at the energy highpoints of the scans. These were found to link both reactants to a common metallophosphorane intermediate, as seen in the small model. The structures of the two transition states, $\mathbf{TS_{6a\text{-}7a}}$ (E = 32.3 kcal/mol) and $\mathbf{TS_{6b\text{-}7a}}$ (E = 30.5 kcal/mol) can be seen in Figure 4.14. As seen in the small model, the activation barrier is smaller when starting from the cis reactant than the trans.

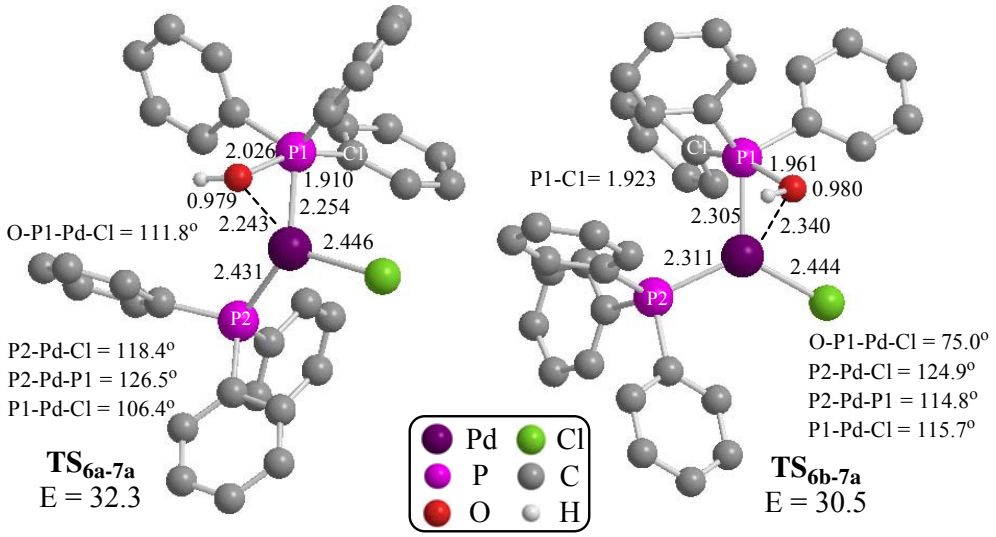

Figure 4.14: The optimised structures of $\mathbf{TS_{6a\text{-}7a}}$ and $\mathbf{TS_{6b\text{-}7a}}$. Bond lengths and distances in Å, energies in kcal/mol.

Looking firstly at $\mathbf{TS_{6a\text{-}7a}}$, the structure exhibits many similar features to $\mathbf{TS_{1a\text{-}2a}}$ in the small model. The additional steric bulk caused by the triphenylphosphines in $\mathbf{TS_{6a\text{-}7a}}$ may contribute to a longer P1···O distance ($\mathbf{TS_{6a\text{-}7a}}$ P1···O =2.026 Å, $\mathbf{TS_{1a\text{-}2a}}$ P1···O =1.901 Å) and a smaller P1-Pd-P2 angle ($\mathbf{TS_{6a\text{-}7a}}$ = 126.5º, $\mathbf{TS_{1a\text{-}2a}}$ = 120.5º) than in the small model. There is a lengthening of the Pd-Cl bond by 0.085 Å in $\mathbf{TS_{6a\text{-}7a}}$ that was not seen in the small model, but cause of which is unclear. The Pd-O bond has elongated, increasing from 2.046 Å in **6a** to 2.24 Å. Pd-P1 has shortened by 0.1 Å compared to the reactant as the other phosphine group moves away from the trans position, leaving a vacant site. Pd-P2 lengthens by 0.06 Å, presumably due to the same orbital factors as in the small model, but to a lesser extent. P1-C1 lengthens from reactant **6a** to $\mathbf{TS_{6a\text{-}7a}}$ as the geometry at P1 changes from tetrahedral to trigonal bipyramidal.

Examination of $\mathbf{TS_{6b\text{-}7a}}$, which links the cis reactant **6b** to intermediate **7a**, shows the same trend of shortening of the Pd-P1 bond (by 0.05 Å) and lengthening of the Pd-Cl bond (by 0.07 Å) as seen in the equivalent small model structure, $\mathbf{TS_{1b\text{-}2a}}$. $\mathbf{TS_{6b\text{-}7a}}$ has a longer P1-O bond ($\mathbf{TS_{6b\text{-}7a}}$ =1.961 Å, $\mathbf{TS_{1b\text{-}2a}}$ =1.837 Å) and a smaller P2-Pd-Cl angle ($\mathbf{TS_{6b\text{-}7a}}$ =124.9°, $\mathbf{TS_{1b\text{-}2a}}$ =136.6°) than in the equivalent small model structure. The P1-Pd-P2 angle is 114.8º in $\mathbf{TS_{6b\text{-}7a}}$, but is 126.5º in $\mathbf{TS_{6a\text{-}7a}}$, probably due to steric crowding caused by the two cis triphenylphosphines.

The two transition states both lead to a common metallophosphorane intermediate, **7a** (E = 26.0 kcal/mol), shown in Figure 4.15. If **7a** is compared to structure **2a** in the small model, similar trends in the bond lengths are observed. For instance, in both intermediates the Pd-P2 bond is shorter than in the corresponding reactant structures, as P2 is now trans to chloride rather than P1. Similarly, the Pd-P1 bond is longer in the intermediates **2a** and **7a** than in their respective reactants. The P2-Pd-Cl angle is 22.2° smaller in **7a**, and the P1-Pd-Cl angle is 12.9° larger. This is likely to be an attempt to ease the steric crowding of having two triphenylphosphine ligands cis to each other.

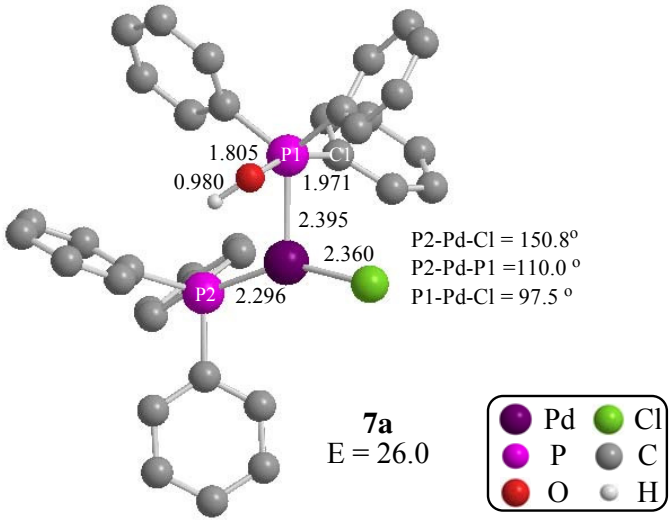

Figure 4.15: The optimised structures of metallophosphorane intermediate **7a**. Bond lengths and distances in Å, energy in kcal/mol.

An important difference between the structures of intermediates **7a** and **2a** is the relative orientation of the hydroxide groups. Comparison of the H-P1-Pd-Cl torsion angles (**7a** =135.3°, **2a** =29.1°) shows that in **2a** the hydroxyl hydrogen is pointing towards the chloride (torsion < 90°) but in **7a** the hydrogen points in the direction of P2 (torsion > 90°). This difference in orientation is also exhibited by the (O)H···Cl distances (**7a** 3.900 Å, **2a** 2.583 Å). The orientation of the hydroxyl in **7a** is consistent with that seen in $\mathbf{TS_{6a\text{-}7a}}$ and $\mathbf{TS_{6b\text{-}7a}}$, but it is possible that a lower energy metallophosphorane structure may exist, with stabilisation from an (O)H···Cl hydrogen-bonding-type interaction. Indeed, a metallophosphorane structure with an orientation more similar to **2a** was identified and will be discussed further in section 4.9.4.

4.9.2 Pathway A: Energy profile

The energy profile for this initial part of the reaction mechanism is shown in Figure 4.16. **TS_{6a-7a}** is the highpoint in the profile, as was its corresponding structure, **TS_{1a-2a}**, in the small model pathway. Furthermore, the activation barrier to form the transition state from the trans reactant is larger in both models than the barrier from the cis isomers. This is consistent with the experimental observations of Grushin and Alper, who reported that the disproportionation occurred more quickly from *cis*-$[PdCl_2(PPh_3)_2]$ than from the trans isomer.[1] However, in their study it was postulated that this was because the strong trans influence of PPh_3 would labilise the chlorides in the cis isomer.

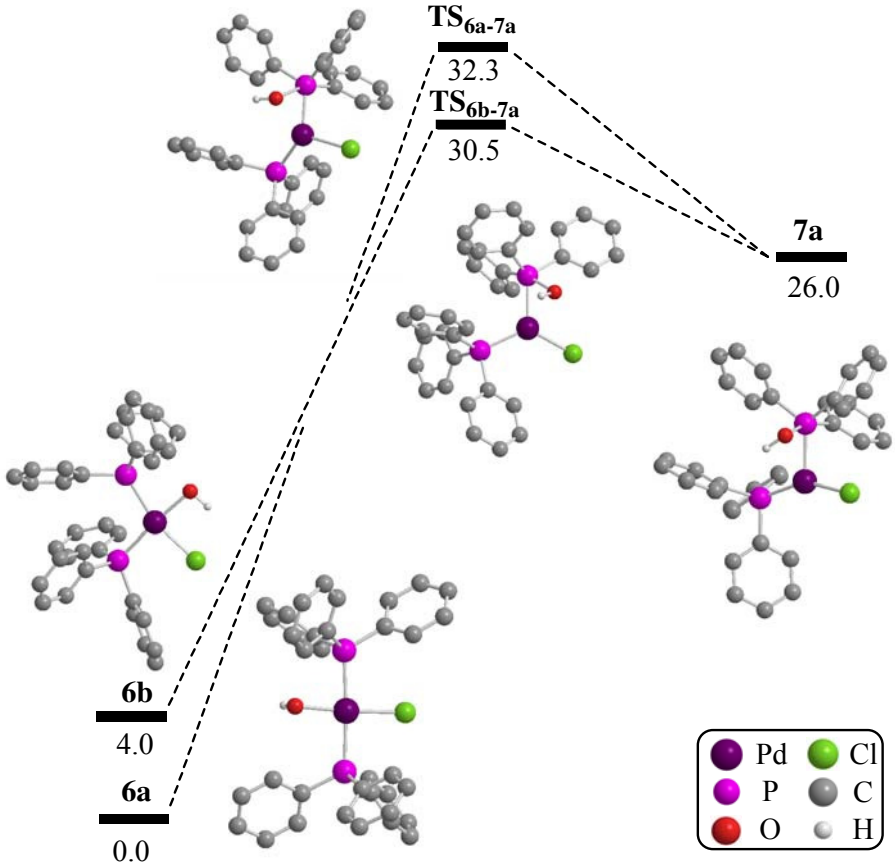

Figure 4.16: P-O bond formation: Pathway A – Energy profile (kcal/mol) for mechanism linking reactants **6a** and **6b** to metallophosphorane **7a**.

Both activation barriers are higher in the large model than in the small model (Large model: ΔE_a(**TS_{6a-7a}**) = 32.3 kcal/mol, ΔE_a(**TS_{6b-7a}**) = 26.5 kcal/mol; Small model: ΔE_a (**TS_{1a-2a}**) = 28.3 kcal/mol, ΔE_a(**TS_{1b-2a}**) = 21.8 kcal/mol). The increase in the activation barriers in the large model is possibly due to the steric hindrance of the bulky phosphines. This may also explain why the metallophosphorane intermediate **7a** is 11.9

kcal/mol less accessible than metallophosphorane **2a** in the small model. As mentioned in the small model, this is a mechanistic route for cis-trans isomerisation.

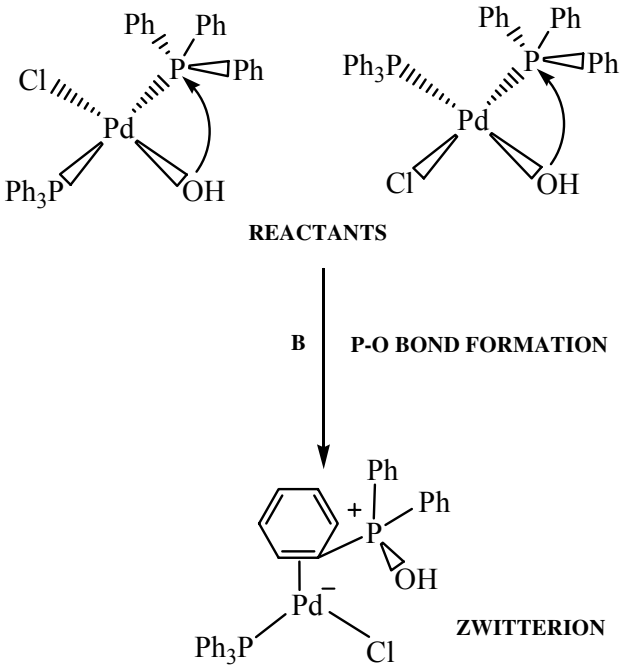

4.9.3 Pathway B

As mentioned earlier in this chapter, it was thought that transition state structures with the hydroxy hydrogen pointing towards chloride may exist in the large model system, analogous to the small model system. To investigate this possibility, the orientation of the hydroxy hydrogen was rotated by 180º around the O-P1 bond in the structures of $\mathbf{TS_{7a\text{-}8a}}$ and $\mathbf{TS_{7b\text{-}8a}}$, and new transition state calculations were run from these geometries. Indeed, two new transition states were found. The structures of $\mathbf{TS_{6a\text{-}8a}}$ (E = 31.7 kcal/mol) and $\mathbf{TS_{6b\text{-}8b}}$ (E = 26.7 kcal/mol) are shown in Figure 4.17.

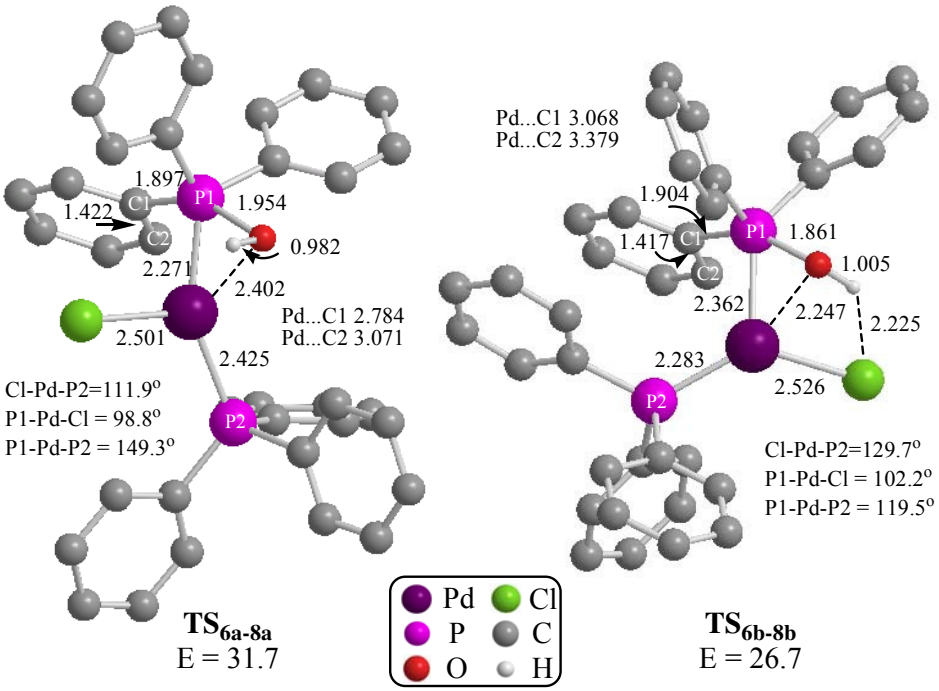

Figure 4.17: The optimised structures of **TS$_{6a-8a}$** and **TS$_{6b-8b}$**. Bond lengths and distances in Å, energies in kcal/mol.

PIRC calculations showed that **TS$_{6a-8a}$** and **TS$_{6b-8b}$** link reactants trans **6a** and cis **6b** to a new type of intermediate, featuring an η^2-interaction between the palladium and a phenyl carbon-carbon bond. The two new transition states are very similar to the two found previously in the large model. Therefore, only the major structural differences will be discussed.

Firstly, comparing **TS$_{6a-8a}$** to **TS$_{6a-7a}$** from Pathway A, the main difference is the orientation of the hydroxy group, with the hydroxy hydrogen now pointing in the direction of the chloride (H-O-Pd-Cl: **TS$_{6a-8a}$** = 16.9º, **TS$_{6a-7a}$** = 169.0º). However, the energies of these two transition states differ by only 0.6 kcal/mol, perhaps because the H···Cl distance is long in both structures (H···Cl: **TS$_{6a-8a}$** = 3.437 Å, **TS$_{6a-7a}$** = 4.741 Å) so there is no hydrogen bonding stabilisation in either. In **TS$_{6a-8a}$** the hydroxy group is closer to P1 than in **TS$_{6a-7a}$** and further from palladium (Pd···O: **TS$_{6a-8a}$** = 2.402 Å, **TS$_{6a-7a}$** = 2.243 Å; P1···O: **TS$_{6a-8a}$** = 1.954 Å, **TS$_{6a-7a}$** = 2.026 Å). Other differences include an even longer Pd-Cl bond than before (Pd-Cl: **TS$_{6a-8a}$** = 2.501 Å, **TS$_{6a-7a}$** = 2.446 Å) and a larger P1-Pd-P2 angle (P1-Pd-P2: **TS$_{6a-8a}$** = 149.3º, **TS$_{6a-7a}$** = 126.5º).

Secondly, the new transition state **TS_{6b-8b}** can be compared to the other transition state which links to cis reactant **6b**, **TS_{6b-7a}**. As before, the different orientation of the hydroxy groups is shown by comparing the H-O-Pd-P torsion angles (H-O-Pd-Cl: **TS_{6b-8b}** = 4.8º, **TS_{6b-7a}** = 134.9º). **TS_{6b-8b}** has a considerably shorter H···Cl distance than in **TS_{6b-7a}** (H···Cl: **TS_{6b-8b}** = 2.225 Å, **TS_{6b-7a}** = 4.123 Å), which means that the 3.8 kcal/mol energy difference between these two transition states could be due to a stabilising intramolecular hydrogen bonding-type interaction in **TS_{6b-8b}**. As seen previously, the P1-Pd-P2 angle is larger in the large model than in the small model (P1-Pd-P2: **TS_{6b-8b}** = 119.5º, **TS_{6b-7a}** = 114.8º, Small model: **TS_{1b-2a}** = 98.9º).

These two new transition states do not lead towards a metallophosphorane intermediate, as seen in the small model. Instead they lead to a new type of structure that features an η^2-interaction between the palladium and a phenyl group from a $\{PPh_3OH^+\}$ ligand. The structures of these new intermediates, **8a** (E = 1.2 kcal/mol) and **8b** (E = 7.1 kcal/mol), can be seen in Figure 4.18. Looking more closely at structure **8a**, one of the major features is that the Pd-P1 bond present in **TS_{6b-7a}** has now broken (Pd···P1 = 3.236 Å). The vacant site on the palladium has been filled by one of the phenyl groups attached to P1 forming an η^2-interaction with palladium (C1-Pd = 2.213 Å and C2-Pd = 2.149 Å). σ-Donation from the carbons to palladium, coupled with π-back donation from palladium into a vacant π^* orbital causes lengthening of the C1-C2 bond, from around 1.39-1.41 Å in reactant **6a**, to 1.469 Å in **8a**. The H···Cl distance has also significantly shortened from 3.437 Å in **TS_{6a-8a}** to 1.914 Å in **8a**, which may have an additional stabilising effect. The Pd-P2 bond has shortened compared to the **TS_{6a-8a}** structure (Pd-P2: **8a** = 2.325 Å, **TS_{6a-8a}** = 2.425 Å). Conversely, the Pd-Cl bond is longer in **8a** than in **TS_{6a-8a}** (Pd-Cl: **8a** = 2.567 Å, **TS_{6a-8a}** = 2.501 Å). The palladium has adopted a structure which is approximately trigonal planar, with the main angles around the palladium adding up to 359.7º. The $\{PPh_3OH^+\}$ ligand is now formally a cation, and can be considered to be interacting with the $\{PdCl(PPh_3)^-\}$ fragment as a zwitterion. Now that P1 is no longer bonded to palladium, it has adopted a tetrahedral geometry with its remaining four substituents (O-P1-C1 = 114.7º, O-P1-C3 = 102.3º, O-P1-C4 = 108.0º).

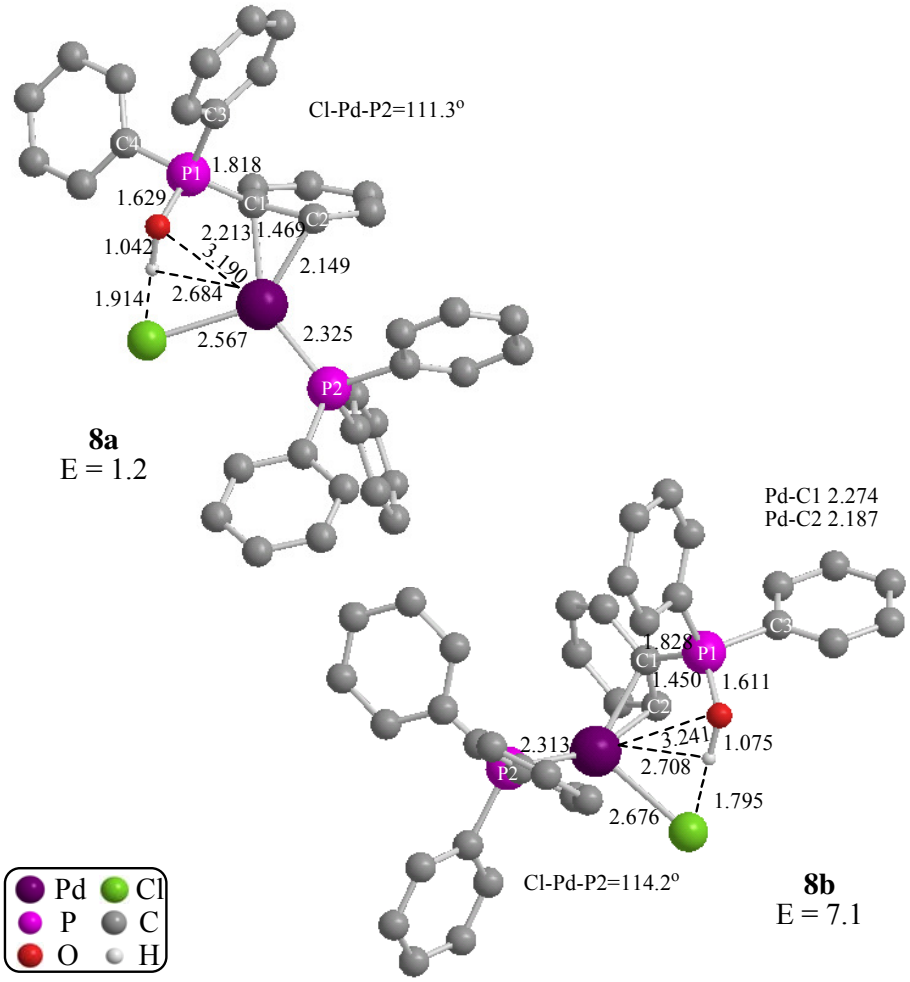

Figure 4.18: The optimised structures of **8a** and **8b**. Bond lengths and distances in Å, energies in kcal/mol.

Intermediate **8b**, which is formed from the cis reactant **6b**, has a similar η^2-bound structure to **8a**. The hydroxyl hydrogen in **8b** has a short interaction with palladium (Pd···H = 2.708 Å) and with chloride (H···Cl = 1.795 Å). The H···Cl hydrogen bonding interaction may contribute to the long Pd-Cl bond (Pd-Cl = 2.676 Å). The main difference between structures **8a** and **8b** is the orientation of the C1-C2 bond with respect to the metal coordination plane. As discussed before, in **8a** the C1-C2 bond lies in the metal coordination plane (C1-C2-Pd-P2 = 168.1º). However, the C1-C2 bond in **8b** is closer to being perpendicular to the plane, with a C1-C2-Pd-P2 torsion angle of 62.3º.

Intermediate **8a** is 5.9 kcal/mol more stable than **8b**. A possible explanation for this is the different orientations adopted by the η^2-phenyl groups coordinated to the palladium. In **8a** palladium interacts with a phenyl ring, which can be simplified to an alkene when looking at the orbitals involved. The Pd···Ph interaction can be modelled by approximating **8a** and **8b** to a d^{10}-ML_2 fragment interacting with ethene.

Generally, alkene ligands show a conformational preference to lie in the metal coordination plane when bonding to a d^{10}-ML_2 C_{2v} fragment, rather than lying perpendicular to the plane. Figure 4.19 illustrates the key frontier π-molecular orbitals in a d^{10} trigonal planar $ML_2(C_2H_4)$ system, and how the interactions change depending on the orientation of the alkene.[6] The diagram only shows the metal orbitals with the correct symmetry to interact with the ligand π^* orbitals and does not include the orbitals involved in σ-bonding as these are independent of the alkene orientation.

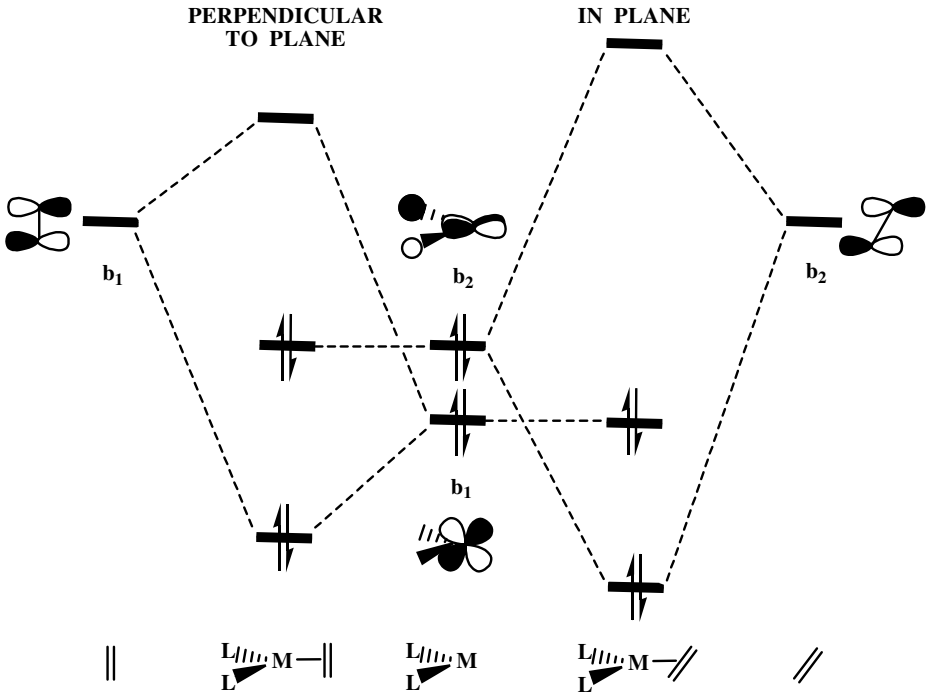

Figure 4.19: Molecular orbital diagram for $ML_2(C_2H_4)$ featuring the interaction between dπ orbitals of ML_2 and π^* orbitals of ethene.

If the alkene is perpendicular to ML_2, as shown on the left hand side of Figure 4.19, its π^* orbital has the correct symmetry to overlap with the metal b_1 orbital, leaving the metal b_2 orbital unaffected and non-bonding. However, if the alkene lies in the metal coordination plane, as shown on the right hand side of Figure 4.19, its π^* orbital has b_2 symmetry, so it overlaps with the metal b_2 orbital, and the metal b_1 orbital is non-

bonding. There is a smaller energy mismatch in the $\pi^* \pm b_2$ combination and the high-lying b_2 orbital is strongly stabilised, resulting in a preference for the in-plane alkene conformation.

Examples of well-characterised zwitterions similar to **8a** and **8b** have been synthesised. An example of an η^2-phosphoniostyrene-palladium(0) complex, [PdBr(*trans*-PhCH=CHPPh$_3$)(PPh$_3$)], was published by Huang *et al*. in 1998.[7] A diagram of the crystallographically determined structure is shown in Figure 4.20. There are several interesting geometric features to this structure. Firstly, the η^2-interacting carbon-carbon bond lies almost coplanar with the halide and PPh$_3$ ligands (C1-C2-Pd-P1 = 6.6°, C2-C1-Pd-I = 11.8°).[8] Furthermore, the {PhCH=CH(PPh$_3$)$^+$} ligand has an unsymmetrical η^2-interaction with the palladium, with a Pd□C1 distance of 2.084(8) Å and a Pd□C2 distance of 2.136(7) Å. This can be explained by the stronger trans influence of the PPh$_3$ ligand on C2 than the bromide exerts on C1. The C1-C2 bond is a similar length (1.435(10) Å) as the analogous bond in **8a** (1.469 Å) and **8b** (1.450 Å).

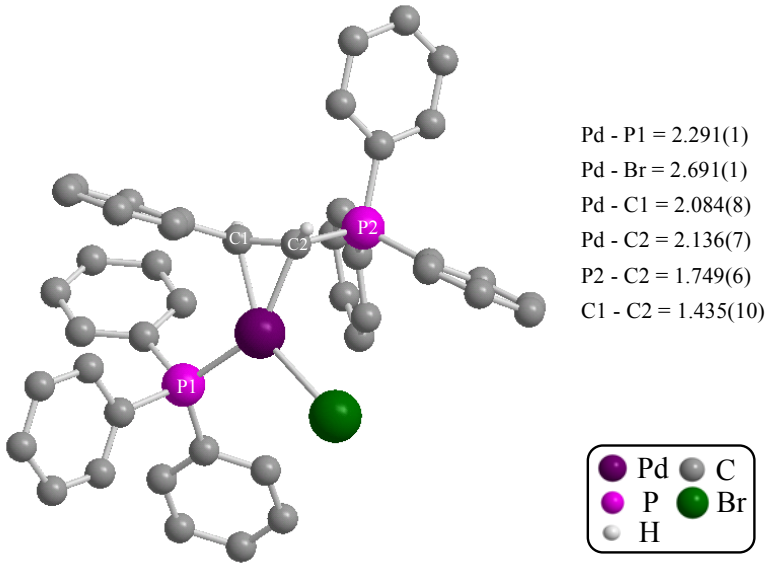

Figure 4.20: The crystallographically determined structure of [PdBr(*trans*-PhCH=CHPPh$_3$)(PPh$_3$)]. Bond lengths in Å.

4.9.4 Pathway B: Energy profile

The energy profile for P-O bond formation via Pathway B is shown in Figure 4.21. As seen in the formation of **7a**, the energy barrier is larger when starting from the trans reactant **6a** (ΔE_a = 31.7 kcal/mol) than from the cis reactant **6b** (ΔE_a = 22.7 kcal/mol).

However, despite the larger barrier, $\mathbf{TS_{6a\text{-}8a}}$ leads to the more thermodynamically stable intermediate, **8a** (+1.2 kcal/mol), due to the more favourable orientation of the η^2-phenyl group. $\mathbf{TS_{6a\text{-}8a}}$ is close in energy to $\mathbf{TS_{6a\text{-}7a}}$ (E = 32.3 kcal/mol) and $\mathbf{TS_{6b\text{-}7a}}$ (E = 30.5 kcal/mol) from Pathway A, while $\mathbf{TS_{6b\text{-}8b}}$ is the most accessible transition state located so far.

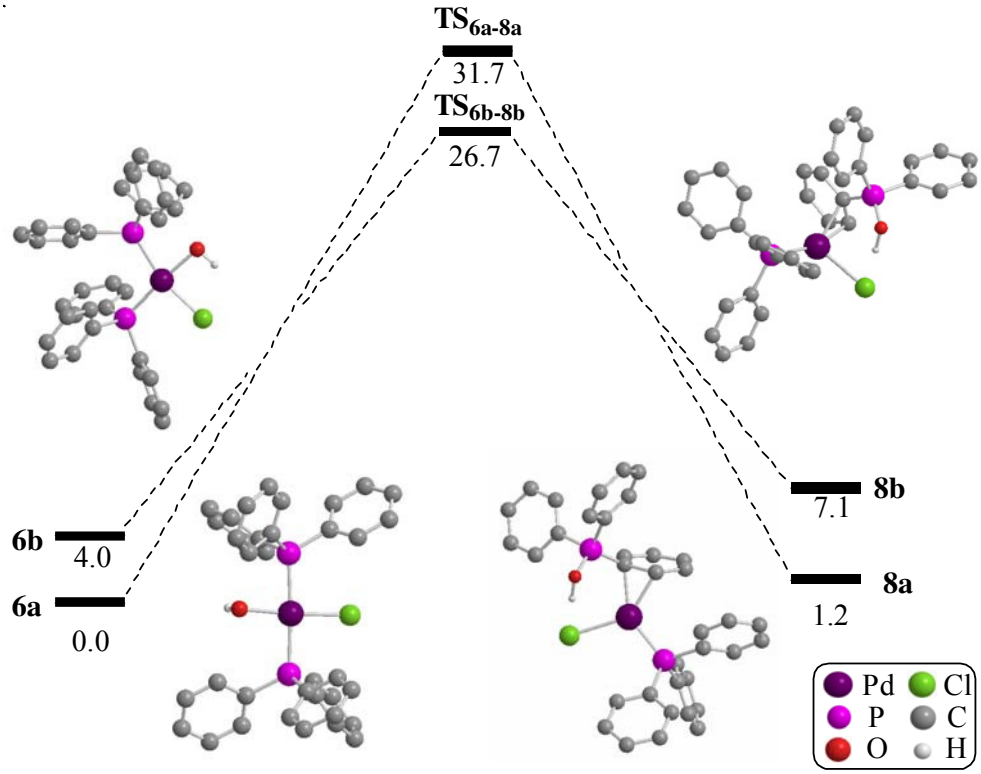

Figure 4.21: P-O bond formation, Pathway B – Energy profile (kcal/mol) for mechanism linking reactants **6a** and **6b** to intermediates **8a** and **8b** respectively.

4.9.5 Pathway A': Route to a new metallophosphorane structure

In the small model it was possible to go from a metallophosphorane intermediate to transfer the hydroxyl hydrogen onto palladium, accompanied by cleavage of the Pd-P1 and O-H bonds. The analogous mechanism was thoroughly investigated in the large model system, by first shortening the Pd···H distance and then lengthening the Pd-P bond, but none of the attempts was successful. Each time the Pd-P bond started to break, a phenyl moved into the new vacant site rather than the hydroxyl hydrogen. Extensive investigations led to the conclusion that it is not possible to transfer the hydroxyl hydrogen onto palladium directly from metallophosphorane **7a**.

However, during these studies the structure of a second metallophosphorane intermediate, **7b** (E = 23.2 kcal/mol), was discovered. In fact, **7b** is similar to metallophosphorane **2a** from the small model pathway, as the hydroxy hydrogen is pointing in the direction of the chloride (H-O-Pd-Cl: **7b** = 28.8º, **2a** = 29.1º) with a reasonably short H···Cl distance (H···Cl: **7b** = 2.482 Å, **2a** = 2.583 Å). This H···Cl interaction, which is not present in metallophosphorane **7a** (H-O-Pd-Cl = 135.3º, H···Cl = 3.900 Å), could account for **7b** being 2.8 kcal/mol more stable than **7a**. The structures of **7b** and the isomerisation transition state linking **7a** and **7b**, $\mathbf{TS_{7a\text{-}7b}}$ (E = 25.6 kcal/mol), corresponding to rotation about the P1-O bond, can be seen in Figure 4.22. There are only small changes in geometry and energy going from **7a**, through $\mathbf{TS_{7a\text{-}7b}}$ to **7b.**

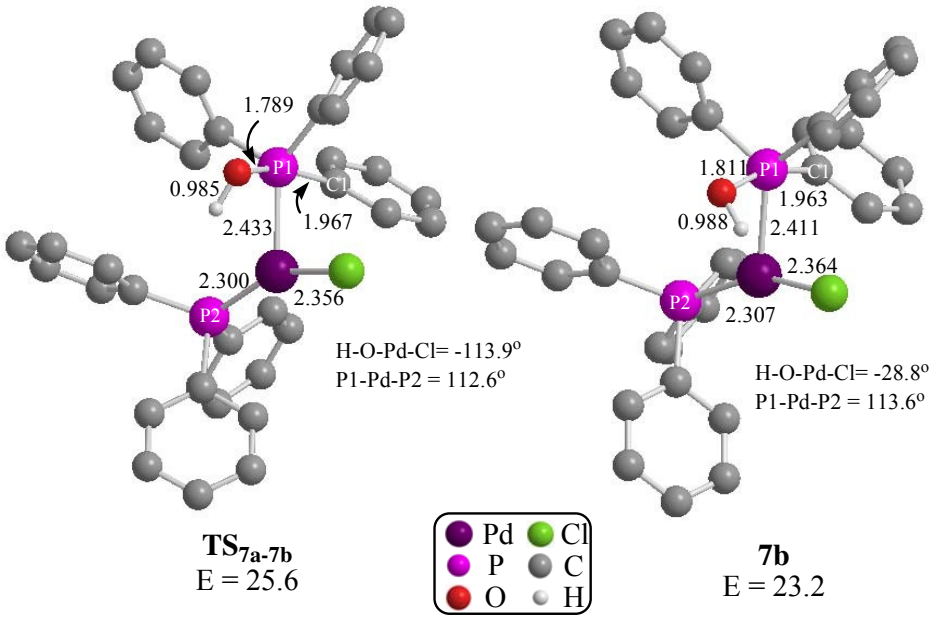

Figure 4.22: The optimised structures of $\mathbf{TS_{7a\text{-}7b}}$ and metallophosphorane **7b**. Bond lengths and distances in Å, energies in kcal/mol.

Attempts were also made to transfer the hydroxy hydrogen from the oxygen to palladium in metallophosphorane **7b**, but as was found with **7a**, this process was not possible. It was discovered, however, that it is possible to transfer the hydroxy group back onto palladium, leading to cis reactant **6b**. This provides a route for the formation of a metallophosphorane from **6b**, with an activation barrier of 23.5 kcal/mol through $\mathbf{TS_{6b\text{-}7b}}$ (E = 27.5 kcal/mol).

The structure of $\mathbf{TS_{6b\text{-}7b}}$, shown in Figure 4.23, is very similar to $\mathbf{TS_{6b\text{-}8b}}$ (Figure 4.16), which links cis reactant **6b** to zwitterion **8b**. Both transition states have an interaction between chloride and the hydroxy hydrogen, with a short H···Cl distance (H···Cl: $\mathbf{TS_{6b\text{-}7b}}$ = 2.511 Å, $\mathbf{TS_{6b\text{-}8b}}$ = 2.225 Å) and a similar orientation (H-O-Pd-Cl $\mathbf{TS_{6b\text{-}7b}}$ = 3.5º, $\mathbf{TS_{6b\text{-}8b}}$ = 4.8º). There are only small differences in bond lengths and distances, notably the Pd···C1 distance is longer in $\mathbf{TS_{6b\text{-}7b}}$ (3.220 Å) than in $\mathbf{TS_{6b\text{-}8b}}$ (3.068 Å), which may explain why they lead to different intermediate species.

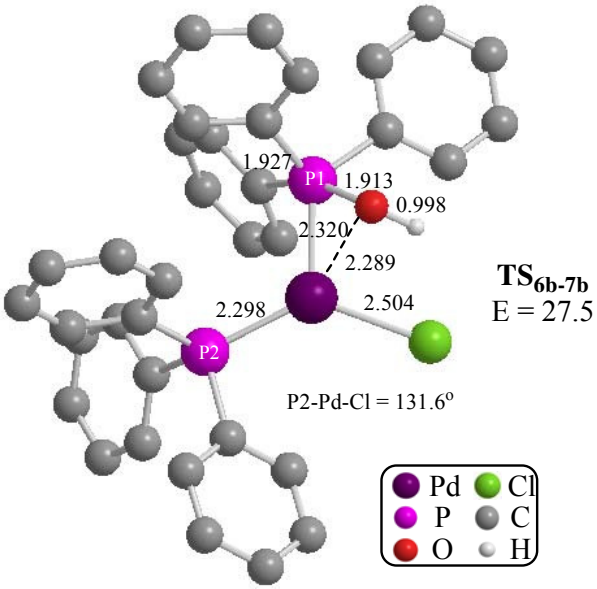

Figure 4.23: The optimised structures of $\mathbf{TS_{6b\text{-}7b}}$. Bond lengths and distances in Å, energy in kcal/mol.

4.9.6 Pathway A': Energy profile

The energy profile leading from the cis reactant **6b** via the new metallophosphorane **7b** to the original metallophosphorane **7a**, is shown in Figure 4.24. The energy highpoint in this part of the mechanism is at $\mathbf{TS_{6b\text{-}7b}}$ (27.5 kcal/mol). This is more accessible than the other two transition states that lead to **7a**, $\mathbf{TS_{6a\text{-}7a}}$ (E = 32.3 kcal/mol) and $\mathbf{TS_{6b\text{-}7a}}$ (E = 30.5 kcal/mol). $\mathbf{TS_{7a\text{-}7b}}$ is comparatively lower in energy than **7a**, due to the zero point correction as discussed previously. This means that isomerisation from **7a** to **7b** is essentially a barrierless process, and also that the energy surface is very flat in this region.

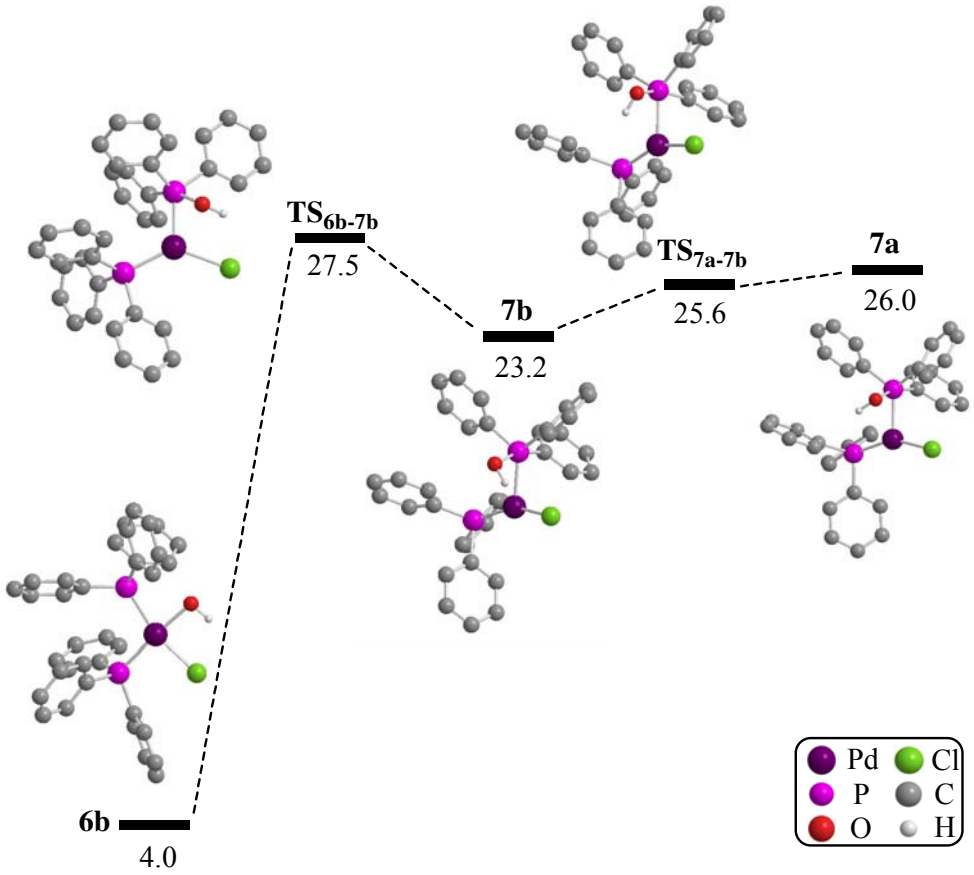

Figure 4.24: Pathway A' – Energy profile (kcal/mol) for mechanism linking reactant **6b** to metallophosphorane intermediate **7a**.

4.9.7 Linking Pathways A and B

As explained previously, it was not possible to find a pathway leading directly from a metallophosphorane intermediate to a product where hydrogen had been transferred to palladium in the analysis of the full experimental species. Nevertheless, a transition state linking metallophosphorane **7a** with zwitterion **8b** was located. This transition state, $\mathbf{TS_{7a\text{-}8b}}$ (E = 25.6 kcal/mol), is a link between Pathways A and B. It was hoped that a mechanism leading to [PdCl(H)PPh_3] and triphenylphosphine oxide from **8b** would subsequently be found. Figure 4.25 shows the structure of $\mathbf{TS_{7a\text{-}8b}}$ in more detail, and the energy profile for this part of the mechanism, linking pathways A and B.

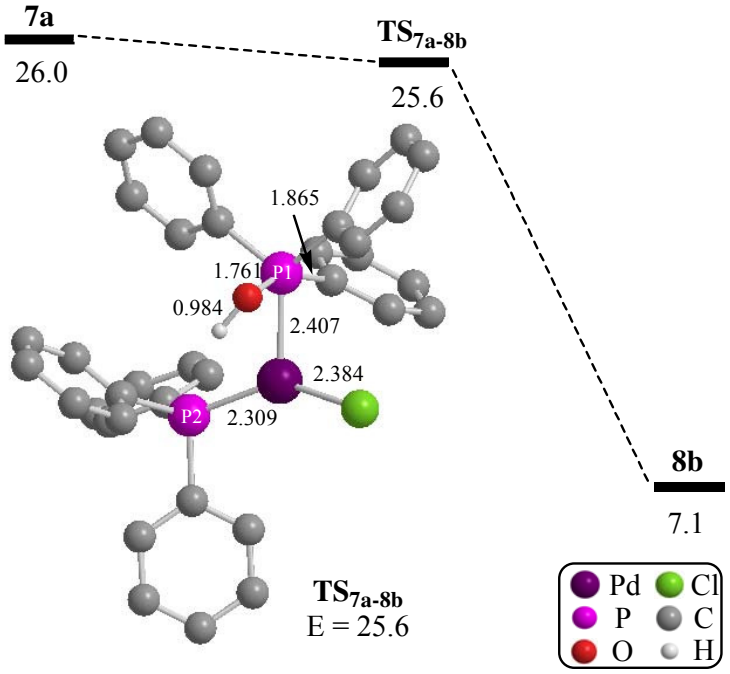

Figure 4.25: Phase 1: Pathway A-B – Energy profile (kcal/mol) for mechanism linking metallophosphorane **7a** to zwitterion **8b**. Bond lengths in Å.

TS$_{7a-8b}$ shows only small structural differences to metallophosphorane **7a**. The greatest differences are seen in the shortening of the P1-O bond from 1.805 Å in **7a** to 1.761 Å in **TS$_{7a-8b}$**, and the P1-C1 bond from 1.971 Å in **7a** to 1.865 Å in **TS$_{7a-8b}$**. The similarity of the structures is mirrored by the very small energy difference (ΔE = 0.4 kcal/mol). As seen in the previous section, the transition state is comparatively lower in energy than **7a**, due to the zero point energy correction, indicating that the potential energy surface is very flat in this region.

Conversely, major structural changes occur between **TS$_{7a-8b}$** and **8b**, accompanied by a substantial stabilisation in energy (ΔE = 18.5 kcal/mol). The changes are very similar to those seen in section 4.9.3 when zwitterion **8b** was formed from **TS$_{6b-8b}$**. The most significant changes are the breaking of the Pd-P1 bond and the formation of a Pd···Ph η^2-interaction.

4.9.7 Comparing Pathways A and B

All of the pathways for P-O bond formation are shown in Figure 4.26. Pathway A is shown from the left of the diagram to the centre, and features the three routes which pass through a metallophosphorane intermediate. The two routes for Pathway B, which lead directly to zwitterions **8a** and **8b**, are shown at the right hand side of the diagram. Four of the five pathways converge at zwitterion **8b**, with the fifth pathway via $\mathbf{TS_{6a\text{-}8a}}$, leading to zwitterion **8a**.

Comparison of the energy highpoints for the five pathways shows that the most accessible route is from cis reactant **6b**, via $\mathbf{TS_{6b\text{-}8b}}$ (E = 26.7 kcal/mol), to intermediate **8b**. The routes from cis **6b** are more accessible than those from trans **6a**, which is consistent with experimental observations.[1]

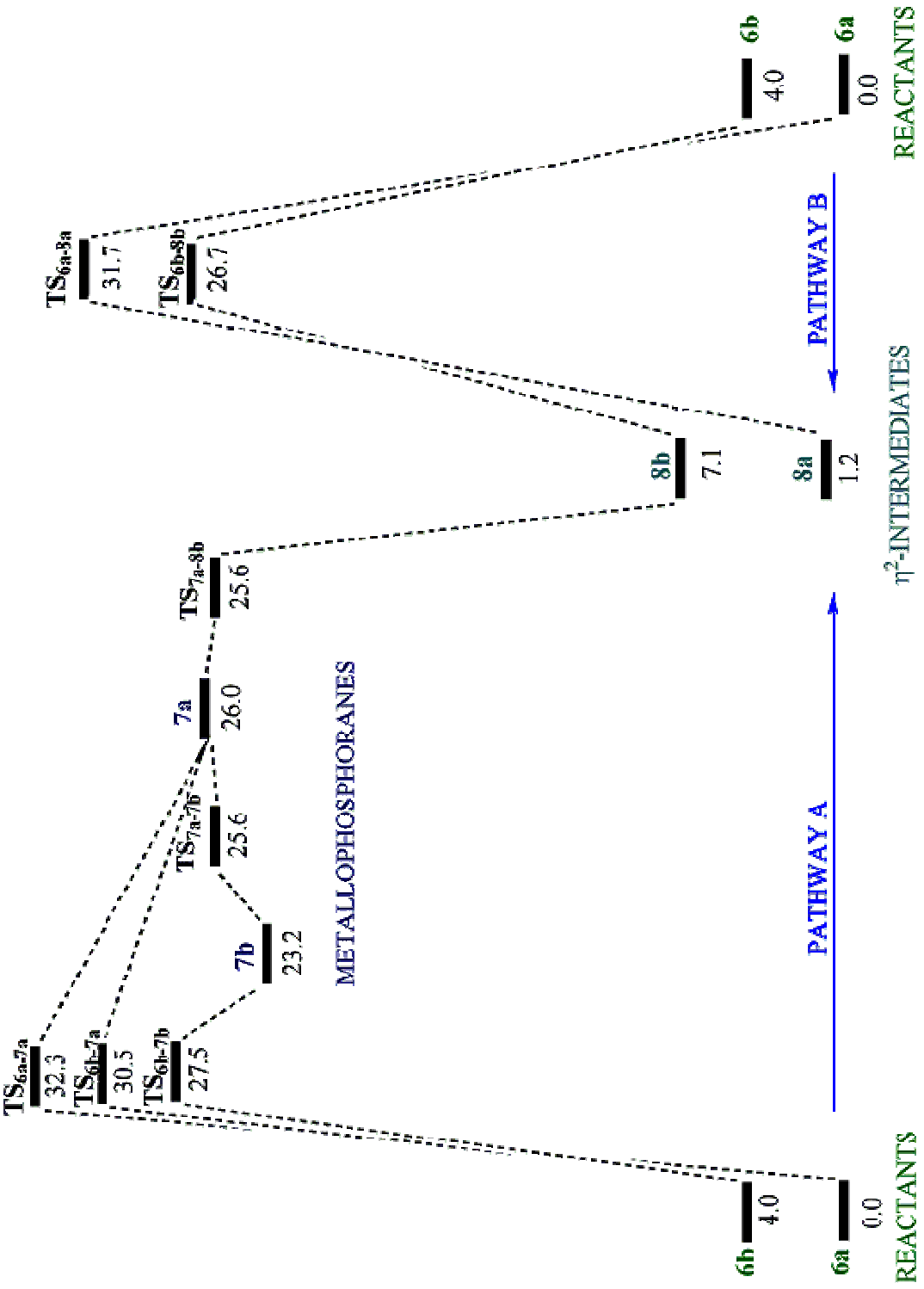

Figure 4.26: P-O Bond Formation: Pathways A and B – Energy profiles (kcal/mol) for both pathways.

4.10 Large model: Hydrogen Transfer

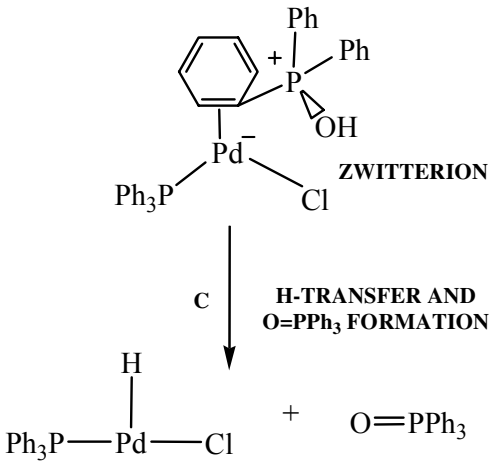

4.10.1 Pathway C: H-transfer and $O=PPh_3$ formation from 8b

As four of the five pathways in the initial part of the mechanism were found to converge at zwitterion structure **8b**, it was hoped that a mechanism could be found to lead from this species and transfer hydrogen from oxygen to palladium.

H-transfer onto palladium should displace the η^2- phenyl ring and break the O-H bond. To achieve this, the Pd···H distance in **8b** was shortened in a stepwise manner. However, rather than leading directly to hydrogen transfer, instead another zwitterion isomer was formed, with a different carbon-carbon bond in the phenyl interacting with palladium. The structures of the transition state, $\mathbf{TS_{8b\text{-}8c}}$ (E = 7.1 kcal/mol), and the new zwitterion structure, **8c** (E = 0.5 kcal/mol), are shown in Figure 4.27.

The isomerisation between **8b** and **8c** is essentially barrierless, as it has an activation energy of less than 0.05 kcal/mol. Not surprisingly, the structure of $\mathbf{TS_{8b\text{-}8c}}$ is very similar to **8b**. The main difference between the two zwitterion structures, **8b** and **8c**, is the way in which the phenyl ring interacts with palladium. In **8b** the η^2-interaction is between palladium, *ipso*-C1 and *ortho*-C2, and the C1-C2 bond lies out of the metal coordination plane (C1-C2-Pd-P2 = 62.3º). In **8c**, however, the palladium interacts with *ortho*-C2 and *meta*-C3, and the C2-C3 bond lies in the metal coordination plane (C2-C3-Pd-P2 = 179.5º). In **8c** the C1···Pd interaction has ceased (C1···Pd = 3.063 Å) and has been replaced by a C3···Pd interaction (C3···Pd: **8b** = 2.876 Å, **8c** = 2.161 Å).

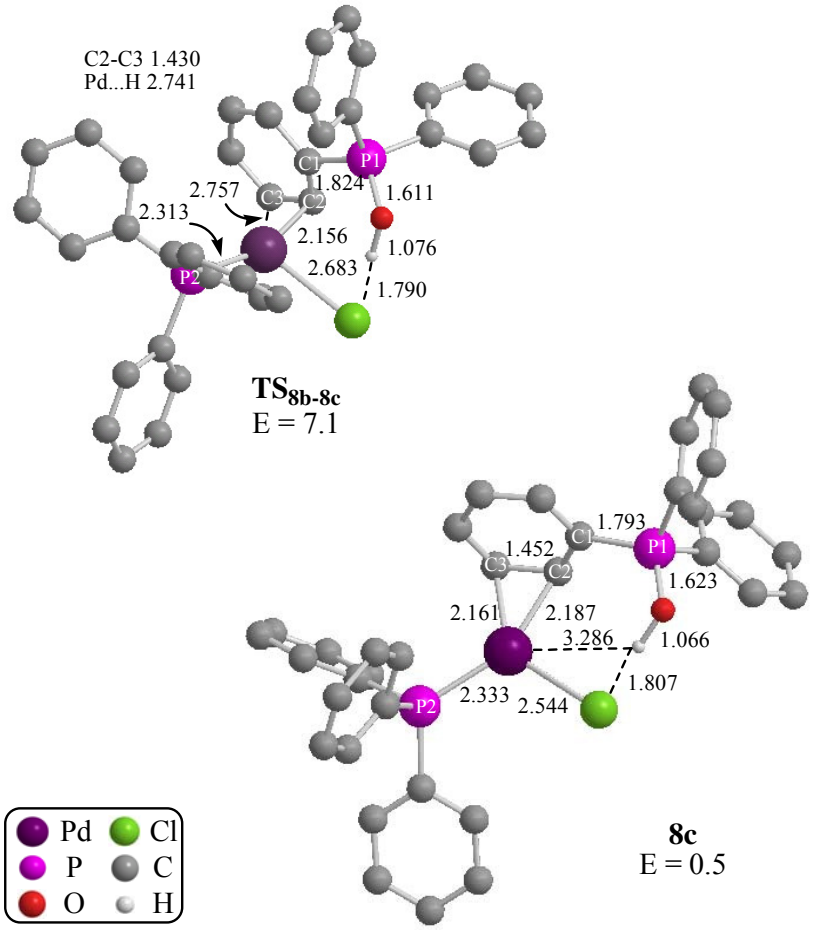

Figure 4.27: Structures of $\mathbf{TS_{8b\text{-}8c}}$ and zwitterion **8c**. Bond lengths and distances in Å and energies in kcal/mol.

Selected bond lengths and distances for structures **8a**, **8b**, $\mathbf{TS_{8b\text{-}8c}}$ and **8c** are shown in Table 4.3. If the carbon-carbon bond lengths (η^2-bound to Pd) are compared for all three zwitterion structures, it can be seen that the longest bond is in **8a**, where the *ipso*-C1- *ortho*-C2 bond is parallel to the metal coordination plane (C1-C2 = 1.469 Å) and this suggests it has the strongest coordination to the metal. The next longest carbon-carbon bond is seen in **8c**, where the *ortho*-C2-*meta*-C3 bond also lies in the plane (C2-C3 = 1.452 Å). The shortest carbon-carbon bond is seen in **8b**, where the *ipso*-C1-*ortho*-C2 bond lies out of the metal coordination plane (C1-C2 = 1.450 Å), so does not coordinate as effectively to palladium. The relative stability of **8c**, as with **8a**, could be explained by the conformational preference for analogous alkene ligands to lie in the metal coordination plane when bonding to a d^{10}-ML_2 fragment, as discussed earlier in the chapter.

Bond	8a	8b	TS_{8b-8c}	8c
Pd – C1	2.213	2.274	2.344	3.064
Pd – C2	2.149	2.187	2.156	2.187
Pd – C3	3.091	2.877	2.757	2.161
C1 – C2	1.469	1.450	1.450	1.452
C2 – C3	1.439	1.429	1.430	1.452

Table 4.3: Selected bond lengths and distances (Å) in structures **8a**, **8b**, $\mathbf{TS_{8b-8c}}$ and **8c**. The values in italics are not directly relevant.

The different orientation in the η^2-phenyl in **8c** causes the whole $\{PPh_3OH^+\}$ fragment to shift its position, resulting in longer Pd···O (4.065 Å) and Pd···P1 (4.134 Å) distances than in **8b** (Pd···O = 3.241 Å; Pd···P1 = 3.271 Å). Since this also means that the Pd···H(O) distance has increased (Pd···H: **8b** = 2.708 Å, **8c** = 3.286 Å) it is surprising that this is indeed a step towards transferring the hydroxy hydrogen onto the palladium. However, despite extensive efforts, no direct route was found from **8b**.

Further reduction of the Pd···H(O) distance from **8c** led to the location of $\mathbf{TS_{8c-9}}$ (E = 14.0 kcal/mol), which was found to lead to palladium hydride complex **9** (E = 4.9 kcal/mol). The structures of these species are shown in Figure 4.28. The major structural change seen in $\mathbf{TS_{8c-9}}$ is the position of the $\{PPh_3OH^+\}$ fragment with respect to palladium. The hydroxy hydrogen has moved away from chloride (H···Cl: **8c** = 1.807 Å, $\mathbf{TS_{8c-9}}$ = 2.853 Å) and closer to palladium (H···Pd: **8c** = 3.286 Å, $\mathbf{TS_{8c-9}}$ = 2.015 Å). Meanwhile, the η^2-phenyl has moved away from palladium ($Pd\cdots MP_{C2-C3}$: **8c** = 2.049 Å (MP = midpoint), $\mathbf{TS_{8c-9}}$ = 2.488 Å) as it is being displaced by the hydroxy hydrogen. Changes seen around palladium include the opening of the P2-Pd-Cl bond from 112.3º in **8c** to 131.0º in $\mathbf{TS_{8c-9}}$ and the shortening of the P2-Pd and Cl-Pd bonds (P2-Pd: **8c** = 2.333 Å, $\mathbf{TS_{8c-9}}$ = 2.297 Å; Cl-Pd: **8c** = 2.544 Å, $\mathbf{TS_{8c-9}}$ = 2.456 Å). The bond lengths and geometry around P1 do not change significantly.

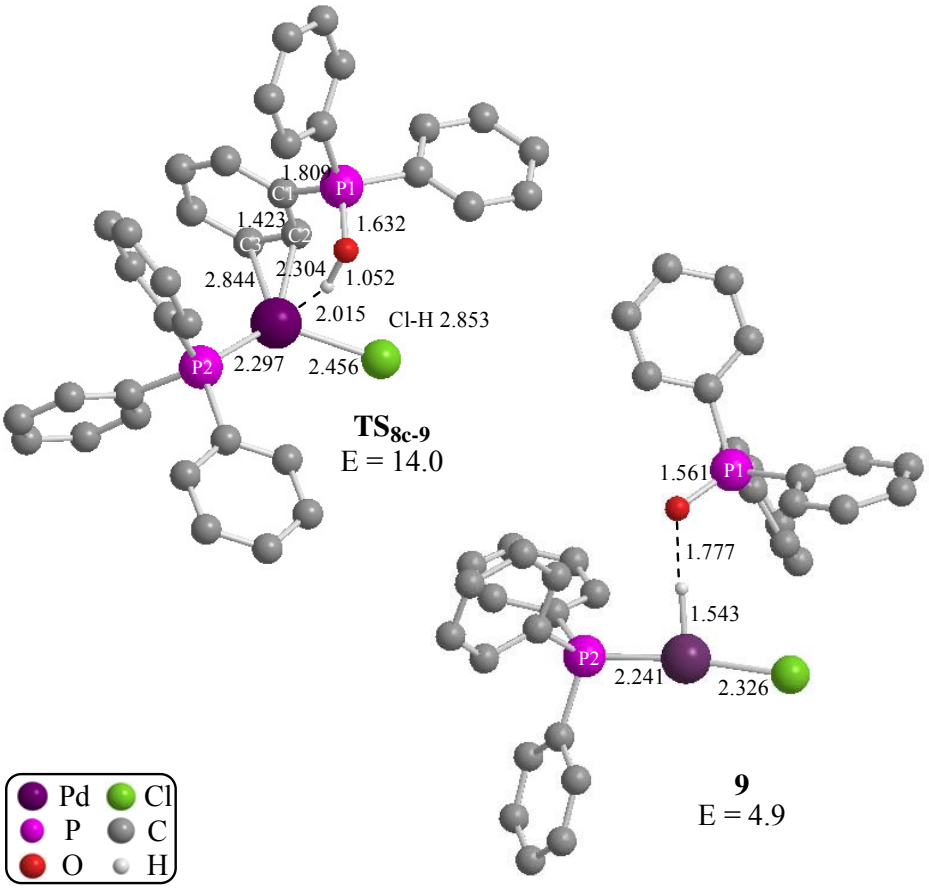

Figure 4.28: The structures of **TS$_{8c-9}$** and **9**. Bond lengths and distances in Å, energies in kcal/mol.

The final structure in the reaction mechanism is **9**, where hydrogen has been transferred onto the metal (Pd-H = 1.543 Å) and the O-H bond has broken (O···H = 1.777 Å). This means that phosphine oxide has been formed, but is still associated with the newly formed [Pd(Cl)H(PPh$_3$)]. The P1-O bond has shortened from 1.623 Å in **8c** to 1.561 Å in **9**, as this is now consistent with a P=O double bond. The Pd-P2 bond has shortened from 2.353 Å in **8c** to 2.241 Å in **9** and similarly the Pd-Cl bond has reduced from 2.544 Å in **8c** to 2.326 Å in **9**. This effect could be due to the change in formal oxidation state of the metal, from Pd(0) in [Pd(Cl)PPh$_3$]$^-$[PPh$_3$OH]$^+$, **8c,** to Pd(II) in **9**.

The structure of **9** is rather different to the analogous species in the small model, complex **3**. The hydrogen is further on in its transfer to palladium in **9**, with a shorter Pd···H distance (**3** = 1.884 Å, **9** = 1.543Å) and a longer O···H distance (**3** = 1.108 Å, **9** = 1.777 Å). Also, the Pd-Cl bond is longer in **3** (2.379 Å) than in **9** (2.326 Å), possibly due to the interaction between chloride and a phosphorus-bound hydrogen in **3**. Species

9 (E = 4.9 kcal/mol) is considerably more comparatively stable than **3** (E = 12.9 kcal/mol). This may be due to the greater reduction of steric interactions in **9** than in **3**.

4.10.2 Pathway C: H-transfer and O=PPh$_3$ formation from 8a

To complete the overall picture of the reaction mechanism, a pathway to link zwitterion **8a**, formed from trans reactant **6a**, to product **9** needed to be located. A transition state, **TS$_{8a-9}$** (E = 9.4 kcal/mol), was located by shortening the Pd···H distance from 2.684 Å in **8a**. The structures of **8a** and **TS$_{8a-9}$** are shown in Figure 4.29.

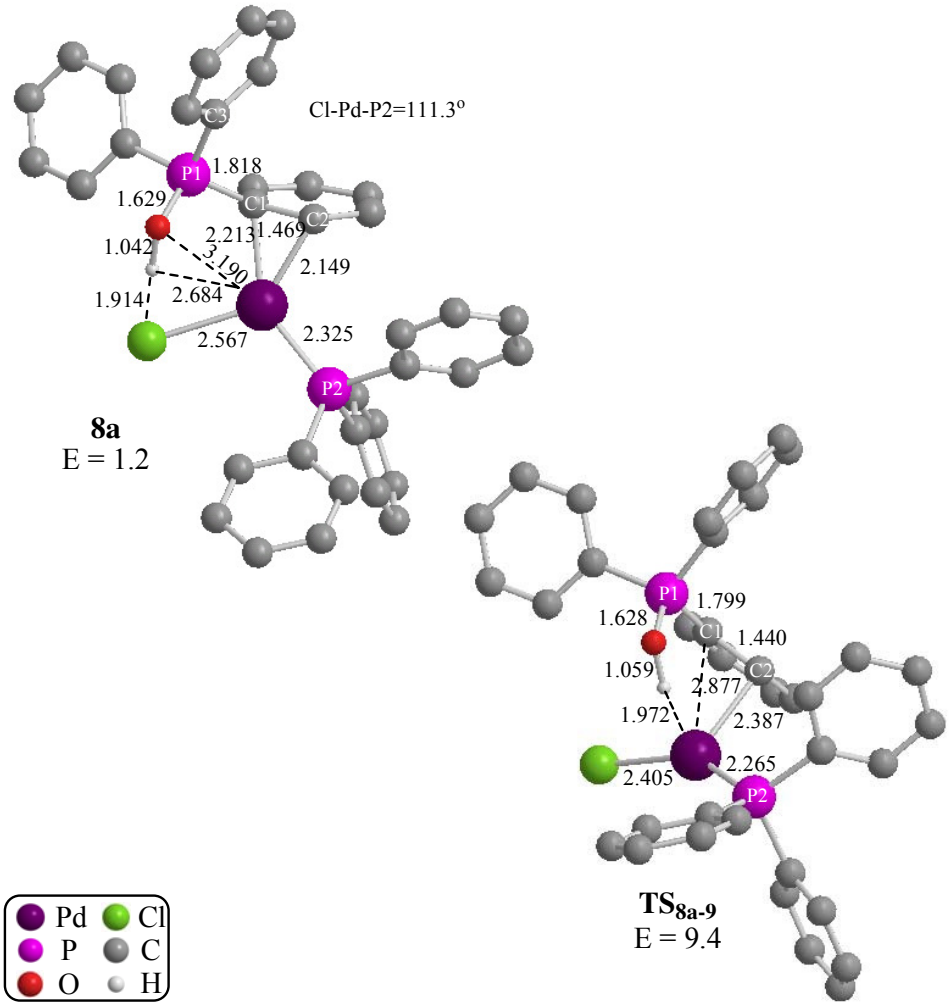

Figure 4.29: Structures of **8a** and **TS$_{8a-9}$**. Bond lengths and distances in Å, energies in kcal/mol.

	Atomic Distance / Å				Bond Length / Å	
Structure	H…Cl	H…Pd	Pd…C1	Pd…C2	Pd-Cl	Pd-P2
8a	1.914	2.684	2.213	2.149	2.567	2.325
TS_{8a-9}	3.184	1.972	2.877	2.387	2.405	2.265
9		1.543			2.326	2.241

Table 4.4: Selected bond lengths and distances (Å) in structures **8a**, **TS_{8a-9}** and **9**.

The structure of **TS_{8a-9}** is similar to **TS_{8c-9}**, as it features a lengthening of the H···Cl distance and a shortening of the H···Pd distance (see Table 4.4). In addition, the η^2-phenyl has begun to move away from palladium, with Pd···C1 increasing by 0.664 Å from **8a** to **TS_{8a-9}** and Pd···C2 increasing by 0.238 Å. As seen in the formation of **9** from **8b**, the Cl-Pd-P2 angle opens when passing from zwitterion **8a** to product **9** (Cl-Pd-P2: **8a** = 111.3º, **TS_{8a-9}** = 144.1º, **9** = 173.7º). There is also a shortening of the Pd-Cl and Pd-P2 bonds as the oxidation state of the palladium changes from Pd(0) to Pd(II).

4.10.3 Pathway C (from 8a to 9): Energy profile

Unlike the route from **8b** to **9**, the pathway from **8a** to **9** is a one-step process (see Figure 4.30). The energy highpoint is low compared to transition states earlier in the mechanism, at 9.4 kcal/mol. Therefore, this process provides a simple and accessible route to **9**.

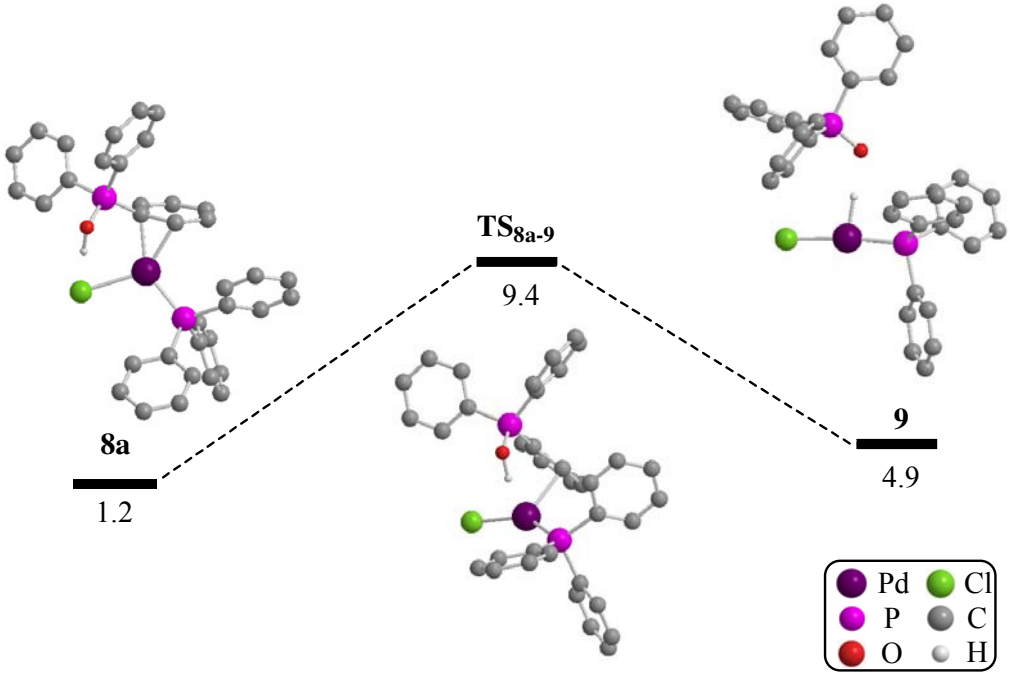

Figure 4.30: Pathway C: Energy profile (kcal/mol) linking **8a** to **9**.

4.10.4 Pathway C (from 8b to 9): Energy profile

The energy profile linking zwitterion **8b** to **9**, with the relevant structures included, is shown in Figure 4.31. The formation of **8c** is essentially a barrierless process, but a barrier of 13.5 kcal/mol must be overcome to transfer the hydrogen from oxygen to palladium, to form **9**. The energy highpoint for this part of the mechanism is $\mathbf{TS_{8c\text{-}9}}$ (E = 14.0 kcal/mol), but this is not a rate-limiting step in the overall reaction as it is considerably lower than the initial transition states to form a P-O bond (lowest initial transition state is $\mathbf{TS_{6b\text{-}8b}}$, E = 26.7 kcal/mol).

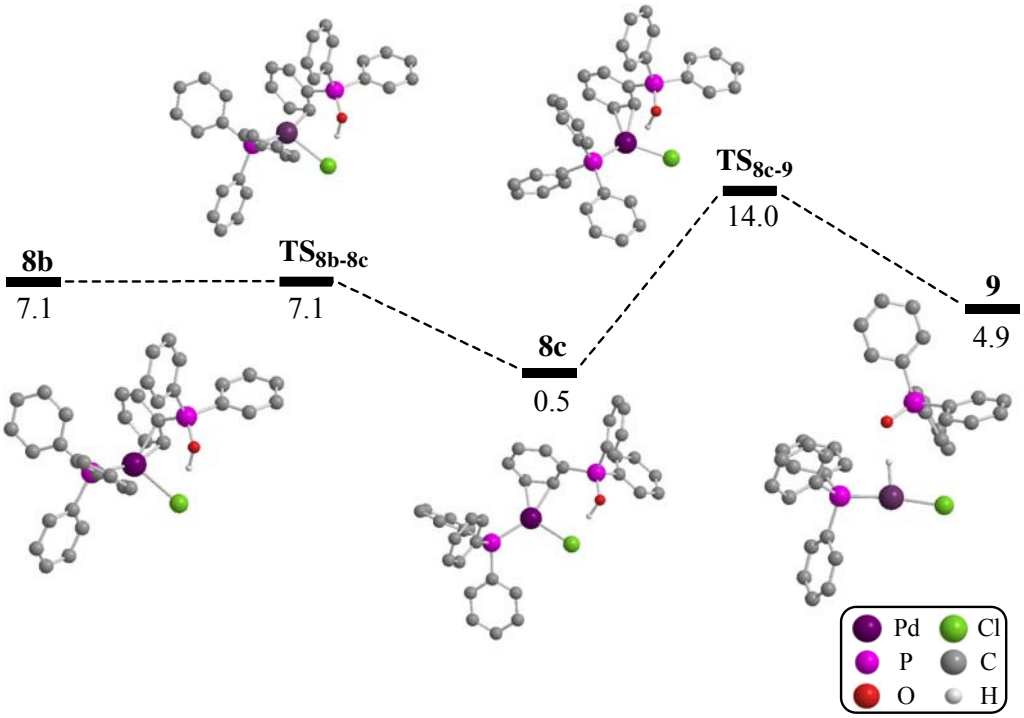

Figure 4.31: Pathway C: Energy profile (kcal/mol) linking **8b** to **9**.

4.11 Large model [PdCl(OH)(PPh_3)$_2$]: Overview

Investigation of the mechanism of the disproportionation reaction found a number of possible routes linking reactants *trans*- and *cis*-[PdCl(OH)(PPh_3)$_2$] (**6a** and **6b**) to [PdCl(H)(PPh_3)] and O=PPh_3. Three routes passed through metallophosphorane intermediate structures, and all five routes passed through zwitterion species. The most energetically accessible route starts from **6b** and has an overall highpoint at **$TS_{6b\text{-}8b}$** of 26.7 kcal/mol. This profile is shown in Figure 4.32. This route does not pass through a metallophosphorane intermediate. However, the most accessible route that does pass through a metallophosphorane species (**7a**) has a highpoint of 27.5 kcal/mol (**$TS_{6b\text{-}7b}$**) which is less than 1 kcal/mol higher than **$TS_{6b\text{-}8b}$**, making it competitive with the globally most accessible route.

If the energies of products [PdCl(H)(PPh_3)] and O=PPh_3 are calculated separately and added together, the combined enthalpy is 13.1 kcal/mol. However, if a correction is made for free energy, the value becomes 0.0 kcal/mol, making the process thermoneutral. This is quite a difference from the energy of the combined products for the small model system, which was 28.9 kcal/mol, decreasing to 19.0 kcal/mol for free energy. It seems that there is a large effect on the energy when the steric bulk is included in the system. Additionally, in the small model it was necessary to overcome a Cl□H interaction which is not present in the large model system.

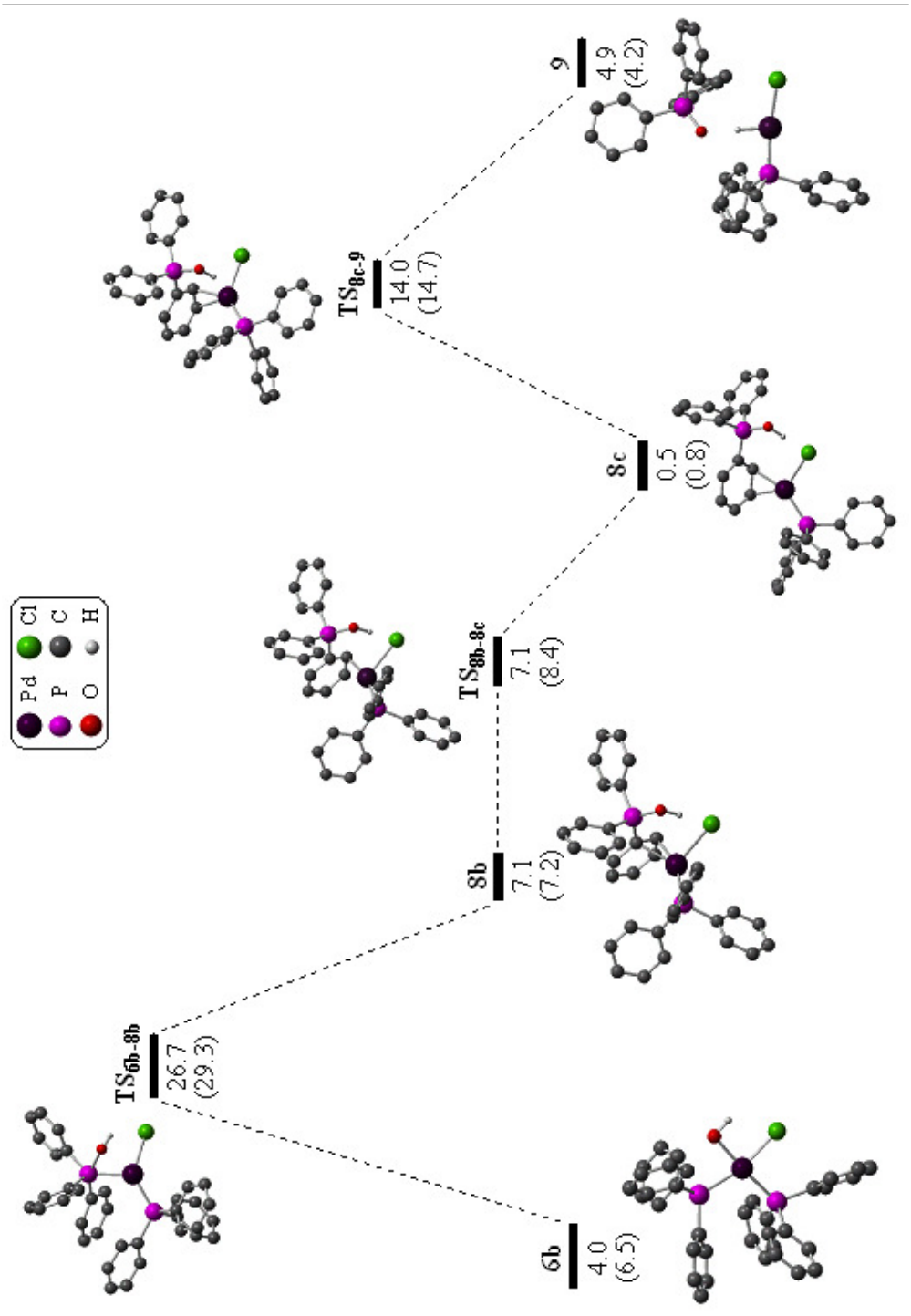

Figure 4.32: Energy profile (kcal/mol) of the lowest route for the disproportionation mechanism in the large model analysis. Free energy values shown in parenthesis.

4.12 Large model: Natural population analysis

All of the structures from the large model were analysed using natural atomic population analysis calculations, as were performed for all the species in the small model earlier in this chapter. As before, the focus of the analysis was on the charges on P1 and palladium, and the values are shown in Table 4.5. The values for only one pathway are shown as the same trends were observed in all of the possible pathways. This pathway was selected because it features both a metallophosphorane and zwitterion intermediates, allowing their charge distribution to be compared.

Structure	q(P1)	q(Pd)
PPh_3	0.95	
6b	1.16	0.34
TS_{6b-7a}	1.52	0.27
7a	1.63	0.14
TS_{7a-8b}	1.70	0.13
8b	2.08	0.20
TS_{8b-8c}	2.08	0.20
8c	2.06	0.24
TS_{8c-9}	2.07	0.11
9	2.06	0.06
$O=PPh_3$	2.04	
$[PdClH(PPh_3)]$		0.13

Table 4.5: Computed natural atomic charges (q) focusing on P1 and Pd for a selected pathway in the large model of the disproportionation mechanism.

As seen in the small model, the negative charge (electron density) on P1 decreases considerably between the reactant **6b** (q = 1.16) and the metallophosphorane intermediate **7a** (q = 1.63). The then negative charge decreases further as zwitterion **8b** (q = 2.08) is formed. This value then remains almost constant through to the product structure, **9** (q = 2.06), and is consistent with the charge on P1 in phosphine oxide (q = 2.04). This suggests that P1 in a zwitterion (**8b** and **8c**) is closer in nature to P(V) than P1 in a metallophosphorane (**7a**).

An increase in negative charge on palladium is seen between the 4-coordinate reactant **6b** (q = 0.34) and the metallophosphorane intermediate **7a** (q = 0.14), as seen in the small model analysis. The negative charge then decreases further with the formation of the zwitterions **8b** (q = 0.20) and **8c** (q = 0.24). As in the small model analysis, the

minimum complex with the lowest negative charge on palladium is the structure where the hydroxy hydrogen is bridging between palladium and oxygen, in this case **9** (q = 0.06). The negative charge falls to around the value of the palladium in **7a** (q = 0.14) when [PdClH(PPh_3)] is formed (q = 0.13). This suggests that there is slightly more electron density on palladium in a metallophosphorane (**7a**) than in a zwitterion (**8b** and **8c**).

4.13 Effects of solvation

Polarisable continuum model (PCM) calculations were performed to investigate whether the energy profiles reported in this chapter would be affected by solvation. Single point values at full DFT level were obtained, and then enthalpy corrections using values from the ONIOM/HF calculations were applied to the values. The experimental work by Grushin and Alper on this disproportionation reaction was carried out in a mixture of benzene and water.[1] Therefore, PCM single point calculations were performed in water and in benzene, and then compared to the enthalpy values in a vacuum that have been reported in this chapter.

There was a clear trend across all the results, namely that the addition of water solvation stabilised the energies along the reaction profile by an average of 2.9 kcal/mol, while solvation in benzene stabilised the energies by an average of 1.4 kcal/mol. It is not surprising that water, a more polar solvent, has a larger effect when stabilising these complexes which do contain a degree of charge separation. However, as the whole profile was affected by solvation to a similar extent, there was no change in the order of the energy highpoints in the key first transition states.

4.14 Conclusions

The analysis of the small model, [PdCl(OH)(PH_3)$_2$], was useful to study routes via metallophosphorane intermediates. However, with PH_3 rather than PPh_3, it was not possible to form species with an η^2-interaction between palladium and a phenyl group.

A greater variety of routes were found when the full experimental complex, [PdCl(OH)(PPh_3)$_2$], was modelled. The most accessible route in the small model analysis had a highpoint of 21.8 kcal/mol (**TS_{6b-7a}**) while in the large model system it was 26.7 kcal/mol (**TS_{6b-8b}**). This may be result of the inclusion of steric factors in the large model system.

Both the small and large model analyses showed that the reaction is more accessible from the cis reactant than the trans, which is consistent with the experimental observations of Grushin and Alper.[1]

Overall, the computational investigations have shown that there are energetically accessible pathways for the hydroxide-induced disproportionation reaction that proceed via an intramolecular attack of hydroxide on a palladium-bound phosphine ligand.

4.15 References

1 Grushin, V. V.; Alper, H., *Organometallics*, **12**, 1890, (1993)

2 Macgregor, S. A.; Neave, G. W., *Organometallics*, **23**, 891, (2004)

3 Ferguson, G.; McCrindle, R.; McAlees, A. J.; Parvez, M., *Acta Crystallogr., Sect. B: Struct. Crystallogr. Cryst. Chem.*, **38**, 2679, (1982)

4 Qin, Z.; Jennings, M. C.; Puddephatt, R. J., *Inorg. Chem.*, **40**, 6220, (2001)

5 Macgregor, S. A.; Wondimagegn, T, *Organometallics*, **26**, 1143, (2007)

6 Albright, T.A.; Burdett, J. K.; Whangbo, M.-H., *Orbital Interactions in Chemistry*, John Wiley and Sons, New York, (1985)

7 Huang, C-C.; Duan, J-P.; Wu, M-Y.; Liao, F-L.; Wang, S-L.; Cheng, C-H., *Organometallics*, **17**, 676, (1998)

8 Torsion angles found from examining 3D structure held in the Cambridge Crystallographic database for ref. 7; Allen, F. H., *Acta Cryst.*, B**58**, 380, (2002)

Chapter 5: A mechanistic study of Ph/Ph' exchange in *trans*-[PdX(Ph)(PPh_3)$_2$] (X = Cl, Br, I)

5.1 Introduction

Aryl/aryl (Ar/Ar') exchange occurs in a wide range of systems, as discussed in Chapter 1. This can be a problem, as it can lead to the formation of unwanted side products, as Chenard *et al*. observed when using [Pd(PPh_3)$_4$] as a catalyst in a Stille cross-coupling reaction.[1] Many cases of Ar/Ar' scrambling have been reported, and some detailed studies have been performed to attempt to understand the mechanism of this type of exchange reaction. Bryant and Abatjoglou,[2] and later Cheng and Kong[3] suggested that exchange may proceed via an oxidative addition across a phosphine P-C bond, followed by a reductive elimination to form a bond between phosphorus and a metal-bound aryl group, as shown in Path 1 in Figure 5.1. Goel, however, proposed that exchange may occur with an initial nucleophilic attack of an aryl onto a coordinated phosphine ligand.[4] The observation that the addition of excess phosphine strongly inhibits exchange led several groups to hypothesise that pre-dissociation of the spectator phosphine was necessary for exchange to occur. Novak *et al.*[5] and Grushin[6] published a possible reaction schemes featuring a phosphonium salt intermediate, as shown in Path 2 in Figure 5.1.

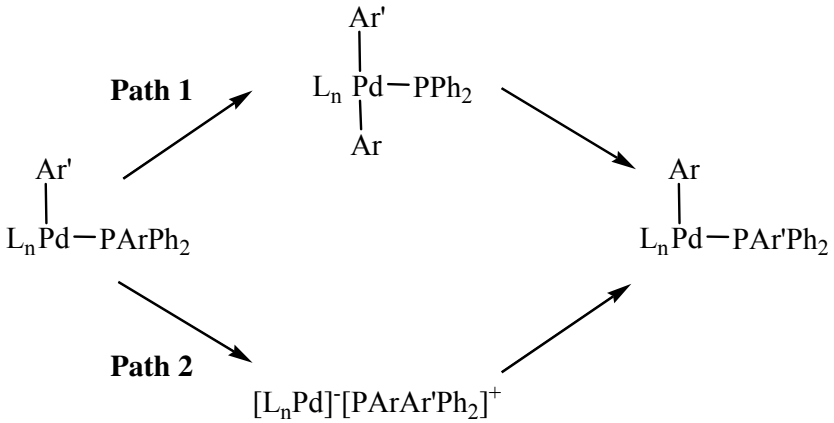

Figure 5.1: Two proposed mechanisms for Ar/Ar' exchange.

This chapter contains a detailed mechanistic study of phenyl/phenyl (Ph/Ph') exchange in *trans*-[PdX(Ph)(PPh_3)$_2$] (X = Cl), followed by an investigation into the effect that changing the halide (X = Br, I) has on the reaction profiles and energies. Drawing from the experimental work that has been conducted in this area, mechanisms based on both Paths 1 and 2 from Figure 5.1 will be investigated.

The ONIOM approach (BP86:HF) was used for this study, as described in Chapter 2. The palladium, phosphorus and halide atoms are at the 'high' level of calculation, as are the carbons and hydrogens of the palladium-bound phenyl ligand and the phosphorus-bound phenyl group that will undergo exchange. The carbon and hydrogen atoms in the five spectator phenyl groups are at the 'low' level of calculation, as depicted in Figure 5.2.

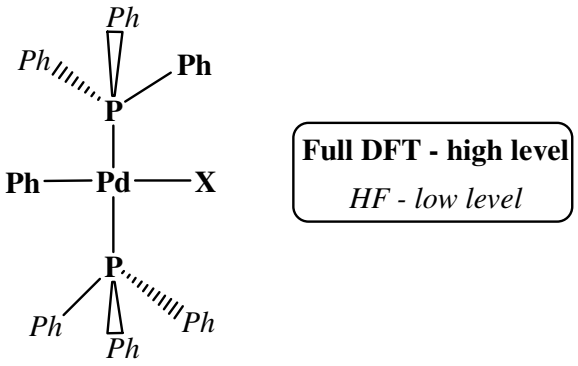

Figure 5.2: *trans*-[PdX(Ph)(PPh_3)$_2$] with the atoms at **high** and *low* level of calculation indicated.

Four distinct mechanisms were investigated for the exchange of the palladium-bound phenyl group with one of the phosphine phenyl groups. The mechanisms differ in their initial step, as to whether this involves attack of the palladium-bound phenyl group on a phosphorus, or the transfer of a phosphine phenyl group onto palladium. Also, a further factor considered was whether the mechanism involves the pre-dissociation of the spectator phosphine group, so that exchange occurs from a 3-coordinate reactant. These mechanisms are shown in Figure 5.3.

Mechanisms **A** and **B** both begin from the 4-coordinate reactant, *trans*-[PdCl(Ph)(PPh_3)$_2$]. Mechanisms **C** and **D** both start from a 3-coordinate reactant, formed by dissociation of the spectator triphenylphosphine in *trans*-[PdCl(Ph)(PPh_3)$_2$]. In principle, this would initially form T_{PPh_3}-[PdCl(Ph)(PPh_3)], however this was found to isomerise to form T_{Ph}-[PdCl(Ph)(PPh_3)]. The second part of this Ph/Ph' exchange study investigates the effect of using iodide and bromide in place of chloride, to enable comparison with the experimental results. Grushin found that exchange was most facile with iodide, followed by bromide and then chloride.[6]

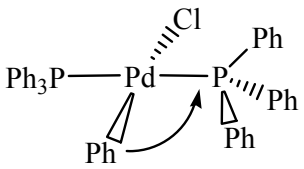

A Transfer of Ph from Pd to P (4 coord)

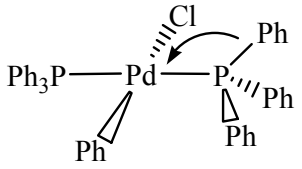

B Transfer of Ph from P to Pd (4 coord)

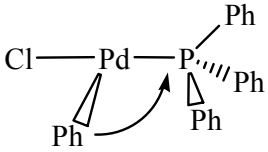

C Transfer of Ph from Pd to P (3 coord)

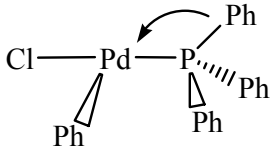

D Transfer of Ph from P to Pd (3 coord)

Figure 5.3: The four initial phenyl transfer steps to be considered for Ph/Ph exchange from *trans*-[PdCl(Ph)(PPh_3)$_2$] (**A** and **B**) and T_{Ph}-[PdCl(Ph)(PPh_3)] (**C** and **D**).

5. 2 Mechanism A

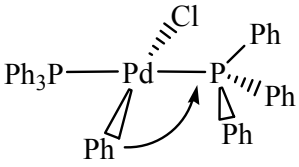

A Transfer of Ph from Pd to P
(4 coord)

The initial structure of the reactant, *trans*-[PdCl(Ph)(PPh_3)$_2$], was optimised starting from the crystallographically determined structure of this species.[7] This provided a conformationally realistic structure from which to begin the reaction profile. The optimised structure of reactant **1a** (E set to 0.0 kcal/mol) is shown in Figure 5.4. All subsequent energies reported in this chapter will be relative to **1a**, unless otherwise stated. The two phenyl groups with numbered carbons are the groups that will exchange, and are therefore at the high level of calculation.

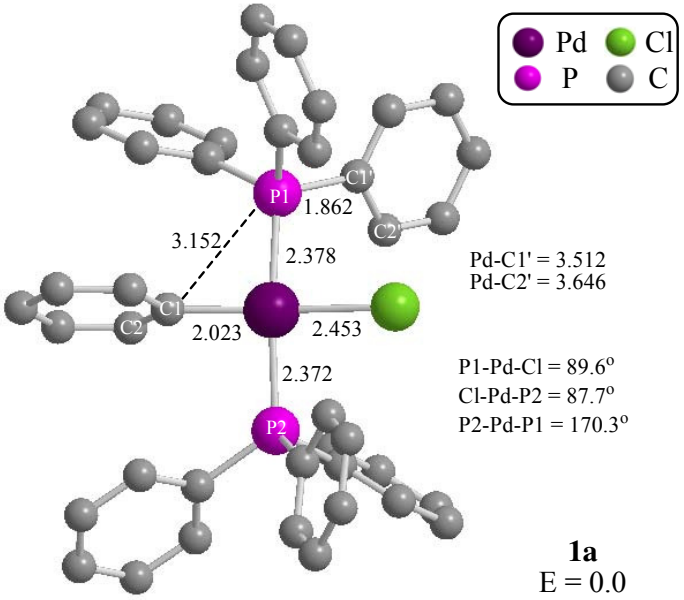

Figure 5.4: The optimised structure of reactant **1a**, *trans*-[PdCl(Ph)(PPh_3)$_2$]. Phenyl hydrogens have been omitted for clarity. Bond lengths and distances in Å, energy in kcal/mol.

If the structure of **1a** is compared to the crystallographically determined structure of *trans*-[PdCl(Ph)(PPh_3)$_2$], they are found to be very similar. Table 5.1 shows selected bond lengths and angles for both structures. Both species have a distorted square planar geometry, with a P1-Pd-P2 angle of 177.55(2)º experimentally and 170.3º in **1a**, which

Atoms	Experimental bond lengths / Å	Calculated bond lengths in **1a** / Å	Atoms	Experimental angles / º	Calculated bond angles in **1a** / º
Pd-P1	2.316(1)	2.378	C1-Pd-P2	91.38(7)	92.8
Pd-P2	2.324(1)	2.372	P1-Pd-C1	90.29(7)	91.2
Pd-Cl	2.407(1)	2.453	P1-Pd-Cl	89.75(2)	89.6
Pd-C1	2.016(3)	2.023	P1-Pd-P2	177.55(2)	170.3

Table 5.1: Selected bond lengths and angles in the crystallographically determined structure of *trans*-[PdCl(Ph)(PPh_3)$_2$][7] and the calculated structure of **1a**.

is presumably less than 180º due to the steric bulk of the palladium-bound phenyl. The calculated bond lengths are all slightly longer than those determined experimentally, but all by less than 3%. For instance, the Pd-P bond lengths are overestimated by <0.06 Å in **1a**. This overestimation was also seen by Macgregor and Wondimagegn[8] in calculated Rh-P bond lengths in [RhF(PPh_3)$_3$] when comparing them to the crystallographically determined structure. To see whether the difference in bond lengths are significant, the four bonds to palladium in **1a** were fixed at the values observed experimentally, and the resulting optimised structure was only 0.8 kcal/mol less stable. Therefore, these small overestimations in bond lengths for a computed structure are not thought to make a significant difference to the computed energies.

To begin the exchange reaction profile, the P1···C1 distance was reduced in a stepwise scan, starting from a distance of 3.152 Å in **1a**. A transition state calculation was run from the maximum energy point in the scan, which led to the location of **TS_{1a-1b}** (E = 31.1 kcal/mol), shown in Figure 5.5. The main geometric change that occurs between **1a** and **TS_{1a-1b}** is the position of the palladium-bound phenyl group. The C1···P1 distance reduces by 0.91 Å, coupled with an increase of 0.110 Å in the Pd···C1 distance. The two phosphorus atoms and the chloride remain in the metal coordination plane, with the P1-Cl-Pd-P2 torsion angle only reducing by 3.5º to 167.2º in **TS_{1a-1b}**. However, the transferring phenyl moves out of the metal coordination plane, with the Cl-P1-Pd-C1 torsion angle reducing from 171.3º in **1a** to 129.6º in **TS_{1a-1b}**. The plane of the transferring phenyl group lies approximately perpendicular to the Pd-P1 bond, as predicted by Hoffmann *et al.*[9] The phenyl group on P1 that lies opposite to the attacking phenyl moves closer to palladium, with the Pd···C1' distance reducing from 3.512 Å in **1a** to 2.705 Å in **TS_{1a-1b}**. The P1-Pd-P2 angle has reduced by 24.5º, so the spectator phosphine group has begun to move into the new vacant site. Other more minor changes in geometry can be observed. For instance, the Pd-P2 bond lengthens by

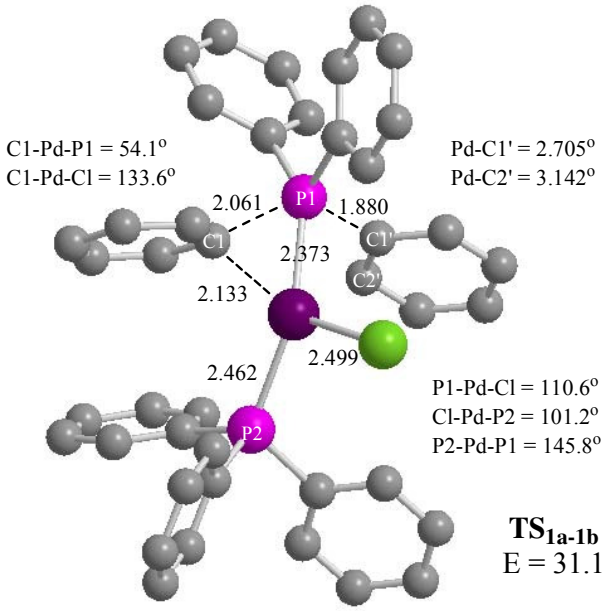

Figure 5.5: The structure of **TS_{1a-1b}**. Bond lengths and distances in Å, energy in kcal/mol.

0.09 Å as the geometry distorts further from a square planar structure, with the Cl-Pd-P1 angle opening by 21.0º and the Cl-Pd-P2 angle opening by 14.5º. There is virtually no change in the Pd-P1 bond length.

Pseudo-intrinsic reaction coordinate (PIRC) calculations were carried out from **TS_{1a-1b}** and they confirmed that the transition state links to **1a** and to intermediate **1b** (E = 22.9 kcal/mol). The structure of **1b** with key bond lengths and angles denoted are shown in Figure 5.6. Major structural changes have occurred in the transition from **1a** to **1b**. These include the breaking of the Pd-C1 and Pd-P1 bonds, and the formation of a P1-C1 bond and an η^2-interaction between palladium and the *ipso-ortho* C1'-C2' bond in the exchanging phenyl group.

The η^2-interaction in zwitterion **1b**, $[Pd(Cl)PPh_3]^-[PPh_4]^+$, was also seen in structures **8a** and **8b**, isomers of $[Pd(Cl)PPh_3]^-[P(OH)Ph_3]^+$, in Chapter 4. As in **8a**, the η^2-C-C bond is almost coplanar with the metal coordination plane in **1b** (C2'-C1'-Pd-P2 = 9.6º). The η^2-interaction with palladium in **1b** is almost symmetrical, with only 0.006 Å difference between the Pd-C1' and Pd-C2' bond lengths. The C1'-C2' bond has lengthened from 1.410 Å in **1a** to 1.473 Å in **1b** as a result of the interaction with palladium.

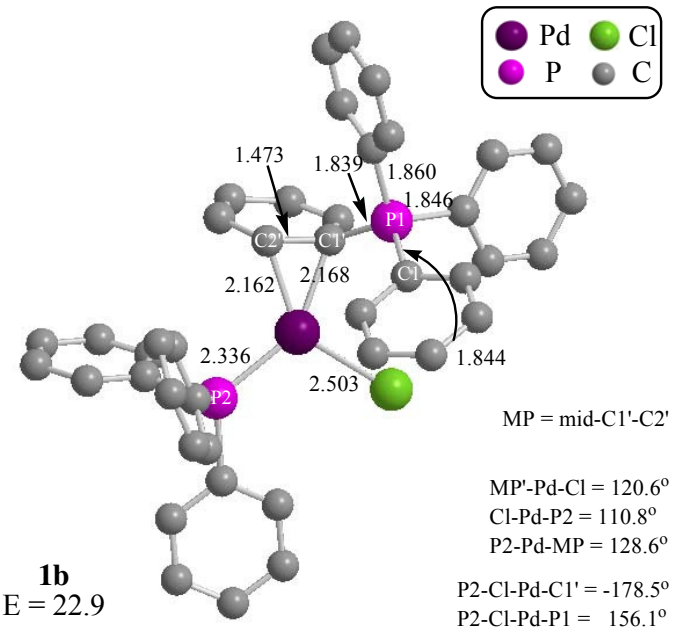

Figure 5.6: The structure of zwitterion **1b** from Mechanism **A**. Bond lengths and distances in Å, energy in kcal/mol.

The geometry around palladium has changed from distorted square planar to distorted trigonal planar, with the main angles around palladium adding up to 360.0º. P1 is now formally cationic, and lies above the metal coordination plane with a P2-Cl-Pd-P1 torsion angle of 156.1º.

The atom labelling in Figure 5.6 shows that the phenyl that was originally bound to palladium is not the phenyl engaged in the η^2-interaction. To move forwards in the exchange process from **1b**, either the C1'-P1 bond must break as Pd-P1 reforms, or one of the other phenyl groups on P1 must transfer onto palladium as Pd-P1 forms. Attempts were made to break the C1'-P1 bond so that the η^2-phenyl group would transfer to the metal, yielding the exchange product, but this was not possible. Instead, it is believed that one of the other phenyls, shown in Figure 5.7 in italics, would transfer onto palladium. This could be achieved by rotation around P1-C1' to place an alternative phenyl group in the position for transfer onto the metal. Unfortunately, it was not possible to locate a transition state (**$TS_{1b-1b'}$**) for the rotation around P1-C1' by 120º, as the phenyl groups on P1 are not equivalent. Due to the type of calculation employed, namely ONIOM, the two phenyl groups shown in italics in Figure 5.6 are at the low level of calculation, while the η^2-interacting phenyl and the phenyl in bold are at

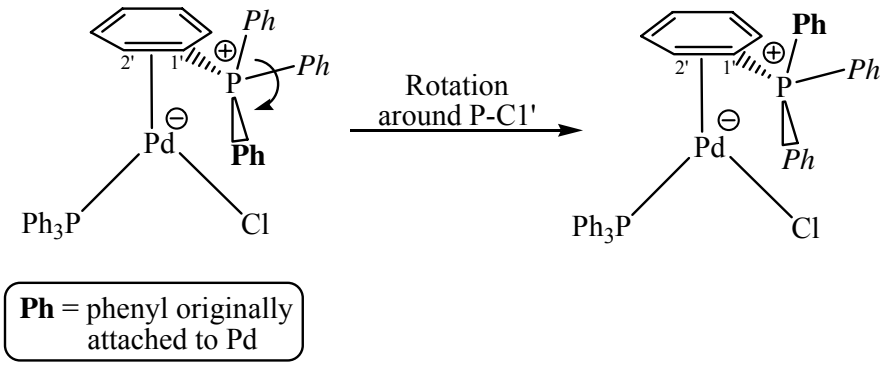

Figure 5.7: Indication of the rotation required in **1b** to allow a different phenyl to transfer back onto the palladium.

the high level. This means that the rotation around P1-C1' by 120º or 240º does not produce energetically equivalent isomers, as it would if the phenyls were all equivalent. The calculations that were performed indicated that the barrier to rotation would be small, at around 5 kcal/mol, meaning it would be lower than $\mathbf{TS_{1a\text{-}1b}}$. Assuming facile rotation occurs, the pathway forwards to the production of the exchange product is the same as the pathway connecting **1a** to **1b**, but now with a different phenyl transferring to palladium. The overall process is thermoneutral, as the product, **1a'** (E = 0.0 kcal/mol), is indistinguishable from reactant **1a**.

The reaction profile, assuming a small barrier for rotation at $\mathbf{TS_{1b\text{-}1b'}}$, can be seen in Figure 5.8. The highest activation barrier for this exchange process corresponds to the transfer of the palladium-bound phenyl onto P1 (E_a = 31.1 kcal/mol). As this is a type of intramolecular nucleophilic attack, it is not surprising that phenyl, a relatively poor nucleophile in this situation, does not readily transfer onto P1. This barrier is of a similar magnitude to the activation energy for the transfer of phenyl from palladium onto P1 from **5a**, *trans*-[PdCl(Ph)(PH_3)$_2$], in Chapter 3 (E_a1 = 32.9 kcal/mol).

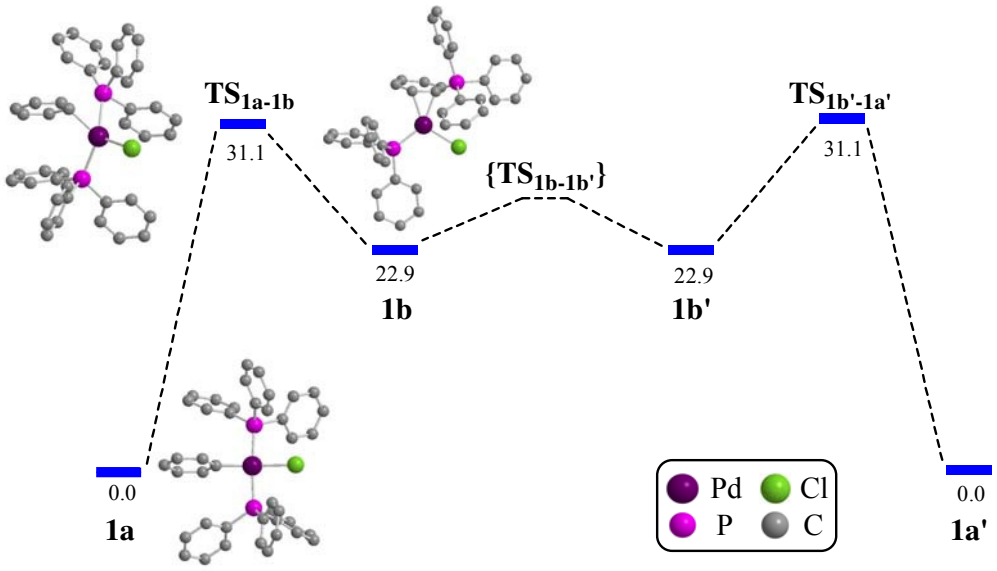

Figure 5.8: Reaction profile for Ph/Ph' exchange via Mechanism **A**, starting from *trans*-[PdCl(Ph)(PPh_3)$_2$], **1a**. **$TS_{1b-1b'}$** could not be located, so an approximation is shown. Energies in kcal/mol.

5.3 Mechanism B

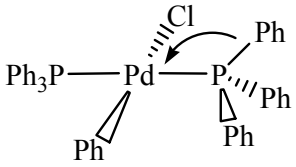

B Transfer of Ph from P to Pd
(4 coord)

The second mechanism considered for Ph/Ph' exchange starts from the same 4-coordinate reactant as before, **1a**, but begins with the transfer of a phenyl group from P1 onto palladium, which is formally an oxidative addition.

Several problems were encountered when investigating this profile. If the P1-C1' bond which is to be broken is simply lengthened in a scan, the phenyl dissociates from the phosphorus without moving towards the palladium. A scan reducing the Pd···C1' distance was therefore run, but this was also unsatisfactory, as the P1-C1' bond would not break. It was, however, possible to optimise the expected square pyramidal structure where the phenyl transfer to palladium had occurred. This 5-coordinate intermediate structure, **1c** (E = 38.1 kcal/mol), is shown in Figure 5.9.

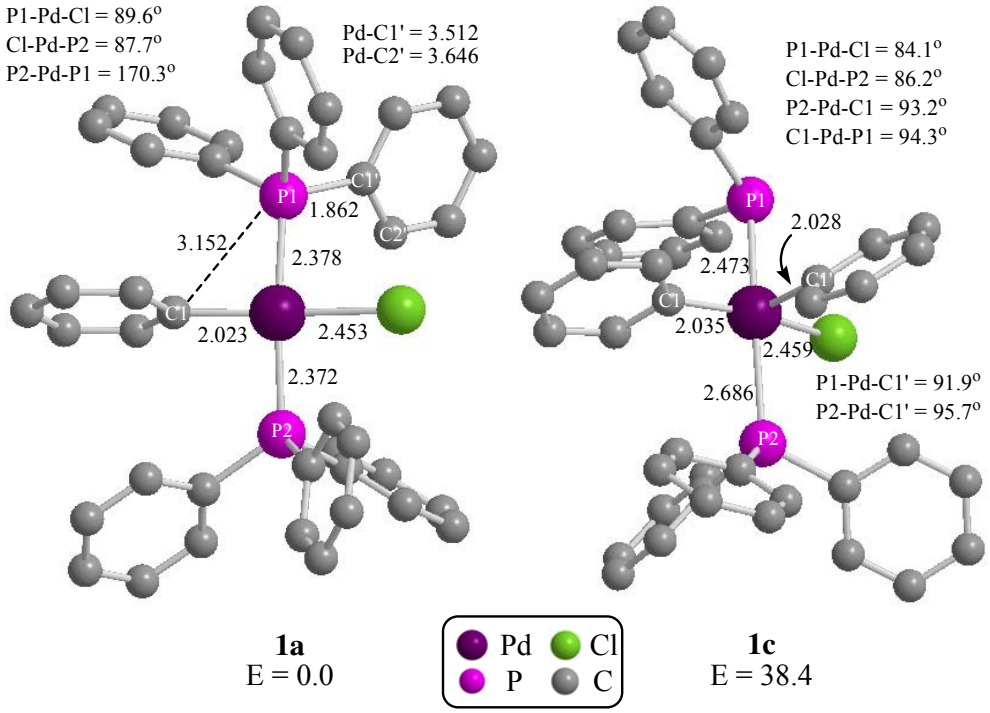

Figure 5.9: The structures of reactant **1a** and intermediate **1c** from Mechanism **B**. Bond lengths and distances in Å, energies in kcal/mol.

The Pd-Cl and Pd-C1 bond lengths are only slightly longer in **1c** than in **1a**. However, the Pd-P bonds are more greatly affected. The PPh_2 ligand in **1c** seems to exert a stronger trans influence than PPh_3, with the Pd-P2 bond lengthening by 0.314 Å. The Pd-P1 bond lengthens by 0.095 Å with the change in the nature of the ligand. Alternative isomeric forms of **1c** were considered by constructing the eight possible isomers, i.e. the cis and trans isomers formed with each variation of the axial group. Each structure was allowed to optimise, but only one other structure was found to be a minimum. This alternative isomer has PPh_2 in the axial site of the square-based pyramid and the two phenyl groups cis to each other, however, due to its high energy of 45.1 kcal/mol it is even less accessible than **1c**.

Intermediate **1c** is higher in energy than $\mathbf{TS_{1a\text{-}1b}}$, which is the highest energy point in Mechanism **A**. A transition state linking **1a** with **1c** would be even higher in energy than **1c**, meaning that Mechanism **B** would be considerably less energetically accessible than Mechanism **B**. Therefore, on this basis, Mechanism **B** is not considered to be a competitive mechanism for Ph/Ph' exchange, therefore the rest of the profile was not investigated.

5.4 Mechanism C

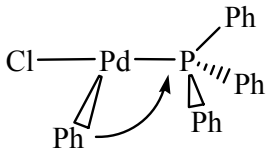

C Transfer of Ph from Pd to P
(3 coord)

The third mechanism considered starts from a 3-coordinate reactant that is formed by the pre-dissociation of the spectator phosphine ligand in **1a**. It is important to investigate the possibility of the reaction mechanism proceeding from a 3-coordinate species since it was found experimentally that addition of excess phosphine strongly inhibits exchange,[3,5,6] implying that phosphine dissociation is involved in the exchange mechanism.

To form a 3-coordinate reactant, the Pd-P2 bond in **1a** was gradually lengthened to dissociate the triphenylphosphine. This process involved a steady increase in energy, but did not pass through a maximum. Once the triphenylphosphine had dissociated to leave T_{PPh_3}-[PdCl(Ph)(PPh_3)], this 3-coordinate palladium complex isomerised resulting in the phenyl ligand lying trans to the vacant site. The optimised structure of **2a**, T_{Ph}-[PdCl(Ph)(PPh_3)], (E = 21.1 kcal/mol) is shown in Figure 5.10.

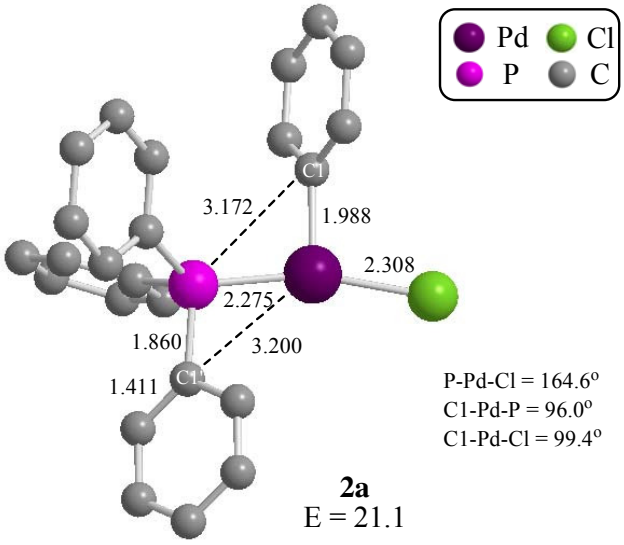

Figure 5.10: The structure of reactant **2a** in Mechanism **C**. Bond lengths and distances in Å. Energy including free PPh_3 in kcal/mol, relative to **1a**.

Comparison of **2a** with 4-coordinate reactant **1a** reveals a shorter Pd-C1 bond in **2a** (Pd-C1: **1a** = 2.023 Å, **2a** = 1.998 Å). This could be attributed to the absence of a ligand trans to C1, however in **2a** the Pd-Cl bond is 0.145 Å shorter and the Pd-P1 bond is 0.103 Å shorter. To investigate the reason for all the bonds around palladium being shorter in **2a** than in **1a**, it is useful to compare **2a** to *cis*-[PdClPh(PPh_3)$_2$] as this species has the same trans influences acting on the ligands.

Figure 5.11 shows that the Pd-C1 bond is 2.6% shorter when opposite to a vacant site in **2a** than trans to PPh_3 in *cis*-[PdClPh(PPh_3)$_2$]. Since there is no change in the trans influence for the chloride and PPh_3(1) groups, the bond lengths would not be expected to change by much. In fact, the Pd-P1 bond is 1.7% shorter and the Pd-Cl bond is 3.5% shorter in **2a** than in *cis*-[PdClPh(PPh_3)$_2$]. This shortening is therefore attributed to a more general effect upon changing from a 4-coordinate to a 3-coordinate species.

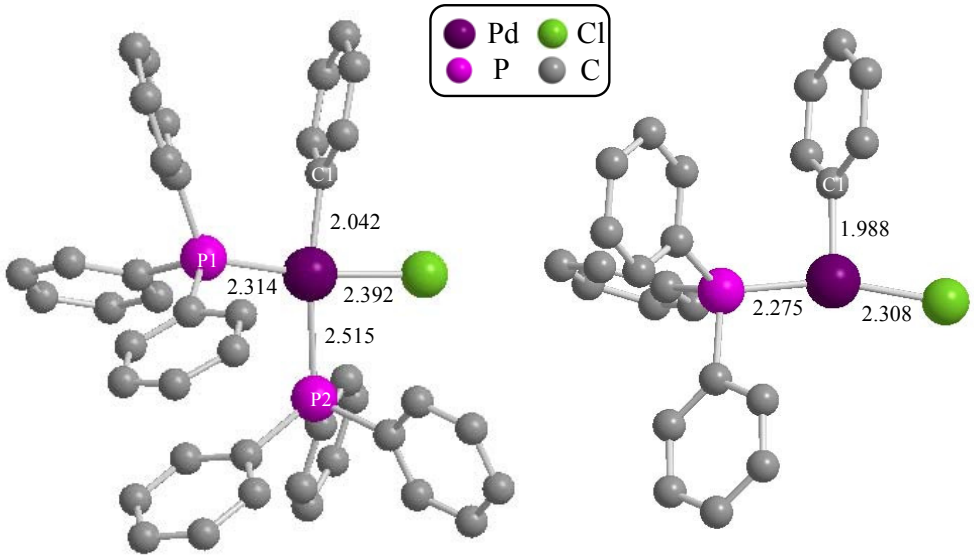

***cis*-[PdClPh(PPh_3)$_2$]** **2a**

Figure 5.11: The structures of *cis*-[PdClPh(PPh_3)$_2$] and **2a**, T_{Ph}-[PdCl(Ph)(PPh_3)]. Bond lengths and distances in Å.

After the loss of PPh_3, Mechanism **C** proceeds in a similar way to **A**, via the attack of the palladium-bound phenyl on P1, therefore the P···C1 distance was reduced in a scan. A transition state calculation was performed at the energy highpoint of the scan, leading to the location of $\mathbf{TS_{2a\text{-}2b}}$ (E = 44.3 kcal/mol), shown in Figure 5.12. The P···C1 distance has reduced, whereas the Pd-C1 bond has lengthened by 0.096 Å. The phenyl maintains a perpendicular orientation during the transfer, as seen in $\mathbf{TS_{1a\text{-}1b}}$. The

chloride has changed its position from trans to triphenylphosphine, to a position trans to C1, with the Cl-Pd-C1 angle increasing from 99.4º in **2a** to 160.9º in $\mathbf{TS_{2a\text{-}2b}}$. This is accompanied by a lengthening of the Pd-Cl bond by 0.039 Å. Although the energy of $\mathbf{TS_{2a\text{-}2b}}$ is comparatively high at 44.3 kcal/mol, the activation energy for this initial step relative to **2a** in Mechanism **C** is 23.2 kcal/mol, which is lower than the corresponding barrier in Mechanism **A** (E_a1 = 31.3 kcal/mol).

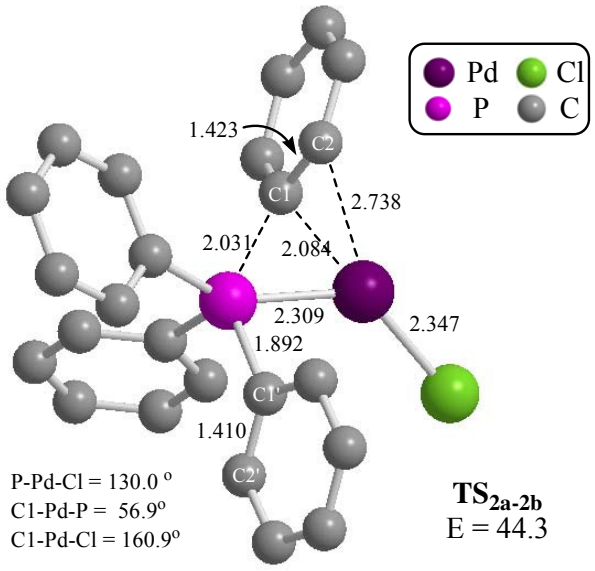

Figure 5.12: The structure of $\mathbf{TS_{2a\text{-}2b}}$ from Mechanism **C**. Bond lengths and distances in Å, energy in kcal/mol.

PIRC calculations revealed that $\mathbf{TS_{2a\text{-}2b}}$ leads to an intermediate structure, **2b** (E = 38.5 kcal/mol), which is a zwitterion featuring an η^2-interaction between palladium and the *ipso-ortho* C1-C2 bond on the previously palladium-bound phenyl group. Figure 5.13 shows the structure of zwitterion **2b**, $[PdCl]^-[PPh_4]^+$. In the formation of **2b**, the Pd-P bond has broken, and the palladium now adopts a distorted linear geometry, with a MP-Pd-Cl angle of 170.7º (MP = midpoint of the C1-C2 bond). Unlike in **1b**, **2b** has an unsymmetrical η^2-interaction between C1-C2 and palladium, with the Pd···C2 distance being the longer of the two. **2b** is 17.4 kcal/mol less stable than 3-coordinate reactant **2a**, while **1b**, the zwitterion in Mechanism **A**, is 22.9 kcal/mol less stable than 4-coordinate reactant **1a**.

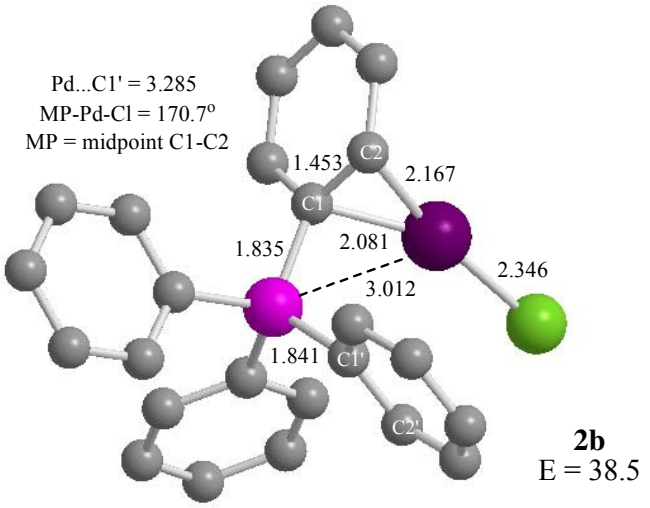

Figure 5.13: The structure of zwitterion **2b** in Mechanism **C**. Bond lengths and distances in Å, energy in kcal/mol.

Intermediate **2b** differs to the zwitterion structure **1b** in the fact that it is the phenyl that was initially bound to palladium in **2a** that engages in an η^2-interaction with palladium in **2b**. This means that a slightly different route must be taken to form the exchange product. In Mechanism **C** it is not necessary to rotate around the Pd-P bond to further the reaction profile; instead the palladium must bind to a different phenyl group. This was achieved by reducing the Pd···C1' distance from its value of 3.285 Å in **2b**. This was successful as it led to the location of $\mathbf{TS_{2b\text{-}2b'}}$ (E = 44.8 kcal/mol), which features the breaking of the C1-C2···Pd interaction and the formation of a C1'-C2'···Pd interaction. The structure of $\mathbf{TS_{2b\text{-}2b'}}$ is shown in Figure 5.14.

In $\mathbf{TS_{2b\text{-}2b'}}$ the Pd···C1 distance has increased by 0.174 Å and the Pd···C2 distance has increased by 0.149 Å as the η^2-interaction has reduced. Simultaneously, the Pd···C1' distance has shortened as this phenyl forms an η^2-interaction to palladium. The Pd···P distance has also shortened by 0.291 Å. The chloride has changed its position such that the Cl-Pd-P angle is 132.7º, giving $\mathbf{TS_{2b\text{-}2b'}}$ a bent geometry around the palladium with almost C_s symmetry. This transition state is easily accessible from **2b** with an activation energy of 6.3 kcal/mol.

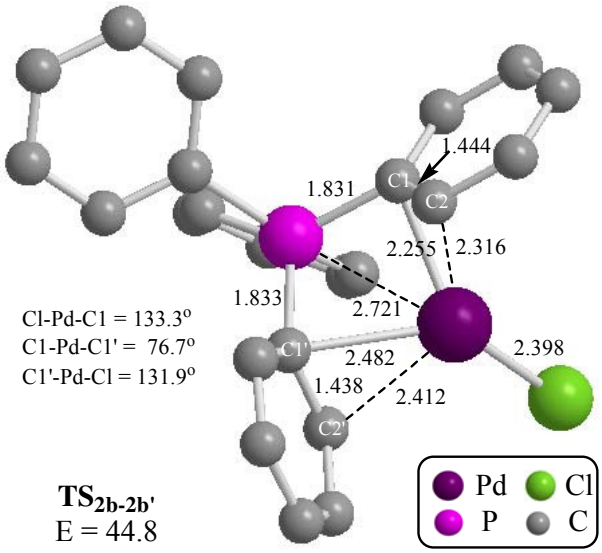

Figure 5.14: The structure of $\mathbf{TS_{2b\text{-}2b'}}$ from Mechanism **C**. Bond lengths and distances in Å, energy in kcal/mol.

PIRC calculations confirmed that $\mathbf{TS_{2b\text{-}2b'}}$ links two isomers that are identical apart from the fact that they have different phenyl groups interacting with the palladium. From this point the exchange process can be completed through an equivalent transition state to $\mathbf{TS_{2a\text{-}2b}}$, which will lead to an exchange product where the phenyl containing C1' is bound to the palladium.

The energy profile for this exchange profile, starting from the 3-coordinate reactant **2a**, is shown in Figure 5.15. The overall energy highpoint in the reaction profile is $\mathbf{TS_{2b\text{-}2b'}}$, however, it is accessible from **2b** with a small activation energy. The first activation barrier is smaller than the equivalent barrier in Mechanism **A**, but due to the pre-dissociation of a triphenylphosphine in this mechanism, all of the energies are high compared to **1a**.

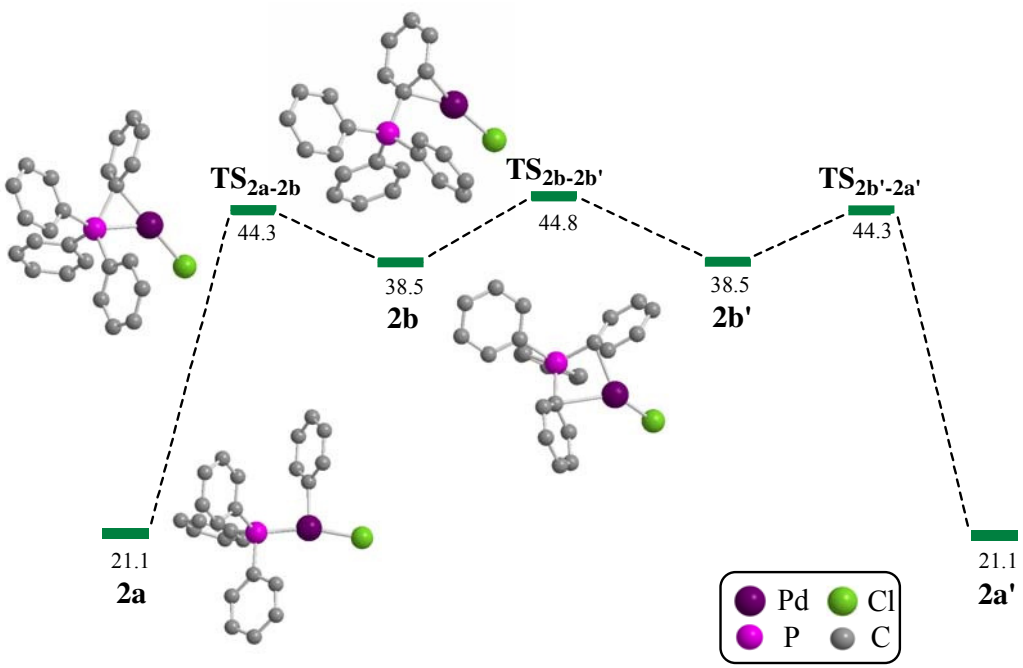

Figure 5.15: Reaction profile for Ph/Ph exchange, starting from T_{Ph}-[PdCl(Ph)(PPh_3)], **2a**. Energies in kcal/mol, relative to the energy of **1a**.

5.5 Mechanism D

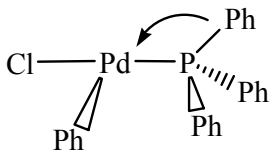

D Transfer of Ph from P to Pd
(3 coord)

The final mechanism that was investigated for Ph/Ph' exchange had the same 3-coordinate starting species, **2a**, as in Mechanism **C**, but features the initial transfer step of oxidative addition of a P-C bond to form a 4-coordinate Pd(IV) intermediate. In order to transfer a phenyl from phosphorus to palladium, the P···C1' distance was reduced from its distance of 3.172 Å in **2a** using a scan, then the 4-coordinate intermediate structure produced by the phenyl-transfer was optimised. The structure of intermediate, **2c** (E = 70.4 kcal/mol), *trans*-[$PdCl(Ph)_2PPh_2$], can be seen alongside **2a** in Figure 5.16.

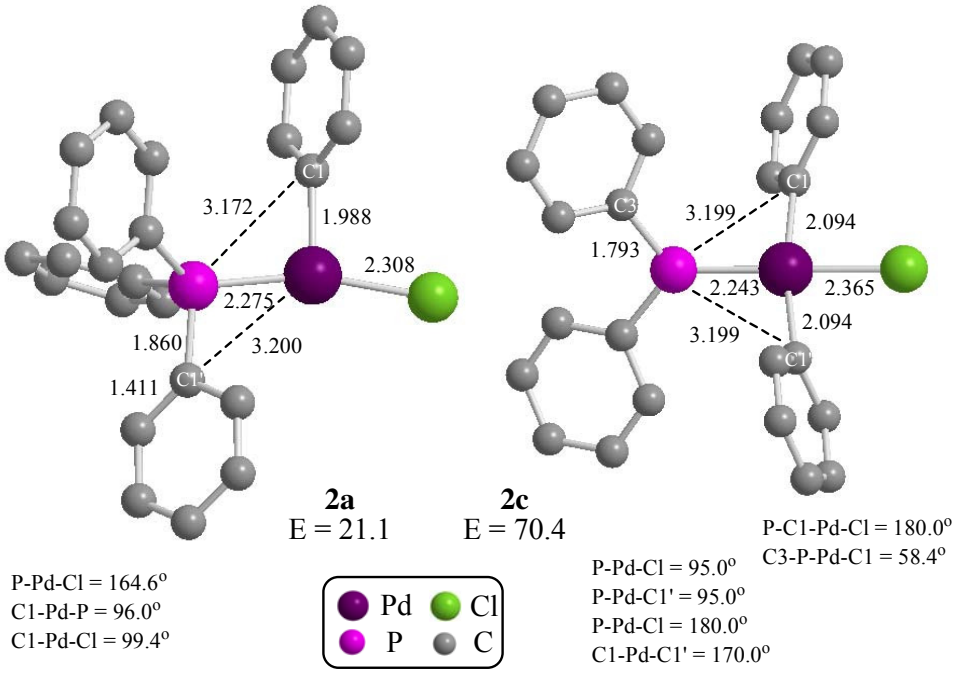

Figure 5.16: The structure of reactant **2a** and intermediate **2c** from Mechanism **D**. Bond lengths and distances in Å. Energies in kcal/mol, relative to the energy of **1a**.

Intermediate **2c** has a distorted square planar structure where all the atoms bonded to palladium lie in the metal coordination plane, with the four main angles around

palladium adding up to 360.0º. The two phenyl groups attached to phosphorus lie out of the metal coordination plane, with a C3-P-Pd-C1 torsion angle of 58.4º. The Pd-Cl bond is 0.057 Å longer in **2c** than in **2a**, suggesting again that PPh_2 exerts a stronger trans influence than PPh_3. The Pd-C1 bond has lengthened considerably, by 0.106 Å, now that it is no longer trans to a vacant site and the complex has changed from 4-coordinate to 3-coordinate.

As in Mechanism **B**, the Pd(IV) intermediate is very high in energy. In this case the activation energy to pass from **2a** to **2c** is likely to be over 50 kcal/mol, and **2c** is 70.4 kcal/mol less comparatively stable than **1a**, making this mechanism very inaccessible. There is no need to locate a transition state for this process, as it is clear that Mechanism **D** is considerably less energetically accessible than Mechanism **C**.

5.6 Comparison of the four exchange mechanisms

Four possible reaction mechanisms for Ph/Ph' exchange in *trans*-[PdCl(Ph)(PPh_3)$_2$] have been investigated, and the energies are compared in Figure 5.17.

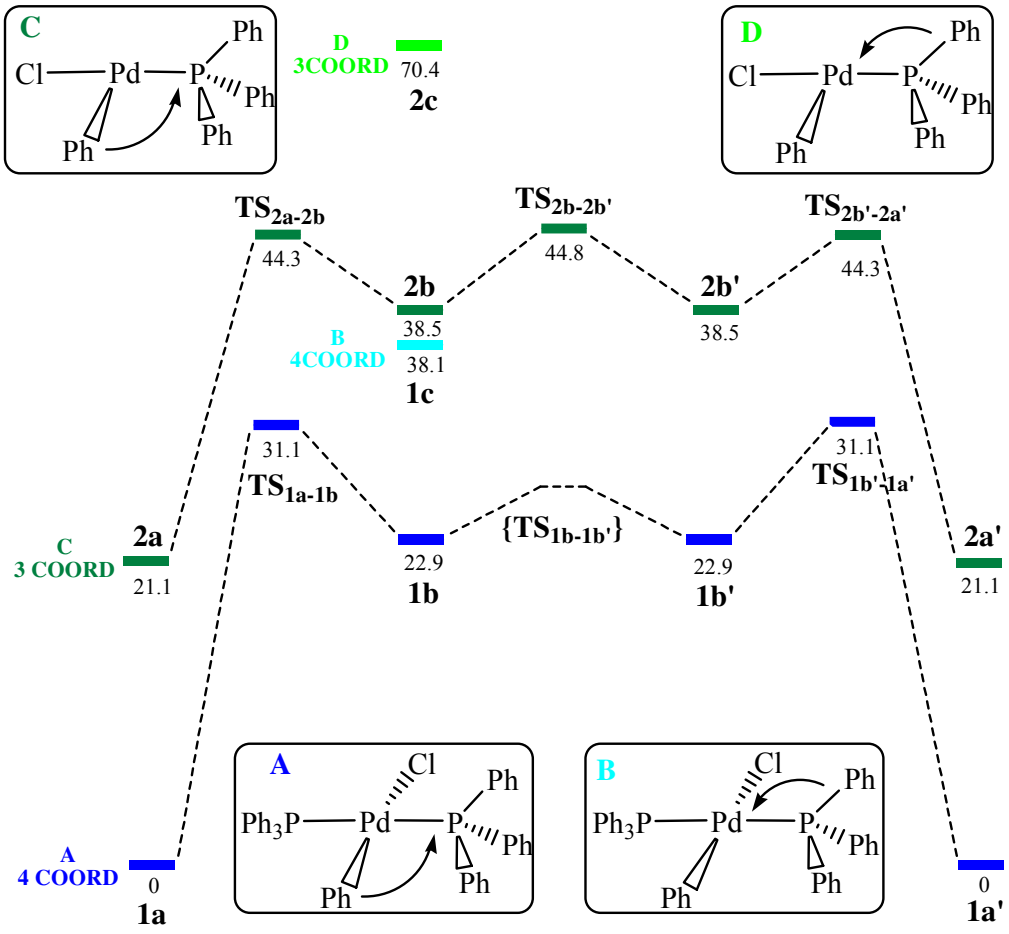

Figure 5.17: Reaction energy profiles (enthalpies relative to **1a**, in kcal/mol) for four possible Ph/Ph' exchange mechanism pathways.

It is clear that Mechanism **D**, where a phenyl initially transfers onto palladium from 3-coordinate **2a**, is not competitive with any of the other three mechanisms as it is considerably higher in energy. The intermediates in Mechanisms **B** and **C** are close in energy, but by far the most accessible pathway is Mechanism **A**. The pre-dissociation of triphenylphosphine results in Mechanisms **C** and **D** starting from their 3-coordinate reactant, **2a**, at 21.1 kcal/mol above the energy of the 4-coordinate reactant **1a**. However, these energies do not reflect the whole situation, as they are enthalpies and entropy is not accounted for. The energies were adjusted to account for entropy, and this resulted in Mechanism **C** becoming much more competitive with Mechanism **A**, due to the phosphine dissociation increasing the entropy of the system. The

comparative free energy reaction profiles for all four mechanisms are shown in Figure 5.18.

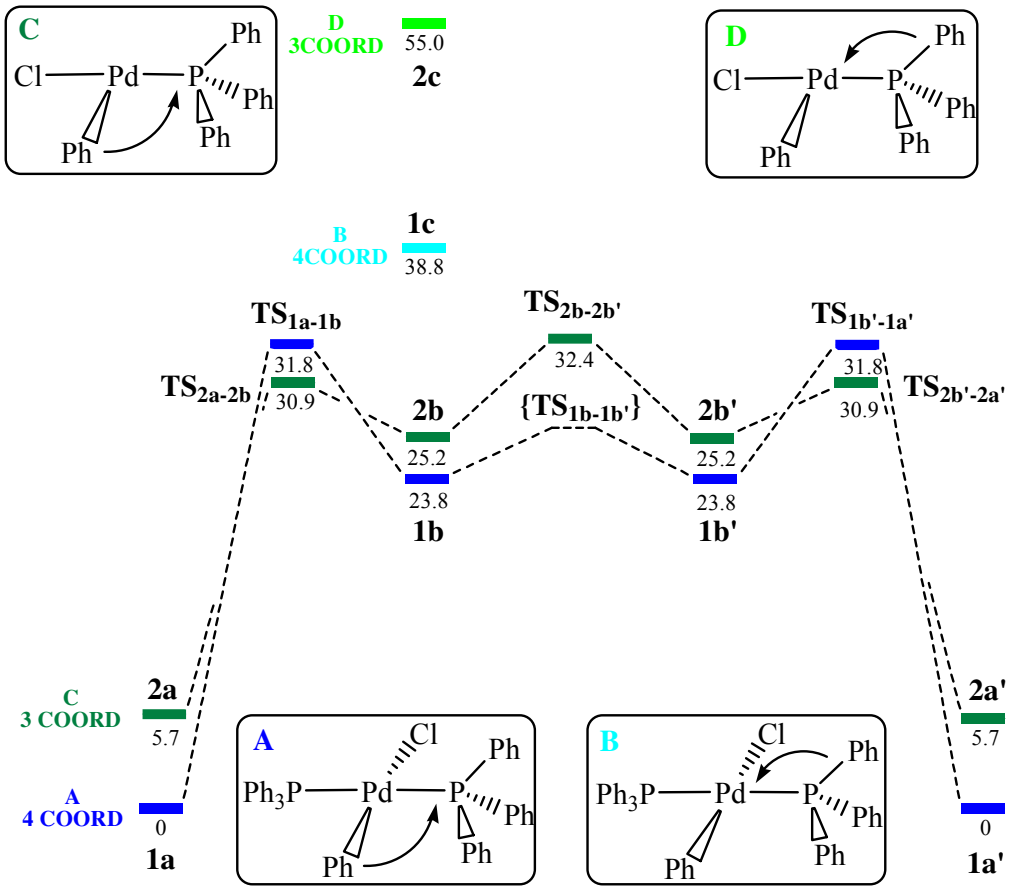

Figure 5.18: Reaction free energy profiles (relative to **1a**, in kcal/mol) for four possible Ph/Ph' exchange mechanisms.

The energy profiles for Mechanisms **A** and **B**, which begin from the same 4-coordinate reactant, **1a**, are largely unaffected by the inclusion of entropy. In contrast, the entropy change associated with the removal of a phosphine stabilises **2a** from its enthalpy value of 21.1 kcal/mol down to 5.7 kcal/mol. This relative stabilisation is seen in all of the species in Mechanisms **C** and **D**. The reactant and intermediate in Mechanism **D**, **2a** and **2c** respectively, have become 15.4 kcal/mol more stable, but intermediate **2c** (55.0 kcal/mol) is still much higher in energy than any of the structures in the other mechanisms, hence it is not a competitive pathway. The key effect of the addition of entropic effects is in the relative stabilisation of the species in Mechanism **C** by up to 15.4 kcal/mol, which makes this mechanism very competitive with Mechanism **A**. The initial activation energy in Mechanism **C** is 25.2 kcal/mol, smaller than the analogous barrier in Mechanism **A** which is 31.8 kcal/mol. The overall energy highpoint in

Mechanism **C** is 32.4 kcal/mol, only 0.6 kcal/mol higher than the highpoint in Mechanism **A**. In terms of free energy, there is very little separating the two mechanisms.

One more factor should be taken into account when comparing the reaction profiles: the effect of solvation. When Ph/Ph' exchange in *trans*-[PdCl(Ph)(PPh_3)$_2$] was studied by Grushin, the reaction was performed in a benzene solvent.[6] Polarisable continuum model (PCM) single point calculations were performed for each of the structures in the four mechanisms in a benzene solvent, and then TΔS corrections using values from the ONIOM calculations were applied to the values. The resultant PCM free energy comparative energies for the two most accessible mechanisms are shown in Figure 5.19. The energies for the structures in Mechanisms **B** and **D** remained relatively much higher, therefore they will not be considered from this point onwards.

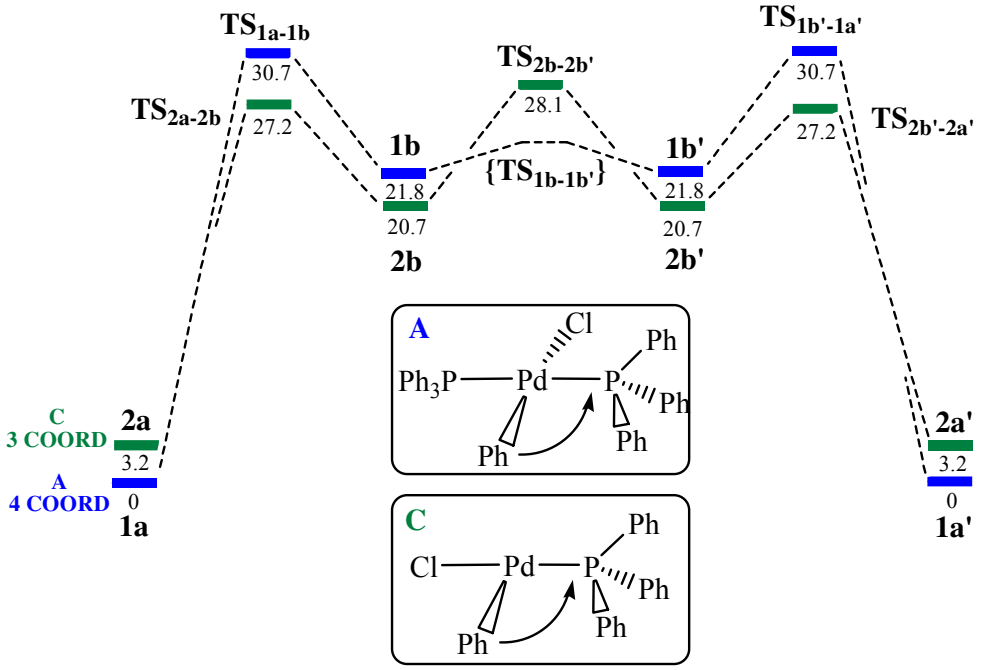

Figure 5.19: Reaction free energy profile with benzene solvation (relative to **1a**, in kcal/mol) for Mechanisms **A** and **C**.

Solvation has stabilised Mechanism **C** by more than Mechanism **A**, resulting in **C** now being the most accessible pathway. This may be due to differences in dipole moments. For instance **1a** has a dipole moment of 2.53 debye, while **2a** is 9.65 debye, which results in **2a** being be more stabilised by solvation than **1a**. Overall, not only does Mechanism **C** have the smallest initial energy barrier of 24.0 kcal/mol, but also the

lowest highpoint, at 28.1 kcal/mol, compared to the Mechanism **A** highpoint of 30.7 kcal/mol.

In conclusion, once the effects of entropy and solvation are included in the analysis of the four different mechanisms, the result is that the 3-coordinate Mechanism **C**, which involves pre-dissociation of the spectator triphenylphosphine followed by attack of the palladium-bound phenyl on P1, is the most accessible mechanism for Ph/Ph' exchange in *trans*-[PdCl(Ph)(PPh_3)$_2$]. This is consistent with the experimental result that Ph/Ph' exchange is strongly inhibited by the addition of excess phosphine, [3,5,6] which would have the effect of suppressing phosphine dissociation.

5.7 Effect of changing the halide

Grushin performed a detailed experimental study on the effect of changing the halide ligand on the rate of Ar/Ar' exchange in *trans*-[PdX(C_6D_5)(PPh_3)$_2$] (X = Cl, Br, I).[6] He observed that the rate of exchange was affected by changing X, and in deuterated benzene at 75ºC the rate constant ratio k_{Cl}:k_{Br}:k_I was approximately 1:4:100.

To investigate these findings, calculations were performed on the four Ph/Ph' exchange reaction mechanisms, changing the halide ligand from chloride to bromide and iodide. The basic features of the mechanisms remained the same for all three halides, with only structural and energetic differences observed. The following discussion will focus Mechanisms **A** and **C**, as they were the two most accessible pathways with X = Cl, and remained so for X = Br and X = I.

5.8 Effect of changing the halide on the energy profile for Mechanism A

Firstly, the effect of changing the halide ligand on the energy profiles will be discussed. Figure 5.20 shows the comparative energies for Mechanism **A** when the halide is varied between chloride, bromide and iodide. The energies of the reactants, *trans*-

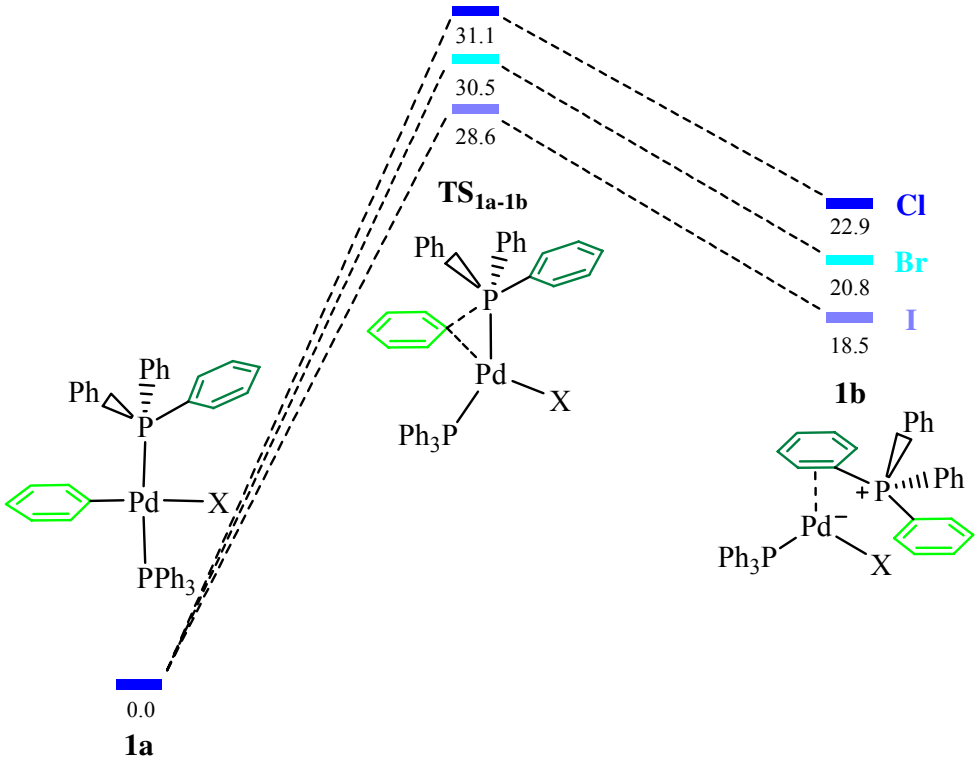

Figure 5.20: Reaction energy profiles showing the effect of varying the halide on the comparative energies (kcal/mol) in Mechanism **A** for Ph/Ph' exchange in *trans*-[PdXPh(PPh_3)$_2$] (X = Cl, Br, I).

[PdX(Ph)(PPh_3)$_2$] (X = Cl, Br, I), have all been set to zero. The relative energies for **TS_{1a-1b}** and **1b** follow the trend Cl > Br > I. The stabilisation is greater for intermediate **1b** (Br = -2.1, I = -4.4 kcal/mol) than for the transition state (Br = -0.6, I = -2.5 kcal/mol).

The three structures for each halide are shown in Figure 5.21, with the bond lengths and energies shown. The values for chloride are shown in bold, those for bromide in italics and for iodide in normal text. Close examination of the structures reveals that changing the halide does not result in many structural changes. Looking firstly at **1a**, a small change in the Pd-C1 bond length can be seen with changing halide, due to the differing trans influence. Experimental[6] and calculated bond lengths for the four bonds around palladium in the reactant **1a** are shown in Table 5.2. The computed data suggest that the strength in trans influence increases as X = Cl < Br < I. There is also a trend of increasing Pd-P1 and Pd-P2 bond lengths as the halide is varied Cl < Br < I. The experimentally determined data also show similar effects on bond lengths around palladium, with the exception of an anomalously short Pd-C1 bond when X = Br. The geometry around palladium remains square planar in all cases.

	Experimental data[6]			Calculated structures		
Bond	Cl	Br	I	Cl	Br	I
Pd-X	2.407(1)	2.532(1)	2.701(8)	2.453	2.583	2.778
Pd-C1	2.016(3)	1.995(6)	2.029(4)	2.023	2.029	2.036
Pd-P1	2.316(1)	2.322(2)	2.338(1)	2.378	2.379	2.383
Pd-P2	2.324(1)	2.327(2)	2.342(1)	2.372	2.376	2.382

Table 5.2: The effect of varying the halide on selected bond lengths (Å) in *trans*-[PdX(Ph)(PPh_3)$_2$] (X = Cl, Br, I) complexes.

The same trends in bond length for the bonds around palladium are seen in the structures of **TS_{1a-1b}**, with the longest bonds seen when X = I. The Pd-P1 bond and bonds in other parts of the transition state structures, further from the palladium centre, are less affected by changing the halide, for instance the P1-C2 bond is only 0.004 Å shorter with X = I than when X = Cl. The angles change by only a small amount when the halide is varied, for instance the P2-Pd-X angle is 101.2º when X = Cl, 102.9º when X = Br and 104.4º when X = I.

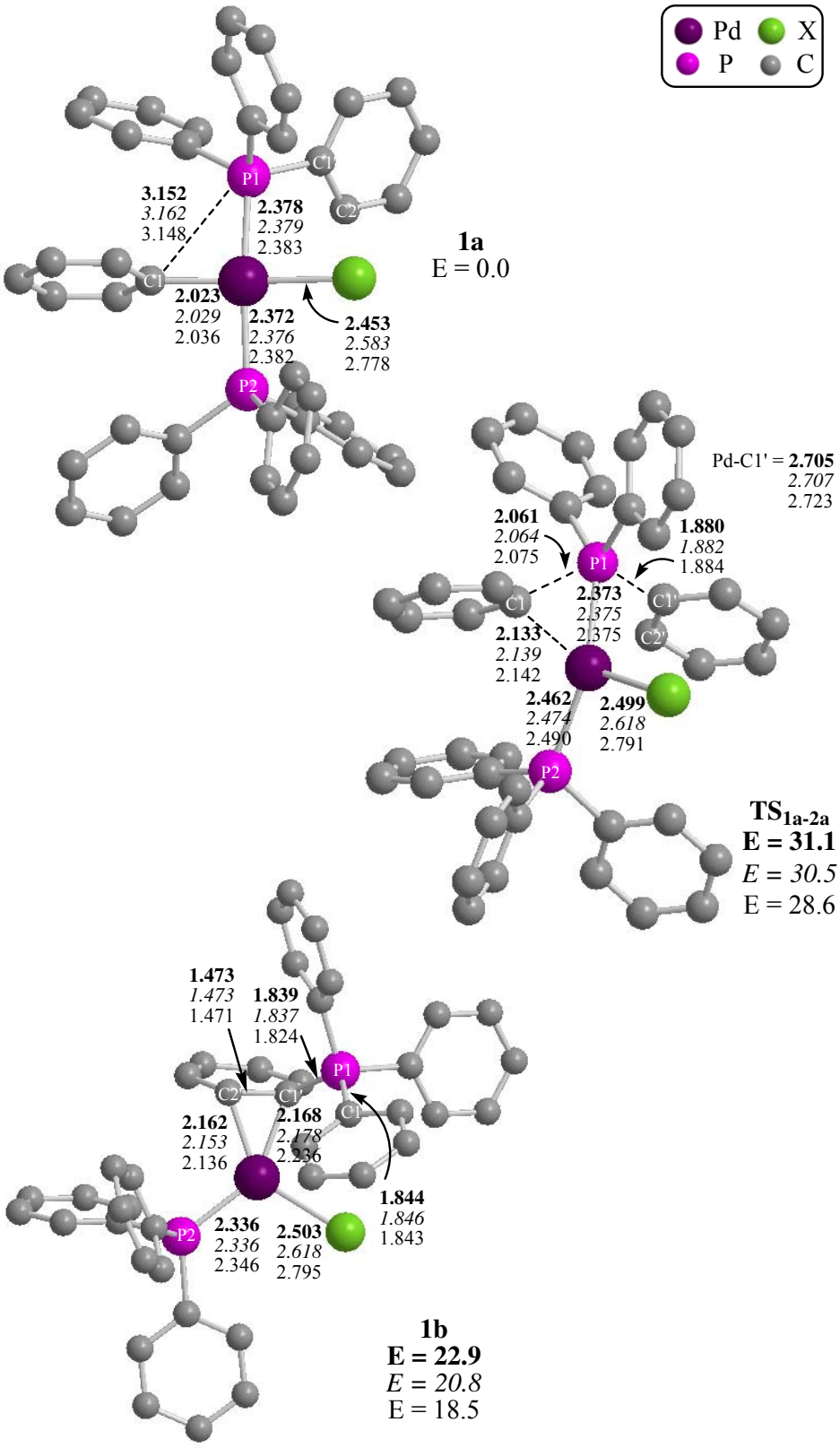

Figure 5.21: The structures of **1a**, $\mathbf{TS_{1a\text{-}1b}}$ and **1b** from Mechanism **A**. Energies (kcal/mol) and bond lengths (Å) are shown for X = **Cl**, *Br* or I in *trans*-[PdX(Ph)(PPh_3)$_2$].

The structures of intermediate **1b** have an exception to the trend of bonds lengthening with changing the halide down group 17. This occurs with the Pd-C2' bond, which shortens from 2.162 Å when X = Cl, to 2.153 Å when X = Br, to 2.136 Å when X = I. However, the Pd-P2 and P1-C1' bonds and the Pd···MP distances lengthen by a small amount in the order Cl < Br < I. The C1'-C2' bond, which has an η^2-interaction with palladium in **1b**, is only 0.002 Å shorter when X = I than when X = Cl or Br. The similarity in the length of this bond when varying the halide is surprising, as this bond may be expected to be sensitive to the environment at the metal centre.

Overall, the structures in Mechanism **A** do not change greatly when the halide is varied. There is a general trend of the bonds around palladium lengthening when the halide is changed, in the order Cl < Br < I.

5.9 Effect of changing the halide on energy profile for Mechanism C

The structures from Mechanism **C** were optimised and a reaction profile was generated for X = Br and I, to compare with the profile and structures for X = Cl. The energy profile is shown in Figure 5.22. The profiles begin at 3-coordinate T_{Ph}-[PdX(Ph)PPh_3], **2a**. The dissociation of phosphine is easier when X = Br (E = 19.9 kcal/mol) and X = I (E = 17.8 kcal/mol) than when X = Cl (21.1 kcal/mol). Grushin proposed[6] that this may be due to the Pd-P bond in *trans*-[PdX(Ph)(PPh_3)$_2$] which breaks to dissociate triphenylphosphine, being longer and thus weaker when X = I. Indeed, the crystallographically determined structures[10] reveal that the Pd-P bonds are longest when X = I, and shortest when X = Cl (see Table 5.2), and the calculations performed also reproduced this trend. To investigate this further, the strengths of the bonding interaction (BI) in the Pd-P1 bonds in *trans*-[PdX(Ph)(PPh_3)$_2$] (X = Cl, Br, I) were calculated using the same method as described in Chapter 3. However, surprisingly, the Pd-P1 bonds in the three species were all of around the same strength (BI(Cl) = 34.4 kcal/mol, BI(Br) = 35.3 kcal/mol, BI(I) = 34.5 kcal/mol). It therefore seems that the halide effect must be present when the 3-coordinate species isomerises from T_{PPh_3}-[PdX(Ph)PPh_3] to T_{Ph}-[PdX(Ph)PPh_3], rather than when the Pd-P1 bond is broken. It is not clear why this should be the case. One possibility is that iodide is a better π-acceptor in T_{Ph}-[PdX(Ph)PPh_3] than chloride or bromide are. The Pd-I bond does shorten slightly more between **1a** and **2a** (6.2%) than the Pd-Br (6.0%) or Pd-Cl (5.9%) bonds do, but the difference is so small that the cause is unclear.

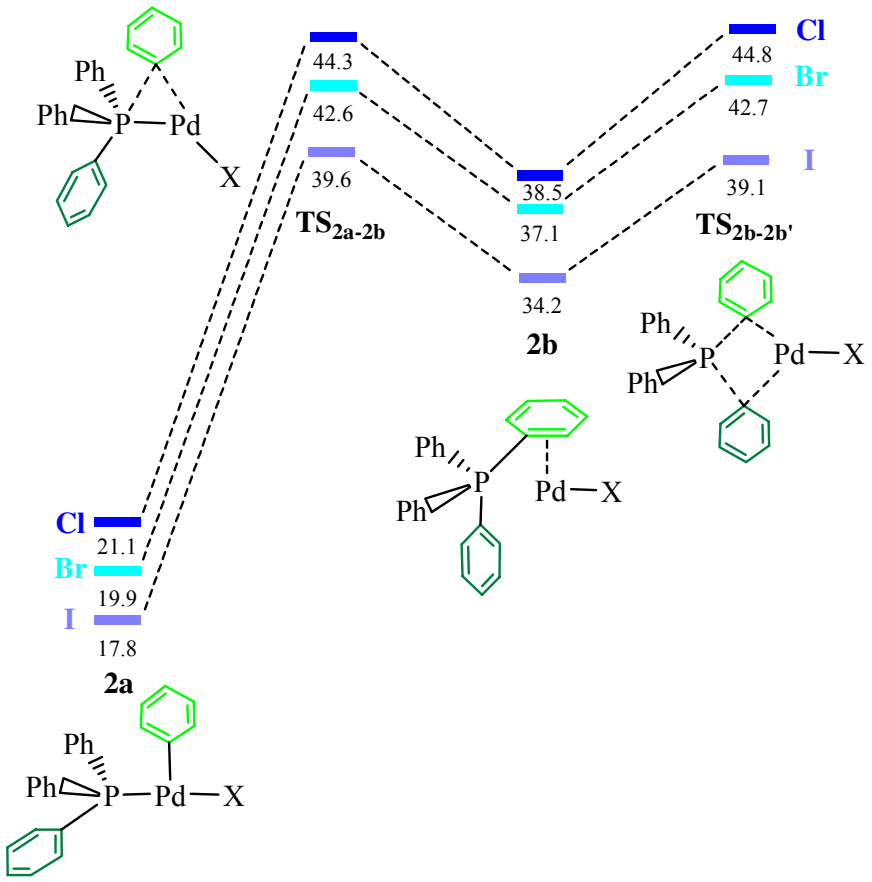

Figure 5.22: Reaction profiles demonstrating the effect of varying the halide on the comparative energies (kcal/mol) in Mechanism **C** for Ph/Ph exchange.

Unlike Mechanism **A**, where the intermediate was more stabilised by changing the halide than the transition state, in Mechanism **C** the transition states were stabilised by more than the minima (e.g. **2a**: Br = -1.2, I = -3.3, $\mathbf{TS_{2a\text{-}2b}}$: Br = -1.7, I = -4.7 kcal/mol). The relatively large stabilisation of $\mathbf{TS_{2b\text{-}2b'}}$ when X = I leads to a switching over of the energy highpoint in the iodide profile, so $\mathbf{TS_{2a\text{-}2b}}$ is the highpoint when X = I, while $\mathbf{TS_{2b\text{-}2b'}}$ is the highpoint when X = Cl or Br. Overall, a similar trend of stabilisation compared to the profile where X = Cl is seen in both Mechanisms **A** and **C** when the halide is varied, with the profile when X = Br being 0.6-2.1 kcal/mol more stable and the profile when X = I being stabilised by 2.5-5.7 kcal/mol.

The structures of **2a**, $\mathbf{TS_{2a\text{-}2b}}$, **2b** and $\mathbf{TS_{2b\text{-}2c}}$ from Mechanism **C**, with the bond lengths for X = Cl, Br and I, are shown in Figure 5.23. In reactant **2a** the Pd-P bond, which lies trans to the halide, is affected most by a change in halide (0.021 Å longer for X = I than X = Cl). The Pd-C1 bond is less sensitive, and is only 0.002 Å longer when X = I than

for X = Br or Cl. The other bonds in the complexes are largely unchanged by varying the halide, and a T-shaped geometry is seen throughout.

In $\mathbf{TS_{2a\text{-}2b}}$ an isomerisation has occurred, so that C1 now lies trans to the halide. Therefore, it is not surprising that the Pd-C1 bond is more sensitive to the nature of the halide than it is in **2a**. The Pd-P bond differs by 0.012 Å between the structures when X = Cl and X = I, despite no longer being trans to the halide. The P-C1 and P-C2 bonds are not particularly affected by a change in halide. The geometry of zwitterion **2b** follows the trend of the bonds around palladium increasing in length as the halide changes (X = Cl < Br < I). The η^2-phenyl lies trans to the halide in a distorted linear structure, and the C1-C2 bond is furthest from the palladium when X = I (Pd···MP (X = Cl) = 1.996 Å, (X = Br) = 2.002 Å, (X = I) = 2.011 Å). As seen in **1b**, the C1-C2 bond length is not affected by a change in halide. Zwitterion **2b** is most stable when X = I, yet this structure has the longest Pd···P distance of 3.098 Å, hence the increased stability is not linked to the proximity of oppositely charged parts of the zwitterion. In $\mathbf{TS_{2b\text{-}2c}}$ the Pd-C1 and Pd-C1' bonds and the Pd···P distances all increase as the halide is varied Cl < Br < I. The P-C1 and P-C1' bonds get slightly shorter (by 0.008 Å) when changing from X = Cl to X = I. However, the C1'-C2' and C1-C2 bonds are not affected, and neither are the other bonds in $\mathbf{TS_{2b\text{-}2b'}}$.

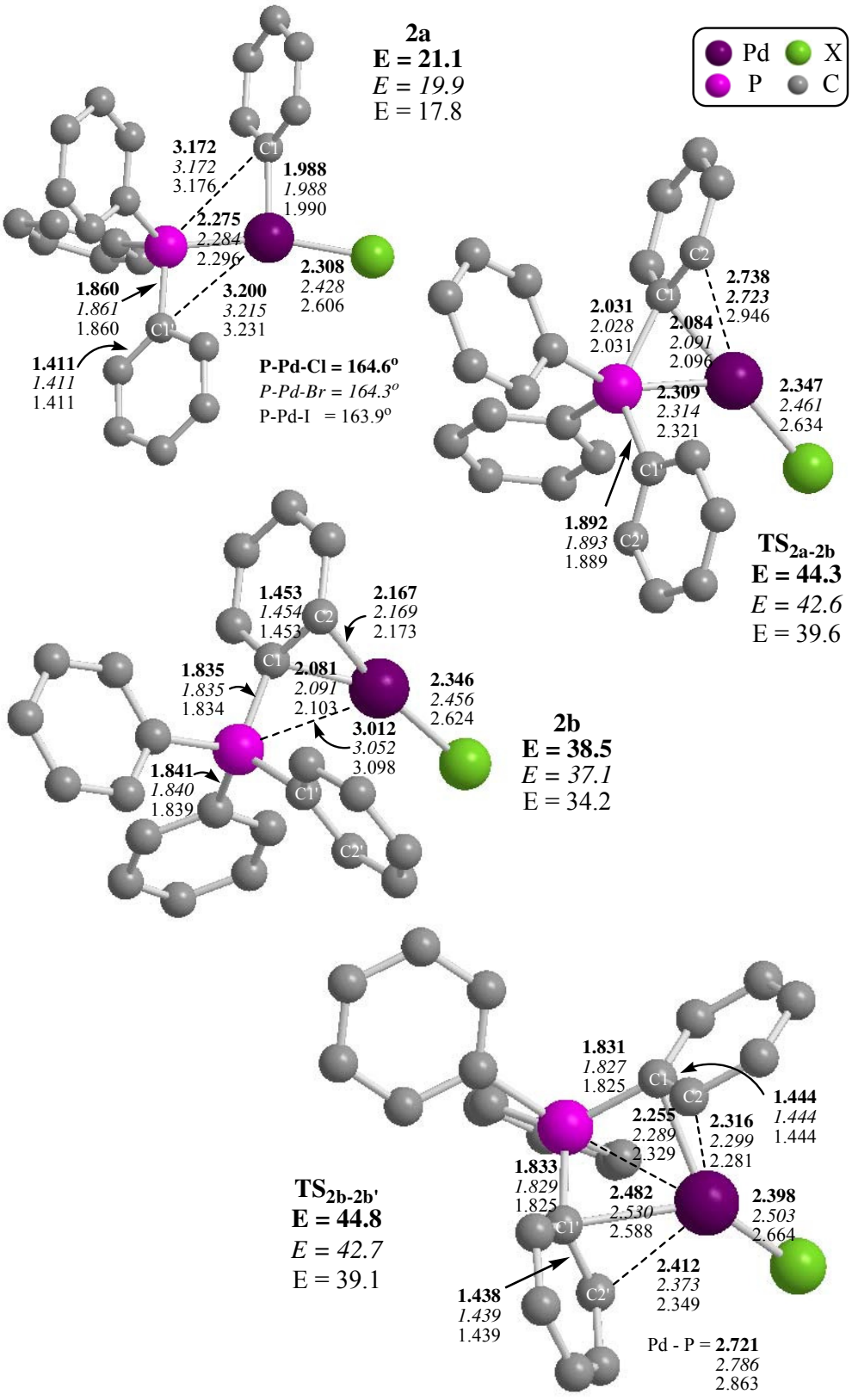

Figure 5.23: The structures of **2a**, $\mathbf{TS_{2a\text{-}2b}}$, **2b** and $\mathbf{TS_{2b\text{-}2c}}$ from Mechanism **C**. Energies in (kcal/mol) and bond lengths (Å) are shown for when X = **Cl**, *Br* and I in T_{Ph}-[PdX(Ph)(PPh_3)].

5.10 The effect of changing the halide on free energy

The analysis of Ph/Ph' exchange in *trans*-[PdCl(Ph)(PPh_3)$_2$] showed that it is important to consider the effects of entropy and solvation when comparing the possible reaction mechanisms. Therefore, it is also relevant to see how all these energies are affected by changing the halide. Figure 5.24 shows the energy highpoints for Mechanisms **A** and **C** when X = Cl, Br or I. The column on the left show the profile highpoints for the enthalpies, the free energy values are shown in the middle column, and the PCM free energy values for solvation in benzene are shown on the right.

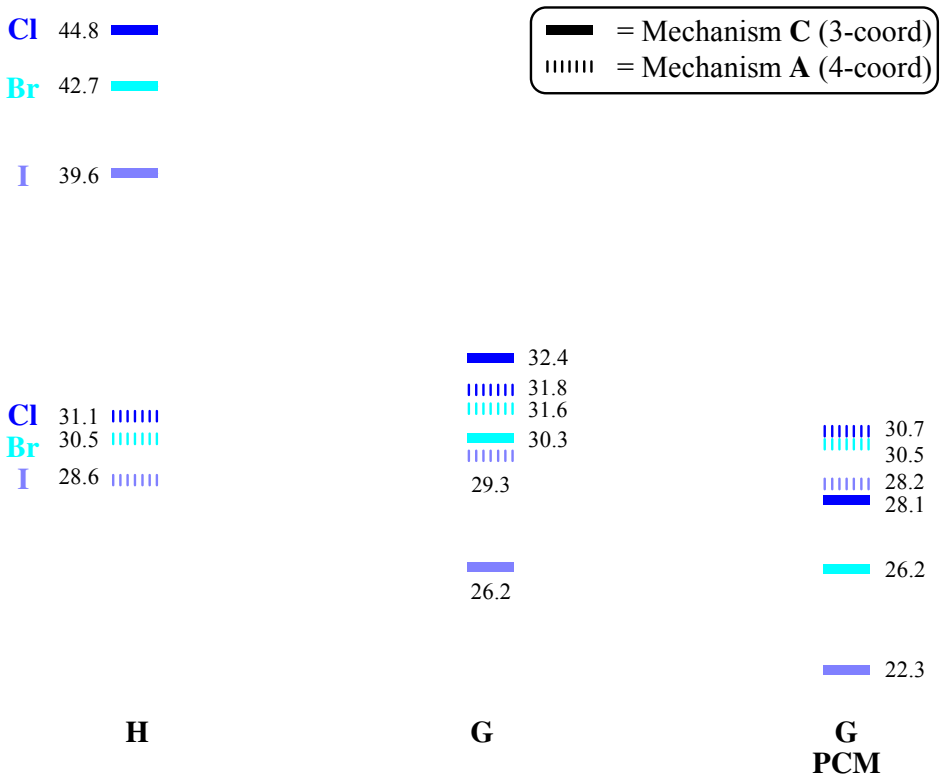

Figure 5.24: Enthalpies (H), free energy (G) and free energy with solvation in benzene (G PCM) (kcal/mol) of the profile highpoints in Mechanism **A** and Mechanism **C** when varying the halide.

In all cases, the energy highpoints in both mechanisms become lower as the halide is varied Cl > Br > I, meaning Ph/Ph' exchange becomes more energetically accessible. Firstly focussing on the dashed lines, which represent the highpoints in Mechanism **A**, inclusion of entropy does not greatly affect the relative energies. This is not surprising as there is no ligand dissociation in Mechanism **A**, thus the complexes are not significantly stabilised by the inclusion of entropy. Conversely, the energy levels in Mechanism **C** are significantly stabilised when comparing free energy values to

enthalpies. Entropy is important in Mechanism **C** due to the initial dissociation of one of the triphenylphosphine ligands. The complexes in Mechanism **C** have larger dipole moments than those in Mechanism **A**, resulting in a greater stabilisation by inclusion of solvation effects. The free energy values for Mechanisms **A** and **C** are very close in value, but once solvation is considered, Mechanism **C** becomes more energetically accessible than Mechanism **A**.

5.11 Conclusions

The calculated results reported in this chapter suggest that the most accessible mechanism for intramolecular Ph/Ph' exchange in *trans*-[PdCl(Ph)(PPh_3)$_2$] in benzene is Mechanism **C**. This involves the dissociation of a triphenylphosphine ligand followed by the transfer of the palladium-bound phenyl group onto the remaining phosphorus. The reaction proceeds via a zwitterion structure containing an η^2-interaction between a phenyl *ipso-ortho* C-C bond and palladium. Swapping the phenyl groups, followed by a reversal of the process to that point completes the exchange. This mechanism is consistent with the experimental finding of Grushin[6] and others,[3,5] that excess phosphine inhibits the exchange process, as excess phosphine would reduce the concentration of 3-coordinate species.

Grushin's experimental results for the effect of changing the halide ligand in *trans*-[PdX(Ph)(PPh_3)$_2$] (X = Cl, Br, I)[6] were reproduced in this investigation. The key trend is that the rate of exchange increases in the order Cl < Br < I. The calculations showed that this trend is not a result of differences in Pd-P bond strengths. Overall, the most accessible pathway for Ph/Ph' exchange for *trans*-[PdCl(Ph)(PPh_3)$_2$] in benzene (X = Cl, Br or I) is via Mechanism **C** when X = I (Highpoint = 22.3 kcal/mol) with no excess phosphine present.

5.12 References

[1] Segelstein, B. E.; Butler, T. W.; Chenard, B. L., *J. Org. Chem.*, **60**, 12, (1995)

[2] Abatjoglou, A. G.; Bryant, D. R., *Organometallics*, **3**, 932, (1984)

[3] Kong, K-C.; Cheng, C.-H., *J. Am. Chem. Soc.*, **113**, 6313, (1991)

[4] Goel, A. B., *Inorg. Chim. Acta*., **86**, L77, (1984)

[5] Goodson, F. E.; Wallow, T. I.; Novak, B. M., *J. Am. Chem. Soc.*, **119**, 12441, (1997)

[6] Grushin, V. V., *Organometallics*, **19**, 1888, (2000)

[7] Flemming, J. P.; Pilon, M. C.; Borbulevitch, O. Y.; Antipin, M. Y.; Grushin, V. V., *Inorg. Chim. Acta*, **280**, 87, (1998)

[8] Macgregor, S. A.; Wondimagegn, T., *Organometallics*, **26**, 5, 1143, (2007)

[9] Ortiz, J. V.; Havlas, Z.; Hoffmann, R., *Helv. Chim. Act*., **67**, 1, (1984)

[10] Flemming, J. P.; Pilon, M. C.; Borbulevitch, O. Ya.; Antipin, M. Yu.; Grushin, V. V., *Inorg. Chim. Acta,* **280**, 87, (1998).

Chapter 6: A mechanistic study of R/Ph exchange in *trans*-[PdI(R)(PPh_3)$_2$] (R = Me, CH_2CF_3)

6.1 Introduction

This chapter follows on from the investigation into the mechanism of Ar/Ar' exchange in Chapter 5, with the focus now turning to R/Ph exchange in the related complexes *trans*-[PdI(R)(PPh_3)$_2$] (R = Me, CH_2CF_3).

In contrast to the extensive experimental work that has been published on Ar/Ar' exchange, there is only one paper which studies alkyl/Ar exchange in depth, published by Norton *et al.*[1] in 1995. They observed Me/Ar scrambling followed by phosphine interchange in *trans*-[PdI(Me)(PAr_3)$_2$] (Ar = C_6H_5) in C_6D_6 at 50ºC. Initially there is an irreversible exchange between the palladium-bound methyl and a phosphine phenyl group, forming complex **2** (see Figure 6.1). This is followed by facile intermolecular phosphine interchange, creating an equilibrium mixture between complexes **2**, **3** and **4**. Further investigations suggested that the mechanism for Me/Ph exchange does not involve the formation of a phosphonium cationic intermediate as none of the unlabelled phenyls from added $[PMePh_3]^+$ exchanged with the deuterated phenyls in *trans*-[PdI(Me)(PAr_3)$_2$] (Ar = C_6D_5). Also, addition of excess phosphine did not affect the rate of Me/Ph exchange, suggesting that phosphine dissociation is not necessary in the mechanism, in contrast to what was proposed for Ar/Ar' exchange.[2]

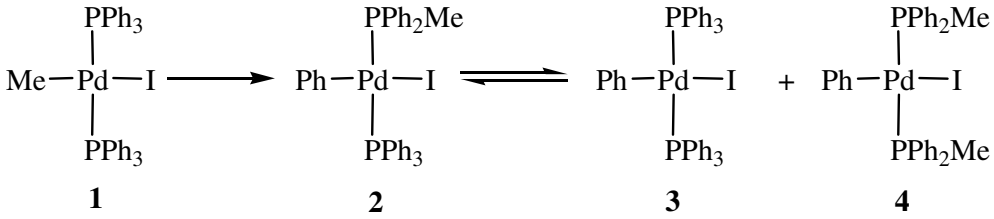

Figure 6.1: Me/Ph exchange in *trans*-[PdI(Me)(PPh_3)$_2$] in C_6D_6 at 50ºC.

This chapter contains a detailed mechanistic study of Me/Ph exchange in *trans*-[PdI(Me)(PPh_3)$_2$], the complex studied experimentally by Norton *et al.*[1] The ONIOM (BP86:HF) approach was used, as described in Chapter 2. The palladium, phosphorus and iodine atoms were at the 'high' level of calculation, along with the carbons and hydrogens from the exchanging methyl and phenyl groups. The remaining five phenyl groups were at the 'low' level of calculation, as shown in Figure 6.2.

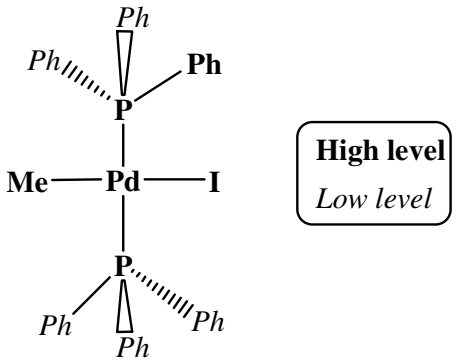

Figure 6.2: *trans*-[PdI(Me)(PPh_3)$_2$] with the atoms which are at **high** and *low* level in ONIOM calculations indicated.

As in Chapter 5, four different possible mechanisms for exchange were investigated. These mechanisms are defined by whether the reactant is 3- or 4-coordinate, and by the initial transfer step in each mechanism, as shown in Figure 6.3.

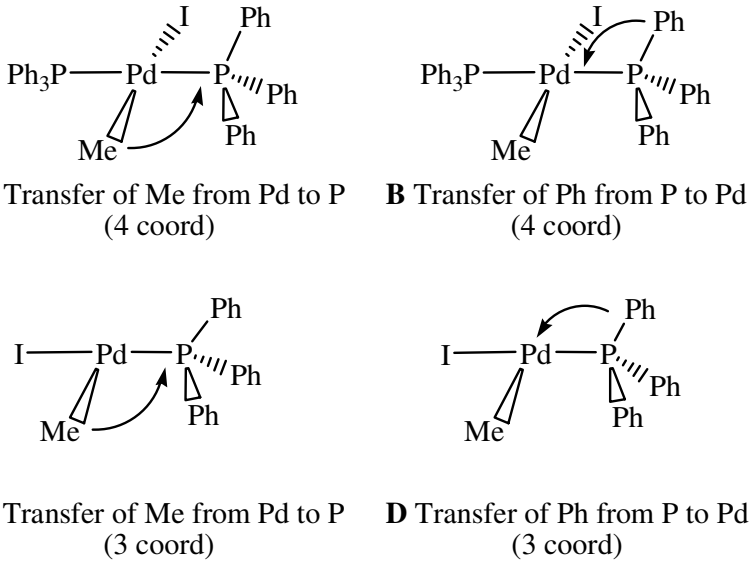

Figure 6.3: The four initial transfer steps to be considered for Me/Ph exchange from *trans*-[PdI(Me)(PPh_3)$_2$] (**A** and **B**) and T_{Me}-[PdI(Me)(PPh_3)] (**C** and **D**).

Mechanisms **A** and **B** begin from the 4-coordinate reactant *trans*-[PdI(Me)(PPh_3)$_2$], with the initial step of methyl attacking a phosphorus in **A**, and a phenyl transferring onto palladium in **B**. A triphenylphosphine ligand has been removed and isomerisation occurs to give the 3-coordinate starting point T_{Me}-[PdI(Me)(PPh_3)] for Mechanisms **C** and **D**, with **C** proceeding via a methyl attack on the phosphorus, while **D** progresses with a phenyl transferring onto palladium.

6.2 Mechanism A

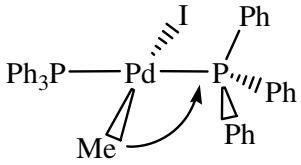

A Transfer of Me from Pd to P
(4 coord)

Before the reaction profile for Mechanism **A** could be investigated, it was necessary to optimise the 4-coordinate reactant structure, *trans*-[PdI(Me)(PPh_3)$_2$]. To obtain a realistic structure, the optimisation began from the structure of *trans*-[PdCl(Me)(PPh_3)$_2$],[3] a related complex whose structure has been crystallographically determined. The halide was changed and the structure was optimised, to produce reactant **3a** (set to 0.0 kcal/mol), as shown in Figure 6.4. All energies for Me/Ph exchange in this chapter will be relative to the energy of **3a**.

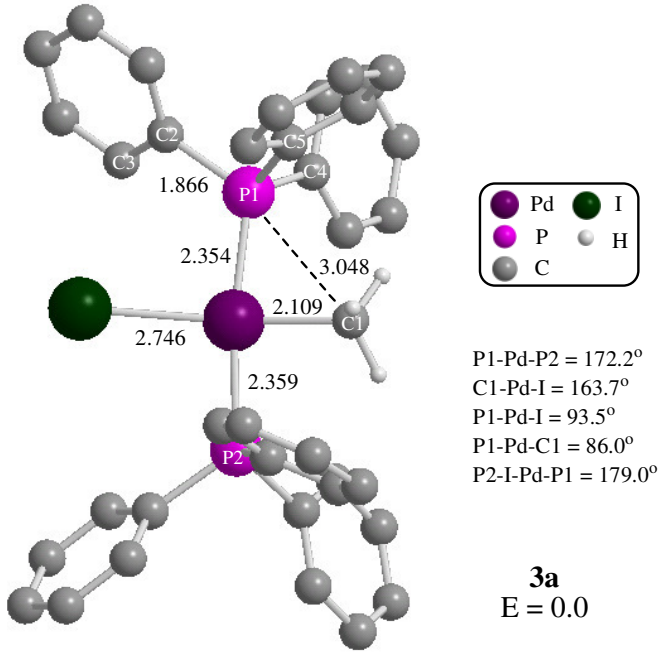

Figure 6.4: Optimised structure of reactant **3a**, *trans*-[PdI(Me)(PPh_3)$_2$]. Phenyl hydrogens are omitted for clarity. Bond lengths and distances in Å, energy in kcal/mol.

Selected bond lengths, angles and torsion angles for **3a** are compared to the crystallographic data for *trans*-[PdCl(Me)(PPh_3)$_2$][3] in Table 6.1. In both structures the palladium has a slightly distorted square planar geometry. The P1-Pd-P2 angle is

smaller than 180º at 177.38(2)º experimentally and 172.2º in **3a**, presumably due to the steric bulk of the iodide. The I-Pd-C1 angle is less than 180º at 175.23(8)º experimentally and 163.7º in **3a**, as the methyl lies slightly out of the metal coordination plane. Since the two structures have different halides coordinated to the palladium, it is not possible to directly compare the Pd-X bond lengths. The Pd-C1 bond is 0.055 Å longer in **3a**, which will be partly due to the stronger trans influence of I in **3a**, as seen in Chapter 5. The Pd-P bonds are overestimated by around 0.03 Å in the calculated geometry, which is a good agreement. When the Pd-P and Pd-C1 bonds in **3a** were fixed at the experimentally determined values, the calculation revealed the constrained structure to be only 0.5 kcal/mol less stable than **3a**, so the difference to the experimental structure was not expected to cause much difference energetically.

Atoms	Experimental bond lengths / Å	Bond lengths in **3a** / Å
Pd-P1	2.3224(7)	2.354
Pd-P2	2.3289(7)	2.359
Pd-X	2.4227(6)	2.746
Pd-C1	2.054(2)	2.109
P1-C2	1.828(2)	1.866
P1-C4	1.830(2)	1.877
P1-C5	1.815(3)	1.869
P1~C1	(3.117)	3.048

Atoms	Experimental angles / º	Angles in **3a** / º
C1-Pd-P2	91.50(7)	86.6
P1-Pd-C1	90.63(7)	86.0
P1-Pd-X	89.03(2)	93.5
P1-Pd-P2	177.38(2)	172.2
C1-Pd-X	175.23(8)	163.7

Table 6.1: Bond lengths and angles in *trans*-[PdX(Me)(PPh_3)$_2$] for the crystallographically-determined structure (X = Cl)[3] and optimised structure **3a** (X = I).

Mechanism **A** starts from structure **3a**, and begins with the palladium-bound methyl attacking one of the phosphorus atoms. Therefore, a scan was performed from **3a**, reducing the P1···C1 distance from 3.048 Å. A transition state calculation was run from the geometry at the energy highpoint of the scan, and this led to the location of $\mathbf{TS_{3a\text{-}3b}}$ (E = 30.5 kcal/mol). The structure of $\mathbf{TS_{3a\text{-}3b}}$ is shown in Figure 6.5. As the methyl attacks P1, the Pd···C1 distance lengthens (Pd···C1: **3a** = 2.109 Å, $\mathbf{TS_{3a\text{-}3b}}$ = 2.405 Å) and the C1···P1 distance shortens (C1···P1: **3a** = 3.048 Å, $\mathbf{TS_{3a\text{-}3b}}$ = 2.115 Å). The methyl group has also moved further out of the metal coordination plane (C1-P1-Pd-I: **3a** = 163.7º, $\mathbf{TS_{3a\text{-}3b}}$ = 92.3º). This results in a change in the coordination environment around palladium, from distorted square planar in **3a** to distorted trigonal planar in $\mathbf{TS_{3a\text{-}3b}}$, if the {$PMePh_3$} moiety is considered as a single ligand. The three angles around palladium reflect this new geometry (P1-Pd-I = 114.0º, I-Pd-P2 = 116.8º,

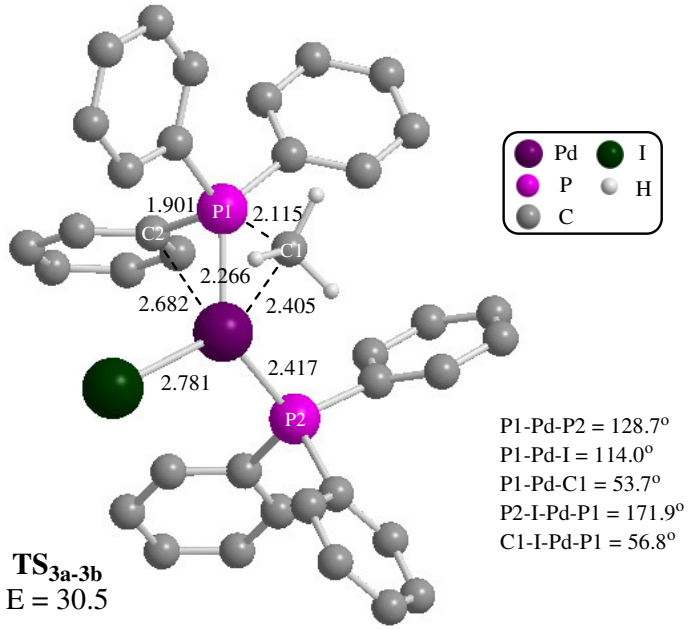

Figure 6.5: Optimised structure of **TS_{3a-3b}**. Bond lengths and distances in Å, energy in kcal/mol.

P1-Pd-P2 = 128.7º) and these angles add up to 359.5º. The phenyl group on the opposite side of P1 from the attacking methyl has dropped down to approach palladium, with a lengthening of the P1-C2 bond (**3a** = 1.866 Å, **TS_{3a-3b}** = 1.901 Å) and a reduction in the C2···Pd distance (C2···Pd: **3a** = 3.670 Å, **TS_{3a-3b}** = 2.682 Å).

Pseudo-intrinsic reaction coordinate (PIRC) calculations revealed that **TS_{3a-3b}** links to the 4-coordinate reactant **3a**, and leads directly to the 4-coordinate exchange product, *trans*-[PdI(Ph)($PMePh_2$)(PPh_3)], **3b** (E = -7.5 kcal/mol). The structure of **3b** with key distances and angles is shown in Figure 6.6. The methyl carbon has formed a bond to P1 (C1-P1 = 1.865 Å), a phenyl group has transferred onto palladium, with a new Pd-C2 bond (2.038 Å), and the P1-C2 bond has completely broken (P1···C2 = 3.063 Å). The geometry around palladium has reverted to being distorted square planar, with the four angles around palladium adding up to 360.7º, and a P2-I-Pd-P1 torsion angle of 174.6º. The Pd-P2 bond is slightly longer in **3b** (2.383 Å) than in **3a** (2.359 Å), which suggests that the $PMePh_2$ ligand exerts a stronger trans influence than PPh_3. Similarly, the Pd-I bond is longer in **3b** (2.774 Å) than in **3a** (2.746 Å), suggesting that phenyl exerts a stronger trans influence than methyl.

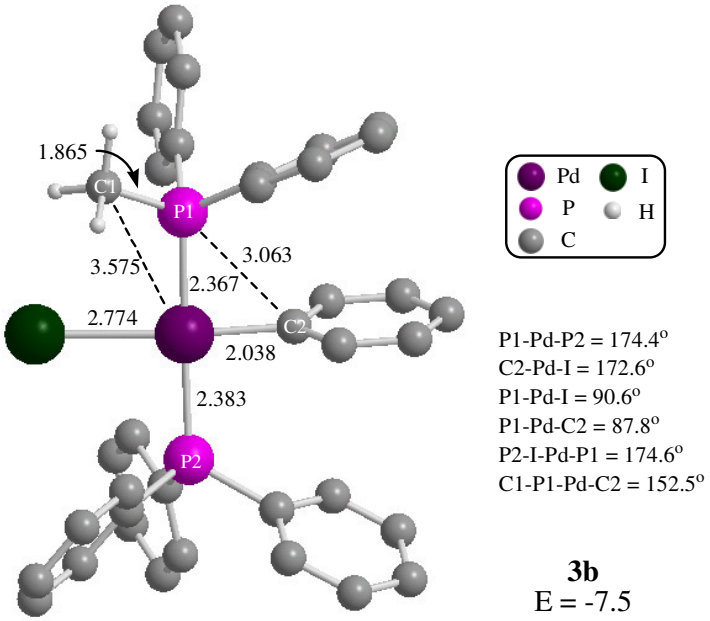

Figure 6.6: Optimised structure of **3b**. Bond lengths and distances in Å, energy in kcal/mol.

The reaction profile for Mechanism **A** is shown in Figure 6.7. The activation barrier (30.5 kcal/mol) is slightly higher than the equivalent barrier for Ph/Ph exchange in *trans*-[PdI(Ph)(PPh_3)$_2$] via Mechanism **A** in Chapter 5, which is 28.6 kcal/mol. As seen in Chapter 3, it is easier to transfer a phenyl group onto PH_3 than a methyl group, as phenyl has a π-system which is able to strengthen the bonding interactions in the transition state, lowering the activation barrier.[4]

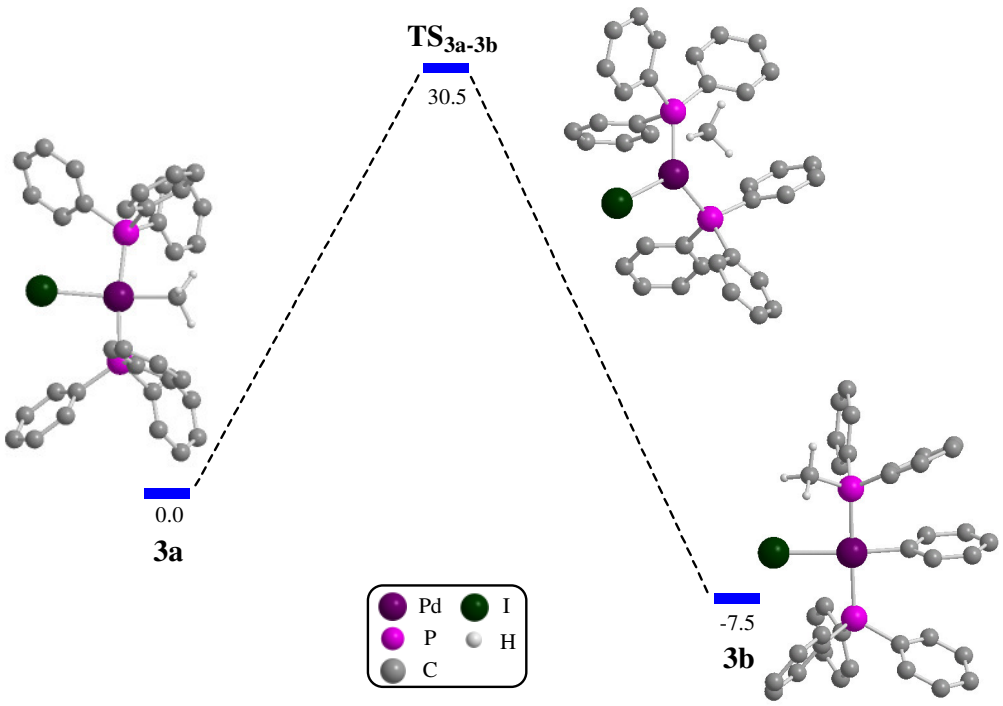

Figure 6.7: Mechanism **A** Me/Ph exchange reaction profile, starting from **3a**, *trans*-[PdI(Me)(PPh_3)$_2$]. Energies in kcal/mol.

It is useful to consider the bond interaction (BI) strengths of the bonds that are made and broken in the exchange process to gain insight into the energetics of the process. This was done using the same techniques as in Chapter 3 and the energies are shown in Table 6.2. The bonds formed (Pd-Ph and P-Me) are collectively stronger (146.6 kcal/mol) than the bonds that are broken (Pd-Me and P-Ph, 131.1 kcal/mol). This is consistent with the fact that the overall process was found to be exothermic in the calculations (ΔE = -7.5 kcal/mol) and irreversible experimentally.[1]

Bond	Complex	BI / kcalmol^{-1}
Pd-Me	**3a**	59.2
P-Ph	**3a**	71.9
P-Me	**3c**	81.4
Pd-Ph	**3c**	65.2

Table 6.2: Bond interaction energies (BI/kcalmol^{-1}) of the bonds broken and formed in Me/Ph exchange in *trans*-[PdI(Me)(PPh_3)$_2$].

6.2.1 The search for a pathway via a zwitterion

A difference between the mechanisms for Ph/Ph and Me/Ph exchange has already come to light. Namely, in Mechanism **A** Me/Ph exchange has a concerted pathway while Ph/Ph exchange was found to be a two-step process via a zwitterion species. Therefore, it was of interest to see whether Me/Ph exchange could also proceed via a zwitterion in Mechanism **A**. A structure containing an η^2-interaction between palladium and a phenyl group was located by allowing ions $[PdIPPh_3]^-$ and $[PMePh_3]^+$ to interact and optimise. The resulting structure was **3c** (E = 10.0 kcal/mol) and is shown in Figure 6.8. This structure bears similarities to other computed zwitterion structures which were discussed in previous chapters, such as **1b**, $[PdClPPh_3]^-[PPh_4]^+$ (a zwitterion bound through a Pd···Ph η^2-interaction), in Chapter 5. The geometry around palladium in **3c** is planar, with the relevant angles adding up to 360.0º. The C2-C3 bond is longer (1.472 Å) than in reactant **3a** (1.413 Å) due to the interaction with the palladium.

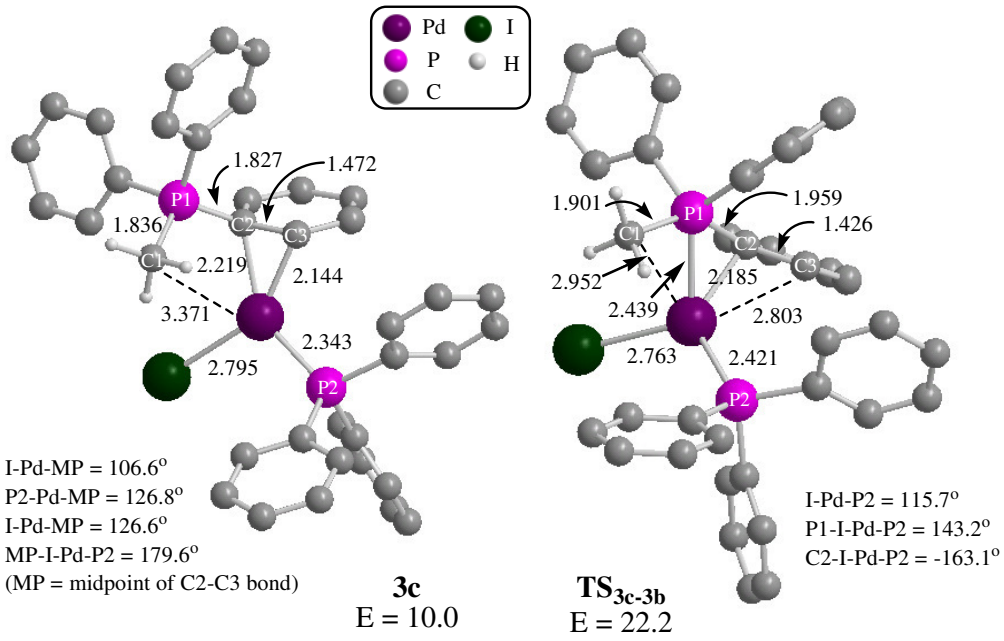

Figure 6.8: Optimised structures of zwitterion **3c** and $\mathbf{TS_{3c\text{-}3b}}$. Bond lengths and distances in Å, energies in kcal/mol.

In order to find a transition state linking reactant **3a** to zwitterion **3c**, a scan was performed reducing the Pd···C1 distance from its value of 3.371 Å in **3c**. A transition state was located from the highpoint of the scan, but when it was characterised using PIRC calculations, it was found to link **3c** to exchange product **3b**. The structure of this transition state, $\mathbf{TS_{3c\text{-}3b}}$ (E = 22.2 kcal/mol), is also shown in Figure 6.8. This

corresponds to a barrier for phenyl-transfer of 12.2 kcal/mol, which is only slightly larger than the analogous barrier in Ph/Ph exchange (X = I) of 10.1 kcal/mol ($\mathbf{TS_{1b'\text{-}1a'}}$ = 28.6 kcal/mol). Extensive efforts were made to try to find a transition state linking reactant **3a** to zwitterion **3c**, but it was not possible to find one. Therefore, although a zwitterion species was found, it does not appear to feature in a pathway for Me/Ph exchange via Mechanism **A**.

6.2.2 Mechanism A starting with *cis*-[PdI(Me)(PPh_3)$_2$]

In the experimental work carried out by Norton *et al.*,[1] it was specified that *trans*-[PdI(Me)(PPh_3)$_2$] (**1**) was the reactant used, and that no free PPh_3 was observed within the limits of the NMR experiment. However, after Me/Ph exchange had occurred to form *trans*-[PdI(Ph)($PMePh_2$)] (**2**), they observed facile intermolecular phosphine exchange, resulting in an equilibrium between **2**, *trans*-[PdI(Ph)(PPh_3)$_2$] (**3**) and *trans*-[PdI(Ph)($PMePh_2$)$_2$] (**4**), as shown in Figure 6.1. It therefore seems possible that there is phosphine dissociation occurring in a solution of **1**, and so there may be equilibrium between the cis and trans isomers of **1**.

There is no crystallographically determined structure for *cis*-[PdI(Me)(PPh_3)$_2$] in the Cambridge Crystallographic Database,[5] so the structure of *cis*-[Pd(H_2O)$_2$(PPh_3)$_2$](OTf)$_2$ was used to get a realistic orientation for the cis triphenylphosphine groups,[6] and the H_2O ligands were replaced by methyl and iodide. The optimised structure for *cis*-[PdI(Me)(PPh_3)$_2$], **3a'** (E = 4.3 kcal/mol), is shown in Figure 6.9. The structure is rather distorted from square planar, with a P1-Pd-P2 angle of 102.6º, caused by the bulky PPh_3 ligands lying cis to each other. The Pd-P2 bond (2.447 Å) is longer than the Pd-P1 bond (2.335 Å) as methyl exerts a stronger trans influence than iodide. The geometry is also distorted from an ideal planar geometry by the iodide lying slightly out of the metal coordination plane (P1-P2-Pd-I = 166.6º). Energetically the cis isomer, **3a'**, is 4.3 kcal/mol less stable than trans isomer **3a**, which is consistent with the fact that only the trans isomer was observed experimentally.[1]

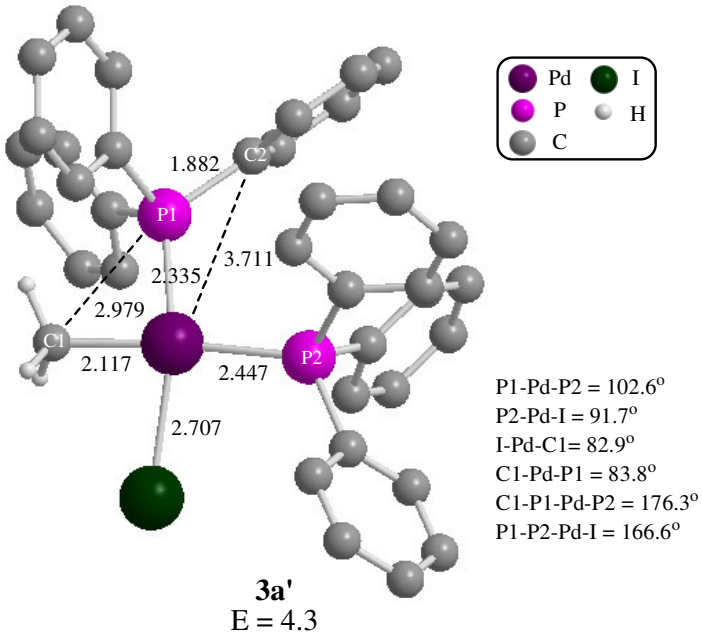

Figure 6.9: Optimised structure of *cis*-[PdI(Me)(PPh_3)$_2$], **3a'**. Bond lengths and distances in Å, energy in kcal/mol.

To investigate Me/Ph exchange from the cis isomer, **3a'**, a scan was performed, which reduced the P1-C1 distance from 2.979 Å. This led to the location of **TS$_{3a'-3b}$** (E = 30.4 kcal/mol), which is shown in Figure 6.10. There are only small differences in bond lengths and angles between **TS$_{3a-3b}$** and **TS$_{3a'-3b}$**, including the methyl group being slightly earlier in its transfer in **TS$_{3a'-3b}$** (Pd···C1: **TS$_{3a-3b}$** = 2.405 Å, **TS$_{3a'-3b}$** = 2.381 Å) and lying closer to the iodide side of the complex (C1-P1-Pd-I: **TS$_{3a-3b}$** = 92.3º, **TS$_{3a'-3b}$** = 83.7º). The methyl group lies out of the metal coordination plane (C1-P1-Pd-P2 = 101.1º) and the Pd-C1 bond is breaking (Pd···C1: **3a'** = 2.117 Å, **TS$_{3a'-3b}$** = 2.381 Å) as a C1-P1 bond is forming (C1···P1: **3a'** = 2.979 Å, **TS$_{3a'-3b}$** = 2.148 Å). The geometry around the metal has changed from distorted square planar to distorted trigonal planar, with the three angles around palladium totalling 359.8º. The energies of the two transition states are very close, with **TS$_{3a'-3b}$** 0.1 kcal/mol more stable.

TS$_{3a'-3b}$ was also found to be a concerted transition state, with PIRC calculations showing that it links to the cis reactant **3a'**, and leads to exchange product **3b**. If indeed there is a presence of the cis isomer [PdI(Me)(PPh_3)$_2$] in the reacting solution, this alternative form of Mechanism **A** would certainly be competitive to the concerted process derived from the trans isomer, as the two pathways have a very similar energy

highpoint. As they are both concerted processes, and form the same products, it would be extremely difficult to distinguish between them experimentally.

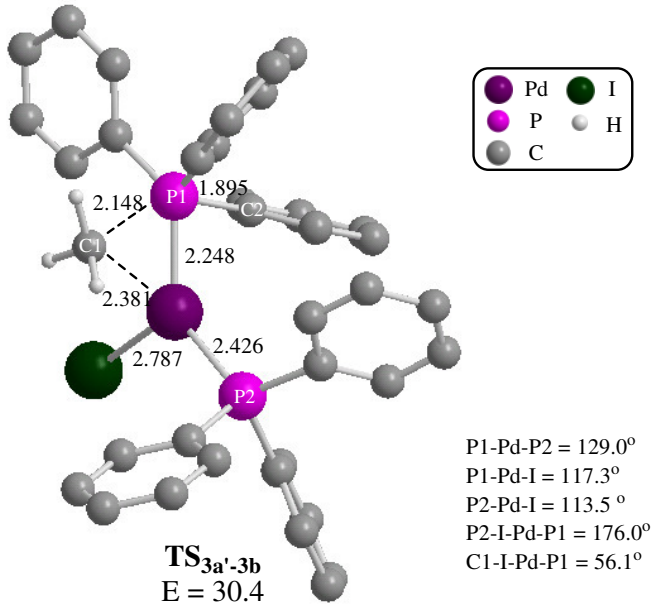

Figure 6.10: Optimised structures of **TS$_{3a'-3b}$**. Bond lengths and distances in Å, energy in kcal/mol.

6.3 Mechanism B

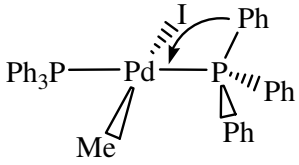

B Transfer of Ph from P to Pd
(4 coord)

The second mechanism to be considered for Me/Ph exchange begins with the oxidative addition of a phenyl group onto palladium. It was presumed that this would lead to a 5-coordinate square pyramidal intermediate species. Such a species, **3d** (E = 35.6 kcal/mol), was formed by reducing the Pd···C2 distance in **3a** using a scan, then optimising the resulting structure. In principle, there are 15 other possible isomers of this 5-coordinate intermediate, as there are 3 isomers for each variation of the axial ligand, hence structures of each were constructed and optimised, to see whether a more relatively stable form could be found. In total three additional local minima which are geometric isomers of **3d** were found, and their structures are shown in Figure 6.11. In all four isomers the PPh_2 ligand lies cis to both the methyl and palladium-bound phenyl

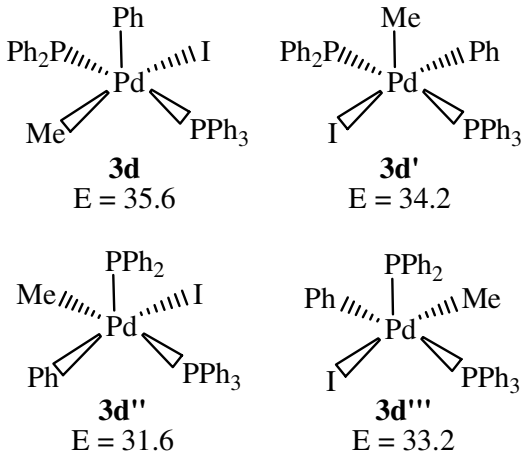

Figure 6.11: Optimised structures of the four stable isomers (**3d**-**3d'''**) of the 5-coordinate oxidative addition intermediate in Mechanism **B**. Energies in kcal/mol.

groups, therefore the transfer of either group onto PPh_2 should be possible without further rearrangement. The most stable isomer is **3d''** (E = 31.6 kcal/mol), which is a distorted square pyramid with PPh_2 in the axial position, and phenyl trans to iodide.

Pathways to link these four species with their appropriate reactants and products were sought by performing scans to reduce the P···C distances to form either PPh_3 or $PMePh_2$. This investigation resulted in two pathways being characterised, both originating from **3a** or **3a'** to form the exchange product **3b**.

6.3.1 Mechanism B starting from 3a

The pathway from trans reactant **3a** was ultimately shown to pass through three 5-coordinate intermediate species and four transition states to produce exchange product **3b**. All of the transition states were located by performing scans starting from each individual intermediate species. Transition states were located from the scans and then PIRCs were run, to see to which local minima each transition state links to. The transition state that was found to link reactant **3a** to an intermediate species is $\mathbf{TS_{3a\text{-}3d}}$ (E = 38.5 kcal/mol), and the structures of $\mathbf{TS_{3a\text{-}3d}}$ and **3d** are shown in Figure 6.12.

In the transfer of the phenyl group (containing C2) from P1 to Pd, the C2-P1 bond breaks (**3a** = 1.866 Å, $\mathbf{TS_{3a\text{-}3d}}$ = 2.595 Å, **3d** = 3.245 Å), and a Pd-C2 bond is formed (**3a** = 3.433 Å, $\mathbf{TS_{3a\text{-}3d}}$ = 2.153 Å, **3d** = 2.060 Å). During this process the four angles

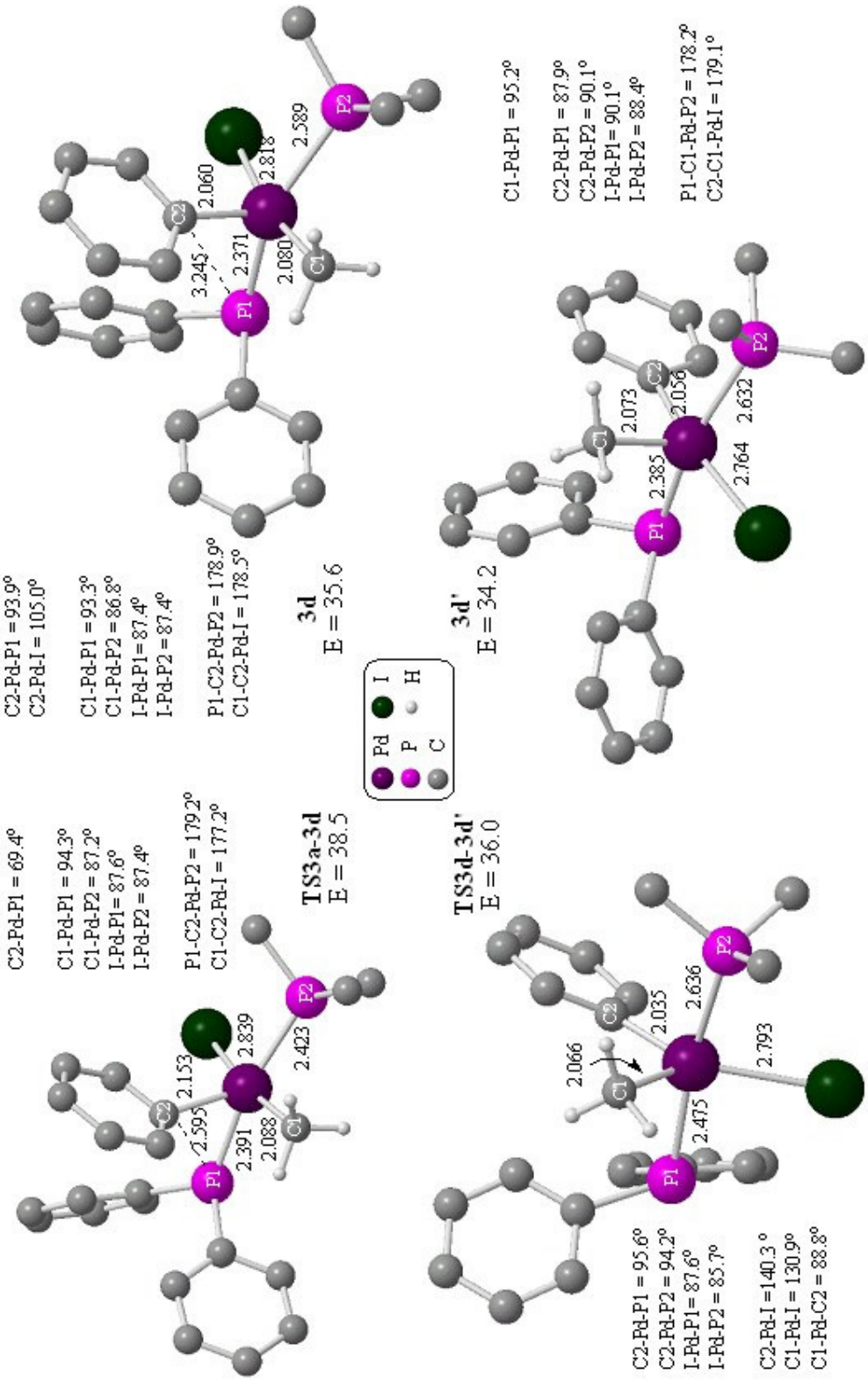

Figure 6.12: Optimised structures of **TS_{3a-3d}**, **3d**, **$TS_{3d-3d'}$** and **3d'** in Mechanism **B**. Bond lengths and distances in Å, energies in kcal/mol. Phenyl groups on P2 have been truncated at the *ipso*-carbons for clarity.

around palladium in the metal coordination plane stay close to 90º. There is a general trend of the metal-ligand bonds being longer in **3d** than in **3a**, with the exception of the Pd-C1 bond which becomes slightly shorter (3a = 2.109 Å, 3d = 2.080 Å). This lengthening may be due to the more crowded environment around palladium with an extra ligand coordinated.

Scans were performed from each intermediate species with a shortening of the P1···C1 distance, to try to find a pathway to form the exchange product **3b**. However, it was not possible to transfer the methyl onto P1 from isomers **3d**, **3d'** or **3d'''**, as each isomerised rather than completing the exchange pathway. A transition state was found to link **3d''** to **3b**, and will be discussed in more detail in due course. Therefore, to complete the pathway between **3d** and **3b**, it was necessary to isomerise before the methyl transfer could occur.

It is not possible to isomerise from **3d** to **3d''** directly, this was instead achieved in a two step process via **3d'**. Firstly, a transition state was sought to change the position of iodide to lie trans to phenyl rather than methyl. This was possible by increasing the C2-Pd-I angle from 105.0º in **3d**, using a scan to find the energy highpoint. Thus $\mathbf{TS_{3d\text{-}3d'}}$ (E = 36.0 kcal/mol) was located, and the structure with key bond lengths, along with the structure of **3d'**, is shown in Figure 6.12. The C2-Pd-I angle has increased to 140.3º in $\mathbf{TS_{3d\text{-}3d'}}$, and C1, C2 and I form a Y-shape around palladium (C1-Pd-C2 = 88.8º, C1-Pd-I = 130.9º), while P1 and P2 remain trans to each other. Both Pd-P bonds become slightly longer in $\mathbf{TS_{3d\text{-}3d'}}$, and though they shorten again when **3d'** is formed, they remain longer than in **3d**. This could be due to having phenyl in the basal plane of the square-pyramid in **3d'**, which is more bulky than the methyl in **3d**. The Pd-C1 bond is slightly shorter in **3d'** than in **3d**, as it no longer has a ligand lying trans and now occupies an axial position. In contrast to this, the Pd-C2 bond is actually slightly shorter in **3d'** than in **3d**, which cannot be attributed to trans influence effects. The energy barrier to pass from **3d** to **3d'** is only 0.4 kcal/mol, indicating that the isomerisation is facile.

A further isomerisation was necessary to form **3d''**, therefore a scan was performed that opened the C1-Pd-P2 angle from 101.0º in **3d'**, to move the triphenylphosphine ligand to lie trans to methyl, leaving PPh_2 in the axial position. A transition state, $\mathbf{TS_{3d'\text{-}3d''}}$ (E

= 36.0 kcal/mol), was located from the energy highpoint of the scan, and the structure of this and **3d''** are shown in Figure 6.13.

In $\mathbf{TS_{3d'-3d''}}$ the C1-Pd-P2 angle has opened to 130.0º and as in $\mathbf{TS_{3d-3d'}}$, P1, C1 and P2 are in a Y-shape around palladium (P1-Pd-P2 = 144.1º, P1-Pd-C1 = 85.7º). The iodide and phenyl ligands remain trans to each other with only small changes in bond length. There is a small activation energy of 1.8 kcal/mol to isomerise from **3d'** to **3d''**. All of the palladium-ligand bonds are slightly longer in **3d''** than in **3d'**, which may be due to the more distorted geometry in **3d''**. There is a distortion from a square pyramidal geometry towards TBP in **3d''** as C2 and I lie slightly below the metal coordination plane (C2-Pd-I = 140.2º, P1-Pd-C2 = 106.1º). The exception to the general trend of bond lengthening is with Pd-P2, which is slightly shorter in **3d''** (2.584 Å) than in **3d'** (2.632 Å).

As mentioned earlier, a transition state which links **3d''** to exchange product **3b**, $\mathbf{TS_{3d''-3b}}$ (E = 37.6 kcal/mol), was located. Its structure is also shown in Figure 6.13. The geometry of $\mathbf{TS_{3d''-3b}}$ is further distorted from square pyramidal than **3d''**, with a shortening of the P1···C1 distance from 3.227 Å in **3d''** to 2.449 Å in $\mathbf{TS_{3d''-3b}}$. As P1 and C1 approach each other, the Pd-C1 bond lengthens by 0.129 Å and simultaneously the Pd-P2 bond trans to C1 shortens by 0.206 Å. The Pd-I and Pd-C2 bonds shorten slightly in $\mathbf{TS_{3d''-3b}}$, and even further in **3b**. The Pd-P1 bond shortens from 2.458 Å in the axial position of **3d''** to 2.367 Å in 4-coodinate square planar **3b**. This step also has a relatively small energy barrier of 6.0 kcal/mol. There is a large stabilisation associated with the formation of 4-coordinate product **3b** (E = -7.5 kcal/mol).

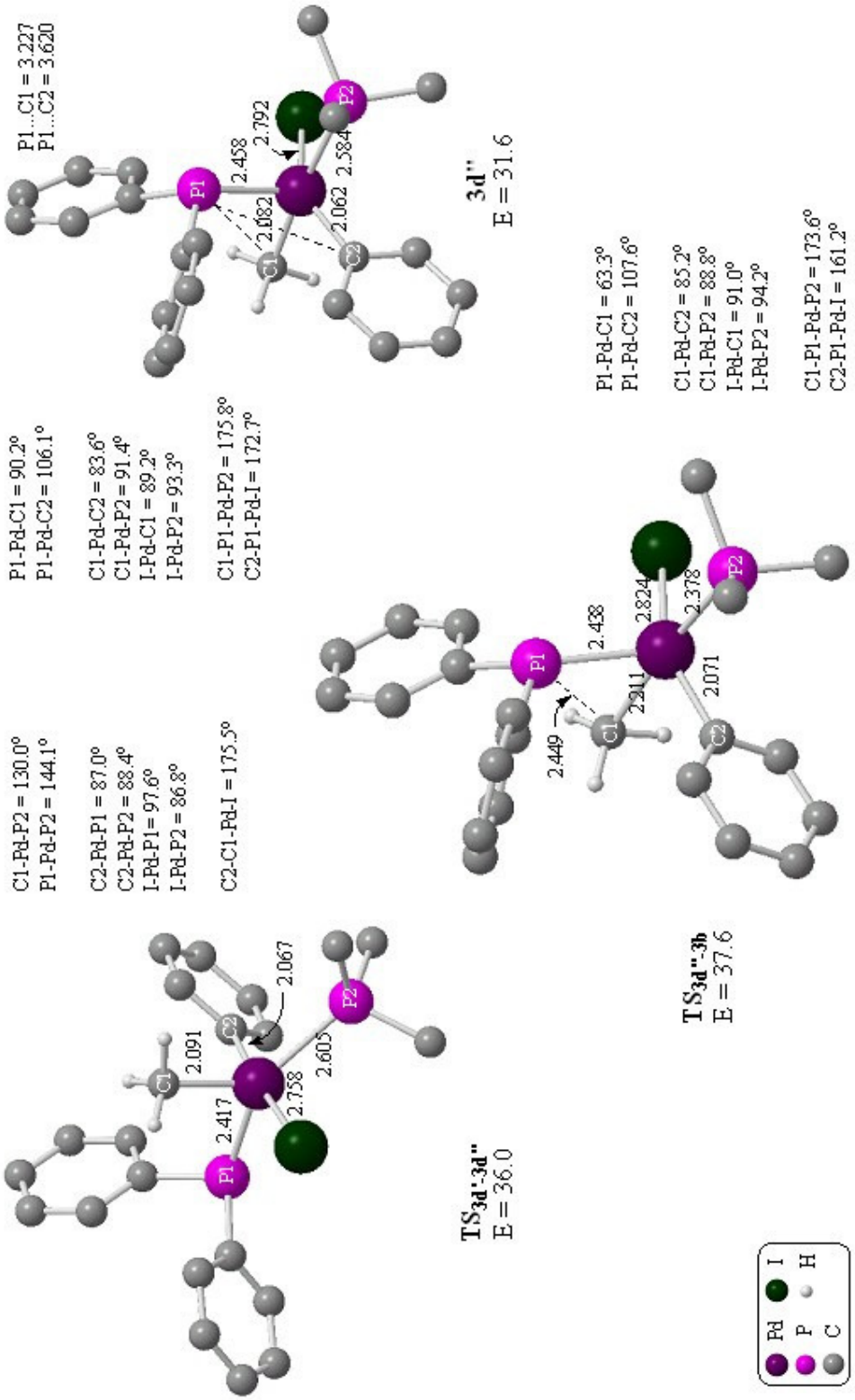

Figure 6.13: Optimised structures of **$TS_{3d'-3d''}$**, **3d''** and **$TS_{3d''-3b}$** in Mechanism **B**. Bond lengths and distances in Å, energies in kcal/mol.

6.3.2 Mechanism B starting from 3a'

A profile to link cis reactant **3a'** to exchange product **3b** via 5-coordinate intermediate **3d''** was found by performing a scan to shorten the P1···C2 distance from 3.620 Å in **3d''**. Thus $\mathbf{TS_{3a'\text{-}3d''}}$ (E = 43.2 kcal/mol) was located, and its structure is shown below in Figure 6.14. The major structural changes occurring are the breaking of the P1-C2 bond (**3a'** = 1.882 Å, $\mathbf{TS_{3a'\text{-}3d''}}$ = 2.458 Å) and the reduction of the Pd···C2 distance (**3a'** = 3.711 Å, $\mathbf{TS_{3a'\text{-}3d''}}$ = 2.145 Å), leading to the formation of a Pd-C2 bond in **3d''** (2.062 Å). There is a general trend of lengthening of the palladium-ligand bonds in $\mathbf{TS_{3a'\text{-}3d''}}$, with the exception of the Pd-C1 bond, as was the case with the analogous transition state, $\mathbf{TS_{3a\text{-}3d}}$, discussed in the previous section. Another similarity is the high activation barrier, in this case 38.9 kcal/mol, required to form a 5-coordinate intermediate species.

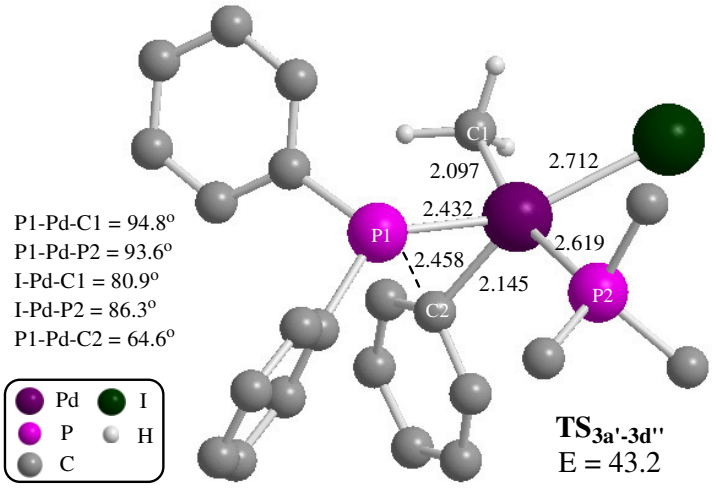

Figure 6.14: Optimised structure of $\mathbf{TS_{3a'\text{-}3d''}}$ in Mechanism **B**. Bond lengths and distances in Å, energies in kcal/mol.

From complex **3d''** it is possible to form the exchange product **3b** via $\mathbf{TS_{3d''\text{-}3b}}$ as discussed in the previous section. Therefore, a simple two-step mechanism links **3a'** to product **3b**.

6.3.3 Mechanism B energy profiles

The two profiles found for Mechanism **B** are shown in Figure 6.15. Although the pathway starting from **3a'** is a simpler process, it also contains the overall energy highpoint at $\mathbf{TS_{3d''\text{-}3b}}$ of 43.2 kcal/mol. The pathway starting from **3a** is slightly more accessible, but involves several isomerisations before the exchange product can be formed. Overall, Mechanism **B**, with a highpoint of 38.5 kcal/mol, is considerably less

accessible than Mechanism **A**, which has an energy highpoint of 30.5 kcal/mol ($\mathbf{TS_{3a\text{-}3b}}$).

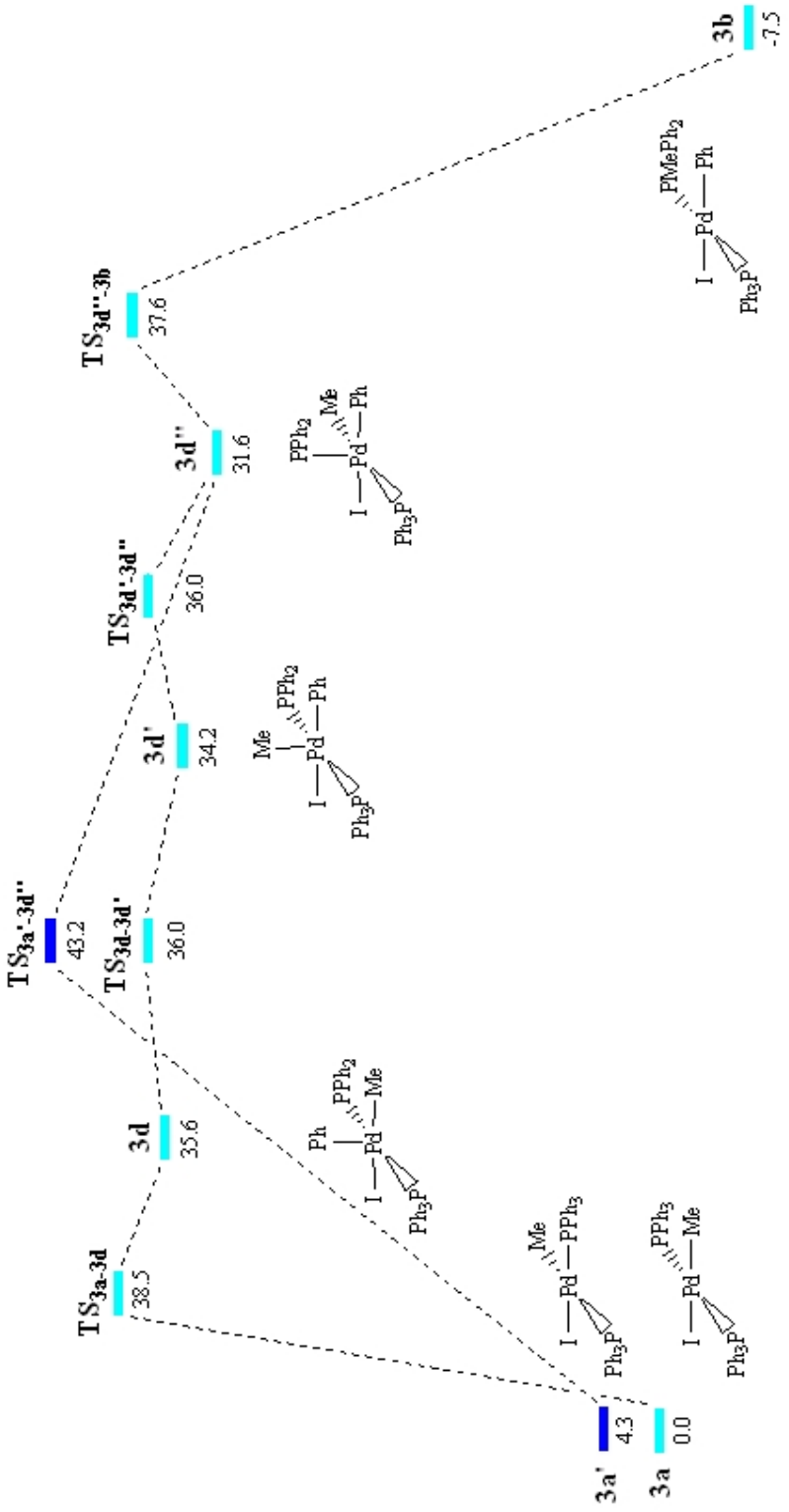

Figure 6.15: Reaction profiles in Mechanism **B**. Energies in kcal/mol.

6.4 Mechanism C

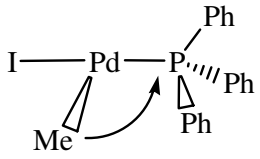

C Transfer of Me from Pd to P
(3 coord)

Mechanism **C** begins from the 3-coordinate reactant T_{Me}-[PdI(Me)(PPh_3)]. This was formed by running a scan to lengthen the Pd···P2 distance from 2.359 Å in **3a**. This process did not pass through an energy maximum, hence the PPh_3 was removed and the remaining complex was allowed to optimise. The complex isomerised so that the methyl group lies opposite the vacant site. The optimised geometry of T_{Me}-[PdI(Me)(PPh_3)], **4a** (E = 16.1 kcal/mol), is shown in Figure 6.16. The geometry around the palladium is T-shaped, with the three angles adding up to 360.1°. The Pd-P bond (2.269 Å) and the Pd-I bond (2.615 Å) are both shorter than in **3a** (2.354 Å and 2.746 Å respectively), as seen before in both Chapters 5 and 6 when going from a 4- to 3-coordinate species.

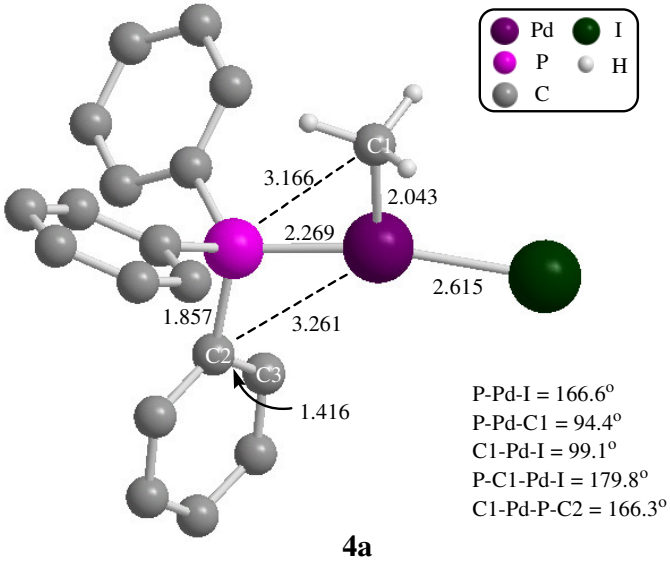

4a
E = 16.1

Figure 6.16: Optimised structures of T_{Me}-[PdI(Me)(PPh_3)], **4a**. Bond lengths and distances in Å, energy in kcal/mol.

A scan reducing the P···C1 distance from its value of 3.166 Å in **4a** was performed, and this led to the discovery of a transition state from the geometry at the energy highpoint, $\mathbf{TS_i}$ (E = 45.1 kcal/mol). However, PIRC calculations showed that this transition state links reactant **4a** forwards to a very shallow minimum, **ii** (E = 45.3 kcal/mol). The structure of the complex at this energy minimum point was very close to that of the transition state, and the energy difference was very small. Further investigation of this very flat area in potential energy revealed a second minimum, **iii** (E = 45.6 kcal/mol) and transition state $\mathbf{TS_{iv}}$ (E = 45.8), both having structures and energies very similar to the other two complexes. Some key bond lengths and distances for these four structures are shown in Table 6.3.

	P-C1	Pd···C1	P-C2	Pd···C2	C1-H1	Pd···H1	E / kcalmol^{-1}
$\mathbf{TS_i}$	1.939	2.261	1.860	2.741	1.161	1.820	45.1
ii	1.906	2.285	1.847	2.727	1.167	1.797	45.3
iii	1.894	2.307	1.843	2.676	1.168	1.795	45.6
$\mathbf{TS_{iv}}$	1.887	2.335	1.841	2.586	1.166	1.807	45.8

Table 6.3: Key bond lengths and distances (Å) and energies (kcal/mol) for structures $\mathbf{TS_i}$, minima **ii** and **iii**, and $\mathbf{TS_{iv}}$.

The bond lengths and distances for these four structures show that the methyl is transferring onto phosphorus and the opposite phenyl group is moving towards palladium. There seems to be an agostic interaction between Pd and H1 (a methyl hydrogen), which is slightly stronger in minima **ii** and **iii** than in the transition states. This may be a factor causing these shallow minima. This section of the potential energy surface is clearly very flat, and in a chemical reaction intermediates **ii** and **iii** would not be isolable. Therefore, the energy highpoint in this region, $\mathbf{TS_{iv}}$, will be taken as the energy barrier for this part of the reaction. From hereon this transition state will be called $\mathbf{TS_{4a\text{-}4b}}$ (E = 45.8 kcal/mol) and its structure is shown in Figure 6.17. In $\mathbf{TS_{4a\text{-}4b}}$ the Pd-C1 bond is breaking (Pd···C1: **4a** = 2.043 Å, $\mathbf{TS_{4a\text{-}4b}}$ = 2.335 Å) and a P-C1 bond is forming (P···C1: **4a** = 3.166 Å, $\mathbf{TS_{4a\text{-}4b}}$ = 1.887 Å). The phenyl group that lies on the opposite side of the phosphorus from the attacking methyl has moved closer to palladium (Pd···C2: **4a** = 3.261 Å, $\mathbf{TS_{4a\text{-}4b}}$ = 2.586 Å). There is now a bent geometry around palladium, with an I-Pd-P angle of 140.7º.

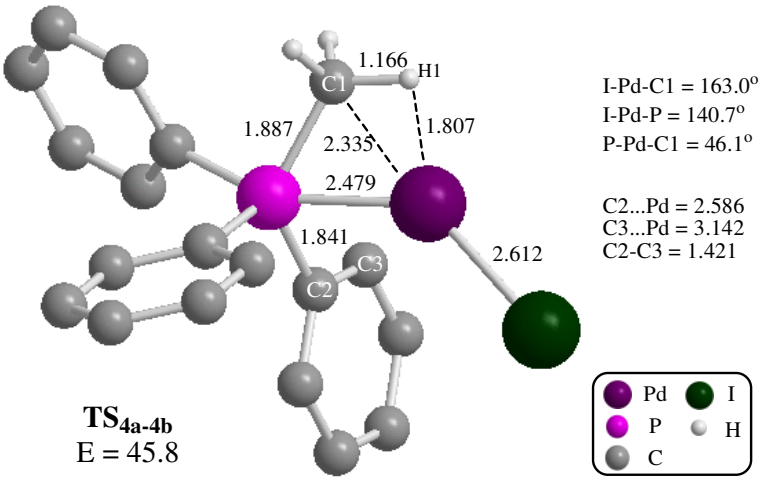

Figure 6.17: Optimised structure of **TS$_{4a-4b}$**. Bond lengths and distances in Å, energy in kcal/mol.

When PIRC calculations were performed from **TS$_{4a-4b}$**, it was found that the transition state leads to an intermediate zwitterion structure, **4b** (E = 27.6 kcal/mol), which is shown in Figure 6.18. The geometry around palladium is distorted by around 10º from being linear (I-Pd-MP = 169.9º). The Pd-P bond has broken and the phosphorus now lies 3.091 Å from palladium. There is an η^2-interaction between the *ipso-ortho* C2-C3 bond in one of the phenyl rings and palladium. As seen in structure **2b** in Chapter 5, the

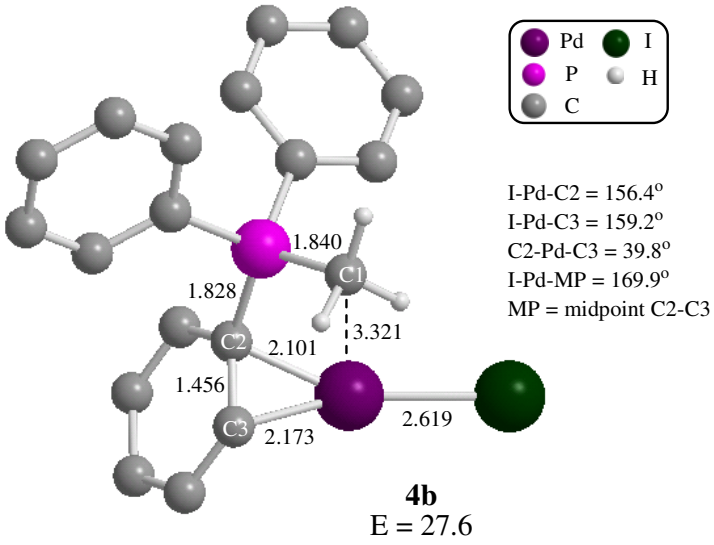

Figure 6.18: Optimised structure of zwitterion **4b** in Mechanism **C**. Bond lengths and distances in Å, energy in kcal/mol.

η^2-interaction is slightly unsymmetrical, with the *ispo*-carbon 0.072 Å closer to palladium than the *ortho*-carbon. The C2-C3 bond here is only 0.003 Å longer than the corresponding bond in **2b**. However, the structures differ in that in **2b**, it is the phenyl that was originally palladium-bound which forms the η^2-interaction with palladium, which is not possible in **4b**. If compared to the 3-coordinate reactant **4a**, intermediate **4b** is rather stable with $\Delta E_{\mathbf{4b\text{-}4a}}$ = 11.5 kcal/mol.

To complete the exchange process, a P-C bond must break to allow a phenyl group to transfer from phosphorus to palladium, and the Pd-P bond must reform. To achieve this, a scan was performed to lengthen the P···C2 distance from its value of 1.828 Å in **4b**. However, this was not successful as the {$PMePh_2$} fragment started to dissociate from the metal, without a Pd-P bond forming. Therefore, the exchange product, T_{Ph}-[PdI(Ph)($PMePh_2$)], was constructed and optimised, then a reverse scan decreasing the P···C2 distance from the product geometry was performed. A transition state was located at the energy highpoint of the scan with a geometry that looked promising, and the energy of the transition state located, $\mathbf{TS_{4b\text{-}4c}}$ (E = 33.1 kcal/mol), is higher than the energy of the zwitterion **4b**. $\mathbf{TS_{4b\text{-}4c}}$ also has a Pd···P distance (2.340 Å) of an intermediate value between **4b** (3.091 Å) and the exchange product (2.289 Å). PIRC calculations were run from $\mathbf{TS_{4b\text{-}4c}}$, and these confirmed that this transition state did indeed link zwitterion **4b** to the exchange product. The structure of $\mathbf{TS_{4b\text{-}4c}}$ is shown in Figure 6.19. If the structure of $\mathbf{TS_{4b\text{-}4c}}$ is compared to **4b**, it can be seen that the η^2-interaction between C2-C3 and palladium has weakened, as the C3···Pd distance has increased by 0.35 Å while the Pd-C2 bond has remained intact. This is highlighted by the shortening of the C2-C3 bond from 1.456 Å in **4b** to 1.427 Å in $\mathbf{TS_{4b\text{-}4c}}$. As mentioned above, the Pd-P bond has reformed as required.

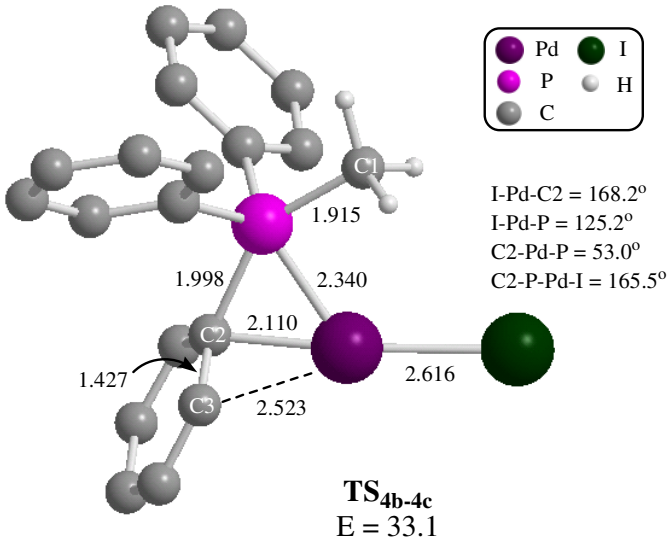

Figure 6.19: Optimised structure of **TS$_{4b-4c}$** in Mechanism **C**. Bond lengths and distances in Å, energy in kcal/mol.

The geometry of the exchange product, T$_{Ph}$-[PdI(Ph)(PMePh$_2$)], **4c** (E = 14.2 kcal/mol), produced in the PIRC calculations from **TS$_{4b-4c}$**, was optimised, and the structure with key bond lengths denoted is shown in Figure 6.20. The geometry around palladium in **4c** is a distorted T-shape, with the three angles adding up to 360.0º and is close to planar with an I-C2-Pd-P torsion angle of 179.4º. The structure is similar to that of **2a** in

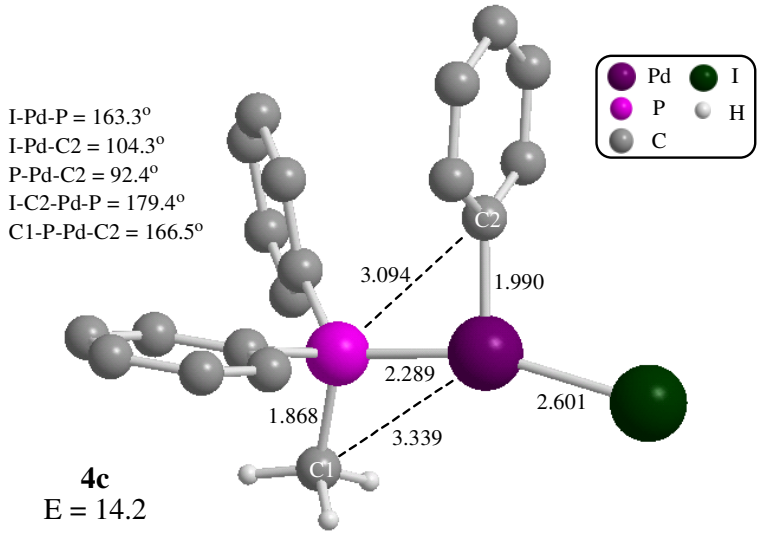

Figure 6.20: Optimised structure of the exchange product T$_{Ph}$-[PdI(Ph)(PMePh$_2$)], **4c**, in Mechanism **C**. Bond lengths and distances in Å, energy in kcal/mol.

Chapter 5, T_{Ph}-[PdCl(Ph)(PPh_3)], with the Pd-C2 bond only 0.002 Å longer in **4c** and the X-Pd-P angle only 1.3º smaller. If the structure of **4c** is compared to **4a**, it can be seen that the Pd-P bond is longer in **4c** (2.289 Å) than in **4a** (2.269 Å) now that the phosphine is $PMePh_2$ rather than PPh_3.

6.4.1 Overview of Mechanism C

Mechanism **C** for Me/Ph exchange proceeds along a similar pathway as was found for the analogous Ph/Ph exchange in Chapter 5. In particular, both pathways proceed via a zwitterion species. The energy profile for Mechanism **C** for Me/Ph exchange is shown in Figure 6.21. The overall energy highpoint in this mechanism is $\mathbf{TS_{4a\text{-}4b}}$ (E = 45.8 kcal/mol), with an activation barrier of 29.7 kcal/mol from **4a**. The barrier for the second transition state, $\mathbf{TS_{4b\text{-}4c}}$, is much smaller at only 5.5 kcal/mol above **4b**. Product **4c** is 1.9 kcal/mol more stable than 3-coordinate reactant **4a**.

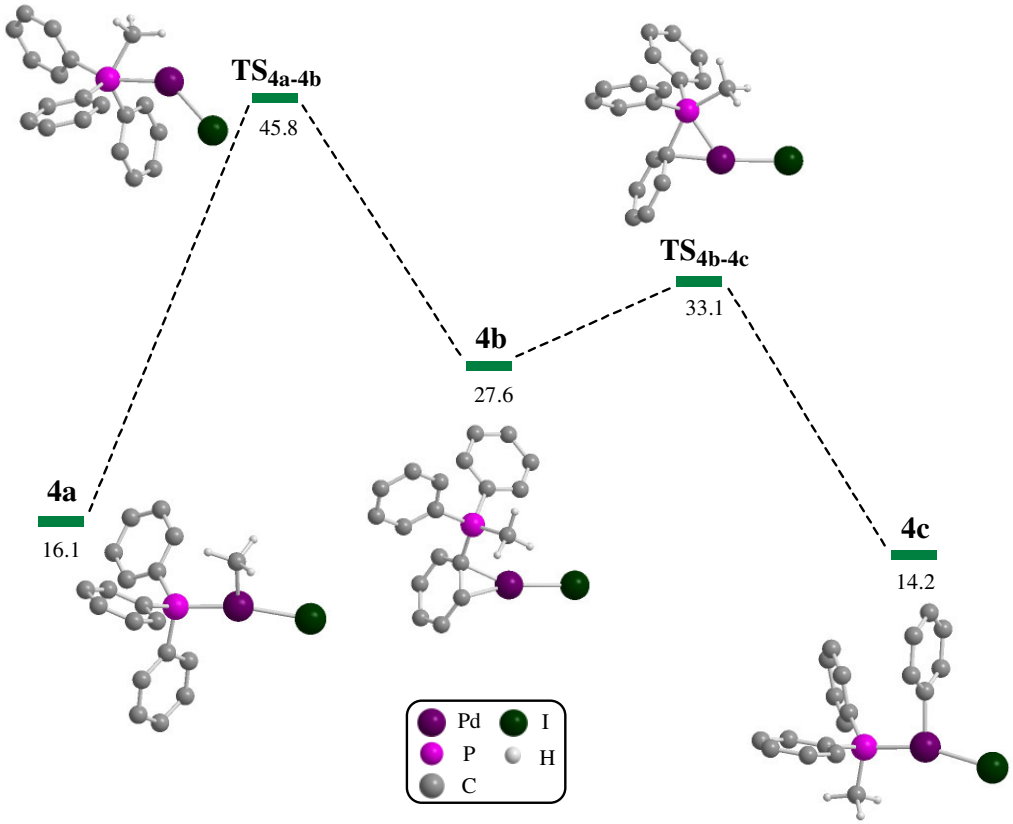

Figure 6.21: Reaction profile for Mechanism **C** in Me/Ph exchange. Energies in kcal/mol, relative to **3a**.

6.5 Mechanism D

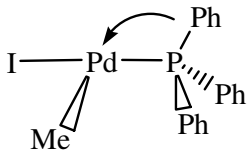

D Transfer of Ph from P to Pd
(3 coord)

The final mechanism to be investigated for Me/Ph exchange features an initial step of a phosphorus-bound phenyl group transferring onto the palladium in **4a**. The 4-coordinate intermediate formed in this process was located by reducing the Pd···C2 distance from 3.261 Å in **4a** down to 2.0 Å, then optimising the end geometry without constraints. The structure formed was confirmed to be a minimum point by running a frequency and the structure of **4d** (E = 61.6kcal/mol) is shown in Figure 6.22.

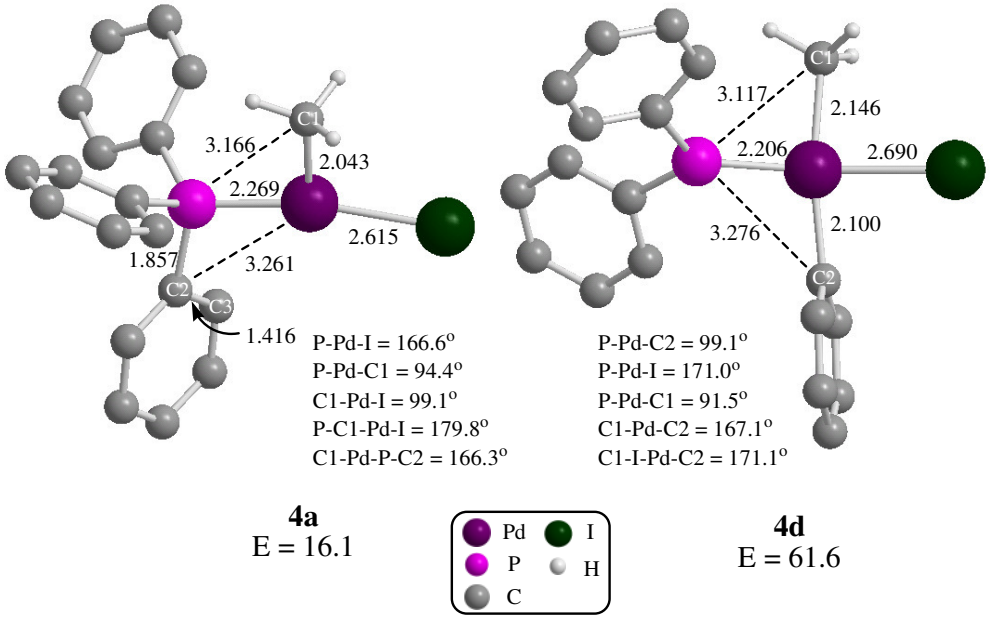

Figure 6.22: Optimised structure of reactant **4a** and intermediate **4d** in Mechanism **D**. Bond lengths and distances in Å, energies in kcal/mol.

The geometry around palladium in **4d** is distorted square planar with a P-Pd-I angle of 171.0º and a P-C1-Pd-I torsion angle of 171.2º. The P-C2 bond has broken and a Pd-C2 bond (2.100 Å) has formed. The Pd-C1 bond has lengthened by 0.103 Å from its value in **4a**, as it is now trans to phenyl rather than a vacant site. The Pd-P bond is 0.063 Å shorter now that the phosphine has become a phosphide, and this PPh_2 ligand appears to exert a stronger trans influence than PPh_3, as seen previously.

With the energy of **4d** being 61.6 kcal/mol less stable than **3a**, it would be expected that the activation energy for this process would be ever larger. This is considerably less accessible than the energy highpoint in Mechanism **C** ($\mathbf{TS_{4a\text{-}4b}}$ = 45.8 kcal/mol), making Mechanism **D** much less favourable. Therefore, the full profile for Mechanism **D** will not be discussed.

6.6 Comparing the four Me/Ph exchange mechanisms

Four mechanisms have been considered for Me/Ph exchange, as depicted in Figure 6.23, and the comparative energies for pathways **A**, **B** and **C** are shown in Figure 6.24. The energies for Mechanism **D** have not been included as they were both found to be too high to be competitive. The mid section of Mechanism **B** has been omitted to make the diagram clearer.

Figure 6.24 clearly shows that Mechanisms **B** and **C** are considerably less accessible than Mechanism **A**. The energy highpoint in Mechanism **A** is 30.5 kcal/mol, compared to 38.5 kcal/mol in **B** and 45.8 kcal/mol in **C**.

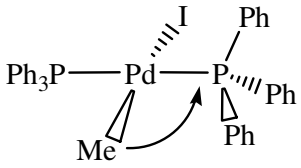

A Transfer of Me from Pd to P (4 coord)

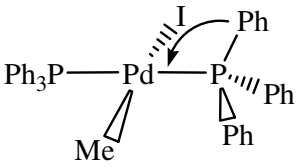

B Transfer of Ph from P to Pd (4 coord)

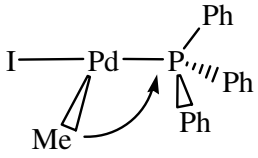

C Transfer of Me from Pd to P (3 coord)

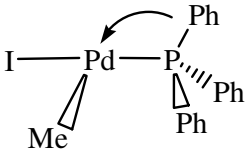

D Transfer of Ph from P to Pd (3 coord)

Figure 6.23: The initial transfer steps considered for alkyl/aryl exchange from *trans*-[PdI(Me)(PPh_3)$_2$] (**A** and **B**) and T_{Me}-[PdI(Me)(PPh_3)] (**C** and **D**).

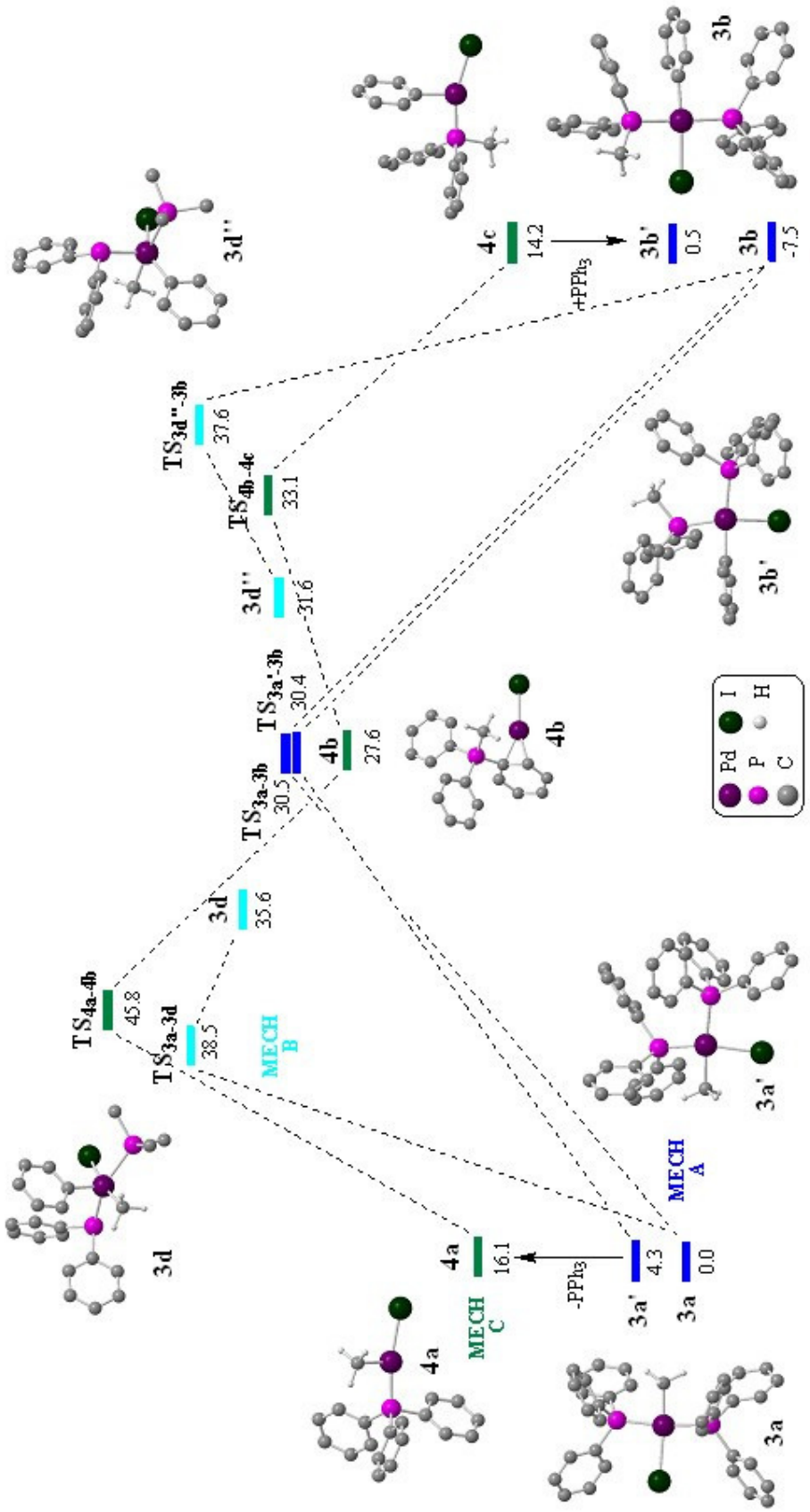

Figure 6.24: Energy profiles (kcal/mol) in Mechanisms **A**, **B** and **C** for Me/Ph exchange from *trans*-[PdI(Me)(PPh_3)$_2$] (**A**&**B**) and T_{Me}-[PdI(Me)(PPh_3)] (**C**).

However, these values are based on computed enthalpies, and as demonstrated in Chapter 5, it is important to compare the free energies for these mechanisms, especially since there is a dissociation in Mechanism **C**. The comparative free energy values for Mechanisms **A**, **B** and **C** are shown in Figure 6.25.

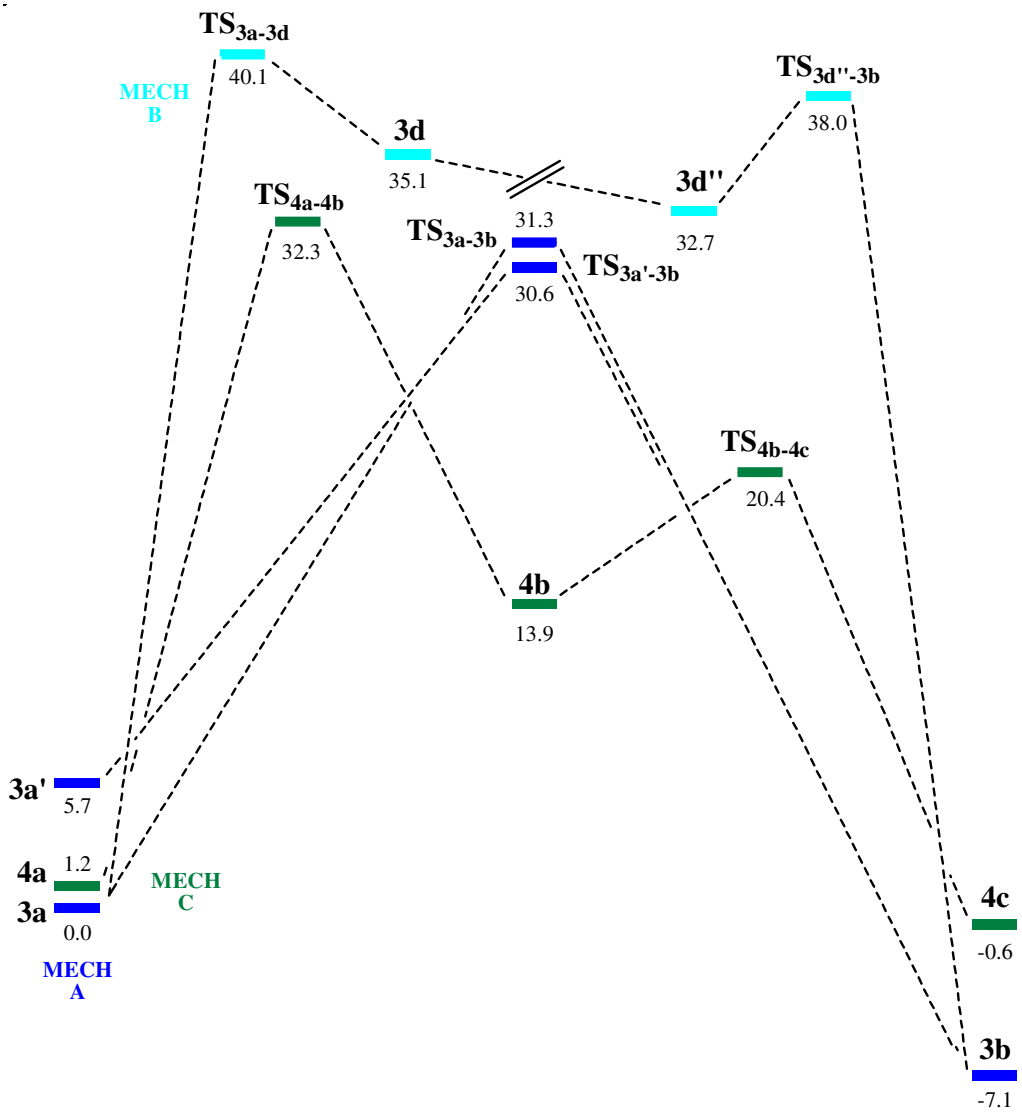

Figure 6.25: Comparative free energies (kcal/mol) in Mechanisms **A**, **B** and **C** for Me/Ph exchange from *trans*-[PdI(Me)(PPh_3)$_2$] (**A**&**B**) and T_{Me}-[PdI(Me)(PPh_3)] (**C**).

As would be expected, the structures in Mechanism **C** have a greater difference between their enthalpy and free energy values than those in Mechanism **A** and **B**, due to the dissociation of triphenylphosphine. Reactant **4a** is now only 1.2 kcal/mol less stable than **3a**, and is more stable than the 4-coordinate cis reactant, **3a'**. **TS_{3a-3d}** is now the

overall energy highpoint for the three mechanisms at 40.1 kcal/mol. The gap between the highpoints in Mechanisms **A** and **C** is now very small at 1.0 kcal/mol.

The final factor that should be taken into account is the effect of solvation on the relative energies of the mechanisms. As in Chapter 5, polarisable continuum model (PCM) calculations with a benzene solvent were performed, and then corrections for TΔS using the values from the ONIOM calculations were added, to give the free energy including solvation for each structure in the three reaction mechanisms. The results are shown in Figure 6.26.

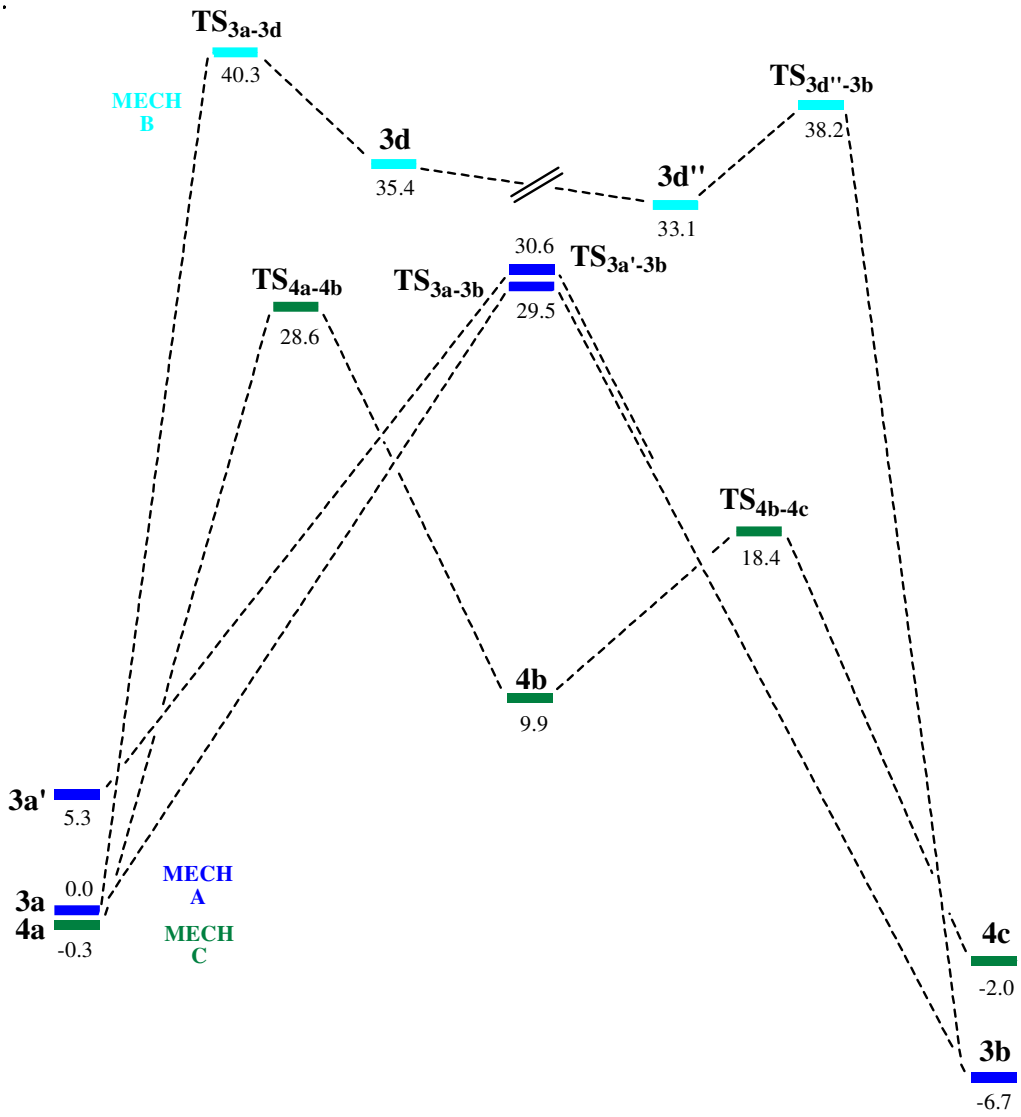

Figure 6.26: Comparative PCM (benzene) free energies (kcal/mol) in Mechanisms **A**, **B** and **C** for Me/Ph exchange from *trans*-[PdI(Me)(PPh_3)$_2$] (**A**&**B**) and T_{Me}-[PdI(Me)(PPh_3)] (**C**).

It can be seen that now 3-coordinate reactant **4a** is 0.3 kcal/mol more stable than 4-coordinate reactant **3a**. There has also been a change in the most accessible mechanism, as the energy of $\mathbf{TS_{4a\text{-}4b}}$ (28.6 kcal/mol, Mechanism **C**) has dropped below both $\mathbf{TS_{3a\text{-}3b}}$ (E = 29.5 kcal/mol) and $\mathbf{TS_{3a'\text{-}3b}}$ (E = 30.6 kcal/mol) (Mechanism **A**).

6.7 Conclusions and comparison with experimental results

To conclude, when the free energies for Mechanisms **A**, **B** and **C** (Figure 6.21) are compared, Mechanism **A** is the most accessible, with its highpoint, $\mathbf{TS_{3a'\text{-}3b}}$ at 30.6 kcal/mol, compared to $\mathbf{TS_{4a\text{-}4b}}$ at 32.3 kcal/mol in Mechanism **C** and $\mathbf{TS_{3a\text{-}3d}}$ at 40.1 kcal/mol in Mechanism **B**. However, when the effect of solvation is taken into account, Mechanism **C** is the most accessible, although the energy highpoints for Mechanisms **A** and **C** are close, with only 0.9 kcal/mol between them. Mechanism **B** is considerably less accessible than the other two mechanisms so is not considered to be competitive.

Mechanism **C** was found to be the most accessible pathway for Ph/Ph exchange in Chapter 5. However, in Ph/Ph exchange (X = I) there was a 5.9 kcal/mol difference in the relative highpoints of free energy with solvation (benzene) between Mechanisms **A** and **C**. In Me/Ph exchange the highpoints of the two mechanisms are much closer in energy, making them more competitive.

The experimental work published by Norton et *al.*[1] on Me/Ph scrambling in *trans*-$[PdI(Me)(PPh_3)_2]$ showed the exchange to be an irreversible process. The fact that exchange was found to be exothermic in the calculations performed, and that a Pd-Ph bond was found to be stronger than a Pd-Me bond supports this observation.

Norton *et al.*[1] found that adding excess triphenylphosphine to the reaction did not inhibit Me/Ph exchange. This finding was not consistent with the results from this chapter, which indicate that a mechanism requiring the pre-dissociation of triphenylphosphine is the most accessible pathway. However, the difference in accessibility between Mechanisms **A** and **C** is very small.

6.8 CH_2CF_3/Ph exchange

Norton *et al*. looked at R/Ph exchange in a range of different [PdI(R)(PPh_3)$_2$] complexes.[1] They found that when R = CF_3CH_2, no exchange occurs in benzene at 50ºC over a 24 hour period. It appears that adding an electron-withdrawing group to the palladium-bound alkyl ligand completely inhibits exchange.

To gain insight into why exchange occurs when R = Me but not when R = CH_2CF_3, the mechanisms for 4- and 3-coordinate exchange when R = CH_2CF_3 were investigated. Since Mechanisms **A** and **C** were found to be the most accessible for both Ph/Ph and Me/Ph exchange, only these two mechanisms were modelled with R = CH_2CF_3 (see Figure 6.27).

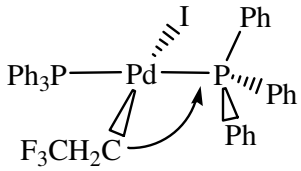

A Transfer of Me from Pd to P (4 coord)

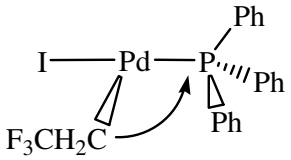

C Transfer of Me from Pd to P (3 coord)

Figure 6.27: Initial transfer steps in Mechanisms **A** and **C** for CH_2CF_3/Ph exchange from *trans*-[PdI(CF_3CH_2)(PPh_3)$_2$] (**A**) and $T_{CH_2CF_3}$-[PdI(CF_3CH_2)(PPh_3)]

6.9 Mechanism A for CH_2CF_3/Ph exchange

The 4-coordinate starting species, *trans*-[PdI(CF_3CH_2)(PPh_3)$_2$], was formed by substituting a methyl hydrogen for CF_3 in structure **3a**, then optimising. The optimised geometry of reactant **5a** (set to 0.0 kcal/mol) is shown in Figure 6.28. The energies for all of the structures in CH_2CF_3/Ph exchange will be reported relative to **5a**.

The structure of **5a** is similar to that of **3a**, with a distorted square planar geometry around palladium. The Pd-I bonds (**3a** = 2.746 Å, **5a** = 2.745 Å) and Pd-C1 bonds (**3a** = 2.109 Å, **5a** = 2.101 Å) are of a similar length in both reactant structures. However, the Pd-P bonds are longer in **5a** (Pd-P1= 2.363 Å, Pd-P2 = 2.375 Å) than in **3a** (Pd-P1= 2.354 Å, Pd-P2 = 2.359 Å). This may be a steric effect as {CH_2CF_3} is bulkier than methyl, which is also suggested by the increase in the P2-Pd-C1 angle from 86.6º in **3a** to 93.4º in **5a**.

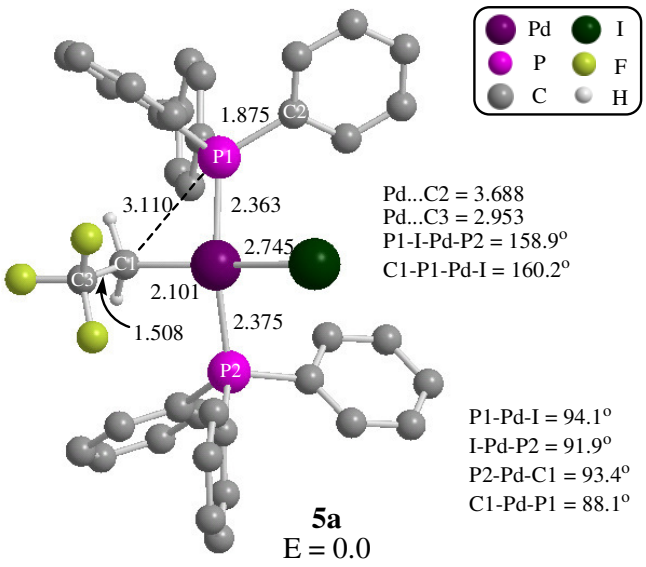

Figure 6.28: Reactant **5a**, *trans*-[PdI(CF_3CH_2)(PPh_3)$_2$] from Mechanism **A** of CH_2CF_3/Ph exchange. Bond lengths in Å, energy in kcal/mol.

The reaction profile was explored in the standard way, by decreasing the P1···C1 distance in a stepwise scan, and running a transition state calculation at the energy highpoint. This led to **$TS_{5a\text{-}5b'}$** (E = 42.8 kcal/mol), which is shown in Figure 6.29.

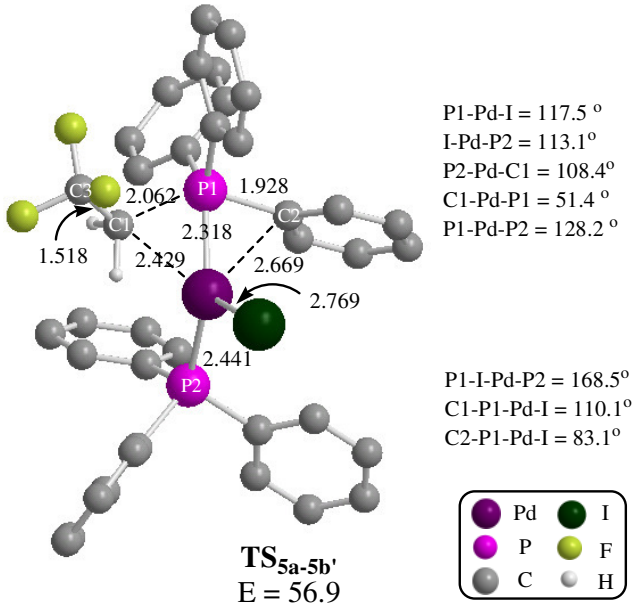

Figure 6.29: $TS_{5a\text{-}5b'}$ from Mechanism **A** of CH_2CF_3/Ph exchange. Bond lengths in Å, energy in kcal/mol.

The structure of $\mathbf{TS_{5a\text{-}5b'}}$ does not differ much from that of $\mathbf{TS_{3a\text{-}3b}}$, the analogous transition state in Me/Ph exchange. The geometry of $\mathbf{TS_{5a\text{-}5b'}}$ could be considered to be later than $\mathbf{TS_{3a\text{-}3b}}$, shown by a shorter P1···C1 distance ($\mathbf{TS_{3a\text{-}3b}}$ = 2.115 Å, $\mathbf{TS_{5a\text{-}5b'}}$ = 2.062 Å) and a shorter Pd···C2 distance ($\mathbf{TS_{3a\text{-}3b}}$ = 2.682 Å, $\mathbf{TS_{5a\text{-}5b'}}$ = 2.669 Å). The activation barrier for this step is considerably higher for CH_2CF_3/Ph exchange (E_a = 42.8 kcal/mol) than in Me/Ph exchange (E_a= 30.5 kcal/mol). A possible reason for this lies in the comparative Pd-C bonding interaction (BI) strengths. The strength of the Pd-C1 bond in **5a** was calculated to be 66.9 kcal/mol, while the same bond in **3a** was weaker, at 59.2 kcal/mol. The energy required to break the stronger Pd-C1 bond in **5a** would lead to a higher activation energy.

PIRC calculations showed that $\mathbf{TS_{5a\text{-}5b'}}$ does not lead to a trans exchange product, as observed in Me/Ph exchange. Instead, the cis exchange product, **5b'** (E = 10.0 kcal/mol), is formed. The structure of $\mathbf{TS_{5a\text{-}5b'}}$ was studied in detail, and compared to $\mathbf{TS_{3a\text{-}3b}}$, but it remains unclear why $\mathbf{TS_{5a\text{-}5b'}}$ leads to a cis product while $\mathbf{TS_{3a\text{-}3b}}$ leads to a trans product. The structure of **5b'** with key bond lengths and distances is shown in Figure 6.30.

The geometry around palladium in **5b'** is rather distorted from square planar. The P1-Pd-P2 angle is large at 107.3º, presumably due to steric interactions between the two phosphine groups. The complex is not planar, with the $P(CH_2CF_3)Ph_2$ ligand lying out of the metal coordination plane (P1-P2-Pd-I = 155.3º).

To enable direct comparison with Mechanism **A** in Me/Ph exchange, the structure of the trans exchange product, **5b** (E = 0.5 kcal/mol) was constructed by substituting the methyl group for CH_2CF_3 in **3b**, and optimising. The structure is also shown in Figure 6.30. With the two bulky phosphine groups lying trans to each other, the geometry around palladium is less distorted from square planar than in **5b'**. All four angles around palladium are within 2º of 90º, and $PCH_2CF_3Ph_2$ lies in the metal coordination plane (P1-I-Pd-P2 = 178.8º). The structure of **5b** is very similar to that of **3b**.

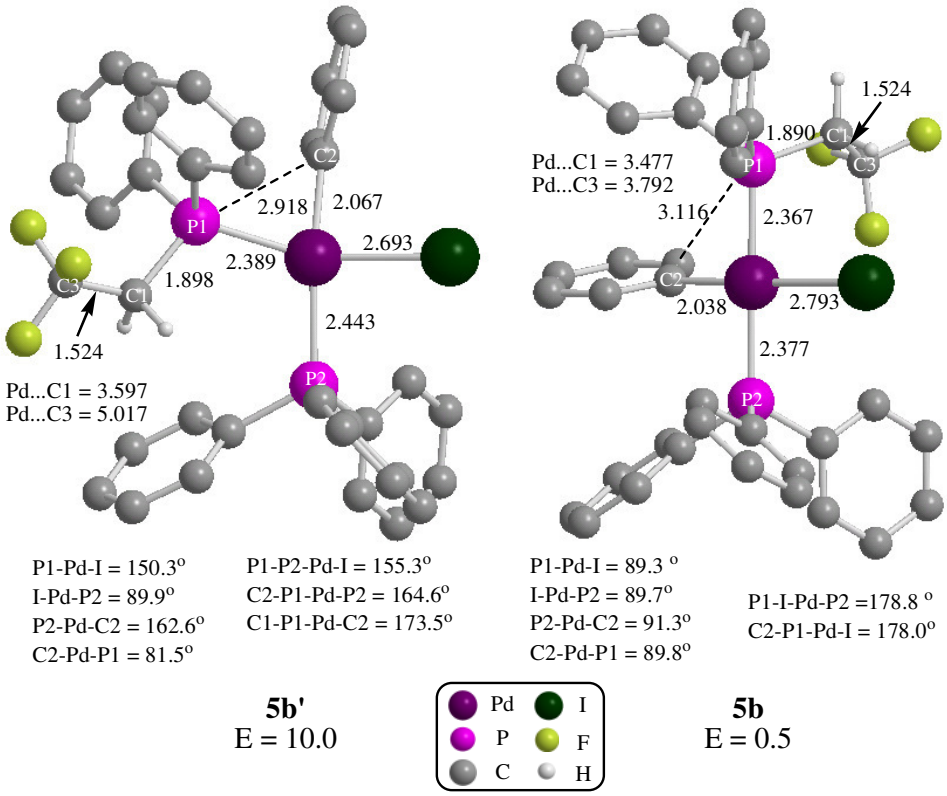

Figure 6.30: 5b and 5b' from Mechanism **A** of CH_2CF_3/Ph exchange. Bond lengths in Å, energy in kcal/mol.

The energy profiles for Mechanism **A** in CH_2CF_3/Ph exchange and Me/Ph exchange can both be seen in Figure 6.31. The energies shown are relative to the respective reactant energies, which are set to zero. As discussed previously, the activation barrier for CH_2CF_3/Ph exchange (E_a = 42.8 kcal/mol) is much higher than for Me/Ph exchange (E_a = 30.5kcal/mol), which can be attributed to the stronger Pd-C bond in **5a** compared to **3a**. The bond interaction (BI) energies for the four bonds broken and formed in exchange were calculated as described in Chapter 3 and are shown in Table 6.4.

Apart from the Pd-C (R) bond that has broken, the other bonds are similar in strength whether R = Me or CH_2CF_3. The overall energy released from bond formation and breaking in CH_2CF_3/Ph exchange is 0.7 kcal/mol, which corresponds to Mechanism **A** being almost thermoneutral ($\Delta E_{(\mathbf{5b'\text{-}5a})}$ = 0.5 kcal/mol). Thus, Mechanism **A** is both thermodynamically and kinetically less accessible when R = CH_2CF_3 than when R = Me.

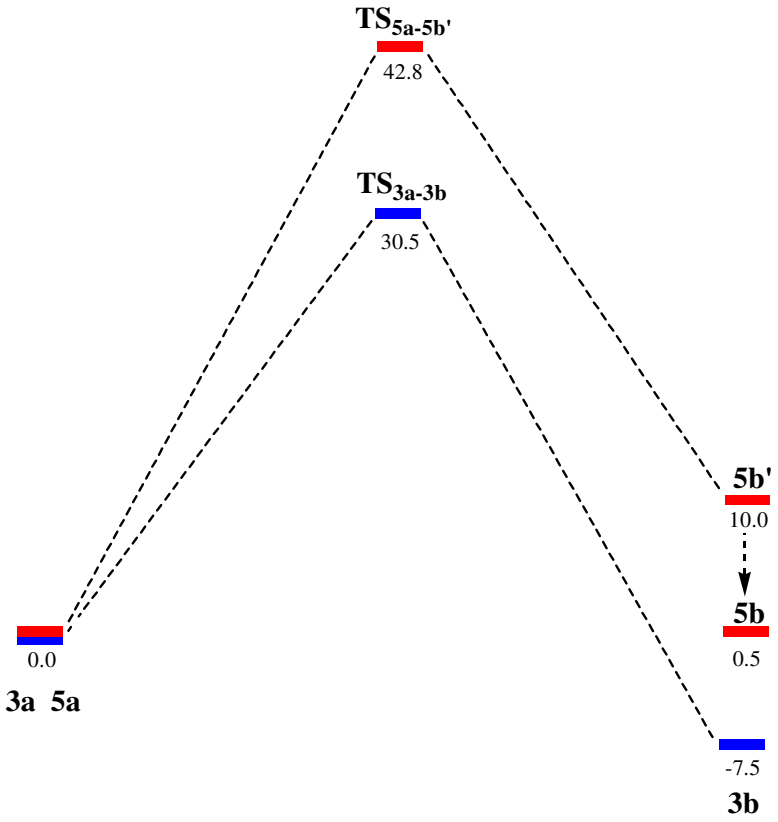

Figure 6.31: Energies for Mechanism **A** in Me/Ph exchange (blue) and CH_2CF_3/Ph exchange (red).

Bond	BI energy (R = Me)	BI energy (R = CH_2CF_3)
Pd-C (R)	59.2	66.9
P-C (Ph)	79.1	79.9
Pd-C (Ph)	65.2	64.9
P-C (R)	81.4	82.7
Total ΔE	-8.3	-0.7

Table 6.4: Comparison of BI energies for the bonds broken and formed during R/Ph exchange (R = Me or CH_2CF_3). Energies in kcal/mol.

6.10 Mechanism C for CH_2CF_3/Ph exchange

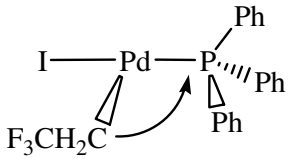

C Transfer of Me from Pd to P
(3 coord)

The 3-coordinate starting species for Mechanism **C** was formed by removing a triphenylphosphine ligand from **5a**, and allowing the remaining complex to optimise. As seen in previous examples, isomerisation occurred to result in the CF_3CH_2 ligand lying trans to the vacant site. The structure of **6a**, $T_{CH_2CF_3}$-[PdI(CF_3CH_2)(PPh_3)], (E = 18.9 kcal/mol) is shown in Figure 6.32. The geometry around palladium is T-shaped and planar, and overall the structure is very similar to that of **4a**.

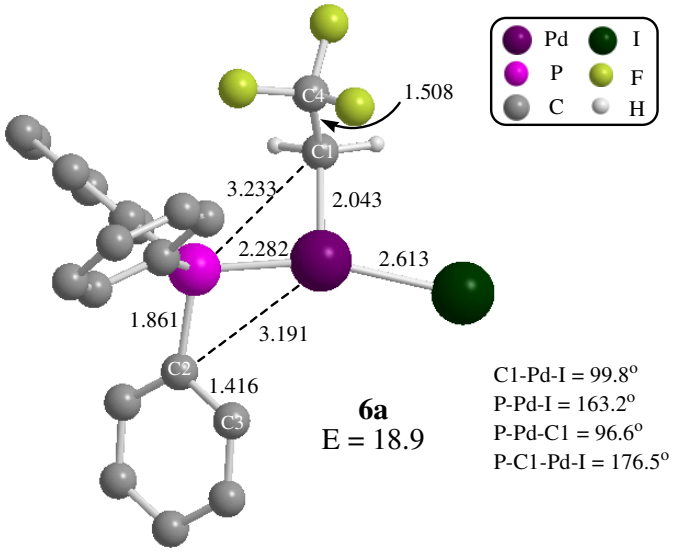

Figure 6.32: Reactant **6a**, $T_{CH_2CF_3}$-[PdI(CF_3CH_2)(PPh_3)], from Mechanism **A** of CF_3CH_2/Ph exchange. Bond lengths in Å, energy in kcal/mol, relative to **5a**.

A scan to reduce the P···C1 distance from its value of 3.233 Å in **6a** was performed, and transition state $\mathbf{TS_{6a\text{-}6b}}$ (E = 56.9 kcal/mol) was located from the energy highpoint. PIRC calculations showed that this transition state connects to a zwitterion species, **6b** (E = 38.5 kcal/mol), and both structures are shown in Figure 2.33.

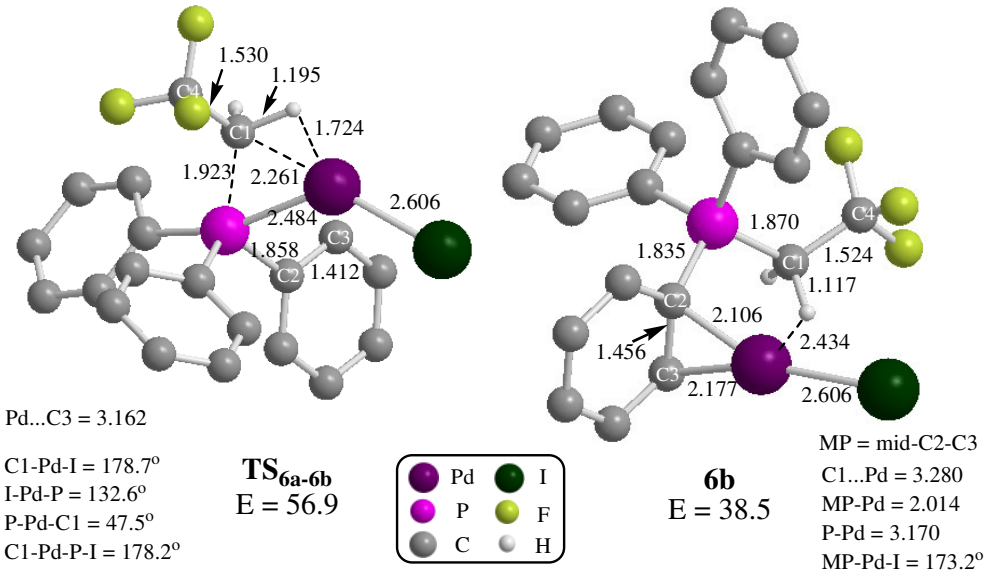

Figure 6.33: The structures of $\mathbf{TS_{6a\text{-}6b}}$ and **6b** from Mechanism **C** of CH_2CF_3/Ph exchange. Bond lengths in Å, energies in kcal/mol.

The structure of $\mathbf{TS_{6a\text{-}6b}}$ is very similar to that of $\mathbf{TS_{4a\text{-}4b}}$, the analogous species in Me/Ph exchange. The main difference between the two structures is that the alkyl group is later in its transfer to palladium in $\mathbf{TS_{6a\text{-}6b}}$, illustrated by a longer P···C1 distance ($\mathbf{TS_{6a\text{-}6b}}$ = 1.923 Å, $\mathbf{TS_{4a\text{-}4b}}$ = 1.887 Å) and a shorter C1···Pd distance ($\mathbf{TS_{6a\text{-}6b}}$ = 2.261 Å, $\mathbf{TS_{4a\text{-}4b}}$ = 2.335 Å). The problems encountered relating to a very flat potential energy surface in this region for Me/Ph exchange were not an issue in this case. The relative energy of $\mathbf{TS_{6a\text{-}6b}}$ is more than 10 kcal/mol less accessible than $\mathbf{TS_{4a\text{-}4b}}$ (E = 45.8 kcal/mol).

PIRC calculations confirmed that $\mathbf{TS_{6a\text{-}6b}}$ leads to zwitterion **6b**, shown in Figure 6.33. The structure of **6b** is similar to the analogous species from the Me/Ph exchange pathway, **4b**. The geometry around palladium is close to linear (MP-Pd-I = 173.2º) and the Pd-I bond is 0.013 Å longer than in **4b**. The C2-C3 bonds are identical in length, at 1.456 Å, and the Pd···MP distance is just 0.005 Å longer in **6b**. However, the comparative energies are quite different, with **6b** (38.5 kcal/mol) being much less accessible than **4b** (27.6 kcal/mol).

As in Mechanism **C** for Me/Ph exchange, it was necessary to construct the exchange product and perform a scan reducing the P···C2(phenyl) distance to locate $\mathbf{TS_{6b\text{-}6c}}$. The structure of the transition state located, $\mathbf{TS_{6b\text{-}6c}}$ (E = 42.7 kcal/mol), is shown in Figure

6.34 along with exchange product **6b** (E = 20.2 kcal/mol). The structure of $\mathbf{TS_{6b\text{-}6c}}$ shows a lengthening of Pd···C3 from its value of 2.177 Å in **6b**, as the Pd···Ph η^2-interaction weakens. A bond has formed between palladium and phosphorus (2.341 Å) and between palladium and C2 (2.097 Å). Although the structure of $\mathbf{TS_{6b\text{-}6c}}$ is similar to that of $\mathbf{TS_{4b\text{-}4c}}$, it is 9.6 kcal/mol less accessible.

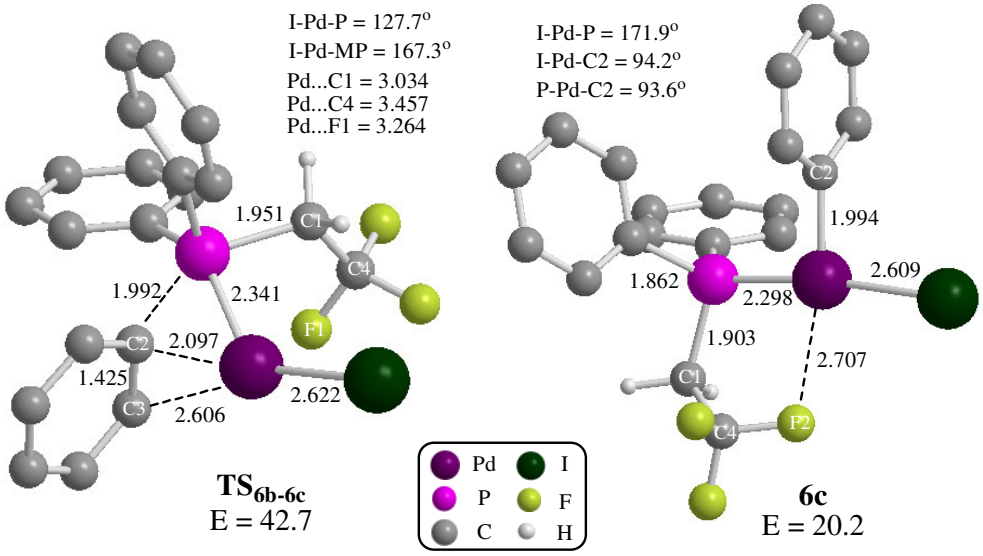

Figure 6.34: The structures of $\mathbf{TS_{6b\text{-}6c}}$ and **6c** from Mechanism **C** of CH_2CF_3/Ph exchange. Bond lengths in Å, energies in kcal/mol.

Exchange product **6b** exhibits a distorted T-shaped planar geometry, with iodide trans to phosphine. The Pd-P (2.298 Å) and Pd-C2 (1.994 Å) bonds have fully formed, and the Pd-I (2.609 Å) bond has lengthened slightly. The geometry and bond lengths in **6c** are very similar to those in **4c**, however **6c** is 6 kcal/mol less accessible.

The energy profiles for Me/Ph and CF_3CH_2/Me exchange via Mechanism **C** are shown in Figure 6.35. Despite reactant **4a** being only 2.8 kcal/mol comparatively higher in energy than **6a**, as the profiles proceed they become further apart energetically. The barrier for formation of the zwitterion intermediates **4b** and **6c** are 29.7 and 38.0 kcal/mol respectively. In both profiles the first transition state is the energy highpoint of the exchange process. The barriers for the second step are of similar magnitude, at 5.5 kcal/mol for Me/Ph exchange and 4.2 kcal/mol for CF_3CH_2/Me exchange, however the transition state is 9.6 kcal/mol less accessible in the latter profile.

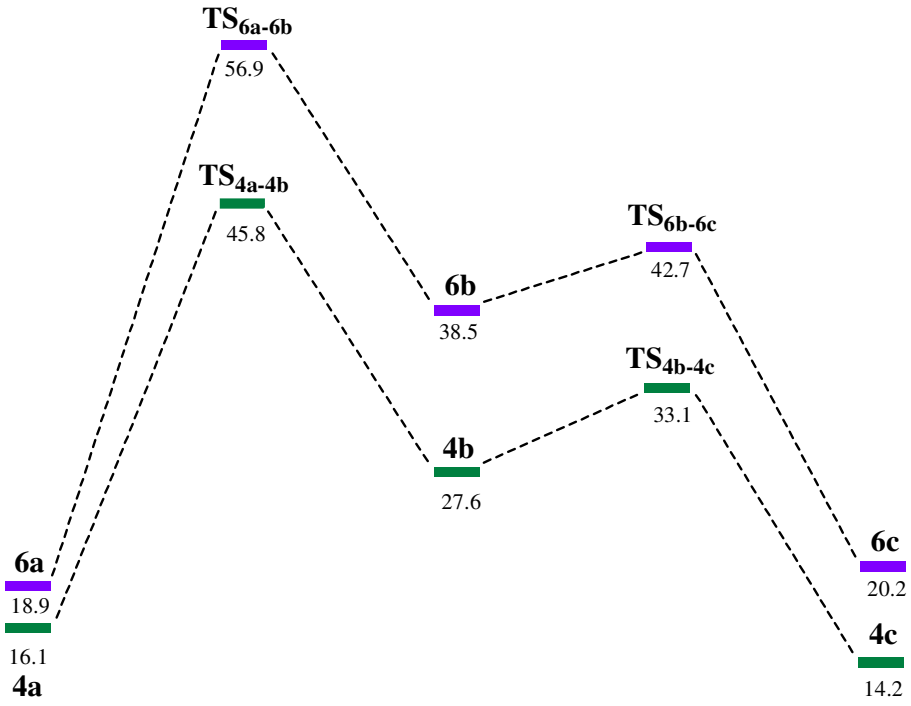

Figure 6.35: Energies (kcal/mol) for Mechanism **C** in Me/Ph exchange (green) and CH_2CF_3/Ph exchange (purple).

6.11 Comparison of Me/Ph and CH_2CF_3/Ph exchange

The values of enthalpy, free energy and free energy with solvation (PCM in benzene) for Mechanisms **A** and **C** are shown in Table 6.5. As seen in Chapter 5, the values with a correction for free energy and solvation are close to the enthalpy values in Mechanism **A**. However, all the minima and transition states in Mechanism **C** are stabilised compared to their enthalpy, with the free energy and solvation corrections applied.

The ΔG (PCM) values for CF_3CH_2/Ph exchange show that Mechanism **C** (highpoint = 40.4 kcal/mol) is more accessible than Mechanism **A** (highpoint = 42.3 kcal/mol), but the difference is small. This is consistent with the findings for Me/Ph exchange.

Comparison of the data for Me/Ph exchange and CF_3CH_2/Ph exchange shows that in Mechanism **A** the highpoint for CF_3CH_2/Ph exchange is 11.9 kcal/mol higher, and in Mechanism **C** the highpoint for CF_3CH_2/Ph exchange is 12.1 kcal/mol higher than for Me/Ph exchange. This difference in accessibility supports the experimental observation that no CF_3CH_2/Ph exchange occurs in benzene at 50ºC over a 24 hour period,[1] whereas Me/Ph exchange is observed under the same conditions.

Mechanism A		ΔH	ΔG	ΔG (PCM)
Me/Ph	**3a**	0	0	0
	TS_{3a-3b}	30.5	31.3	30.4
	3b	-7.5	-7.1	-6.7
CF_3CH_2/Ph	**5a**	0	0	0
	TS_{5a-5b}	42.8	43.1	42.3
	5b'	10	10.2	10.1
	5b	0.5	0.7	1.2
Mechanism C				
Me/Ph	**4a**	16.1	1.2	-0.3
	TS_{4a-4b}	45.1	31.4	28.3
	4b	27.6	13.9	9.9
	TS_{4b-4c}	33.1	20.4	18.4
	4c	14.2	-0.6	-2.0
CF_3CH_2/Ph	**6a**	18.9	2.9	1.8
	TS_{6a-6b}	56.9	43.2	40.4
	6b	38.5	24	20.2
	TS_{6b-6c}	42.7	28.8	26.9
	6c	20.2	4.2	2.6

Table 6.5: Enthalpy (ΔH), free energy (ΔG) and free energy with solvation (ΔG(PCM)) for Me/Ph and CH_2CF_3/Ph exchange via Mechanisms **A** and **C**. Energies in kcal/mol.

6.15 References

[1] Morita, D. K.; Stille, J. K.; Norton, J. R., *J. Am. Chem. Soc.,* **117**, 8576, (1995)

[2] a) Kong, K-C.; Cheng, C.-H., *J. Am. Chem. Soc.*, **113**, 6313, (1991) b) Goodson, F. E.; Wallow, T. I.; Novak, B. M., *J. Am. Chem. Soc.*, **119**, 12441, (1997) c) Grushin, V. V. *Organometallics*, **19**, 1888, (2000)

[3] Otto, S., *Acta Crystallogr., Sect. E: Struct. Rep. Online*, **57**, M75, (2001)

[4] Ortiz, J. V.; Havlas, Z.; Hoffmann, R., *Helv. Chim. Acta,* **67**, 1, (1984)

[5] http://www.ccdc.cam.ac.uk/ ; Allen, F. H., *Acta Cryst.*, **B58**, 380, (2002)

[6] Qin, Z.; Jennings, M. C.; Puddephatt, R. J., *Inorg. Chem.*, **40**, 6220, (2001)

Chapter 7: Computational background

7.1 Introduction

This chapter contains an overview of the main concepts in density functional theory (DFT), the main computational method utilised in this thesis. The discussion will begin with some important principles from quantum mechanics and continue with an overview of the Hartree-Fock approximation. This is followed by the key points in the development of DFT and some practical considerations when performing calculations. Finally, the results of benchmark calculations to compare different methodologies, functionals and basis sets are presented.

7.2 Basic quantum mechanics

When seeking to use quantum mechanics to model the type of chemical system discussed in this thesis, the aim is to solve the time-independent Schrödinger equation,[1] the general form of which is:

$$H\Psi = E\Psi \qquad (7\text{-}1)$$

where H is the Hamiltonian operator, which acts on the wave function, Ψ, to produce an eigenvalue, E, the energy of the system.

The Hamiltonian operator is constructed from the sum of potential and kinetic energy operators.

$$H = -\frac{\hbar^2}{2m}\nabla^2 + V \qquad (7\text{-}2)$$

Kinetic energy — Potential energy

The potential energy part, represented by V, describes the field resulting from the repulsive force between electrons or nuclei and the electron-nuclear attraction. The kinetic energy is composed of contributions from all the nuclei and electrons in a system with particles of mass, m. The Laplacian operator, ∇^2, is defined in Equation 7-3, where x, y and z are Cartesian coordinates.

$$\nabla^2 = \frac{\partial^2}{\partial x^2} + \frac{\partial^2}{\partial y^2} + \frac{\partial^2}{\partial z^2} \qquad (7\text{-}3)$$

The total Hamiltonian operator can be expressed in terms of the kinetic (T) and potential (V) energies of the nuclei (N) and electrons (e), as shown in (7-4).

$$H_{tot} = T_N + T_e + V_{Ne} + V_{ee} + V_{NN} \tag{7-4}$$

There are several approximations which can be made to simplify the task of solving the Schrödinger equation, which are outlined in the following sections.

7.3 The Born-Oppenheimer approximation

The considerable difference in mass between nuclei and electrons is exploited in the Born-Oppenheimer approximation,[2] resulting in the simplification of the Schrödinger equation. The smallest possible nucleus, a proton, is more than 1800 times heavier than an electron. This difference means that nuclei move extremely slowly compared to electrons, and consequently electrons can adjust almost instantaneously to a change in nuclear position. The nuclei can therefore be considered to be fixed points with respect to the electrons, thus T_N in equation (7-4) becomes zero and V_{NN} is a constant. Now the Schrödinger equation can be approached using an electronic Hamiltonian for each fixed nuclear geometry.

$$H_e = T_e + V_{Ne} + V_{ee} \tag{7-5}$$

7.4 The variational principle

The variational principle is important to many quantum mechanical applications, as it provides a way of homing in on the ground state wave function of a system. It states that any energy calculated from a trial wave function will be higher than the actual ground state energy, E_0.

$$E_0 \leq \min_{\Psi} E[\Psi] \tag{7-6}$$

Thus, it is possible to assess the quality of trial wave functions, as the lower the energy, the better the trial wave function.

7.5 The Slater determinant

Only certain mathematical functions are suitable as wave functions. They must obey certain constraints, for instance Ψ must be finite, single-valued and continuous. A suitable function must also obey Pauli's exclusion principle and forbid two electrons from occupying the same state.

In 1929 Slater realised that a type of matrix called a determinant was a convenient way of expressing wave functions.[3] Equation (7-7) shows a Slater determinant, Φ_{SD}, of N electrons.

$$\Psi_0 \approx \Phi_{SD} = \frac{1}{\sqrt{N!}} \begin{vmatrix} \chi_1(x_1) & \chi_2(x_1) & \cdots & \chi_N(x_1) \\ \chi_1(x_2) & \chi_1(x_1) & \cdots & \cdots \\ \cdots & \cdots & \cdots & \cdots \\ \chi_1(x_N) & \cdots & \cdots & \chi_N(x_N) \end{vmatrix} \qquad (7\text{-}7)$$

$1/\sqrt{N!}$ is used to normalise the wave function and each electron is represented by a one-particle wave function known as a spin orbital, $\chi_N(x_N)$, encompassing an electron's position (x_N) and spin angular momentum (α or β). A Slater determinant is antisymmetric with respect to the interchange of any two electrons. This means that swapping two rows will result in a change of sign in Φ_{SD}. If two columns are the same, corresponding to two electrons occupying the same spin orbital, Φ_{SD} goes to zero, thus obeying the Pauli exclusion principle.

7.6 The Hartree-Fock approximation

The Hartree-Fock (HF) approximation[4] is a common method used to attempt to solve the electronic Schrödinger equation resulting from using the Born-Oppenheimer approximation on the time-independent Schrödinger equation.

The approximation makes the assumption that the wave function of a chemical system can be described by a single Slater determinant composed of spin orbitals, each representing one electron. Each electron feels the field of the nuclei and an average repulsion from the other electrons present.

Hartree-Fock theory adopts a self-consistent field (SCF) approach which works by starting with an initial set of guess spin orbitals and improves them iteratively. The

guess orbitals are solved using the Fock equation (7-8) and then compared to the input orbitals. If the new orbitals are lower in energy, these then replace the guess orbitals. This cycle continues, lowering the total energy until the new energy does not vary by more than a certain threshold when compared to the previous energy.

The Fock operator, f_i, can be defined as,

$$f_i = -\frac{1}{2}\nabla_i^2 - \sum_A \frac{Z_A}{r_{iA}} + V_i^{HF} \qquad (7\text{-}8)$$

where the first term is the kinetic energy, the second term is the attractive potential energy between electron *i* and the nucleus and the third term, V_i^{HF}, is the Hartree-Fock potential. V_i^{HF} is one of the key approximations in the theorem, representing the average repulsion felt by an electron due to all the other electrons in the system. It consists of two parts, the Coulomb operator, *J*, and the exchange operator, *K*.

$$V^{HF}(x_1) = \sum_j^N \left(J_j(x_1) - K_j(x_1)\right) \qquad (7\text{-}9)$$

The Coulomb operator, $J_j(x_1)$, represents the potential experienced by an electron due to another electron in χ_j. It is defined in equation (7-10) as,

$$J_j(x_1) = \int dx_2 \left|\chi_j(x_2)\right|^2 \frac{1}{r_{12}} \qquad (7\text{-}10)$$

where an average potential is calculated by integrating the r_{12}^{-1} interaction over all space and possible positions of another electron, weighted by the probability that the other electron is in position x_2.

The second term, the exchange operator, $K_j(x_1)$, does not have a classical interpretation. It needs to be defined by its effect when operating on a spin orbital, as in Equation 7-11.

$$K_j(x_1)\chi_i(x_1) = \left[\int dx_2 \chi_j^*(x_2)\frac{1}{r_{12}}\chi_i(x_2)\right]\chi_j(x_1) \qquad (7\text{-}11)$$

As in Equation 7-10, the value is inversely proportional to the distance between two electrons (r_{12}), and is integrated over all possible positions of the second electron in space. However, Equation 7-12 also features an exchange of the two electrons in the two spin orbitals, χ_i and χ_j. $K_j(x_1)$ is considered to be non-local as it depends on the value of χ_i over all space, not just at position x_1. The exchange operator also serves a useful purpose by removing the inaccuracy of 'self-interaction' in a one-electron system, which is a problem created by the Coulomb operator. Basically, when $i=j$ is input into $J_j(x_1)$, the result is non-zero, despite the fact that there is no electron-electron interaction possible in a one-electron system. $K_j(x_1)$ removes this problem by producing an identical value to $J_j(x_1)$ when $i=j$, thus when $K_j(x_1)$ is subtracted in Equation 7-9, the result is zero.

7.7 Electron correlation

Electron correlation is essentially the interaction of electrons within a system. This can be divided into dynamic correlation, where the electron feels repulsion from each of the other electrons in the system, and static correlation, where a single determinant is not flexible enough for the system in question.

The major weakness of the Hartree-Fock approximation is its failure to represent electron correlation. In Hartree-Fock each electron experiences an average field contribution from the other electrons present in the chemical system. This does not accurately model a molecule because in reality two electrons would have a direct Coulomb repulsion between them and electrons do not move independently of each other. The correlation energy is negative due to the overestimation of dynamic electron-electron repulsion in Hartree-Fock. The electron correlation energy, E_{corr}, can be defined as the error in energy between the Hartree-Fock energy and the true ground state energy, E_0.[5]

$$E_{corr} = E_0 - E_{HF} \qquad (7\text{-}12)$$

The approximation also fails to correctly model the behaviour of infinitely separated particles, as a single Slater determinant is not a sufficient model in these types of cases. This failure is seen when considering an H_2 molecule.[6] The Hartree-Fock approximation models H_2 well at the equilibrium bond length, but fails as $r_{HH} \rightarrow \infty$. This static correlation energy gets larger at greater distances of r_{HH}, and there is a

probability of both electrons being on the same nucleus factored into the calculation. This is unrealistic as H_2 dissociates to give two neutral atoms, and results in an overestimation of the interaction energy.

7.8 Density functional theory

Density functional theory (DFT) is centred on the experimentally evincible property of electron density, ρ. In DFT, ρ is used to calculate the ground state energy of a system, moving the primary focus away from the wave function. Electron density represents the probability of finding an electron at a point in space, and the density tends to zero as the distance from the nucleus tends to infinity. A major strength of DFT is that electron density only has 3 spatial variables regardless of the size of the system. This is much simpler than wave function approaches which have 3N variables for an N-electron system, making calculations on large systems extremely complex.

In the 1920s Thomas[7] and Fermi[8] were the first to use electron density rather than wave functions to investigate chemical systems. However, it was not until 1964 that a paper by Hohenberg and Kohn[9] laid the foundations on which modern DFT is built.

The first Hohenberg-Kohn theorem legitimises the use of electron density to find the ground state energy, and thus all other properties, of a system. The ground state energy of a system can now be expressed purely as a functional of ρ.

$$E_0[\rho] = T[\rho_0] + V_{Ne}[\rho_0] + V_{ee}[\rho_0] \qquad (7\text{-}13)$$

This equation can then be separated into two parts, defined by whether each term is system dependent. This gives rise to a system independent term, the Hohenberg-Kohn functional, $F_{HK}[\rho_0]$, as defined in Equation 7-15.

$$E_0[\rho_0] = \int \rho_0(r) V_{Ne} dr + F_{HK}[\rho_0] \qquad (7\text{-}14)$$

$$F_{HK}[\rho_0] = T[\rho_0] + V_{ee}[\rho_0] \qquad (7\text{-}15)$$

The first term in Equation 7-14 is system dependent, meaning that it depends on properties unique to the molecule or system studied. Conversely, $F_{HK}[\rho_0]$ is independent of the system being investigated, and is therefore universal. The electron-

electron interaction ($V_{ee}[\rho_0]$) can be divided into a classical Coulomb repulsion ($J[\rho]$) and a non-classical part ($E_{ncl}[\rho]$), as shown in Equation 7-16.

$$V_{ee}[\rho_0] = \frac{1}{2}\iint \frac{\rho(r_1)\rho(r_2)}{r_{12}} dr_1 dr_2 + E_{ncl}[\rho] = J[\rho] + E_{ncl}[\rho] \quad (7\text{-}16)$$

The non-classical term contains the exchange-correlation energy, which is one of the terms that is particularly difficult to calculate.

The second Hohenberg-Kohn theorem is related to the variational principle outlined in Section 7.4. It states that the energy calculated from a trial density conforming to the appropriate boundary conditions will always be higher than the energy of the ground state density, E_0.

$$E_0 \leq E[\rho_{trial}] \quad (7\text{-}17)$$

Thus, E_0 can only be calculated if the ground state density, ρ_0, is known exactly.

In 1979 Levy[10] published a paper which proposed a method of using the variational principle to find the ground state energy of a system using the electron density. The Levy constrained-search approach consists of a two step search. The first step searches through the subset of antisymmetric wave functions which yield a certain density on integration. The second step searches over all densities to produce a ground state energy. This can be expressed as shown in Equation 7-18, where the inner minimisation is the first step.

$$E_0 = \min_{\rho \to N}\left(\min_{\Psi \to \rho} \langle \Psi | T + V_{Ne} + V_{ee} | \Psi \rangle \right) \quad (7\text{-}18)$$

By separating this equation according to which terms are system dependent (as in Equation 7-14), and employing the Hohenberg-Kohn functional, the equation can be simplified.

$$E_0 = \min_{\rho \to N}\left(F_{HK}[\rho] + \int \rho(r) V_{Ne} dr \right) \quad (7\text{-}19)$$

This approach is good in theory, but in practice it is not possible to search over all possible densities, so further development was needed to turn these ideas into practical methods.

7.9 The Kohn-Sham approach

Additional developments towards the application of density functional methods to chemical problems were made by Kohn and Sham in 1965.[11] They realised that by using a reference system of non-interacting electrons built from one-electron functions, a large part of the kinetic energy can be calculated very accurately. The remaining part of the kinetic energy contribution is approximated along with the non-classical part within E_{XC}. This results in only a small part of the total energy being approximated.

The non-interacting reference system is constructed from a Slater determinant as seen before in the Hartree-Fock approximation, where φ represents a Kohn-Sham orbital.

$$\Theta_s = \frac{1}{\sqrt{N!}} \det[\varphi_1 \varphi_2 ... \varphi_N] \tag{7-20}$$

The kinetic energy for non-interacting electrons, T_s, is expressed as it was in the Hartree-Fock approximation. Thus, the overall DFT energy can be defined as:

$$E[\rho] = T_s[\rho] + E_{Ne}[\rho] + J[\rho] + E_{XC}[\rho] \tag{7-21}$$

Where E_{XC}, the exchange-correlation energy, can be defined as:

$$E_{XC}[\rho] = (T[\rho] - T_s[\rho]) + (V_{ee}[\rho] - J[\rho]) = T_C[\rho] + E_{ncl}[\rho] \tag{7-22}$$

The variational principle is then applied, where the best spin orbitals correspond to the lowest energy, expressed as,

$$f^{KS}\varphi_i = \varepsilon_i \varphi_i \tag{7-23}$$

where f^{KS} is the one-electron Kohn-Sham operator, as defined in 7-24.

$$\left[-\frac{1}{2}\nabla^2 + V_{eff}(r)\right]\varphi_i = \varepsilon_i\varphi_i \qquad (7\text{-}24)$$

V_{eff}, the Kohn-Sham effective potential, consists of the components of $J[\rho]$, E_{xc} and $E_{Ne}[\rho]$. The exchange correlation potential, V_{xc}, resulting from E_{xc}, can be defined as:

$$V_{XC} = \frac{\partial E_{XC}}{\partial \rho} \qquad (7\text{-}25)$$

Unfortunately, the exact functional for E_{xc} is unknown and has to be approximated.

7.10 The local density approximation

In fact the search to find accurate values for $E_{xc}[\rho]$ is still the greatest challenge in DFT. A common starting point for modelling $E_{xc}[\rho]$ is considering that the exchange and correlation energy for each particle, ε_{XC}, can be calculated from the local value of electron density at that point. One case where this is possible is the uniform electron gas, which is a model with a structure similar to an idealised metal, where electrons move uniformly against a background of positive cores. This model is used because the exchange is known exactly and the correlation energy is known very accurately. In the local density approximation (LDA), $E_{XC}[\rho]$ can be defined as,

$$E_{XC}^{LDA}[\rho] = \int \rho(r)\varepsilon_{XC}(\rho(r))dr \qquad (7\text{-}26)$$

which is the exchange-correlation energy per particle of a uniform electron gas with the density $\rho(r)$. ε_{XC} can be split into separate contributions from exchange and correlation.

$$\varepsilon_{XC}(\rho) = \varepsilon_X(\rho) + \varepsilon_C(\rho) \qquad (7\text{-}27)$$

The exchange part of a particle's energy, $\varepsilon_X(\rho)$, can be calculated by using an equation similar to one developed earlier by Slater.[12]

$$\varepsilon_x(\rho) = -\frac{3}{4}\left(\frac{3\rho(r)}{\pi}\right)^{\frac{1}{3}} \qquad (7\text{-}28)$$

However, there is no such equation known for the correlation energy, $\varepsilon_C(\rho)$. Therefore, accurately calculated values from Monte-Carlo simulations of a uniform electron gas are commonly used.[13]

The LDA approximation represents a major step forward for DFT, and it performs better than the Hartree-Fock approximation for many systems.[14] However, a major drawback with LDA is that it overestimates atomisation energies, resulting in overbinding.

7.11 The generalised gradient approximation

Real molecular systems do not have uniform electron density. Therefore, a correction must be added to any energy calculated using LDA to represent a real system more closely. The generalised gradient approximation (GGA) is a method which has been developed to improve on the LDA by making ε_C depend not only on the local density at point r, $\rho(r)$, but on the extent to which the local density is changing, $\nabla\rho(r)$. The GGA functional can be expressed as:

$$E_{XC}^{GGA}[\rho] = \int f(\rho, \nabla\rho)dr \qquad (7\text{-}29)$$

The exchange and correlation parts of E_{xc} can be considered separately. The exchange part, E_x, can be expressed as,

$$E_X^{GGA} = E_x^{LDA} - \sum_\sigma \int F(s_\sigma)\rho_\sigma^{4/3}(r)dr \qquad (7\text{-}30)$$

where s_σ is a local inhomogeneity parameter, dependent on the gradient and electron density of the particular point on the potential energy surface.

$$s_\sigma(r) = \frac{|\nabla\rho_\sigma(r)|}{\rho_\sigma^{4/3}(r)} \qquad (7\text{-}31)$$

There are two widely used types of GGA exchange functionals, the first of which was developed by Becke[15] and is commonly abbreviated to 'B'. It can be defined as,

$$F^{B} = \frac{\beta s_\sigma^2}{1 + 6\beta s_\sigma \sinh^{-1} s_\sigma} \qquad (7\text{-}32)$$

It employs an empirical parameter, β, which has been fitted to exactly known exchange energies of the six noble gases. Other functionals similar to the Becke approach are CAM[16] and PW91.[17]

The second class of GGA exchange functionals do not contain any empirical parameters. Instead they use a rational function expansion of the reduced density gradient. Examples of this approach include B86,[18] P86,[19] LG[20] and PBE.[21]

$$F^{P86} = \left(1 + 1.296\left(\frac{s_\sigma}{(24\pi^2)^{1/3}}\right)^2 + 14\left(\frac{s_\sigma}{(24\pi^2)^{1/3}}\right)^4 + 0.2\left(\frac{s_\sigma}{(24\pi^2)^{1/3}}\right)^6\right)^{1/15} \qquad (7\text{-}33)$$

There are several correlation functionals which are commonly used. One was developed alongside the Perdew 1986 exchange functional, which contains an empirical parameter fitted to the neon atom. Perdew and Wang developed this E_c functional further in 1991 (PW91)[17] to become free of the empirical parameter. A different approach was made by Lee, Yang and Parr in 1988 when they developed E_c^{LYP}.[22] This was derived from a correlated wave function that provides the correlation energy for the helium atom.

The exchange and correlation functionals can be paired together to give some of the popular functionals used today, such as BP86, BPW91 and BLYP.

7.12 Hybrid functionals

The use of hybrid functionals was first introduced by Becke in 1993.[23] The idea was to calculate an exact value for E_x as calculated in the Hartree-Fock approximation, but using Kohn-Sham orbitals rather than Hartree-Fock orbitals. However, this did not reproduce experimental data particularly well. Therefore, the exact exchange is combined with exchange and correlation contributions calculated using the local density approximation.

Becke proposed an approach that included empirical parameters to tailor the weight of contribution from each term. These parameters were chosen to make the calculations reproduce experimental data.

$$E_{XC}^{B3} = E_{XC}^{LDA} + a(E_{XC}^{\lambda=0} - E_{X}^{LDA}) + bE_{X}^{B} + cE_{C}^{PW91} \qquad (7\text{-}34)$$

In Equation 7-36, '$\lambda = 0$' refers to a non-interacting system where electron correlation is not present. This led to the development of the popular B3LYP functional by Stephens *et al.*,[24] which is similar to Becke's hybrid functional, but uses LYP rather than PW91.

$$E_{XC}^{B3LYP} = (1-a)E_{X}^{LDA} + aE_{XC}^{\lambda=0} + bE_{X}^{B88} + cE_{C}^{LYP} + (1-c)E_{C}^{LDA} \qquad (7\text{-}35)$$

7.13 Basis sets

In ab initio methods molecular orbitals are represented by a linear combination of basis functions. Slater-type orbitals (STOs) would be the ideal choice of function as they closely model the radial form of atomic orbitals. However, when these methods were first developed STOs were too computationally demanding for most applications, so basis sets consisting of gaussian-type orbitals (GTOs) were developed instead. The functions are as follows:

$$\text{STO:} \quad \chi_{\zeta,n,l,m}(r,\theta,\varphi) = NY_{l,m}(\theta,\varphi)r^{n-1}\exp(-\zeta r) \qquad (7\text{-}36)$$

$$\text{GTO:} \quad \chi_{\zeta,n,l,m}(r,\theta,\varphi) = NY_{l,m}(\theta,\varphi)r^{2n-2-l}\exp(-\zeta r^{2}) \qquad (7\text{-}37)$$

N is a normalisation constant, r, θ and φ are spherical coordinates, $Y_{l,m}$ is angular momentum and n, l and m are quantum numbers. Although GTOs are much easier to compute, their r^2 exponential dependence means they fail to accurately model the cusp at the nucleus or the wave function at large values of r. The model can be improved by using a linear combination of several primitive GTOs to model each STO.

The minimal basis set only contains the number of basis functions required to accommodate all the electrons in the ground state neutral molecule. A popular minimal basis set is STO-3G[25] where 3 primitive GTOs are combined to simulate each STO.

These simple basis sets can be improved upon by increasing the number of basis functions used to describe each atom. For instance, a double zeta basis set has twice as many basis functions as a minimal basis set. This allows the flexibility needed to create a better model of electrons both close to and further away from the nuclei. Since most chemistry is governed by the actions of the valence electrons, it makes sense to dedicate more computing power to those regions. The use of 'split valence' can allow the core and valence electrons to be treated appropriately. A widely used example of a split valence basis set is 3-21G,[26] where the core electrons are represented by a contraction of 3 GTOs while the valence electrons are described by 2 basis functions constructed from 2 GTOs and 1 GTO.

Basis sets can be further improved, for example by adding d-orbital polarisation functions onto heavy atoms and possibly by also adding p-orbital polarisation onto hydrogen atoms. This is indicated by one or two asterisks respectively, for example 6-31G** has polarisation on all heavy atoms and hydrogens. The addition of polarisation enables much better, more flexible modelling of systems where the electron cloud on a particular atom is distorted, for instance by the presence of other nuclei.

When modelling a system with a considerable amount of electron density away from the nuclei, for example in an anion, it can be useful to use a basis set with added diffuse functions. These are symbolised using a plus sign, +. These functions use gaussians with a small exponent so that the function decays slowly as the distance from the nucleus increases.

It is important to find the most appropriate basis set for each application. It must be a sensible choice for the chemical system, but also be a balance between accuracy and computing time.

When the chemical system of interest contains elements from the second row of the periodic table and beyond, it is not necessary to accurately model the chemically-inert core electrons in such elements. The use of effective core potentials (ECPs) can be employed to greatly reduce the complexity of calculations on heavier atoms, while adequately modelling the nucleus and core electrons of an atom. Examples of ECPs commonly used include LANL[27] and SDD.[28]

7.14 Hybrid DF/HF methods

A balance between accuracy and computing time must also be sought when choosing the most appropriate methodology for the chemical system to be studied. The full experimental systems studied in this thesis contain over seventy atoms and it was not practical to compute these systems using purely DF methods with the computing resources available. Therefore, a hybrid DF/HF method was used, which allows the user to calculate the parts of the molecule important for reactivity at the high DF level, and the less important outer parts of the molecule at the lower HF level of calculation.

This was achieved using the ONIOM (our own N-layered integrated molecular orbital + molecular mechanics) method developed by Morokuma *et al*.[29] Within ONIOM the user can define either two or three different layers in a given molecule, which will be calculated using different computational methods. Figure 7.1 shows how *trans*-[Pd(Cl)OH(PPh_3)$_2$] from Chapter 4 is divided into two levels of calculation. The atoms in blue are calculated at the high DF level and the phenyl groups in black are calculated at the lower HF level.

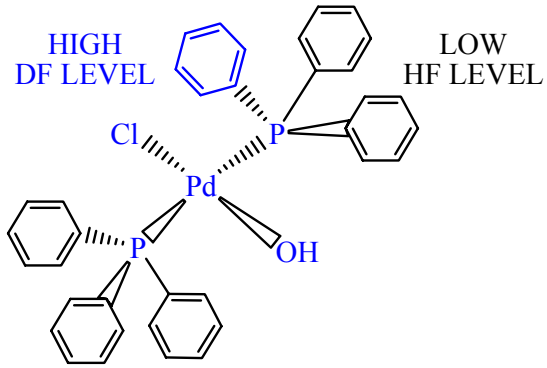

Figure 7.1: The different levels of calculation in *trans*-[Pd(Cl)OH(PPh_3)$_2$] using the DF/HF ONIOM method.

The energy of the molecule is then calculated using Equation 7.39, where the whole molecule is calculated using HF, then the HF energy of the high region is subtracted, and then finally the DF energy of the high region is added.

$$E_{tot} = E_{HF}(\text{whole}) - E_{HF}(\text{high}) + E_{DF}(\text{high}) \qquad (7\text{-}38)$$

The high and low regions of the molecule are connected using 'linker' atoms. In the ONIOM calculations performed in this thesis hydrogen atoms were used as linker atoms

in place of the P-C covalent bonds in the high model system. Thus, the high model system is considered as $[PdCl(OH)(PH_3)_2]$ in the example in Figure 7.1. This is necessary so that the high model region makes chemical sense when it is calculated.

The DF/HF ONIOM method was used to compute all of the large model complexes in Chapters 4, 5 and 6. Initial testing of the method, as described in Chapter 4, showed that this method produces geometries with a good structural agreement to those calculated using pure DF methods, but is much less computationally demanding.

7.15 Comparing functionals and basis sets

There are many different options when it comes to choosing an appropriate functional and corresponding basis sets to use on a project. As there are no suitable experimental data available for the systems investigated in this thesis, it is not possible to make a quantitative comparison between experiment and calculation. However, it is possible to compare the different computational methods to each other, in order to try to strike a balance between accuracy and computing time.

To this end, a range of calculations using different functionals and basis sets were performed using Gaussian 98[30] to compare their performance. The F/H exchange mechanism for $[PdCl(F)(PH_3)_2]$ from Chapter 3 was used for the comparison. Table 7.1 shows the comparative energies (in kcal/mol) of the exchange reaction profile calculated using six different functionals, Hartree-Fock and post Hartree-Fock methods. In each case the same basis sets were used, namely SDD[31] on palladium, SDD with added polarisation on chlorine and phosphorus, and 6-31G**[32] on fluorine and the hydrogens.

	BP86	BLYP	BPW91	B3P86	B3LYP	B3PW91	RHF	MP2
Reactant	0.0	0.0	0.0	0.0	0.0	0.0	0.0	0.0
TS 1	29.0	29.5	29.1	30.8	31.3	30.8	42.4	32.3
Intermed	15.4	18.3	15.5	16.6	19.4	16.9	35.5	15.7
TS 2	24.2	29.4	26.1	27.9	31.1	28.3	-	24.6
Product	-9.7	-6.7	-8.9	-10.2	-7.7	-9.6	0.8	-10.8

Tables 7.1: F/H exchange profile (kcal/mol) for $[PdCl(F)(PH_3)_2]$ computed using different functionals.

The first three columns show the results using pure DF methods, and they show similar values with TS1 consistently the energy highpoint and the exchange being exothermic

overall. Columns 4-6 in Table 7.1 show the results using the corresponding hybrid functionals of the columns 1-3. The values are slightly higher but maintain the key trends. An important difference when using hybrid functionals is the extra time taken for a calculation compared to using the pure functional. For instance, it took 55 seconds for one step in the optimisation of the reactant species using BLYP, whereas it took 66 seconds (20% longer) for a step with the same number of cycles in the same optimisation using B3LYP. Column 7 in Table 7.1 shows the comparative energies using Hartree-Fock methods. These results are significantly different from the other functionals as there is no allowance for electron correlation in the HF approximation. Column 8 in Table 7.1 shows a post-HF function based on Møller-Plesset perturbation theory,[33] which does allow for electron correlation effects but takes considerably longer (145 seconds for one step comparable with data above). However, these results are much more consistent with the DF results.

The next comparison conducted was to assess the importance and impact of adding polarisation to the basis sets used. Table 7.2 shows the results for the pure density functional BP86, while in Table 7.3 the hybrid functional B3LYP was used.

BP86			
Basis Sets on Pd, P + Cl: Basis Sets on F + H:	SDDALL 6-31G	SDDALL+pol 6-31G**	SDDALL+pol 6-311G**
Reactant	0.0	0.0	0.0
TS 1	41.5	29.0	28.2
Intermed	35.7	15.4	15.3
TS 2	52.1	24.2	26.2
Product	7.3	-9.7	-8.6

B3LYP			
Basis Sets on Pd, P + Cl: Basis Sets on F + H:	SDDALL 6-31G	SDDALL+pol 6-31G**	SDDALL+pol 6-311G**
Reactant	0.0	0.0	0.0
TS 1	44.5	31.3	30.3
Intermed	39.8	19.4	19.2
TS 2	58.8	31.1	32.0
Product	9.5	-7.7	-6.3

Tables 7.2 and 7.3: F/H exchange profile (kcal/mol) for $[Pd(F)(PH_3)_2]$ computed using BP86 / B3LYP and varying the basis sets.

Columns 1 and 2 in Tables 7.2 and 7.3 show the effect of adding polarisation to the basis sets of all the atoms except palladium in the system on the comparative profile

energies. With both functionals the absence of polarisation causes the comparative energy for all stationary points to be higher, the overall profiles highpoint to change to TS 2 and the overall process to become endothermic. This demonstrates the major differences that inclusion of polarisation makes to an energy profile. The polarisation on hydrogen was particularly important as TS 2, the H-transfer step, is most affected by adding polarisation. Columns 2 and 3 in Tables 7.2 and 7.3 show the effect of changing from a double zeta to a triple zeta basis set for the fluorine and hydrogen atoms. As discussed earlier in the chapter, this should improve the description of the outer region of the valence orbitals. In fact, for this reaction profile it makes no significant changes to the comparative energies.

A further comparison between the data in column 2 of Table 7.2 and the computed energies with the addition of f orbitals on palladium was performed. This made no significant difference to the comparative energies for the reaction profile.

In conclusion, it has been demonstrated that no significant advantage would be gained by using a hybrid functional over a pure DF theory method. In addition, it is important to include polarisation in the basis sets for all atoms in the system except palladium, but not much is gained by using a triple rather than double zeta basis set on the lighter atoms.

7.16 References

[1] a) Schrödinger, E., *Annalen der Physik,* 734, (1926) b) Schrödinger, E., *Phys. Rev.* **28**, 6, 1049, (1926)

[2] Born, M.; Oppenheimer, R., *Annalen der Physik,* **84**, 457, (1927)

[3] Slater, J. C., *Phys. Rev.*, **34**, 1293, (1929)

[4] a) Hartree, D. R., *Proc. Camb. Phil. Soc.*, **24**, 89, (1928) b) Fock, V., *Z. Phys.*, **61**, 126, (1930)

[5] Löwdin, P. –O., *Adv. Chem. Phys.,* **2**, 207, (1959)

[6] Cook, M.; Karplus, M., *J. Chem. Phys.,* **91**, 31, (1987)

[7] Thomas, L. H., *Proc. Camb. Phil. Soc.,* **23**, 542, (1927)

[8] Fermi, E., *Rend. Accad. Lincei.,* **6**, 602, (1927)

[9] Hohenberg, P.; Kohn, W., *Phys. Rev. B*, **136**, 864, (1964)

[10] Levy, M, *Proc. Natl. Acad. Sci. USA*, **76**, 6062, (1979)

[11] Kohn, W.; Sham, L. J., *Phys. Rev.*, **140**, A1133, (1965)

[12] Slater, J. C., *Phys. Rev.,* **81**, 385, (1951)

[13] Ceperley, D. M.; Alder, B. J., *Phys. Rev. Lett.*, **45**, 566, (1980)

[14] Koch, W.; Holthausen, M. C., *A Chemists Guide to Density Functional Theory*, 2nd Edn., Wiley-VCH, Weinheim, (2002)

[15] Becke, A. D., *Phys. Rev. A,* **38**, 3098, (1988)

[16] Laming, G. J.; Termath, V.; Handy, N. C., *J. Chem. Phys.,* **99**, 8765, (1993)

[17] a) Perdew, J. P., *Electronic Structure of Solids*, Akademie Verlag, Berlin (1991) b) Burke, K.; Perdew, J. P.; Wang, Y., *Electron Density Functional Theory. Recent progress and New Directions*, Plenum Press, New York (1998)

[18] Becke, A. D., *J. Chem. Phys.,* **84**, 4524, (1986)

[19] Perdew, J. P., *Phys. Rev. B,* **33**, 8822, (1986)

[20] Lacks, D. J.; Gordon, R. G., *Phys. Rev. A,* **47**, 4681, (1993)

[21] Perdew, J. P.; Burke, K.; Ernzerhof, M., *Phys. Rev. Lett.,* **77**, 3865, (1996)

[22] Lee, C.; Yang, W.; Parr, R. G., *Phys. Rev. B*, **37**, 785, (1988)

[23] a) Becke, A. D., *J. Chem. Phys.,* **98**, 1372, (1993) b) Becke, A. D., *J. Chem. Phys.,* **98**, 5648, (1993)

[24] Stephens, P. J.; Devlin, J. F.; Chabalowski, C. F.; Frisch, M. J., *J. Phys. Chem.,* **98**, 11623, (1994)

[25] a) Hehre, W. J.; Stewart, R. F.; Pople, J. A., *J. Chem. Phys.,* **51**, 2657, (1969) b) Collins, J. B.; Schleyer, P. v. R.; Binkley, J. S.; Pople, J. A., *J. Chem. Phys.,* **64**, 5142, (1976)

[26] a) J. S.; Binkley, J. A.; Pople, W. J., Hehre, *J. Am. Chem. Soc.,* **102**, 939, (1980) b) Gordon, M. S.; Binkley, J. S.; Pople, J. A.; Pietro, W. J.; Hehre, W. J., *J. Am. Chem. Soc.,* **104**, 2797, (1982) c) Pietro, W. J.; Francl, M. M.; Hehre, W. J.; Defrees, D. J.; Pople, J. A.; Binkley, J. S., *J. Am. Chem. Soc.,* **104**, 5039, (1982) d) Dobbs, K. D.; Hehre, W. J., *J. Comp. Chem.,* **7**, 359, (1986) e) Dobbs, K. D.; Hehre, W. J., *J. Comp. Chem.,* **8**, 861, (1987) f) K. D. Dobbs and W. J. Hehre, *J. Comp. Chem.,* **8**, 880 (1987)

[27] Hay, P. J.; Wadt, W. R., *J. Chem. Phys.*, **82**, 270, (1985)

[28] Dolg, M, *Theor. Comput. Chem.,* **11**, 793, (2002)

[29] a) Maseras, F.; Morokuma, K., *J. Comp. Chem.*, **16**, 1170, (1995) b) Humbel, S.; Sieber, S.; Morokuma, K., *J. Chem. Phys.,* **105**, 1959 (1996) c) Matsubara, T.; Sieber, S.; Morokuma, K., *Int. J. Quant. Chem.,* **60**, 1101 (1996) d) Svensson, M.;

Humbel, S.; Froese, R. D. J.; Matsubara, T.; Sieber, S.; Morokuma, K., *J. Phys. Chem.,* **100**, 19357 (1996) e) Svensson, M.; Humbel, S.; Morokuma, K., *J. Chem. Phys.,* **105**, 3654 (1996) f) Dapprich, S.; Komáromi, I.; Byun, K. S.; Morokuma, K.; Frisch, M. J., *J. Mol. Struct. (Theochem),* **462**, 1 (1999) g) Vreven T.; Morokuma, K., *J. Comp. Chem.,* **21**, 1419 (2000)

[30] Frisch, M. J.; Trucks, G. W.; Schlegel, H. B.; Scuseria, G. E.; Robb, M. A.; Cheeseman, J. R.; Zakrzewski, V. G.; Montgomery Jr., J. A.; Stratmann, R. E.; Burant, J. C.; Dapprich, S.; Millam, J. M.; Daniels, A. D.; Kudin, K. N.; Strain, M. C.; Farkas, Ö.; Tomasi, J.; Barone, V.; Cossi, M.; Cammi, R.; Mennucci, B.; Pomelli, C.; Adamo, C.; Clifford, S.; Ochterski, J.; Petersson, G. A.; Ayala, P. Y.; Cui, Q.; Morokuma, K.; Salvador, P.; Dannenberg, J. J.; Malick, D. K.; Rabuck, A. D.; Raghavachari, K.; Foresman, J. B.; Cioslowski, J.; Ortiz, J. V.; Baboul, A. G.; Stefanov, B. B.; Liu, A.; Liashenko, G.; Piskorz, P.; Komáromi, I.; Gomperts, R.; Martin, R. L.; Fox, D. J.; Keith, T.; Al-Laham, M. A.; Peng, C. Y.; Nanayakkara, A.; Challacombe, M.; Gill, P. M. W.; Johnson, B.; Chen, W.; Wong, M. W.; Andres, J. L.; Gonzalez, C.; Head-Gordon, M.; Replogle, E. S.; Pople, J. A., *Gaussian 98* (Gaussian, Inc., Pittsburgh, PA, 1998)

[31] Perdew, J. P.; Wang, Y. *Phys. Chem Rev. B,* **45***,* 13244, (1992)

[32] a) Ditchfield, R.; Hehre, W. J.; Pople, J. A., *J. Chem. Phys.,* **54**, 724, (1971) b) Hehre, W. J.; Ditchfield, R.; Pople, J. A., *J. Chem. Phys.,* **56**, 2257, (1972) c) Hariharan P. C.; Pople, J. A., *Mol. Phys.,* **27**, 209, (1974) d) Gordon, M. S., *Chem. Phys. Lett.,* **76**, 163, (1980) e) Hariharan P. C.; Pople, J. A., *Theo. Chim. Acta,* **28**, 213, (1973) f) Blaudeau, J.-P.; McGrath, M. P.; Curtiss, L. A.; Radom, L., *J. Chem. Phys.,* **107**, 5016, (1997) g) Francl, M. M.; Pietro, W. J.; Hehre, W. J.; Binkley, J. S.; DeFrees, D. J.; Pople, J. A.; Gordon, M. S., *J. Chem. Phys.,* **77**, 3654, (1982) h) Binning Jr. R. C.; Curtiss, L. A., *J. Comp. Chem.,* **11**, 1206, (1990) i) Rassolov, V. A.; Pople, J. A.; Ratner, M. A.; Windus, T. L., *J. Chem. Phys.,* **109**, 1223, (1998) j) Rassolov, V. A.; Ratner, M. A.; Pople, J. A.; Redfern, P. C.; Curtiss, L. A., *J. Comp. Chem.,* **22**, 976, (2001)

[33] Møller, C.; Plesset, M. S. *Phys. Rev.*, **46**, 618, (1934)

7.17 Bibliography

Cramer, C. J., *Essentials of Computational Chemistry, Theories and Models,* 2nd Edn., John Wiley & Sons Ltd, West Sussex (2004)

Jensen, F., *Introduction to Computational Chemistry,* John Wiley & Sons Ltd, West Sussex (1999)

Koch, W.; Holthausen, M. C., *A Chemists Guide to Density Functional Theory*, 2nd Edn., Wiley-VCH, Weinheim (2002)

Parr, R. G.; Yang, W., *Density-Functional Theory of Atoms and Molecules,* Oxford University Press, New York, (1994)